CIRCULATIONS AND WATER MASS BALANCES IN THE BRAZIL BASIN

by

Huai-Min Zhang

M.S. Institute of Atmospheric Physics, Academia Sinica
(1987)

Submitted in partial fulfillment of the
requirements for the degree of

Master of Science

at the

MASSACHUSETTS INSTITUTE OF TECHNOLOGY

and the

WOODS HOLE OCEANOGRAPHIC INSTITUTION

September 1991

Signature of Author.....
Joint Program in Physical Oceanography
Massachusetts Institute of Technology
Woods Hole Oceanographic Institution
August 26, 1991

Certified by.....
Nelson G. Hogg
Senior Scientist
Thesis Supervisor

Accepted by.....
Lawrence J. Pratt
Chairman, Joint Committee for Physical Oceanography
Massachusetts Institute of Technology
Woods Hole Oceanographic Institution

CIRCULATIONS AND WATER MASS BALANCES IN THE BRAZIL BASIN

by
Huai-Min Zhang

Submitted in partial fulfillment of the requirements for the degree of
Master of Science at the Massachusetts Institute of Technology
and the Woods Hole Oceanographic Institution
August 26, 1991

Abstract

Based on the Levitus atlas, we find that the application of the Montgomery streamfunction to the isopycnal surfaces induces an error which can not be ignored in some regions in the ocean. The error arises from the sloping effect of the specific volume anomaly along isopycnal surfaces. By including the major part of this effect, new streamfunctions, namely the pressure anomaly and main pressure streamfunctions, are suggested for the use in potential density coordinates.

By using the newly proposed streamfunction and by including the variations of specific volume anomaly along isopycnal surfaces, the inverse model proposed by Hogg (1987) is modified for increasing accuracy and applied to the Brazil Basin to study the circulation, diffusion and water mass balances. The equations in the model, i.e. the dynamic equation, continuity equation, integrated vorticity equation, and conservation equations for heat, salt and oxygen (in which a consumption sink term is allowed), are written in centered finite difference form with lateral steps of 2 degree latitude and longitude and 8 levels in the vertical. This system of equations with constraints of positive diffusivities and oxygen consumption rates is solved by the inverse method. The results indicate that the circulation in the upper oceans is consistent with previous works, but that in the deep ocean is quite different. In the NADW region, we find a coincidence of the flows with the tongues of water properties. The diffusivities and diapycnal velocities seem stronger in the region near the equator than in the south, with reasonable values. Diffusion plays an important role in the water mass balance. Examples show that similar property fields may resulte from different processes.

Thesis Supervisor:
Dr. Nelson Hogg , Senior Scientist
Woods Hole Oceanographic Institution

Contents

Chapter 1

INTRODUCTION

1.1 Overview

The investigation of the ocean circulation is very important in the study of the heat transport in the ocean and thus the global climate system. Unfortunately, direct measurement of ocean currents, especially those in the deep oceans, is extremely difficult. On the other hand, hydrographic data, such as temperature, salinity, oxygen, etc., are much more accessible. Thus one primary task for oceanographers is to deduce the ocean circulation from the available hydrographic data.

Understanding the physical mechanisms for balances in the water properties is not only itself an important topic, it is also essential for the inference of the circulation from the hydrographic data (water properties). For example, if one believed that advection is the only process in the water property balance, one would infer that the flows are along the isopleths of the property. On the other hand, if processes other than advection, like mixing due to diffusion etc. are also present in the balances, as is almost always true in the ocean, one must utilize a different approach to infer the circulation.

Traditionally, there are two approaches to deducing the ocean circulation from hydrographic data: one is the descriptive method (water mass analysis or the "core

method"), and the other is the dynamic method. In the descriptive method, the fields of the water properties (such as temperature, salinity, oxygen, etc.) are used to deduce the circulation configurations. In *Wüst's* (1935) core layer method, the extremes of the water properties are interpreted as the primary "spreading" pathways of the flows. The isentropic analysis (Montgomery, 1938) is another example of the descriptive method. Since the distributions of water properties generally depend on both advective and diffusive processes, the water mass deduced flows can only give us a flow pattern in a general sense, but cannot correctly give us the detailed structure of the flow field. On the other hand, in the dynamic method, the distributions of the density field are used to derive the shear flows or relative flows through the hydrostatic and geostrophic equations. To get the absolute velocities, the so called "reference-level" or "level-of-no -motion" issue must be resolved. Early attempts to obtain the reference level velocities are based on the assumption that there must exist some levels at which velocity vanishes, such as the ocean bottom, an interface between two water masses which appear to flow in opposite directions, and so on. But there are no dynamic justifications for the existence of the level of no motion. An alternate attempt to get the reference level velocities is to measure them directly, but again there are practical difficulties.

By using the conservation equations for mass, heat, salt, carbon-14 and oxygen in a box model, Wright (1969) determined the deep water transports in the Western Atlantic. More recently, Wunsch (1977) applied the general inverse theories to the field of the oceanography to determine the reference level velocities; and independently, Stommel and Schott(1977) proposed the β-spirial method to solve essentially the same problem, and this method was further developed by Olbers et al (1985). Instead of exactly satisfying geostrophy (implied by solving the reference velocity), as in the two previous works, Hogg(1987) combined the dynamic method with the conservation laws for the water properties to determine the absolute velocities(actually the streamfunctions) at all levels simultaneously by the least square fit or the inverse method. (More detailed

comparisions among these models are discussed in the following sections). Calculating the velocities relative to the ocean bottom initially, and then adding and adjusting the so called *barotropic* components to the relative velocities to make the flows consonant with the property distributions and mass conservations, Reid (1989) determined the adjusted steric heights for the absolute flows and transports in the South Atlantic. His model and results will be discussed in Chapter 4 for comparison with our model results.

1.2 Comparisons of the Inverse Models

The basic assumptions in Wunsch's box inverse model (1977, 1978) are that the oceans are in hydrostatic equilibrium, flows are in geostrophic balance, and the conservative water properties, such as mass, heat, salt, etc., are conserved in *closed* volumes. The mathmatical expressions for the first two assumptions are

$$\frac{\partial p}{\partial z} = -g\rho \tag{1.1}$$

$$fv = \frac{1}{\rho}\frac{\partial p}{\partial x} \tag{1.2}$$

$$fu = \frac{-1}{\rho}\frac{\partial p}{\partial y}. \tag{1.3}$$

Combining these equations yields the "thermal wind" relations:

$$f\frac{\partial v}{\partial z} = \frac{-g}{\rho}\frac{\partial \rho}{\partial x} \tag{1.4}$$

$$f\frac{\partial u}{\partial z} = \frac{g}{\rho}\frac{\partial \rho}{\partial y} \tag{1.5}$$

Integrating the above equations with respect to z from the reference level, z_0 to any level z , we get the absolute velocity at the level z as

$$fv(x,y,z) = fv(x,y,z_0) - \frac{g}{\rho}\int_{z_0}^{z}\frac{\partial \rho}{\partial x}dz \tag{1.6}$$

$$fu(x,y,z) = fu(x,y,z_0) + \frac{g}{\rho}\int_{z_0}^{z}\frac{\partial \rho}{\partial y}dz \tag{1.7}$$

Substituting the above expressions for u and v into the conservation equations for the water properties, we obtain a simultaneous equation system concerning the unknown reference velocities, and the solutions can be obtained by the inverse method he used. Unlike the models discussed below, Wunsch (1978) generally applies the conservation laws over large closed volumes so that the data noise may be smaller (mass conservation is more accurate in large volumes than in small volumes). These box models are especially good at determining velocities and transports *across* the hydrographic sections, but not particularly suitable for determining the interior (within the boxes) flows.

In the β-spirial method postulated by Stommel and Schott(1977), in addition to the basic assumptions in Wunsch's model (hydrostatics, geostrophy), it is also explicitly assumed that sea water is incompressible: [1]

$$\frac{\partial u}{\partial x} + \frac{\partial v}{\partial y} + \frac{\partial w}{\partial z} = 0. \tag{1.8}$$

and that the density equation is in the conservation form (for the steady state and without diffusion):

$$u\frac{\partial \rho}{\partial x} + v\frac{\partial \rho}{\partial y} + w\frac{\partial \rho}{\partial z} = 0 \tag{1.9}$$

Reorganizing all the above equations, and expressing the density gradients by the slopes of the constant density surfaces($h = h(x,y)$), the β-spirial equation is derived as

$$u\frac{\partial^2 h}{\partial x \partial z} + v(\frac{\partial^2 h}{\partial y \partial z} - \frac{\beta}{f}) = 0 \tag{1.10}$$

[1]Note that if the compressibility of the sea water is considered, nondivergency Eq.(1.9) is still a good first order approximation, but the density equation may have more complicated form than Eq.(1.8). Ref. to Chapter 3 for detail.

Principally, the absolute velocities at all depths can be obtained in the following way. Firstly, the direction of the velocity at all depths is given from Eq.(1.10) by

$$tan\theta = \frac{v}{u} = -\frac{\partial^2 h}{\partial x \partial z} / (\frac{\partial^2 h}{\partial y \partial z} - \frac{\beta}{f}) \tag{1.11}$$

Secondly, if one of the coefficients of u and v in Eq.(1.10) vanishes without the other vanishing at a particular depth, then obviously that component of u and v which is associated with the non-zero coefficients also vanishes at that depth, and thus the level of no motion for that component is decided. Therefore the absolute velocities for that component at all depths are consequently determined by the thermal wind relation, and the other component is likewisely determined by the direction relation, eq.(1.11).

In practice, the coefficients for u and v are not well determined because of the large data noise which has impacts on the second order derivatives. Actually, in the application of the β-spirial method, instead of finding the level of no motion, an equation system for the velocities (u_0, v_0) at a previously selected "reference level" is formulatted as follows. Decomposing the absolute velocity $\vec{V}$ at any depth into the known shear velocity $\vec{V}_r$, which is obtained from the density field by the thermal wind relation, and the unknown reference velocity $\vec{V}_0$, substitution into eq.(1.10) yields

$$u_0 \frac{\partial^2 h}{\partial x \partial z} + v_0 (\frac{\partial^2 h}{\partial y \partial z} - \frac{\beta}{f}) = -u_r \frac{\partial^2 h}{\partial x \partial z} - v_r (\frac{\partial^2 h}{\partial y \partial z} - \frac{\beta}{f}) \tag{1.12}$$

This equation can be applied at any grid points where the derivatives h_{xz}, h_{yz} exist, so that a system of equations for u_0, v_0 is derived, and the solutions can be obtained by the general inverse method (But this is generally overdetermined because there are just two

unknowns). As in Wunsch's model, conservation equations for other water properties can also be added to give more constraints to the solution. The work by Olbers et al (1985) is one example. Different from the box model, the conservation equations are written on a point-wise basis.

In all the above models, the unknowns are the velocities at the reference levels. The absolute velocities at all other levels are then calculated using the thermal wind relation. This implies that geostrophy is satisfied exactly in these models. In the oceans, geostrophy is a quite good first order *approximation* for the large-scale flows (Pedlosky, 1987), thus the real ocean flows may deviate from geostrophy to some extent. Based on essentially the same assumptions as above, but instead of calculating the reference velocities, Hogg(1987) formulated a model to determine the absolute velocities(actually the streamfunctions) at all levels directly. By computing the velocities at all depths simultaneously, the artificially enforced exact satisfaction of geostrophy is relaxed. The extent to which geostrophy is satisfied depends on the relative weights for the dynamic equations and other conservation equations(this can be seen from the data resolutions). In the present work, Hogg's model is first modified to make it more exact for the potential density coordinates, then the model is applied to the Brazil Basin to study the circulation and diffusion processes in that region. A more detailed discussion of the assumptions and formulations of this model is given in Chapter 3.

1.3 The Brazil Basin

The Brazil Basin is chosen as the region to apply the model, because in this basin there are many uncertainties about the circulation and mass conversion processes. The Brazil Basin contains a rich water mass structure, namely: the central water in the surface; the Antarctic intermediate water(AAIW), circumpolar water(CPW), Antarctic bottom water(AABW) from the south; and the North Atlantic deep water(NADW) from the

north. Even more water masses can be idenfied by the extremes of the water properties. All these waters meet in the Brazil Basin, flowing over and mixing with each other in the interfaces to adjust their characteristics. Nevertheless, the exact pathways of the flows and the mechanisms by which the water masses are modified are still unclear. Because of the large and complicated vertical distributions of the water properties, mixing may be the important process in the water property conversions, which not only has direct significance on the tracer distributions, but also has significance on the circulation through its impact on the stratification of the ocean(Tziperman, 1987). However, there are many physical processes which can be responsible for the mixing: from mesoscale eddies to small scale turbulence, and to molecular diffusion. In the case where only molecular diffusion is important in the mixing, double diffusion may also be effective because of the different diffusivities for heat and salt (Turner, 1973). Schmitt (1979) shows that the salt fingering is mostly active when $1 < R_\rho < 2$, where $R_\rho = \alpha\theta_z/\beta S_z$ is the ratio of the density fluxes due to heat and salt. The profiles of $R_{\rho(z)}$ shown in Fig.1.1 suggest that at some depths double diffusion is potentially important. Because other processes, such as wave breaking, cabbeling, etc. (Turner, 1980), may also occur, the actual effectiveness of the double diffusion depends on the relative strengths of all these processes, and is still an open question.

The purposes of this work are try to answer some of the questions raised above. In Chapter 2, a new, appoximate streamfunction for the potential density surfaces (hereafter defined as isopycnal surfaces) is deduced based on the data analysis. Chapter 3 gives a detailed description of the model, and a brief discussion of the Levitus atlas and basic techniques in the inverse model used in this work. The model results and their analysis are presented in Chapter 4, followed by a brief summary and remarks.

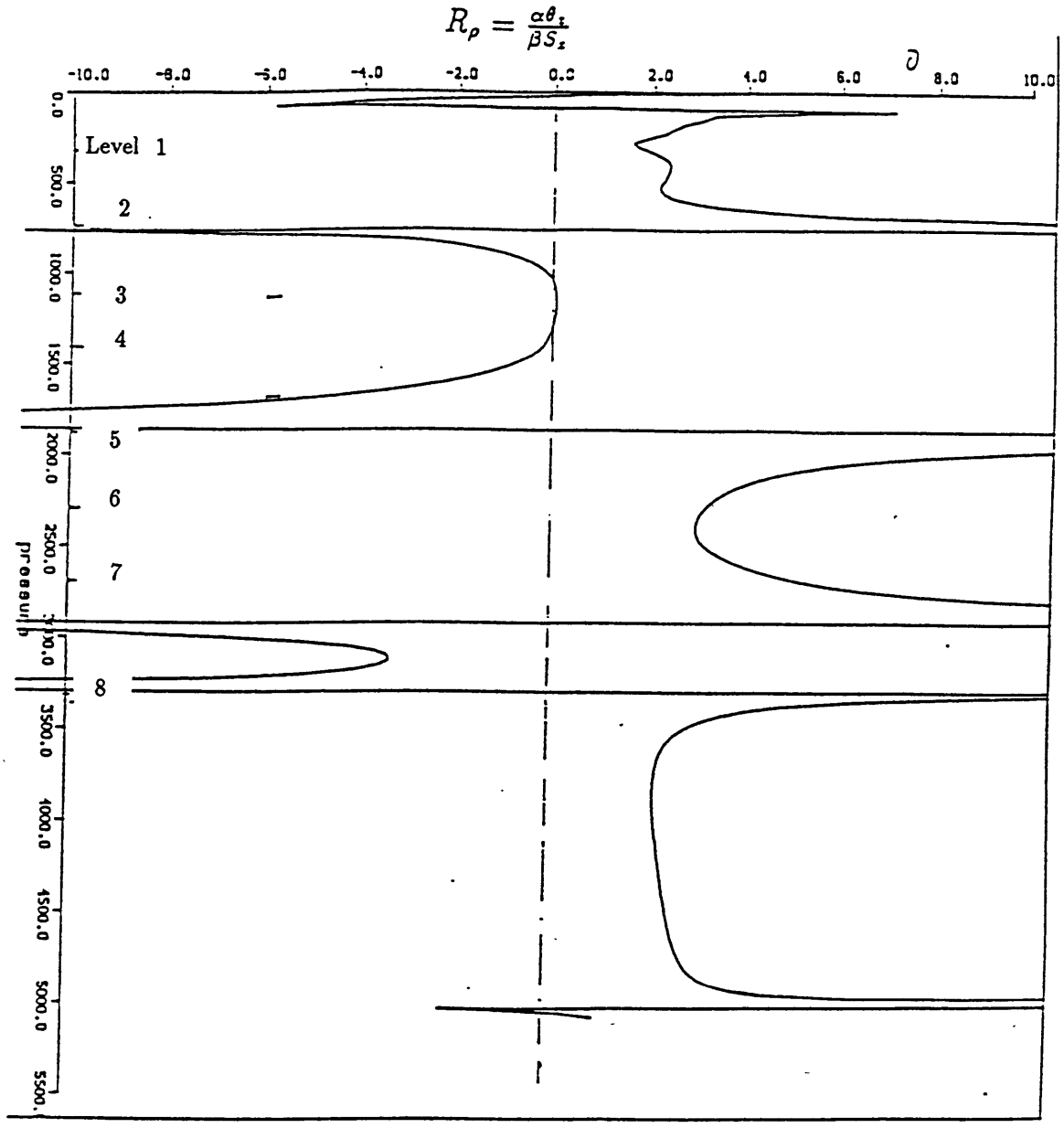

Fig.1.1 Profile of the stability parameter (R_ρ) at (26.5°W,6.5°S)

Chapter 2

STREAMFUNCTIONS FOR POTENTIAL DENSITY SURFACES

2.1 Introduction

A well known fact about the oceans is that the flows and mixing are much stronger in the horizontal than in the vertical. Thus it is possible to find surfaces along which the velocities and mixing have their major components while those across are minimized.The very early choice of such surfaces is the potential density surfaces (Montgomery, 1938), where the potential density is defined as the density a fluid parcel would have if it were isentropically and adiabatically moved to an arbitrarily chosen but fixed pressure, for example, the ocean surface pressure. Although the *in situ* density ρ generally increases monototically with depth, which means that the ocean is statically stable, inversion of *potential* density gradient is still possible, because the static stability is not simply determined

by the gradient of potential density (*Wüst*,1933;Ekman,1934). [1] Ekman(1934) proposes the use of potential densities at different depths with reference to different pressures, and even suggests notations σ_1, σ_2,etc. which are widely used till today. By definition, fluid parcels having the same potential density can be freely moved around on the reference pressure surface p_r without experiencing buoyancy forces. However, with respect to the *in situ* pressure, there is no such property. Recently,McDougall (1977) suggested the use of the *neutral surfaces*, which are defined as the surfaces on which small isentropic and adiabatic displacements of a fluid parcel do not produce buoyant restoring forces on the parcel. In principal,these are the surfaces we want. But in practice,the computation and interpretation of the neutral surfaces are far more difficult than that of the historically used isopycnal ones. As neutral and isopycnal surfaces coincide at the reference pressure, if the potential densities at different depths are with reference to different pressures, and if the *in situ* pressure is never allowed to be more than 500 *dbars* from the reference pressure, the deviation of the isopycnal surface from the neutral surface should be small. Therefore,the more commonly used isopycnal surfaces will be used in this work.

Streamfunctions for several different vertical coordinates have been found, such as pressure for geopotential surfaces, dynamic height for pressure surfaces,Montgomary streamfunctions for steric (specific volume) anomaly surfaces and for steric or *in situ* density surfaces (McDougall, 1989). Nevertheless, exact streamfunctions for isopycnal surfaces have not been found yet. In his work,Hogg(1987) applied Montgomary streamfunction on isopycnal surfaces. The data analysis presented in the later sections shows

[1]The criterior for static stability in terms of potential density is such that

$$\frac{1}{g}N^2 = -C\frac{1}{\rho_\theta}\frac{d\rho_\theta}{dz} - B\frac{dS}{dz} > 0 \tag{2.1}$$

where N is the Brunt-V*ässalä* frequency,$C = \frac{\rho_\theta}{\rho}(\frac{\partial\rho}{\partial\rho_\theta})_{p,S}$, $B = \frac{1}{\rho}(\frac{\partial\rho}{\partial S})_{p,\rho_\theta}$, and S is salinity.See Gill(1982) for detail.

that this application implies that a potentially important term has been neglected. By including the major part of this term in the Montgomery streamfunction, an approximate, but more accurate streamfunction for the potential density coordinate can be obtained which will be derived next.

2.2 Operators in Potential Density Coordinates

To work in potential density coordinates,it is necessary first to derive the expressions for the linear oprators in this system. In an arbitrary curvilinear (*orthogonal*) coordinate as shown in Fig.2.1,the general three dimensional gradient operator is

$$\nabla A = (\frac{1}{H_1}\frac{\partial A}{\partial \xi_1} \ , \ \frac{1}{H_2}\frac{\partial A}{\partial \xi_2} \ , \ \frac{1}{H_3}\frac{\partial A}{\partial \xi_3}) \ , \tag{2.2}$$

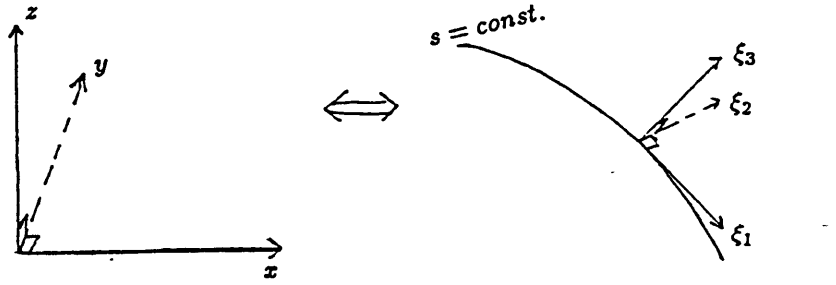

Fig.2.1 A Curvilinear Coordinate

the three dimensional divergence operator is

$$\nabla \cdot \vec{\mathbf{A}} = \frac{1}{H_1 H_2 H_3}[\frac{\partial(H_2 H_3 A_1)}{\partial \xi_1} + \frac{\partial(H_3 H_1 A_2)}{\partial \xi_2} + \frac{\partial(H_1 H_2 A_3)}{\partial \xi_3}], \tag{2.3}$$

and the three dimensional Laplacian operator is

$$\nabla^2 A = \frac{1}{H_1 H_2 H_3} \sum_{i=1}^{3} \partial\left(\frac{H_1 H_2 H_3}{H_i^2} \frac{\partial A}{\partial \xi_i}\right)/\partial \xi_i \tag{2.4}$$

where

$$H_i^2 = \left(\frac{\partial x}{\partial \xi_i}\right)^2 + \left(\frac{\partial y}{\partial \xi_i}\right)^2 + \left(\frac{\partial z}{\partial \xi_i}\right)^2 = \left[\left(\frac{\partial \xi_i}{\partial x}\right)^2 + \left(\frac{\partial \xi_i}{\partial y}\right)^2 + \left(\frac{\partial \xi_i}{\partial z}\right)^2\right]^{-1}. \tag{2.5}$$

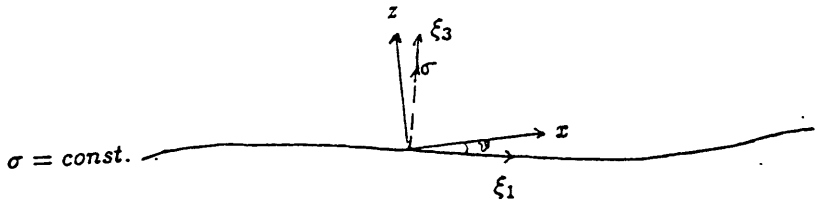

Fig.2.2 Relation Between Coordinates (x, y, z) *And* (ξ_1, ξ_2, σ)

For the σ-coordinate (hereafter,σ represents the *potential* density surfaces, which can be σ_θ or σ_1 to σ_4), as shown in Fig.2.2, the σ surfaces are generally so gentle that we can make the following approximations:

$$\xi_1 = x \cdot cos\vartheta - z \cdot sin\vartheta \approx x \cdot 1 - z \cdot \vartheta \approx x + z \cdot \frac{\sigma_x}{\sigma_z} \approx x \quad , \tag{2.6}$$

and similarly,

$$\xi_2 = y, \tag{2.7}$$

$$\xi_3 \equiv \sigma = \sigma(x, y, z) \quad , and\ thus \quad z = z(x, y, \sigma) \tag{2.8}$$

$$\tag{2.9}$$

Using the above approximations, we have

$$H_1^2 = 1^2 + 0^2 + \left(\frac{\partial z}{\partial x}\right)_\sigma^2 = 1 + \left(\frac{\sigma_x}{\sigma_z}\right)^2 \approx 1 \; ; H_1 \approx 1 \tag{2.10}$$

$$H_2^2 = 0^2 + 1^2 + \left(\frac{\partial z}{\partial y}\right)_\sigma^2 = 1 + \left(\frac{\sigma_y}{\sigma_z}\right)^2 \approx 1 \; ; H_2 \approx 1 \tag{2.11}$$

$$H_3^2 = \left(\frac{\partial z}{\partial \sigma}\right)^2 \; ; \quad H_3 = \frac{\partial z}{\partial \sigma} = \frac{1}{\sigma_z} \tag{2.12}$$

Therefore, the 3-D gradient and divergence operators in the σ-coordinate are

$$\nabla A = \hat{i}\frac{\partial A}{\partial x} + \hat{j}\frac{\partial A}{\partial y} + \hat{k}\sigma_z\frac{\partial A}{\partial \sigma} \equiv \nabla_\sigma A + \hat{k}\sigma_z\frac{\partial A}{\partial \sigma} \tag{2.13}$$

$$\nabla \cdot \vec{\mathbf{A}} = \sigma_z\left[\frac{\partial(\frac{A1}{\sigma_z})}{\partial x} + \frac{\partial(\frac{A2}{\sigma_z})}{\partial y} + \frac{\partial A3}{\partial \sigma}\right] \equiv \nabla_h \cdot \vec{\mathbf{A}} + \sigma_z\frac{\partial A3}{\partial \sigma} \tag{2.14}$$

where ∇_σ *and* ∇_h are the 2-D lateral gradient and divergence operators defined in the σ-coordinate:

$$\nabla_\sigma \equiv \hat{i}\frac{\partial}{\partial x} + \hat{j}\frac{\partial}{\partial y} \tag{2.15}$$

$$\nabla_h \equiv \sigma_z\left[\hat{i}\frac{\partial}{\partial x}\frac{1}{\sigma_z} + \hat{j}\frac{\partial}{\partial y}\frac{1}{\sigma_z}\right] \tag{2.16}$$

Partial Differential Relations between the z-coordinate and the σ-coordinate

In the two different coordinates, any property A can be expressed as

$$A = A(x,y,z) = A(x,y,z(x,y,\sigma)) \quad or \quad A = A(x,y,\sigma) = A(x,y,\sigma_(x,y,z)) \tag{2.17}$$

Hence the partial differential relation can be derived as

$$\left(\frac{\partial A}{\partial x}\right)_\sigma = \left(\frac{\partial A}{\partial x}\right)_z + \left(\frac{\partial A}{\partial z}\cdot\frac{\partial z}{\partial x}\right)_\sigma \tag{2.18}$$

$$\left(\frac{\partial A}{\partial y}\right)_\sigma = \left(\frac{\partial A}{\partial y}\right)_z + \left(\frac{\partial A}{\partial z}\cdot\frac{\partial z}{\partial y}\right)_\sigma \tag{2.19}$$

or, in terms of the 2-D gradient operator,

$$\nabla_z A = \nabla_\sigma A - \frac{\partial A}{\partial z} \cdot \nabla_\sigma z \tag{2.20}$$

2.3 Streamfunctions for Isopycnal Surfaces

In this section, we will first figure out the error term associated with the application of the Montgomery streamfunction to the isopycnal surfaces. Then using the Levitus atlas values, we will show that this error may not be negligible in some regions in the ocean. New streamfunctions will then be proposed for the isopycnal surfaces. Note that in this work,the streamfunction is not conventional (which implies horizontal, or more precisely, two dimensional nondivergent flow); instead, this streamfunction is defined for $f\vec{V}$ which implies $f\vec{V}$ is nondivergent,and in the β-plane, divergence of the lateral flows may be allowed.

We start our derivation with the general geostrophic relation in the z- coordinate, i.e.

$$\hat{k} \times f\vec{\mathbf{V}} = -\frac{1}{\rho} \nabla_z p \tag{2.21}$$

where $\hat{k}$ is the unit vector in z direction,$\vec{\mathbf{V}}$ is the 2-D lateral velocity,and ∇_z is the 2-D gradient operator in the z-coordinate. In an arbitrary vertical s-coordinate (e.g., $s = \sigma$), by applying $eq.(2.20)$ and the hydrostatic equation($\frac{\partial p}{\partial z} = -g\rho$),the above equation can be written as

$$\hat{k} \times f\vec{\mathbf{V}} = -\frac{1}{\rho}[\nabla_s p - \frac{\partial p}{\partial z} \nabla_s z]$$

$$= -[\frac{1}{\rho} \nabla_s p + g \nabla_s z]$$
$$= -[\alpha \nabla_s p + \nabla_s(g \cdot z)] \quad (2.22)$$

where $\alpha = \frac{1}{\rho}$ is the specific volume. Generally, a reference level is needed when using the geostrophic relation. Assume $\vec{\mathbf{V}}_r$ is the geostrophic velocity at the reference s_r-surface, i.e.,

$$\hat{k} \times f\vec{\mathbf{V}}_r = -[\alpha \nabla_s p + \nabla_s(g \cdot z)]_{s_r} \quad (2.23)$$

then we have

$$\hat{k} \times f(\vec{\mathbf{V}} - \vec{\mathbf{V}}_r) = -[\alpha \nabla_s p - \alpha_r \nabla_s p_r + \nabla_s(g \cdot (z - z_r))]$$
$$= -[\alpha \nabla_s p - \alpha_r \nabla_s p_r - \nabla_s \int_{p_r}^{p} \alpha \cdot dp] \quad (2.24)$$

in which the hydrostatic equation has been used. Using the specific volume anomaly defined by

$$\delta = \alpha(S,T,p) - \alpha_(35,0,p) \equiv \alpha - \alpha_p \quad (2.25)$$

where S and T are salinity and temperature respectively,and $\alpha_p = \alpha(35,0,p)$ is the specific volume for the standard seawater at $S = 35\ psu$ and $T = 0°$, thus α_p is a function of p only, then the above equation becomes

$$\hat{k} \times f(\vec{\mathbf{V}} - \vec{\mathbf{V}}_r) = -[\delta \nabla_s p - \delta_r \nabla_s p_r + \alpha_p \nabla_s p - \alpha_{p_r} \nabla_s p_r - \nabla_s \int_{p_r}^{p} \delta \cdot dp - \nabla_s \int_{p_r}^{p} \alpha_p \cdot dp] \quad (2.26)$$

Note that

$$\nabla_s \int_{p_r}^{p} \alpha_p \cdot dp = \nabla_s \int_{p_r(x,y)}^{p(x,y)} \alpha_p(p') \cdot dp' = \alpha_p \nabla_s p - \alpha_{p_r} \nabla_s p_r \ , \quad (2.27)$$

then *eq.*(2.26) becomes

$$\hat{k} \times f(\vec{\mathbf{V}} - \vec{\mathbf{V}}_r) \;=\; -[\delta \bigtriangledown_s p - \delta_r \bigtriangledown_s p_r \;-\; \bigtriangledown_s \int_{p_r}^{p} \delta \cdot dp] \quad , \tag{2.28}$$

i.e. *eq.*(2.24) is also exactly valid for the specific volume anomaly δ.

In short-hand notation,and keeping in mind that *eq.*(2.28) is a relative relation between two s surfaces, we can simply write it as

$$\hat{k} \times f\vec{\mathbf{V}} \;=\; -[\delta \bigtriangledown_s p - \bigtriangledown_s \int^{p} \delta \cdot dp] \quad , \tag{2.29}$$

$$\;=\; -[\alpha \bigtriangledown_s p - \bigtriangledown_s \int^{p} \alpha \cdot dp]. \tag{2.30}$$

As examples several known streamfunctions can be derived from *eq.*(2.29) or *eq.*(2.30) directly:

A. For $s = z$ being the *geopotential* surface,the second term in eq.(2.30) vanishes by the hydrostatic equation.Thus

$$\hat{k} \times \rho f\vec{\mathbf{V}} = - \bigtriangledown_z p \tag{2.31}$$

and the *streamfunction* for $\rho f\vec{\mathbf{V}}$ is simply the pressure p.

B. For $s = p$,namely the *pressure* coordinate, $\bigtriangledown_s p = 0$, and it is obvious that

$$\hat{k} \times f\vec{\mathbf{V}} \;=\; \bigtriangledown_s \int^{p} \delta \cdot dp \;\; ,or \quad \hat{k} \times f\vec{\mathbf{V}} \;=\; \bigtriangledown_s \int^{p} \frac{1}{\rho} \cdot dp \quad , \tag{2.32}$$

and the streamfunctions for $f\vec{\mathbf{V}}$ are the dynamic height or geopotential:

$$\psi_p = -\int^p \delta \cdot dp \ , \quad or \quad \psi_p = -\int^p \frac{dp}{\rho}. \tag{2.33}$$

C. For $s = \delta$,i.e. the steric anomaly surfaces, the δ can be taken into the gradient operator, thus the Montgomery streamfunction is derived as

$$\psi_M = p\delta - \int^p \delta \cdot dp \tag{2.34}$$

D. Also for s=$\alpha = \frac{1}{\rho}$, we similarly get the Montgomery streamfunction for the *in situ* density coordinate:

$$\psi = \frac{p}{\rho} - \int^p \frac{dp}{\rho}. \tag{2.35}$$

E. However,for the isopycnal surfaces($s = \sigma$) since δ is generally a function of (x, y) on these surfaces, thus a closed or precise form for the streamfunctions cannot be derived. How large will the error be if we apply the Montgomery streamfunction on the isopycnal surfaces?Taking δ into the gradient operator, eq.(2.29) can be manipulated to become

$$\hat{k} \times f\vec{\mathbf{V}} = -[\nabla_\sigma(\delta p) - \nabla_\sigma \int^p \delta \cdot dp - p \nabla_\sigma \delta] \tag{2.36}$$

The first two terms are just the two components in the Montgomery streamfunction, thus the last one will be the error term:

$$ER_M = p \bigtriangledown_\sigma \delta, \tag{2.37}$$

Table 2.1 shows the ratios of this error term to the gradient term of the Montgomery streamfunction between two isopycnal surfaces $\sigma_1 = 31.8$ and $\sigma_1 = 32.3$ in the Mediterranean Water tongue region by using the data set of the Levitus climatological hydrographic atlas (Levitus,1982). It can be seen that in some areas,the magnitude of the error term can be as large as, and even larger than that of the Montgomery streamfunction gradient term, and more seriously even in opposite sign. One interesting fact that should be pointed out is that, each component of the two gradient terms of the Montgomery streamfunction $(\bigtriangledown_\sigma(\delta p), or\ -\bigtriangledown_\sigma \int^p \delta \cdot dp)$ can have a magnitude an order larger than that of the error term,but as the two components often have opposite sign , their residual is greatly reduced and generally of the same magnitude as the error term. Mathematically, although

$$\left|\frac{p \bigtriangledown_\sigma \delta}{\bigtriangledown_\sigma(\delta p)}\right| \sim \left|\frac{p \bigtriangledown_\sigma \delta}{\bigtriangledown_\sigma \int^p \delta \cdot dp}\right| \ll 1 \ , \tag{2.38}$$

we still have

$$\left|\frac{p \bigtriangledown_\sigma \delta}{\bigtriangledown_\sigma(\delta p - \int^p \delta \cdot dp)}\right| \sim O(1) \tag{2.39}$$

Table 2.1 Examples of ratio $[p \bigtriangledown_\sigma \delta / \bigtriangledown_\sigma (p\delta - \int^p \delta \cdot dp)]_{\sigma_1=32.3}^{\sigma_1=31.8}$ in the Mediterranean tongue region (45.5°W — 19.5°W, 23.5°N — 45.5°N).

-0.1325	-0.0385	-0.5515	-2.0823	-0.5305	-2.8817	-3.5620	-2.4832	-1.2285	-0.0609	-0.0131	-0.1010			
0.0000	-0.2630	-0.2449	-0.4656	-0.3696	-0.8274	-1.1636	-1.4598	-1.4353	-4.3047	-2.0999	-0.4450	-0.1416	-0.1274	-0.1942
-0.1533	0.1357	0.0809	-0.3829	3.3783	34.4087	1.4277	0.4958	0.0549	-0.0751	-0.1197	-0.2025			
0.0000	-0.2000	-0.0791	-0.3743	-0.5929	-1.2125	-1.5425	-1.7662	-1.5059	-2.8020	-1.6267	-0.4075	-0.0740	-0.0244	-0.0665
-0.0214	-0.0213	-0.2533	-1.0031	-2.8263	4.6693	0.5193	0.2191	0.1225	-0.0757	-0.1645	-0.2642			
0.0000	-0.1727	-0.0069	-0.3141	-0.5834	-1.5825	-2.2764	-2.2966	-2.1332	-6.3966	-1.4639	-0.3033	0.0541	0.0675	0.0214
-0.0107	-0.2095	-0.4309	-1.1193	-2.8378	3.7184	0.4288	0.3895	0.4917	0.1722	-0.1859	0.4998			
0.0000	-0.2262	0.0511	-0.1551	-0.5645	-1.5332	-2.6510	-3.4218	-6.5580	-12.3368	-1.5223	-0.0812	0.3345	0.1299	0.0271
-0.0277	-0.3371	-0.7933	-1.4049	-2.8436	-19.0730	1.1416	1.1216	0.3280	13.0523	-3.9713	18.5606			
0.0000	-0.2217	-0.0380	-0.2348	-0.8946	-1.5895	-2.5069	-6.5219	-56.3030	-9.5582	-0.6094	0.2004	0.6385	0.1394	0.0565
-0.3569	-0.7404	-1.2861	-1.4372	-1.3382	-2.9793	39.4316	1.6303	-0.7997	-1.8767	-1.1539	-1.9520			
0.0000	-0.2661	-0.3375	-0.5341	-1.0606	-1.6974	-3.6365	-5.2121	14.9683	33.9567	1.0540	1.2906	0.8920	0.2704	-0.1577
-0.8373	-1.2173	-1.8129	-1.5475	-1.4973	-1.8145	-2.0038	-1.1903	-0.8099	-0.8045	-1.5973	-1.2401			
0.0000	-0.9233	-0.7762	-1.3524	-1.3170	-2.1902	-3.3420	-12.5314	207.4020	-0.9112	7.8756	6.5554	1.6396	0.7807	-0.4727
-1.0004	-1.6275	-1.9338	-1.7255	-1.6135	-1.7085	-1.3728	-0.8425	-0.7033	-0.8631	-1.0271	-1.3306			
0.0000	-1.5395	-1.1437	-3.2592	-2.6765	-4.3035	-3.9398	-4.8574	-3.6066	-7.6824	163.6494	-19.5544	********	1.5992	-0.8072
-1.5535	-1.8183	-2.1314	-1.8398	-1.8989	-1.5130	-1.1013	-0.8442	-0.8485	-0.9258	-1.0491	-1.1978			
0.0000	-1.6749	-1.6435	-3.3393	-3.4658	-22.5396	-24.8741	-2.9321	-2.3908	-27.3981	-11.8009	-3.3331	-4.3700	2.9480	-1.0866
-1.8532	-1.7759	-2.1335	-2.1423	-1.8051	-1.3148	-1.0182	-0.9184	-0.8542	-1.0489	-1.0849	-1.3539			
0.0000	-0.8647	-1.4783	-1.9913	-4.1910	-6.7538	-4.1586	-2.9854	-2.7099	7.8673	-1.2415	-2.4406	-4.0486	1.6316	-0.9756
-1.4329	-1.7532	-2.1494	-1.8308	-1.5815	-1.2995	-0.9910	-0.9374	-0.9499	-1.0881	-1.1859	-1.2783			
0.0000	-0.4934	-0.7620	-1.1004	-1.3092	-1.6366	-1.8810	-2.1461	-3.4625	4.7223	0.0945	-0.4627	-1.1811	-0.1868	-0.6573
-1.1439	-1.4253	-1.4919	-1.6286	-1.5931	-1.3259	-1.1705	-1.0401	-1.0890	-1.1228	-1.2078	-1.2005			
0.0000	-0.4406	-0.4794	-0.5718	-0.7603	-0.9145	-1.0987	-1.6387	-2.9332	1.1488	0.4346	0.1468	0.2047	-1.1060	-0.8428
-0.9223	-1.0716	-1.2330	-1.3445	-1.4678	-1.7850	-1.3714	-1.2832	-1.2552	-1.1292	-1.1421	-1.1891			
0.0000	-0.3757	-0.4254	-0.4663	-0.5811	-0.7003	-0.8253	-1.2594	-6.0455	0.9922	0.2666	0.1529	0.4016	-23.5354	-1.2490
-1.0384	-1.0207	-1.0959	-1.0699	-1.4727	-1.8197	-1.6725	-1.8880	-1.3981	-1.1707	-1.0971	-1.1143			
0.0000	-0.3315	-0.3924	-0.4724	-0.5450	-0.6023	-0.6795	-1.0719	-10.4352	0.2479	0.0015	0.1537	0.4505	0.9173	-2.3520
-1.3064	-1.1158	-1.0821	-1.2487	-1.2318	-1.9083	-1.3531	-2.1799	-1.6793	-1.1535	-1.1109	-1.0941			
0.0000	-0.2837	-0.3360	-0.4340	-0.5525	-0.6161	-0.6768	-0.8673	22.8660	0.0056	0.0003	0.0763	0.1569	0.6555	25.3518
-1.8469	53.0028	53.0101	-1.2271	-1.5377	52.9550	0.0000	52.8756	0.5236	-1.2193	-1.1083	-1.1064			
0.0000	-1.0533	-1.0129	-0.8522	-0.7592	-0.6768	-0.8039	-0.9238	-6.9507	0.0874	-0.0165	-0.0092	0.0710	0.4588	1.1010
-9.9549	-1.5983	52.9418	0.0003	52.9377	-1.3564	-1.2858	3.8521	-1.8046	-1.2940	-1.1551	-1.1671			
0.0000	-0.1281	-0.0532	0.0299	0.1903	-3.2964	-1.3970	-1.1412	-1.6793	0.1401	-0.0122	-0.0008	-0.0222	0.1951	0.4765
0.3757	-3.9911	-1.8840	-1.2454	-1.2343	-1.0885	-1.1988	-1.5454	-1.8834	-1.3428	-1.3451	-1.2797			
0.0000	-0.0340	-0.0442	-0.0071	-0.0256	0.0142	1.0715	2.3243	-2.9995	0.2483	0.1095	-0.0680	-0.0091	0.0752	0.2473
0.2282	1.8049	-4.0942	-1.5078	-1.2559	-1.2774	-1.3974	-1.9374	-1.7980	-1.6824	-1.4525	-1.5599			
0.0000	-0.1666	-0.0515	0.0153	-0.0529	-0.0156	-0.1432	-0.5187	-0.6809	0.0007	0.0182	0.1931	-0.0022	0.1380	0.1957
0.4320	1.3283	3.6428	-2.7220	-1.3734	-2.1710	-2.5920	-3.1435	-2.5385	-2.1124	-1.8455	-1.7183			
0.0000	-0.0727	-0.1533	-0.0414	-0.0274	-0.0341	-0.1647	-0.5076	-0.5275	2.3677	0.4371	0.3628	0.2248	0.2091	0.2583
0.3375	0.6346	1.7229	9.9250	-2.2104	-5.4592	-6.7279	5.5867	-1.9182	-4.4204	-2.6917	-2.1300			
0.0000	0.1411	-0.0585	-0.2066	-0.0712	-0.1031	-0.0973	-0.1349	-0.2356	-2.0512	-11.7471	3.6256	0.4632	0.3752	0.2900
0.3602	0.2567	0.2345	1.1424	2.5257	-5.8419	-3.5522	-2.5443	-3.5556	-6.2389	-9.2927	-5.5244			
0.0000	0.1240	-0.0417	-0.0567	-0.2549	-0.1860	-0.1520	-0.1586	-0.0935	-2.3208	-3.0123	1.4169	0.8516	0.3694	0.1256
0.4608	0.4252	0.6725	0.5166	0.7935	1.0550	1.3139	0.9126	1.0151	1.9083	1.5201	0.7580			
0.0000	0.1146	0.2088	-0.1572	-0.0965	-0.2656	-0.2545	-0.2477	-0.2522	0.7584	-15.0117	5.4345	0.6532	0.4953	0.3242
0.3918	0.4234	0.5198	0.3859	0.5245	0.5061	0.6910	0.4670	0.4976	0.6126	0.5054	1.0597			

Table 2.2 Examples of ratio $[p' \nabla_\sigma \delta / \nabla_\sigma (p\delta - \int^p \delta \cdot dp)]_{\sigma_1=32.3}^{\sigma_1=31.8}$ in the Mediterranean tongue region (45.5°W — 19.5°W, 23.5°N — 45.5°N).

0.0673	-0.0693	0.0586	-0.0521	0.1693	0.0728	0.0452	0.0407	0.0483	0.0379	0.0366	0.0326			
0.0000	-0.0112	-0.0079	-0.0300	-0.0433	-0.1862	0.6234	0.2803	0.3670	-0.1550	0.3362	-0.0317	0.0246	0.0354	0.0411
0.0436	0.0308	0.0383	-0.0815	0.0651	0.0435	0.0394	0.0425	0.0350	0.0274	0.0306	0.0221			
0.0000	-0.0204	-0.0117	-0.0297	-0.0525	0.3464	0.1748	0.1696	0.2393	0.1460	0.2505	-0.0279	0.0133	0.0215	0.0241
0.0261	0.0245	0.0182	-1.2391	0.0559	0.0345	0.0278	0.0377	0.0278	0.0243	0.0081	-0.0076			
0.0000	-0.0336	-0.0202	-0.0354	-0.0671	0.1131	0.0894	0.1146	0.1456	0.0979	0.3099	-0.0241	0.0084	0.0100	0.0090
0.0037	0.0039	-0.0092	0.1978	0.0421	0.0295	0.0229	0.0238	0.0243	0.0101	-0.0185	-0.0009			
0.0000	-0.0463	-0.0273	-0.0346	-0.0761	0.1062	0.0706	0.0752	0.0735	0.0746	0.2499	-0.0097	0.0094	-0.0025	-0.0071
-0.0078	-0.0229	-0.1013	0.1178	0.0537	0.0398	0.0236	0.0235	0.0008	0.0122	0.0170	0.0052			
0.0000	-0.0613	-0.0420	-0.0527	-0.1835	0.1147	0.0690	0.0516	0.0481	0.0577	-0.0966	-0.0018	0.0038	-0.0140	-0.0191
-0.0528	-0.1034	0.2127	0.1512	0.1251	0.0651	0.0412	0.0127	-0.0918	0.0495	0.1742	0.0441			
0.0000	-0.0908	-0.0904	-0.1050	17.7384	0.1126	0.0465	0.0462	0.0322	0.0359	0.0112	0.0031	-0.0074	-0.0219	-0.0294
-0.0321	0.2073	0.0790	0.1272	0.1543	0.1131	0.1008	0.4201	-0.3608	-0.1238	0.1050	0.1894			
0.0000	-0.5362	-0.2483	0.4391	0.1830	0.0509	0.0337	0.0300	0.0277	-0.5406	0.0972	-0.0052	-0.0135	-0.0290	-0.0450
-1.1207	0.0542	0.0627	0.0582	0.1329	0.1305	0.2379	-0.2127	-0.1101	-0.2061	-3.0149	0.1521			
0.0000	0.2573	1.0748	0.0601	0.0166	0.0134	0.0180	0.0299	0.0301	-0.0079	-0.0044	-0.0143	-0.0296	-0.0347	-0.0707
0.0038	0.0234	0.0107	0.0777	0.1129	0.1525	1.2294	-0.2158	-0.2027	-0.3358	4.3543	0.2557			
0.0000	0.1294	0.1301	0.0215	0.0062	-0.0072	0.0016	0.0230	0.0371	-0.0285	-0.0289	-0.0334	-0.0435	-0.0492	-0.0663
-0.0224	0.0130	0.0291	0.0528	0.1039	0.2059	-1.3576	-0.3134	-0.1957	3.6731	1.2324	0.1371			
0.0000	-0.2559	0.0926	0.0233	-0.0144	-0.0144	-0.0029	0.0152	0.0286	0.0386	-0.1779	-0.0577	-0.0566	-0.0475	-0.3507
-0.0283	0.0027	0.0190	0.0483	0.0328	0.1600	-0.7740	-0.3161	-0.3594	0.6051	0.2121	0.1458			
0.0000	-0.0757	-0.0548	0.1311	-0.0167	-0.0159	0.0007	0.0153	0.0176	0.0096	0.0249	0.0637	-0.3544	-0.0496	-0.0766
0.0179	0.0045	0.0291	0.0388	0.0544	0.0885	0.1686	1.1707	0.4574	0.2389	0.1431	0.1635			
0.0000	-0.0423	-0.0386	-0.0236	-0.0064	-0.0196	0.0457	0.0141	0.0099	0.0027	0.0011	0.0082	0.0199	0.4410	-0.0789
-0.0597	0.0599	0.0451	0.0374	0.0329	0.0256	0.0435	0.0592	0.0744	0.1559	0.1824	0.1420			
0.0000	-0.0322	-0.0237	-0.0189	-0.0113	-0.0130	-0.0246	0.0161	0.0012	-0.0042	0.0002	-0.0003	0.0011	0.0058	-0.0004
0.0918	0.0505	0.0656	0.0929	0.0171	0.0182	0.0207	0.0211	0.0398	0.0893	0.1813	0.2022			
0.0000	-0.0248	-0.0116	-0.0095	-0.0076	-0.0084	-0.0049	-0.0266	-0.0037	-0.0046	-0.0025	-0.0033	-0.0044	-0.0068	-0.0165
-0.0171	-0.0237	0.0781	0.0173	0.0303	0.0207	0.0532	0.0073	0.0248	0.0555	0.1253	0.2086			
0.0000	-0.0007	0.0079	0.0023	0.0065	0.0061	0.0035	0.0539	-0.0101	-0.0010	-0.0044	-0.0059	-0.0076	-0.0123	-0.0151
-0.0227	38.3580	-0.0317	0.0327	0.0123	17.3618	0.0000	0.0224	-0.0023	0.0505	0.1191	0.1828			
0.0000	-1.2596	-0.9365	0.6724	0.1070	0.0424	0.0725	0.2147	-0.0101	0.0025	-0.0022	-0.0057	-0.0096	-0.0153	-0.0166
-0.0164	-0.0242	28.6341	0.0000	0.0107	0.0279	0.0754	0.0082	0.0240	0.0443	0.0795	0.0807			
0.0000	-0.0066	-0.0156	-0.0231	-0.0324	-0.0463	-0.0982	-0.1413	-0.0297	0.0135	0.0025	-0.0052	-0.0096	-0.0173	-0.0211
-0.0157	-0.0244	-0.0146	0.0130	0.0274	0.1039	0.0527	0.0285	0.0224	0.0352	0.0397	0.0573			
0.0000	0.0397	-0.0005	-0.0076	-0.0096	-0.0114	-0.0297	0.0261	0.1293	0.0322	0.0042	0.0016	-0.0093	-0.0193	-0.0245
-0.0305	-0.0255	-0.0232	-0.0179	0.0035	0.0142	0.0222	0.0141	0.0183	0.0228	0.0313	0.0345			
0.0000	0.0454	0.0070	-0.0027	-0.0064	-0.0152	0.0077	0.0482	2.0029	0.1021	0.0224	-0.0131	-0.0085	-0.0235	-0.0269
-0.0331	-0.0348	-0.0307	-0.0260	-0.0141	-0.0025	0.0035	0.0078	0.0139	0.0193	0.0215	0.0304			
0.0000	0.0787	0.0527	0.0071	0.0016	-0.0001	0.0154	0.0554	0.2434	0.1151	-0.0010	-0.0262	-0.0246	-0.0260	-0.0316
-0.0307	-0.0327	-0.0324	-0.0274	-0.0175	-0.0095	-0.0004	0.0033	0.0073	0.0122	0.0155	0.0230			
0.0000	0.0254	0.0145	0.0765	0.0192	0.0135	0.0104	0.0219	0.0753	-0.0415	-0.1965	-0.0465	-0.0421	-0.0359	-0.0291
-0.0295	-0.0268	-0.0296	-0.0253	-0.0194	-0.0126	-0.0035	0.0007	0.0054	0.0053	0.0119	0.0135			
0.0000	0.0334	0.1430	0.1085	0.1256	0.0525	0.0391	0.0273	0.0219	-0.1945	-0.1930	-0.0870	-0.0664	-0.0570	-0.0307
-0.0253	-0.0252	-0.0252	-0.0192	-0.0155	-0.0117	-0.0059	-0.0001	0.0026	0.0036	0.0044	0.0054			
0.0000	0.1159	-0.0287	0.3020	0.1249	0.1752	0.1125	0.0520	0.0705	-0.0936	-0.1960	-0.1465	-0.0670	-0.0460	-0.0292
-0.0252	-0.0257	-0.0255	-0.0182	-0.0177	-0.0086	-0.0058	0.0015	0.0022	0.0018	0.0017	-0.0905			

From the above analysis,we see that the Montgomery streamfunction may not be suitable for the isopycnal surfaces in some regions. Note that the error term arises from the variations of the specific volume anomaly along the isopycnals. Since the climatological data set is used, one may doubt whether the sloping signals are really significant because of the data noise(errors due to measurements,averaging,ect.). Unfortunately, the data I have for the time being cannot answer this question. Another question that may be asked is whether it is necessary to include this error term compared with the terms neglected in the geostrophy assumption. The geostrophic relation for the large scale motions in the ocean has been strongly supported both by theory (e.g., Pedlosky , 1987) and by observations (e.g., Bryden, 1977), thus we do not expect that the neglected time varying and nonlinear terms are in the same order as the Coriolis and pressure gradient terms. In conclusion, because of the large size of this error term, we believe it should not be neglected, and a streamfunction for isopycnal surfaces is needed.

The following discussions are not only true for isopycnal surfaces, but also true for any *gently* sloping surfaces.Define the pressure anomaly as

$$p' = p - \bar{p} \tag{2.40}$$

where $\bar{p}$ is the lateral mean pressure on the s-surface,then by definition,

$$\nabla_s \bar{p} = 0. \tag{2.41}$$

Then eq.(2.29) is identical to

$$\hat{k} \times f\vec{\mathbf{V}} = -[\delta \nabla_s p' - \nabla_s \int^p \delta \cdot dp] \tag{2.42}$$

$$= -[\nabla_s (p'\delta - \int^p \delta \cdot dp] + p' \nabla_s \delta \tag{2.43}$$

If we now define an approximate streamfunction(hereafter labeled with pressure *anomaly* streamfunction) as

$$\psi_a \;=\; p'\delta \;-\; \int^p \delta \cdot dp, \tag{2.44}$$

then the error in the use of ψ_a on the s-surface will be

$$ER_a \;=\; p' \bigtriangledown_s \delta \tag{2.45}$$

which is proportional to the "*residual*" or anomaly pressure p'. For gently sloping surfaces (such as isopycnal ones),and if the surfaces are not too near to the ocean surface, i.e. if p is large enough, we generally have

$$\frac{ER_a}{ER_M} \;= \frac{p'}{p} \ll 1 \;\;, \tag{2.46}$$

and we would expect that the use of this streamfunction on the s- surfaces produces much smaller errors. Actually,as shown in Table 2.2,the Levitus atlas values shows that

$$\left| \frac{p' \bigtriangledown_\sigma \delta}{\bigtriangledown_\sigma (p'\delta \;-\; \int^p \delta \cdot dp)} \right| \;\sim\; O(10^{-2} \;\sim\; 10^{-1}) \tag{2.47}$$

Consequently we can conclude that the streamfunction ψ_a defined by (2.44) is a fairly good one for the isopycnal surfaces, with the errors of at most 10% or less. The only difference between the anomaly or approximate streamfunction ψ_a and the Montgomery streamfunction ψ_M is the use of the pressure anomaly instead of the total pressure in the term $p\delta$. The reason for this modification can also be clearly seen from eq.(2.37) in

the following way. We see that there are two parameters in the error term:the slope of the specific volume anomaly and the total pressure p.The slope itself is really small,it is the large value of p that makes the product comparable to the gradient term of the Montgomery streamfunction term.In the derivation of *eq.*(2.36), the error term $-p \bigtriangledown_\sigma \delta$ appears by taking δ into the lateral gradient operator $\bigtriangledown_\sigma$. Therefore the p in this term acts only as a coefficient of the term $\bigtriangledown_\sigma \delta$, because the lateral variations of p are still kept in the gradient of the product term $\bigtriangledown_\sigma(p\delta)$.Therefore if we decompose p into $\bar{p} + p'$, and for $p' \ll \bar{p}$, the error term $p \bigtriangledown_\sigma \delta$ can be approximated by $\bar{p} \bigtriangledown_\sigma \delta$ (with the error $p' \bigtriangledown_\sigma \delta$) .Using this approximation,*eq.*(2.36) becomes

$$\begin{aligned} \hat{k} \times f\vec{\mathbf{V}} &= -[\bigtriangledown_\sigma(\delta p) - \bigtriangledown_\sigma \int^p \delta \cdot dp - \bar{p} \bigtriangledown_\sigma \delta] \\ &= -\bigtriangledown_\sigma (p'\delta - \int^p \delta \cdot dp) \end{aligned} \tag{2.48}$$

and this again leads to the definition of ψ_a.

Although the streamfunction ψ_a is *approximate* for the generalized s-coordinate, the generalized geostrophic relation(2.29) is *exactly* true for all kinds of s-coordinates. To interpret this relation physically, the following discussion reveals that this relation is no more than the application of the dynamic relation (in the p-coordinate) to the generalized $s - coordinate$. For simplicity,we only discuss one component of *eq.*(2.29):

$$f(V_1 - V_2) = \frac{\partial}{\partial x})_s \int_{p1}^{p2} \delta \cdot dp + \delta_1 \frac{\partial}{\partial x})_s p_1 - \delta_2 \frac{\partial}{\partial x})_s p_2 \tag{2.49}$$

As shown in Fig.2.3, the pressures on the two surfaces s_1 *and* s_2 at the two stations A *and* B are p_{1A}, p_{1B}, p_{2A} *and* p_{2B} respectively, and M_1, N_1, M_2, N_2 are separately the mid-points between stations A *and* B on the pressure surfaces p_{1B}, p_{1A}, p_{2B} *and* p_{2A} . The dynamic relation on the pressure surfaces read as:

$$f(V_{M1} - V_{M2}) = \frac{\partial}{\partial x} \int_{p_{1B}}^{p_{2B}} \delta \cdot dp \approx \frac{1}{L}[\int_{p_{1B}}^{p_{2B}} \delta_B \cdot dp - \int_{p_{1B}}^{p_{2B}} \delta_A \cdot dp] \tag{2.50}$$

$$f(V_{N1} - V_{N2}) = \frac{\partial}{\partial x}\int_{p_{1A}}^{p_{2A}} \delta \cdot dp \approx \frac{1}{L}[\int_{p_{1A}}^{p_{2A}} \delta_B \cdot dp - \int_{p_{1A}}^{p_{2A}} \delta_A \cdot dp] \quad (2.51)$$

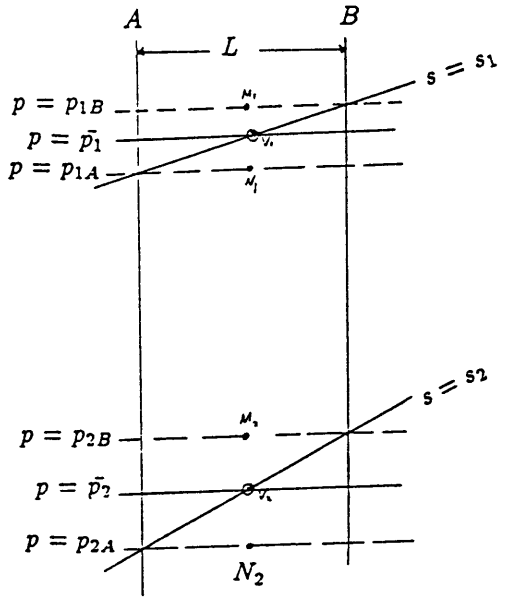

Fig.2.3 Geostrophic Relations Between Two Stations On The $s - Surfaces$

Approximating the velocity at the mid-point on the s_1 surface by $V_1 \approx \frac{1}{2}(V_{M1} + V_{N1})$, and on the s_2 surface by $V_2 \approx \frac{1}{2}(V_{M2} + V_{N2})$, then adding $eq.(2.50)$ to $eq.(2.51)$ yields

$$\begin{aligned}
f(V_1 - V_2) &= \frac{1}{2L}[\int_{p_{1B}}^{p_{2B}} \delta_B \cdot dp - \int_{p_{1A}}^{p_{2A}} \delta_A \cdot dp + \int_{p_{1A}}^{p_{2A}} \delta_B \cdot dp - \int_{p_{1B}}^{p_{2B}} \delta_A \cdot dp] \\
&= \frac{1}{2L}[2(\int_{p_{1B}}^{p_{2B}} \delta_B \cdot dp - \int_{p_{1A}}^{p_{2A}} \delta_A \cdot dp) + \int_{p_{1A}}^{p_{2A}} (\delta_B + \delta_A) \cdot dp \\
&\qquad - \int_{p_{1B}}^{p_{2B}} (\delta_A + \delta_B) \cdot dp] \\
&= \frac{1}{2L}[2(\int_{p_{1B}}^{p_{2B}} \delta_B \cdot dp - \int_{p_{1A}}^{p_{2A}} \delta_A \cdot dp) \\
&\quad + (\int_{p_{1A}}^{p_{2B}} + \int_{p_{2B}}^{p_{2A}})(\delta_B + \delta_A) \cdot dp - (\int_{p_{1B}}^{p_{1A}} + \int_{p_{1A}}^{p_{2B}})(\delta_A + \delta_B) \cdot dp] \\
&= \frac{1}{L}[(\int_{p_{1B}}^{p_{2B}} \delta_B \cdot dp - \int_{p_{1A}}^{p_{2A}} \delta_A \cdot dp) + \int_{p_{2B}}^{p_{2A}} \frac{(\delta_B + \delta_A)}{2} \cdot dp \\
&\qquad - \int_{p_{1B}}^{p_{1A}} \frac{(\delta_A + \delta_B)}{2} \cdot dp] \\
&\approx \frac{1}{L}[(\int_{p_{1B}}^{p_{2B}} \delta_B \cdot dp - \int_{p_{1A}}^{p_{2A}} \delta_A \cdot dp)
\end{aligned}$$

$$+\frac{(\delta_{2A}+\delta_{2B})}{2}(p_{2A}-p_{2B}) \;-\; \frac{(\delta_{1A}+\delta_{1B})}{2}(p_{1A}-p_{1B})] \tag{2.52}$$

which is exactly the difference form of *eq.*(2.49).These argumests clearly indicate the geometric implications of V_1 and V_2 .

From the above geometric arguments as shown in Fig.2.3, one may also expect the following approximation:

$$f(V_1 - V_2) \;\approx\; \frac{\partial}{\partial x}\int_{\bar{p_1}}^{\bar{p_2}} \delta \cdot dp \tag{2.53}$$

and thus the following approximate streamfunction for the s-coordinate:

$$\bar{\psi} \;=\; \int_{\bar{p_1}}^{\bar{p_2}} \delta \cdot dp \tag{2.54}$$

Actually, this is also a good approximation, and can also be derived mathematically as follows. As shown in Fig.2.4, note the integrating approximation that

$$\begin{aligned}\int_{p_1}^{p_2} \delta \cdot dp \;&=\; \int_{\bar{p_1}}^{\bar{p_2}} \delta \cdot dp \;-\; \int_{\bar{p_1}}^{\bar{p_1}+p_1'} \delta \cdot dp \;+\; \int_{\bar{p_2}}^{\bar{p_2}+p_2'} \delta \cdot dp \\ &\approx\; \int_{\bar{p_1}}^{\bar{p_2}} \delta \cdot dp \;-\; \delta_1 p_1' \;+\; \delta_2 p_2', \end{aligned} \tag{2.55}$$

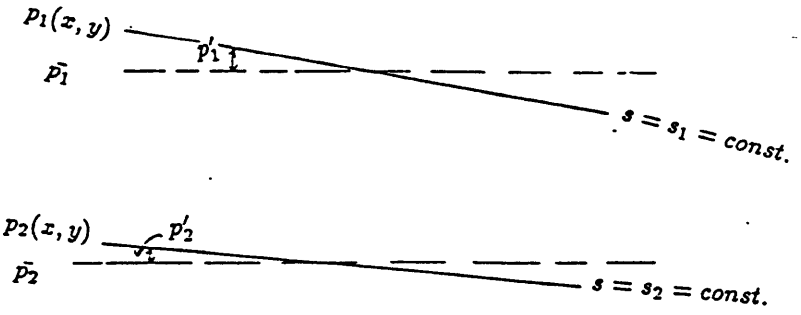

Fig.2.4 Integrating Approximations on the Gently Sloping s surfaces

Using *eq.*(2.36), the geostrophic relation can be developed to

$$\begin{aligned}
\hat{k} \times f(\vec{\mathbf{V}}_1 - \vec{\mathbf{V}}_2) &= -[\nabla_s \int_{p_1}^{p_2} \delta \cdot dp + \delta_1 \nabla_s p_1 - \delta_2 \nabla_s p_2] \\
&= -[\nabla_s (\int_{\bar{p_1}}^{\bar{p_2}} \delta \cdot dp - \delta_1 p_1' + \delta_2 p_2') \\
&\qquad + \delta_1 \nabla_s (\bar{p_1} + p_1') - \delta_2 \nabla_s (\bar{p_2} + p_2')] \\
&= -[\nabla_s \int_{\bar{p_1}}^{\bar{p_2}} \delta \cdot dp - p_1' \nabla_s \delta_1 + p_2' \nabla_s \delta_2] \qquad (2.56)
\end{aligned}$$

In this equation, the last two terms on the RHS are exactly the error terms neglected in the definition of ψ_a, and for the same reason they can be ignored here, hence the expression for the streamfunction $\bar{\psi}$ is attained(hereafter labelled as *mean* pressure streamfunction).

To show the effectiveness of the use of the pressure *anomaly* and *mean* pressure streamfunfunctions,the ψ_a's and $\bar{\psi}$'s for the isopycnals and the $\bar{\psi}$'s for the specific volume anomaly surfaces in the Mediterranean Water tongue region are computed from the Levitus atlas values and displayed in Fig.2.5. Also shown in this figure are the *exact* streamfunctions for the the specific volume anomaly surfaces(Montgomery streamfunction) and for the pressure surfaces(Dynamic Height) as well as the Montgomery streamfunction on the isopycnal surfaces. (The two values for δ and p in Fig.2.5 correspond to their mean values on the two isopycnal surfaces).It can be seen that all streamfunctions show similar lateral flow patterns between the two depths except the one from the Montgomery streamfunction on the isopycnal surfaces. It implies that the errors on the use of the Montgomery streanfunction on the isopycnal surfaces are effectively large in the southern part of the region.It also shows the use of ψ_a and $\bar{\psi}$ on the isopycnal surfaces is extremely good. In this work we will use the ψ_a as the streamfunction for the σ-coordinate, because in deriving $\bar{\psi}$, another approximation–the integrating approximation (however small the error) was used.

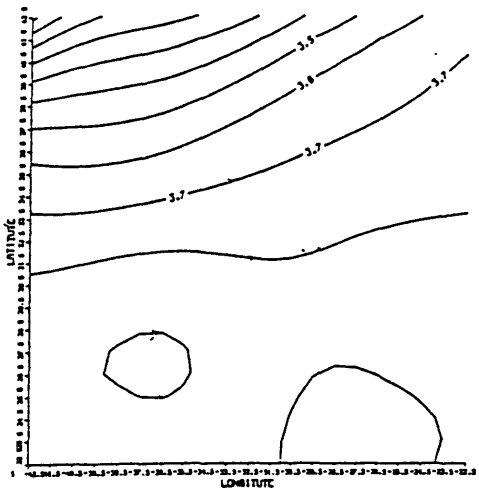

(a) ψ_a between $\sigma_1 = 31.8$ *and* $\sigma_1 = 32.3$

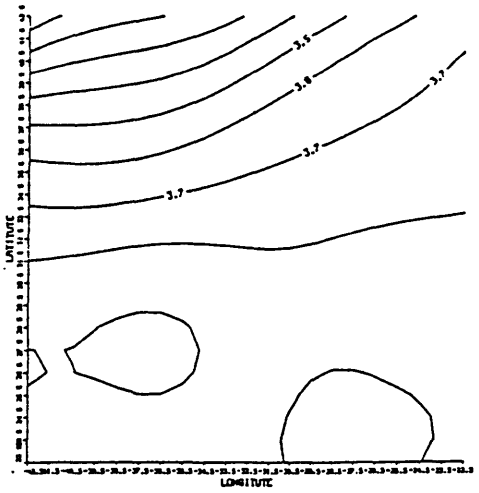

(b) $\bar{\psi}$ between $\sigma_1 = 31.8$ *and* $\sigma_1 = 32.3$

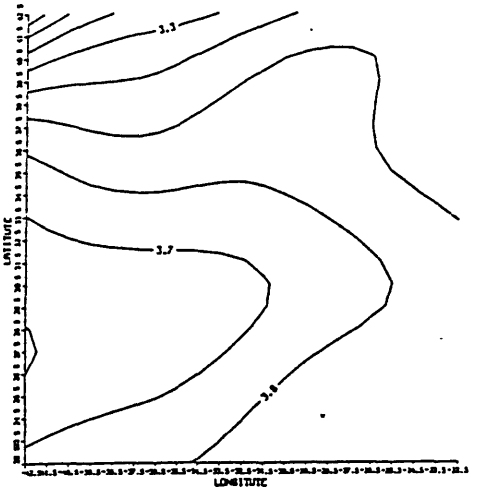

(c) ψ_M between $\sigma_1 = 31.8$ *and* $\sigma_1 = 32.3$

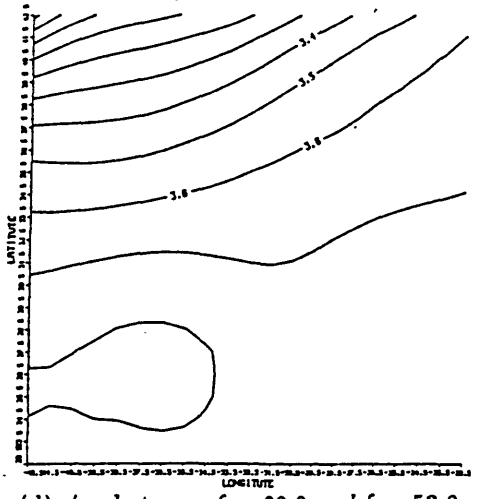

(d) ψ_M between $\delta = 89.0$ *and* $\delta = 52.0$

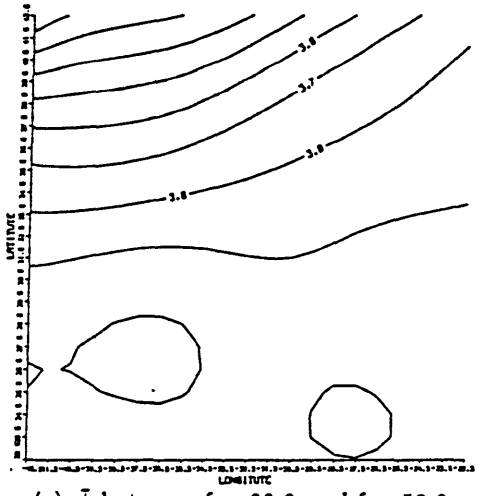

(e) $\bar{\psi}$ between $\delta = 89.0$ *and* $\delta = 52.0$

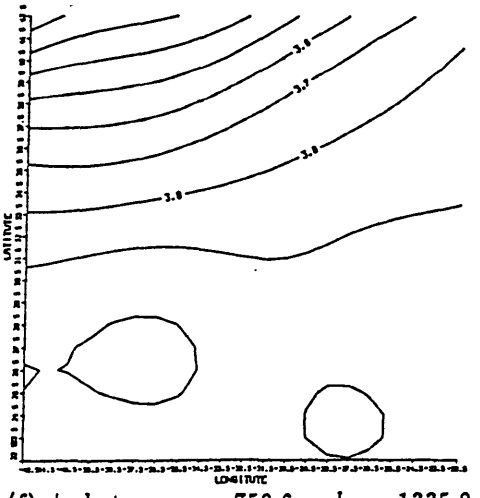

(f) ψ_p between $p = 759.6$ *and* $p = 1335.9$

Fig.2.5 Various Streamfunctions For Different Coordinates

2.4 SUMMARY

In this chapter, we showed that when the dynamic method is applied to isopycnal surfaces, the variation of the specific volume anomaly along isopycnal surfaces has dynamical importance. By considering this variation, two streamfunctions have been formulated for any gently sloping surfaces, such as the isopycnal surface, neutral surface and so on. One is the pressure *anomaly* streamfunction which is analogous to the Montgomery streamfunction,but the the pressure anomaly is used instead of the pressure itself, i.e.

$$\psi = p'\delta - \int^{p} \delta dp \tag{2.57}$$

The other is the *mean* pressure streamfunction which is analogious to the dynamic height, but the mean pressure is used instead of the pressure itself.

$$\psi = -\int_{p_1}^{p_2} \delta dp \tag{2.58}$$

These streamfunctions are defined for laterally nondivergent quantity $f\vec{V}$:

$$\hat{k} \times f\vec{V} = \nabla_s \psi \tag{2.59}$$

The lateral divergence of $\vec{V}$ itself is allowed. The application of these two streamfunctions on the isopycnal surface generally induces errors in velocity less than 10%.

Chapter 3

DESCRIPTION OF THE MODEL

3.1 Introduction

The model used in this work is basically the one proposed by Hogg(1987), which has the following assumptions: flows are in hydrostatic equilibrium and geostrophic balance; mass is conservative at each grid point (Continuity Equation), and mass is conservative between isopycnal surfaces (Integrated Vorticity Equation); water properties like heat, salt, oxygen (a sink or consumption term is allowed for the oxygen equation) etc. are conservative. Instead of calculating the two components of the velocity, streamfunctions are calculated. (One practical advantage of this procedure is that the unknowns associated with the velocity field are reduced by half). Some modifications of the model have been made. Specifically, in the dynamic equation the new streamfunction for the potential density surfaces which includes the variations of the specific volume anomaly on the isopycnal surfaces has been used to replace the Montgomery streamfunction; consistently, by considering these sloping effects, a new form of the integrated vorticity equation has been reformulated; an exact potential density equation has been deduced by considering the variations of the thermal expansion and saline contraction coefficients with temperature and salinity as well as the possible differences in diffusivities for heat and salt; finally, as more levels are included in this work, the controlling equations are written in

three – dimensional difference forms by a staggered finite difference frame (which will be discussed in the following sections) which permits us to remove the derivatives of the diffusive parameters as unknowns. In this chapter, we will first present the formulations and their implications for the equations, followed by brief discussions on the Levitus atlas and inverse techniques.

3.2 Formulation of the Equations

3.2.1 Dynamic Equation

As discussed in the previous sections, the assumptions of hydrostatic and geostrophic balances result in the thermal wind or shear flow relation. In the σ-coordinate and in terms of the newly defined streamfunction, this relation can be expressed as

$$\psi_{k(x,y)} - \psi_{k+1(x,y)} = \int_{p_k}^{p_{k+1}} \delta \cdot dp + p'_k \delta_k - p'_{k+1} \delta_{k+1}, \quad k = 1, 2, ..., K-1 \qquad (3.1)$$

where K is the level number of the isopycnals in the model. Eq.(3.1) will be called the "Dynamic Equation" in this work.

3.2.2 Mass Conservations at the grid points—Continuity or Potential Vorticity Equations

The complete or precise form of the mass conservation for a fluid parcel is

$$\frac{1}{\rho}\frac{d\rho}{dt} + \nabla \cdot \vec{\mathbf{V}} = 0. \qquad (3.2)$$

The sea water is compressible ($\frac{d\rho}{dt} \neq 0$), but it is generally believed that the compressibility is small compared to the divergence term, i.e.

$$\left| \frac{\frac{1}{\rho}\frac{d\rho}{dt}}{\nabla \cdot \vec{\mathbf{V}}} \right| \ll 1. \tag{3.3}$$

Therefore to the first approximation, sea water may be considered as *three dimensinally* nondivergent(the *nondivergency* is only in the sense of eq.(3.3), it doesn't mean sea water is incompressible), and the continuity equation is thus written as

$$\nabla \cdot \vec{\mathbf{V}} = 0. \tag{3.4}$$

or, using the operators for the σ-coordinate,

$$\nabla_h \cdot \vec{\mathbf{u}} + \sigma_z \frac{\partial w^*}{\partial \sigma} = 0. \tag{3.5}$$

where $\vec{\mathbf{u}}$ represents the 2-D lateral velocity and the superscript $*$ appended to w emphasizes explicitly that w^* is the *cross isopycnal* velocity. As discussed by Hogg(1987), *eq.*(3.5) can also be interpreted as the statement of the conservation of the potential vorticity ($f\frac{\partial \sigma}{\partial z}$, ignoring the relative vorticity) as follows:

Multiply *eq.*(3.5) by $f\sigma_z$, we have

$$f\sigma_z \nabla_h \cdot \vec{\mathbf{u}} = -f{\sigma_z}^2 {w^*}_\sigma \tag{3.6}$$

Note that

$$\nabla_h \cdot (f\sigma_z \vec{\mathbf{u}}) = f\sigma_z \nabla_h \cdot \vec{\mathbf{u}} + \vec{\mathbf{u}} \cdot \nabla_\sigma (f\sigma_z) \tag{3.7}$$

and that

$$\nabla_h \cdot (f\sigma_z \vec{\mathbf{u}}) = \nabla_\sigma \cdot (f\vec{\mathbf{u}}) = 0 \quad , \tag{3.8}$$

we obtain

$$\vec{\mathbf{u}} \cdot \nabla_\sigma (f\sigma_z) = f{\sigma_z}^2 {w^*}_\sigma \tag{3.9}$$

which states that the variation of the potential vorticity $f\sigma_z$ along the streamfunction is caused by the cross-isopycnal stretching term. Thus the continuity equation combined with geostrophy may also be called the potential vorticity equation.

Note that the streamfunction is defined for $f\vec{\mathbf{u}}$, not for $\vec{\mathbf{u}}$ itself. Hence it is $f\vec{\mathbf{u}}$ that is laterally nondivergent, thus $\nabla_h \cdot \vec{\mathbf{u}}$ also involves the divergence of the planetary vorticity f, and this variation can be expressed explicitly as follows. From the definition

$$\hat{k} \times \vec{\mathbf{u}} = -\frac{1}{f} \nabla_\sigma \psi \tag{3.10}$$

or

$$\vec{\mathbf{u}} = \frac{1}{f} \hat{k} \times \nabla_\sigma \psi \tag{3.11}$$

we have

$$\begin{aligned} \nabla_h \cdot \vec{\mathbf{u}} &= \nabla_h \cdot (\frac{1}{f}\hat{k} \times \nabla_\sigma \psi) = \frac{1}{f_0} \nabla_h \cdot (\hat{k} \times \nabla_\sigma \psi) + (\hat{k} \times \nabla_\sigma \psi) \cdot \nabla_\sigma (\frac{1}{f}) \\ &= \nabla_h \cdot (\frac{1}{f_0}\hat{k} \times \nabla_\sigma \psi) - (\hat{k} \times \nabla_\sigma \psi) \cdot \frac{\nabla_\sigma f}{{f_0}^2} \\ &= \nabla_h \cdot \vec{\mathbf{u_g}} - \frac{\beta}{f_0} v_g \end{aligned} \tag{3.12}$$

where f_0 is a local constant and $\vec{\mathbf{u_g}}$ is laterally nondivergent, defined as

$$\vec{\mathbf{u_g}} = \frac{1}{f_0}\hat{k} \times \nabla_\sigma \psi = \frac{f}{f_0}\vec{\mathbf{u}}. \tag{3.13}$$

Therefore the continuity equation can be rewitten as

$$\nabla_h \cdot \vec{\mathbf{u_g}} - \frac{\beta}{f_0} v_g + \sigma_z \frac{\partial w^*}{\partial \sigma} = 0. \tag{3.14}$$

This is the exact equation used by Hogg(1987).

3.2.3 Integrated Vorticity Equation—Mass or Potential Vorticity Conservation between Two Isopycnal Surfaces

Eq.(3.5) is the statement of mass conservation on each individual isopycnal surface. Our purpose is to establish an expression for the mass conservation between two isopycnal surfaces, and this expression is important because it contains the inhomogeneous terms to give the system unique non-zero solutions (the only other inhomogeneous terms come from the dynamic relation, *eq.*(3.1)). For the same reason we introduced the new streamfunction for the potential density coordinates, the variations of specific volume anomaly and pressure on the isopycnals will be included in the derivation of the integrated potential vorticity equation.

Thermal Wind Relation in σ-coordinate

In order to get the desired expression, the thermal wind relation in the σ - coordinate is needed. Note that

$$\int^p \delta \cdot dp = p\delta - \int^\delta p \cdot d\delta \quad , \tag{3.15}$$

the geostrophic relation, *eq.*(2.29) can be rewritten as

$$\hat{k} \times f\vec{\mathbf{u}} = p \bigtriangledown_\sigma \delta - \bigtriangledown_\sigma \int^\delta p \cdot d\delta. \tag{3.16}$$

Differentiating the above relation with respect to σ, we get

$$\begin{aligned} \hat{k} \times f\frac{\partial \vec{\mathbf{u}}}{\partial \sigma} &= p_\sigma \bigtriangledown_\sigma \delta + p \bigtriangledown_\sigma \frac{\partial \delta}{\partial \sigma} - \bigtriangledown_\sigma (\frac{\partial}{\partial \sigma} \int^\delta p \cdot d\delta) \\ &= p_\sigma \bigtriangledown_\sigma \delta + p \bigtriangledown_\sigma \frac{\partial \delta}{\partial \sigma} - \bigtriangledown_\sigma (\frac{\partial \delta}{\partial \sigma} \cdot \frac{\partial}{\partial \delta} \int^\delta p \cdot d\delta) \end{aligned} \tag{3.17}$$

i.e.

$$\hat{k} \times f\frac{\partial \vec{\mathbf{u}}}{\partial \sigma} = p_\sigma \bigtriangledown_\sigma \delta - \frac{\partial \delta}{\partial \sigma} \bigtriangledown_\sigma p \tag{3.18}$$

or (3.19)

$$f\frac{\partial u}{\partial \sigma} = +\frac{\partial p}{\partial \sigma}\frac{\partial \delta}{\partial y} - \frac{\partial \delta}{\partial \sigma}\frac{\partial p}{\partial y} \tag{3.20}$$

$$f\frac{\partial v}{\partial \sigma} = -\frac{\partial p}{\partial \sigma}\frac{\partial \delta}{\partial x} + \frac{\partial \delta}{\partial \sigma}\frac{\partial p}{\partial x}. \tag{3.21}$$

These are the exact(no approximation used) thermal wind relations in the σ-coordinate.

Integrated Vorticity Equation

Dividing the continuity equation, eq.(3.14), by σ_z, yields

$$\frac{\partial}{\partial x}(\frac{u}{\sigma_z}) + \frac{\partial}{\partial y}(\frac{v}{\sigma_z}) + \frac{\partial w^*}{\partial \sigma} = 0 \tag{3.22}$$

or

$$\frac{\partial}{\partial x}(\frac{\partial z}{\partial \sigma}u) + \frac{\partial}{\partial y}(\frac{\partial z}{\partial \sigma}v) + \frac{\partial w^*}{\partial \sigma} = 0. \tag{3.23}$$

Hence

$$\frac{\partial}{\partial x}[\frac{\partial}{\partial \sigma}(zu) - z\frac{\partial u}{\partial \sigma}] + \frac{\partial}{\partial y}[\frac{\partial}{\partial \sigma}(zv) - z\frac{\partial v}{\partial \sigma}] + \frac{\partial w^*}{\partial \sigma} = 0. \tag{3.24}$$

or

$$\frac{\partial}{\partial \sigma}[\frac{\partial}{\partial x}(zu) + \frac{\partial}{\partial y}(zv)] - [\frac{\partial}{\partial x}(z\frac{\partial u}{\partial \sigma}) + \frac{\partial}{\partial y}(z\frac{\partial v}{\partial \sigma})] + \frac{\partial w^*}{\partial \sigma} = 0. \tag{3.25}$$

The following operations

$$\frac{\partial}{\partial x}[z \cdot \frac{1}{f} \cdot Eq.(3.20)] + \frac{\partial}{\partial y}[z \cdot \frac{1}{f} \cdot Eq.(3.21)] \tag{3.26}$$

result in

$$\frac{\partial}{\partial x}(z\frac{\partial u}{\partial \sigma}) + \frac{\partial}{\partial y}(z\frac{\partial v}{\partial \sigma}) = \frac{1}{f}\{[p_\sigma(z_x\delta_y - z_y\delta_x) + z\frac{\partial}{\partial \sigma}(p_x\delta_y - p_y\delta_x)] + \frac{\beta}{f}z(p_\sigma\delta_x - \delta_\sigma p_x)\} \tag{3.27}$$

For p in *Pascal*, we have $z \approx -10^{-4}p$. Substituting the z in the RHS of *eq.*(3.27) by $-10^{-4}p$, recombining the terms, we get

$$\frac{\partial}{\partial x}(z\frac{\partial u}{\partial \sigma}) + \frac{\partial}{\partial y}(z\frac{\partial v}{\partial \sigma}) = \frac{-10^{-4}}{f}\{\frac{\partial}{\partial \sigma}[p(p_x\delta_y - p_y\delta_x)] + \frac{\beta}{f}p(p_\sigma\delta_x - \delta_\sigma p_x)\} \tag{3.28}$$

Substituting *eq.*(3.28) into *eq.*(3.25), we obtain

$$\frac{\partial}{\partial \sigma}[\frac{\partial}{\partial x}(zu) + \frac{\partial}{\partial y}(zv)] + \frac{10^{-4}}{f}\frac{\partial}{\partial \sigma}[p(p_x\delta_y - p_y\delta_x)] + \frac{10^{-4}\beta}{f^2}p(p_\sigma\delta_x - \delta_\sigma p_x) + \frac{\partial w^*}{\partial \sigma} = 0. \tag{3.29}$$

The 3^{rd} term can be manipulated as

$$\begin{aligned} p(p_\sigma\delta_x - \delta_\sigma p_x) &= \frac{1}{2}[(p^2)_\sigma\delta_x - \delta_\sigma(p^2)_x] \\ &= \frac{1}{2}\{\frac{\partial}{\partial x}[(p^2)_\sigma\delta] - \delta(p^2)_{x\sigma} - \frac{\partial}{\partial\sigma}[(p^2)_x\delta] + \delta(p^2)_{x\sigma}\} \\ &= \frac{1}{2}\{\frac{\partial}{\partial x}[(p^2)_\sigma\delta] - \frac{\partial}{\partial\sigma}[(p^2)_x\delta]\} \qquad (3.30) \\ &= \frac{\partial}{\partial x}[pp_\sigma\delta] - \frac{\partial}{\partial\sigma}[pp_x\delta] \qquad (3.31) \end{aligned}$$

Thus *eq.*(3.29) becomes

$$\frac{\partial}{\partial\sigma}[\frac{\partial}{\partial x}(zu) + \frac{\partial}{\partial y}(zv)] + \frac{10^{-4}}{f}\frac{\partial}{\partial\sigma}[p(p_x\delta_y - p_y\delta_x)] - \frac{10^{-4}\beta}{f^2}\frac{\partial}{\partial\sigma}[pp_x\delta] \qquad (3.32)$$

$$+ \frac{\partial w^*}{\partial\sigma} = -\frac{10^{-4}\beta}{f^2}\frac{\partial}{\partial x}[pp_\sigma\delta] \qquad (3.33)$$

Integrating the above equation with respect to σ from σ_k to σ_{k+1}, yields

$$\begin{aligned} [\nabla_\sigma\cdot(z\vec{\mathbf{u}})]_k^{k+1} &+ \frac{10^{-4}}{f}[p(p_x\delta_y - p_y\delta_x)]_k^{k+1} - \frac{10^{-4}\beta}{f^2}[pp_x\delta]_k^{k+1} + [w^*]_k^{k+1} \\ &= -\frac{10^{-4}\beta}{2f^2}\frac{\partial}{\partial x}\int_{\sigma_k}^{\sigma_{k+1}}\delta\frac{\partial}{\partial\sigma}(p^2)\cdot d\sigma \\ &= -\frac{10^{-4}\beta}{2f^2}\frac{\partial}{\partial x}\int_{p_k}^{p_{k+1}}\delta\cdot d(p^2) \\ &= -\frac{10^{-4}\beta}{f^2}\frac{\partial}{\partial x}\int_{p_k}^{p_{k+1}}\delta p\cdot dp \qquad (3.34) \end{aligned}$$

Note that $\nabla_\sigma\cdot(z\vec{\mathbf{u}}) = \nabla_\sigma\cdot(z\frac{f_0}{f}\vec{\mathbf{u_g}}) = \nabla_\sigma\cdot(z\vec{\mathbf{u_g}}) - z\frac{\beta v_g}{f_0}$,

for p in $dbar = 10^4 Pascal$, thus $z \approx -p$, then

$$\begin{aligned} [w^*]_{k+1}^k - [\nabla_\sigma\cdot(p\vec{\mathbf{u_g}})]_{k+1}^k + [p\frac{\beta v_g}{f_0}]_{k+1}^k &= \frac{10^4}{f}[p(p_x\delta_y - p_y\delta_x)]_k^{k+1} - \frac{10^4\beta}{f^2}[pp_x\delta]_k^{k+1} \\ &+ \frac{10^4\beta}{f^2}\frac{\partial}{\partial x}\int_{p_k}^{p_{k+1}}\delta p\cdot dp \qquad (3.35) \end{aligned}$$

In this equation, the first term on the LHS is the diapycnal velocity difference, or the diapycnal streching; the second term on the LHS is the isopycnal divergence term, or

the vertical streching due to the isopycnal sloping (because $\nabla_\sigma \cdot (p\vec{\mathbf{u}_g}) = \vec{\mathbf{u}_g} \cdot \nabla_\sigma p$); the third on the LHS is the planetary divergence term; and finally, the RHS are the terms associated with the slopings of δ and p along the isopycnal surfaces. Note that

$$[pv_g]_k^{k+1} = \frac{1}{f}[p_{k+1}\psi_{k+1_x} - p_k\psi_{k_x}] = \frac{1}{f}[(p_{k+1} - p_k)\frac{\psi_{k_x} + \psi_{k+1_x}}{2} + \frac{p_k + p_{k+1}}{2}(\psi_{k+1_x} - \psi_{k_x})], \tag{3.36}$$

hence the above equation (3.35) becomes

$$[w^*]_{k+1}^k - [\nabla_\sigma(\vec{\mathbf{u}_g}p)]_{k+1}^k - \frac{\beta}{f^2}\frac{p_{k+1} - p_k}{2}(\psi_{k_x} + \psi_{k+1_x}) \tag{3.37}$$

$$= -\frac{\beta}{f^2}\frac{p_{k+1} + p_k}{2}\frac{\partial}{\partial x}DYN1_k + \frac{10^4\beta}{f^2}\frac{\partial}{\partial x}DYN2_k \tag{3.38}$$

$$+\frac{10^4}{f}[p(p_x\delta_y - p_y\delta_x)]_k k + 1 - \frac{10^4\beta}{f^2}[\delta p p_x]_k^{k+1} \tag{3.39}$$

where p is in *dbar* except in the definition of DYN1 where it is in *Pascal*:

$$DYN1_k \equiv \psi_k - \psi_{k+1} = \int_k^{k+1} \delta \cdot dp - p'_{k+1}\delta_{k+1} + p'_k\delta_k \tag{3.40}$$

whereas

$$DYN2_k \equiv \int_k^{k+1} p\delta \cdot dp \tag{3.41}$$

All other variables are in the SI units.

3.2.4 Conservation Equations for Water Properties

To see what the so called *eddy* diffusivities really mean, we derive the conservation equation for heat in more detail. For a fluid parcel, the energy conservation equation is

(e.g., Gill, 1982)

$$\rho C_p \frac{dT}{dt} - \alpha T \frac{dp}{dt} = \nabla \cdot (\kappa \nabla T) + Q \tag{3.42}$$

where T is the absolute temperature, Q is the source/sink term, here assumed to be zero. κ is the molecular heat diffusivity. In terms of the potential temperature, *eq.*(3.42) is in the form of

$$\rho C_p \frac{T}{\theta} \frac{d\theta}{dt} = \nabla \cdot (\kappa \nabla T) \tag{3.43}$$

In the eddy field, the quantity is decomposed into the mean and the perturbed parts, i.e.

$$\theta = \Theta + \theta' \;\; ; \qquad \vec{u} = \vec{U} + \vec{u'}, \tag{3.44}$$

then we have

$$\frac{d\theta}{dt} = \frac{\partial \theta}{\partial t} + \vec{u} \cdot \nabla \theta = \frac{\partial \Theta}{\partial t} + \vec{U} \cdot \nabla \Theta + \vec{u'} \cdot \nabla \theta' \tag{3.45}$$

$$= \frac{\partial \Theta}{\partial t} + \nabla \cdot (\vec{U} \Theta) + \nabla \cdot (\vec{u'} \theta') \tag{3.46}$$

where the Reynolds averaging and the nondivergence equations

$$\nabla \cdot \vec{u} = 0 \; , \;\; \nabla \cdot \vec{U} = 0 \; , \qquad \nabla \cdot \vec{u'} = 0 \; , \tag{3.47}$$

have been used. The eddy heat fluxes are usually parameterized by

$$\overline{u'\theta'} = -A \frac{\partial \Theta}{\partial x} \; , \quad \overline{v'\theta'} = -A \frac{\partial \Theta}{\partial y} \; , \quad \overline{w^{*'}\theta'} = -K \sigma_z \frac{\partial \Theta}{\partial \sigma} \; , \tag{3.48}$$

where A and K are the along- and cross- isopycnal surface eddy diffusivity. For the steady field, *eq.*(3.46) in the σ-coordinate can be written as

$$\nabla_h \cdot (\vec{\mathbf{U}}\Theta) + \sigma_z \frac{\partial}{\partial \sigma}(w^*\Theta) = \nabla_h \cdot A \nabla_\sigma \Theta + \sigma_z \frac{\partial}{\partial \sigma}(K\sigma_z \frac{\partial \Theta}{\partial \sigma}) \tag{3.49}$$

where, since the molecular diffusive term $\frac{\Theta}{T}\frac{1}{\rho C_p} \nabla (\kappa \nabla T)$ is much smaller than the eddy flux terms, it has been ignored.

Similarly, the conservation equation for water properties (like salinity (S), oxygen (O_2), etc.) with concentration C is derived in the $\sigma - coordinate$ as

$$\nabla_h \cdot (\vec{\mathbf{U}}C) + \sigma_z \frac{\partial}{\partial \sigma}(w^*C) = \nabla_h \cdot A \nabla_\sigma C + \sigma_z \frac{\partial}{\partial \sigma}(K\sigma_z \frac{\partial C}{\partial \sigma}) + Q \tag{3.50}$$

in which Q is the possible source/sink term associated with biological or/and chemical processes. In the deeper ocean, oxygen is generally consumed, and the sink term may be parameterized as (Jenkins, 1984)

$$Q = -\lambda C. \tag{3.51}$$

Unlike the molecular diffusivities which are determined by the physical properties of the medium, the eddy-flux induced *eddy* diffusivity or mixing coefficients A, K depend on the flow fields. In eq.(3.44), the mean quantities should be the ensemble means , which require infinite samples in theory and large number of samples in practice. However in reality, the means are usually substituted by the sample-limited time or space means or

a combination of them. Different averaging methods result in different mean and eddy fields and thus different eddy diffusivities. Using a six cruise data set, Tziperman(1988) shows different orders of inverting and averaging may result in different eddy diffusivities. One thing we can learn from the above arguments is that one must interpret one's results based on one's data and model.

Along isopycnals, the eddy diffusivities are generally much greater than the molecular ones. Since the eddy diffusivity is *eddy-* or flow-field- determined, we may assume it is the same for all the water proterties. On the other hand, double diffusion processes may also be important in the cross isopycnal mixing, thus the total diapycnal diffusivities for heat and salt may be different. Since the molecular diffusivity for oxygen is more like that for salt [1] , we assume the diffusivities for salt and oxygen are the same. Another assumption is that $A_x = A_y$, this implies that the eddies must be isotropic laterally. This may not be a bad asumption in the ocean interior.

In order to single out the planetary vorticity divergence term, using the definition of $\vec{\mathbf{u}}_g$ and its relation with $\vec{\mathbf{u}}$ (3.13), then we get

$$\nabla_h \cdot (\vec{\mathbf{U}} C) = \nabla_h \cdot (\frac{f_0}{f} \vec{\mathbf{U}}_\mathbf{g} C) = \nabla_h \cdot (\vec{\mathbf{U}}_\mathbf{g} C) + \vec{\mathbf{U}}_\mathbf{g} C \cdot \nabla_\sigma (\frac{f_0}{f}) \tag{3.53}$$

$$= \nabla_h \cdot (\vec{\mathbf{U}}_\mathbf{g} C) - \frac{\beta V_g C}{f_0} \tag{3.54}$$

and thus *eq.*(3.50) can be rewriten as

$$\nabla_h \cdot (\vec{\mathbf{U}}_\mathbf{g} C) - \frac{\beta V_g C}{f_0} + \sigma_z \frac{\partial}{\partial \sigma} (w^* C) = \nabla_h \cdot A \nabla_\sigma C + \sigma_z \frac{\partial}{\partial \sigma} (K \sigma_z \frac{\partial C}{\partial \sigma}) - \lambda C \tag{3.55}$$

[1] The molecular diffusivities for heat, salt and oxygen are

$$\kappa_T \sim 1 \times 10^{-7} m^2/s; \quad \kappa_S \sim 1 \times 10^{-9} m^2/s; \quad \kappa_{o2} \sim 1 \times 10^{-9} m^2/s \tag{3.52}$$

(κ_T and κ_S are from Pond and Pickard (1983), κ_{o2} is from Broecker and Peng (1982))

This is exactly the equation used by Hogg(1987). To reduce data noise, the equations for the concentration anomaly $C' = C - \bar{C}$, with $\bar{C}$ the laterally mean value on the isopycnal surfaces, are used and derived by multiplying the continuity equation, *eq.*(3.14) by $\bar{C}$, and substracting it from the above equation, the result is

$$\nabla_h \cdot (\vec{\mathbf{U}}_g C') - \frac{\beta V_g C'}{f_0} + \sigma_z C' \frac{\partial w^*}{\partial \sigma} + \sigma_z w^* \frac{\partial C}{\partial \sigma} = \nabla_h \cdot A \nabla_\sigma C + \sigma_z \frac{\partial}{\partial \sigma}(K \sigma_z \frac{\partial C}{\partial \sigma}) - \lambda C \quad (3.56)$$

3.2.5 Equation for Potential Density

In the absense of diffusion, water parcels preserve their potential densities. In the presence of diffusion, Hogg(1987) assumed that the potential density obeys the conservation laws in form of eq.(3.50), just like heat and salt. In the σ-coordinate, this equation is simplified as

$$w^* = \frac{\partial}{\partial \sigma}(K \sigma_z). \quad (3.57)$$

But how is the density or potential density equation derived and does it really have the conservation form? This has long been a puzzle to me. For example, in the presence of diffusion, and in the case that heat and salt have different diffusivities (such as when double diffusion is effective), then how is the density mixed? Is is mixed like heat or salt? What is the controlling equation for this density? In this section I'll try to solve this puzzle by deriving an exact equation for the potential density starting with the state equation of sea water. I will conclude that only under certain assumptions does the potential density have the conservation form.

As mentioned before, sea water is actually compressible, thus $\frac{d\rho}{dt} \neq 0$. The equation for density can be derived from the state equation of sea water:

$$\rho = \rho_{(S,T,p)} \tag{3.58}$$

or, in terms of potential density and potential temperature,

$$\rho_\theta = \rho_{(S,\theta)} \equiv \rho_{\theta\ (S,\theta)} \tag{3.59}$$

Using the above relation, the total differetial of ρ_θ is

$$d\rho_\theta = \frac{\partial \rho_\theta}{\partial S} dS + \frac{\partial \rho_\theta}{\partial \theta} d\theta \tag{3.60}$$

$$= \rho_\theta(\beta dS - \alpha d\theta) \tag{3.61}$$

where

$$\beta = \frac{1}{\rho_\theta}\frac{\partial \rho_\theta}{\partial S}\ ;\quad \alpha = -\frac{1}{\rho_\theta}\frac{\partial \rho_\theta}{\partial \theta} \tag{3.62}$$

are the saline and thermal contraction/expansion coefficients of sea water. Consequently, the equation for the potential density is derived as

$$\frac{1}{\rho_\theta}\frac{d\rho_\theta}{dt} = \beta\frac{dS}{dt} - \alpha\frac{d\theta}{dt} \tag{3.63}$$

or, using $\sigma = \rho_\theta - 1000.$ and the the equations for S and θ,

$$\frac{1}{\rho_\theta}\frac{d\sigma}{dt} = \beta[\nabla_h \cdot A_s \nabla_\sigma S + \sigma_z \frac{\partial}{\partial \sigma}(K_s \sigma_z \frac{\partial S}{\partial \sigma})] - \alpha[\nabla_h \cdot A_\theta \nabla_\sigma \theta + \sigma_z \frac{\partial}{\partial \sigma}(K_\theta \sigma_z \frac{\partial \theta}{\partial \sigma})] \tag{3.64}$$

where the subscripts θ and s appended to A and K distinguish the possible differences of the eddy diffusivity for heat and salt. On the isopycnal surfaces, the lateral eddy diffusivity is mainly determined by the flow fields, and thus we may assume that $A_s = A_\theta \equiv A$ for an isentropic eddy field($A_x = A_y$, and this may be the case in the ocean interior). On the other hand, the cross-isopycnal mixing is caused by small scale processes like wave breaking, cabbeling, etc., and the double diffusive processes may be important, thus K_s and K_θ are used to discriminate between them.

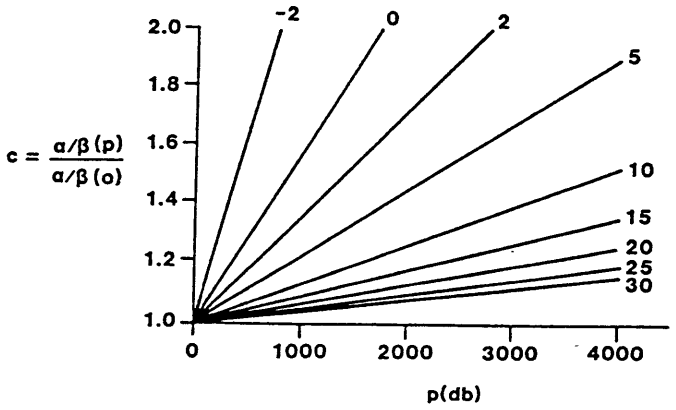

Fig.3.1. Plots of the parameter $c = \frac{\alpha}{\beta}(p) \Big/ \frac{\alpha}{\beta}(p_r)$ for $S = 35.0$ psu and for various values of θ ($\theta = -2°C$, $0°C$, $2°C \cdots 30°C$) as a function of pressure. The reference pressure, p_r, is 0 db in this figure. (From McDougall, 1987)

Following the above arguments, *eq.*(3.64) can be rewritten as

$$\frac{1}{\rho_\theta}\frac{d\sigma}{dt} = \beta[\nabla_h \cdot A\,\nabla_\sigma\, S + \sigma_z\frac{\partial}{\partial\sigma}(K_s\sigma_z\frac{\partial S}{\partial\sigma})] - \alpha[\nabla_h \cdot A\,\nabla_\sigma\,\theta + \sigma_z\frac{\partial}{\partial\sigma}(K_\theta\sigma_z\frac{\partial\theta}{\partial\sigma})] \quad (3.65)$$

and this is a generalized equation for the potential density. In what situations can (3.65) be simplified to the conservative form? If we assume that

$$a). \quad K_s = K_\theta \equiv K \quad (3.66)$$

$$b). \quad \alpha = const., \quad \beta = const. \quad (3.67)$$

then *eq.*(3.65) can be simplified as

$$\begin{aligned}\frac{1}{\rho_\theta}\frac{d\sigma}{dt} &= \nabla_h \cdot A(\beta\,\nabla_\sigma\, S - \alpha\,\nabla_\sigma\,\theta) + \sigma_z\frac{\partial}{\partial\sigma}[K\sigma_z(\beta\frac{\partial S}{\partial\sigma} - \alpha\frac{\partial\theta}{\partial\sigma})] \\ &= \frac{1}{\rho_\theta}[\nabla_h \cdot A\,\nabla_\sigma\,\sigma + \sigma_z\frac{\partial}{\partial\sigma}(K\sigma_z\frac{\partial\sigma}{\partial\sigma})] \quad (3.68) \\ &= \frac{1}{\rho_\theta}\frac{1}{\sigma_z}\frac{\partial}{\partial\sigma}(K\sigma_z) \quad (3.69)\end{aligned}$$

or

$$w^* = \frac{\partial}{\partial\sigma}(K\sigma_z) \quad (3.70)$$

If the above derivations are carried out in the z-coordinate, and under the assumptioms (3.66) and (3.67), we similarly end up with

$$\frac{d\sigma}{dt} = \nabla_z \cdot A\,\nabla_z\,\sigma + \frac{\partial}{\partial z}(K\frac{\partial\sigma}{\partial z}) \quad (3.71)$$

and this is the conventional form of the conservation equations for water properties.

The above arguments elucidate that, under the two assumptions stated in (3.66) and (3.67), the potential density is advected and diffused *like* a passive tracer. But

one may doubt the validity of the two assumptions. Where double diffusion is effective, $K_T \neq K_S$. Further, α and β are generally functions of θ and S, and thus functions of x and y. (Polynomial expressions for α and β as functions of θ, S, p can be found in McDougall (1987), and examples are shown in Fig.3.1). Therefore the more generalized form of the potential density equation, *eq.*(3.65), will be used. In the σ- coordinate and for the steady state, it simplifies as

$$\frac{\sigma_z}{\rho_\theta} w^* = \beta[\nabla_h \cdot A \nabla_\sigma S + \sigma_z \frac{\partial}{\partial \sigma}(K_s \sigma_z \frac{\partial S}{\partial \sigma})] - \alpha[\nabla_h \cdot A \nabla_\sigma \theta + \sigma_z \frac{\partial}{\partial \sigma}(K_\theta \sigma_z \frac{\partial \theta}{\partial \sigma})] \quad (3.72)$$

This expression signifies that the cross-isopycnal velocity is only caused by diffusive processes, but both vertically and laterally. If there is no diffusion in all directions, then there wil be no diapycnal advection. A similar potential density equation in neutral surface coordinates is derived by McDougall (1991).

The significance of the derivation of the potential density equation is that, firstly, it gives the exact form of potential density equation, and it shows under what conditions this equation can be simplified to the conservative form. Secondly, it directly shows the relations between the diapycnal velocity and diffusion. In practice, the equations for potential temperature, salinity and potential density are not independent (they are related by the state equation of the sea water), and only two of them provide independent information. As the potential density is computed from the potential temperature and salinity, more error may be involved in it, and therefore the equations for potential temperature and salinity will be used in this study.

3.3 Data Presentation

The hydrographic data set used in this work is the climatological hydrographic atlas prepared by Levitus (1982). This atlas represents a synthesis of all temperature, salinity, and oxygen data available from the National Oceanographic Data Center (NODC) before 1978. These parameters have been analyzed in a consistant, objective manner at standard oceanographic levels on a one-degree latitude-longitude grid from ocean surface to bottom with a maximum depth of 5500 meters (with a 10m increment in the top 30m, increases to a 100m increment betweem 300m and 1500m, and a 500m increment below 2000m). Detailed descriptions of the data sources, data reduction and quality control, representativeness of the data, and the objective analysis scheme are given by Levitus (1982). There are certain limitations due to the nature of the data base which is non-synoptic and scattered in space. To qualitatively show how scattered the data are in space, we reproduce the distributions of temperature observations in the world oceans for the annual period in Fig.3.2. More quantatively, we show the annual potential temperature statistics (means, standard deviations, and observation numbers) by 5-degree squares at the 6 levels corresponding to Fig.3.2 in the South Atlantic Ocean in Fig.3.3.

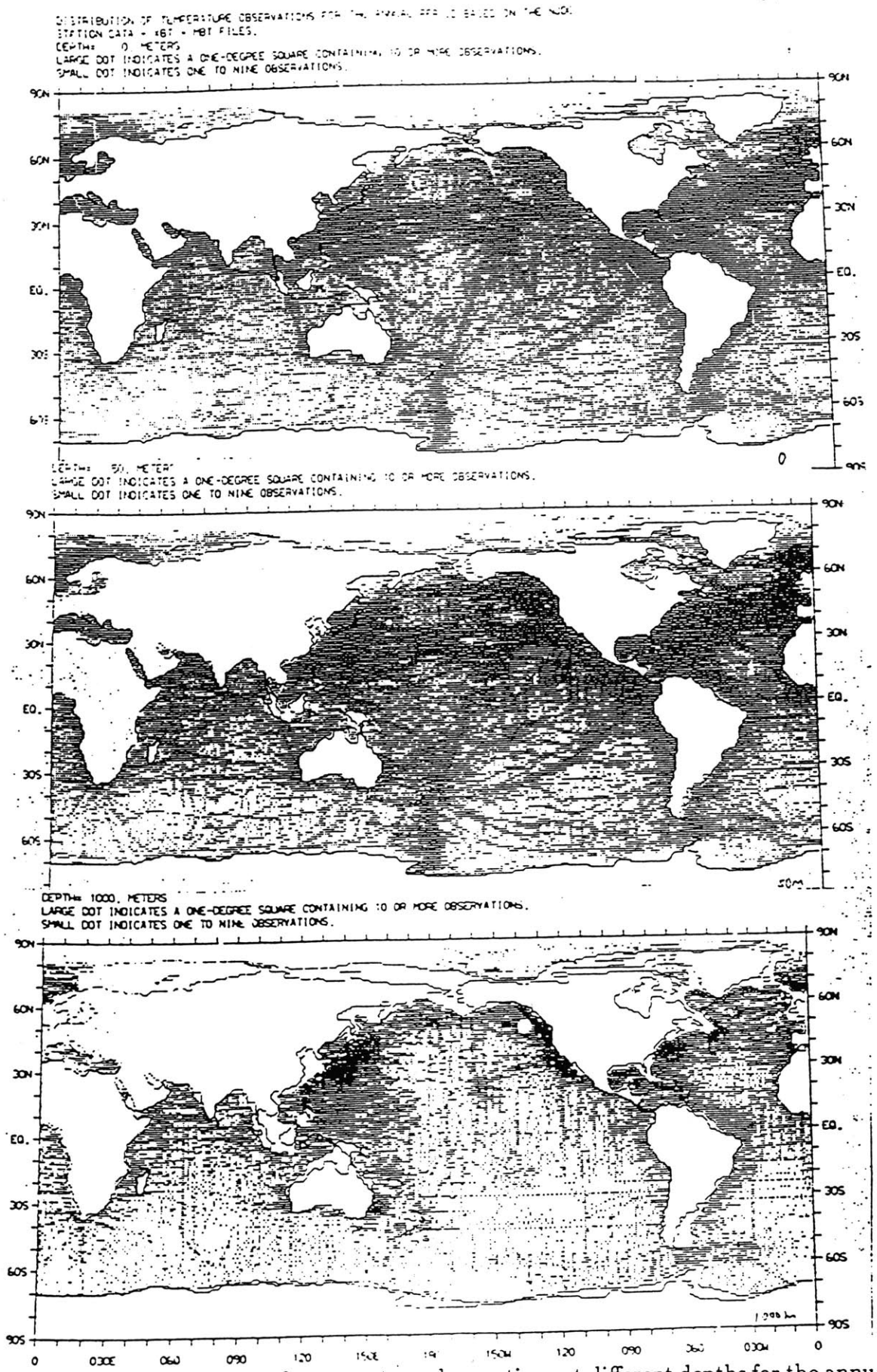

Fig.3.2 Distributions of temperature observations at different depths for the annual period. From Levitus, 1982 (microfiches)

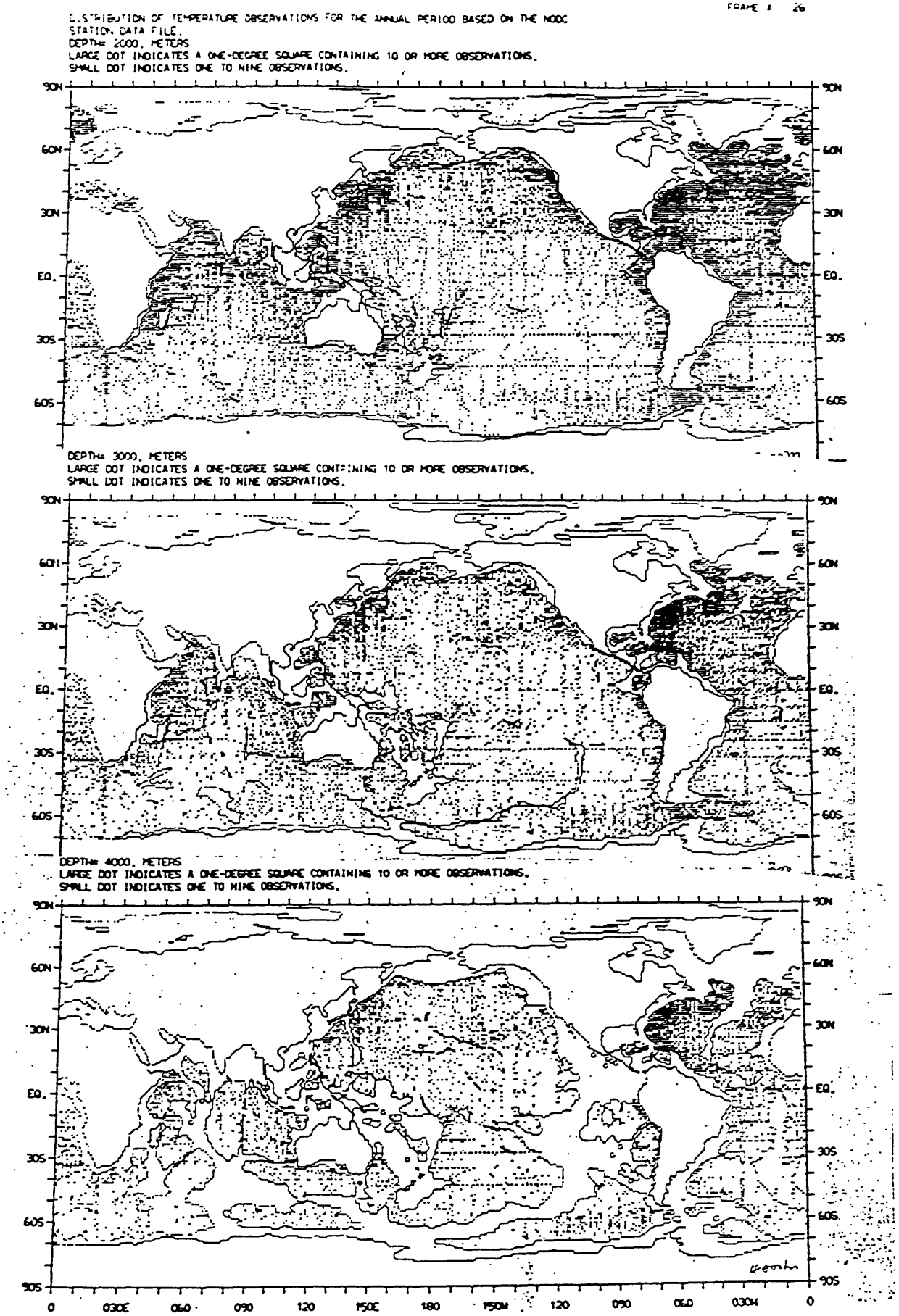

Fig.3.2 (continued)

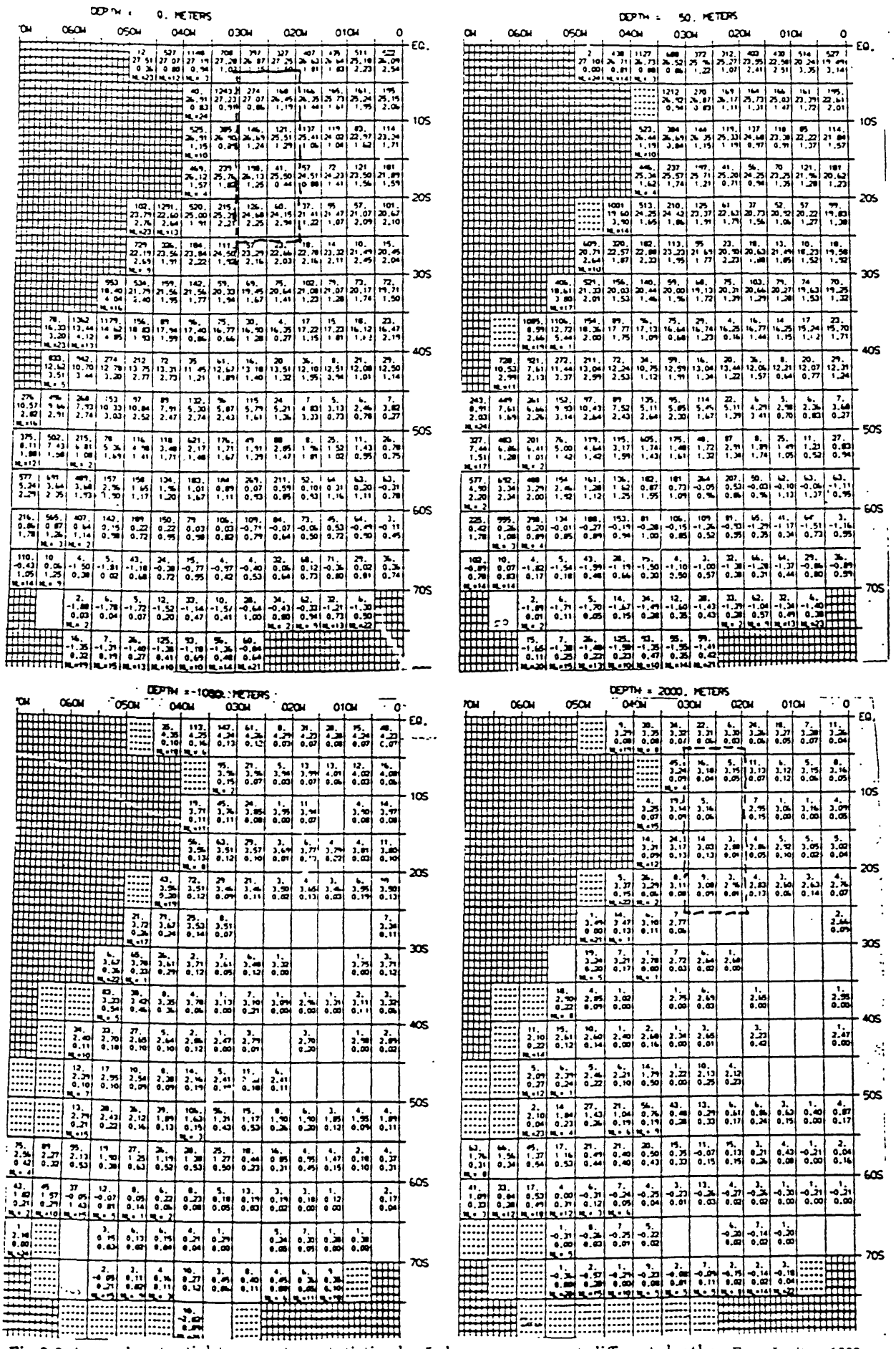

Fig.3.3 Annual potential temperature statistics by 5-degree squares at different depths From Levitus, 1982.

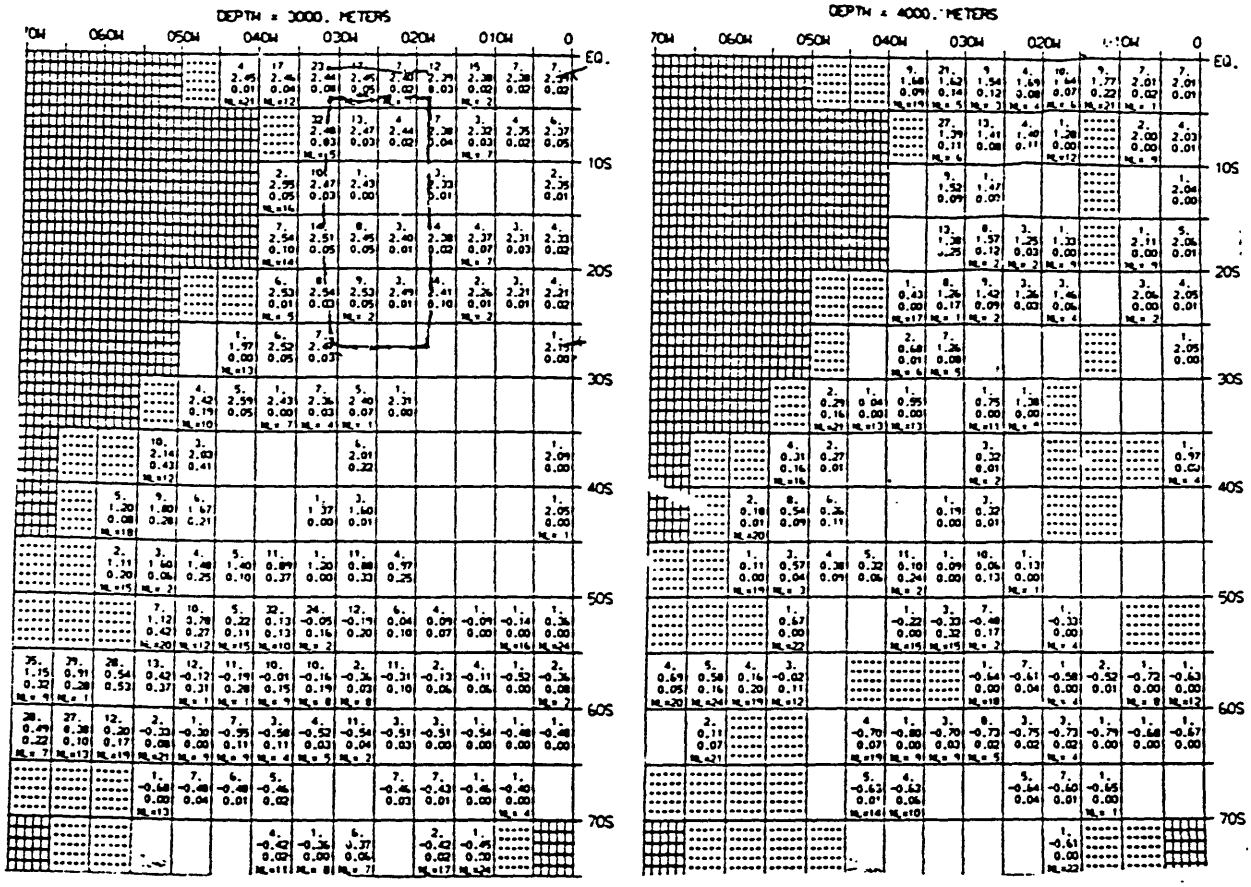

Fig.3.3 (continued)

Since topography and irregular boundary features have not yet been included in our model for the present time, the topography restricts our modeled areas. To run the model in as large a horizonal area as possible and to extend it as deep as possible without touching the bottom, we choose the area extending from 3°S to 27°S and from 32°W to 18°W in the Brazil basin (Fig.3.4) as our modeling area. As mentioned before, the water masses in the Brazil basin are very complicated. In order to study the flow patterns and balances of all these water masses in this basin, eight isopycnal surfaces are chosen in the vertical. The values of the 8 isopycnals and their relations to the water masses as well as the depth ranges they extend are listed in Table 3.1 and shown in Figs.3.5, which are the vertical section contours of potential temperature, salinity, and oxygen as well as σ_0, σ_1, σ_2, and σ_3. Note that in Figs.3.5, the vertical coordinate is the standard oceanographic level number, thus it is not uniform in depth. The relation between the standard oceanographic level numbers and the depths are firstly shown in Fig.3.5a. The dashed lines in the potential density contours are corresponding to the eight chosen isopycnals. These levels correspond to those of Fu (1981), Rintoul (1988) and Reid (1989), but the values for the isopycnals are not exactly the same, because the water masses extend to different depths in different areas. What we know from the Levitus atlas are the values of the water properties at the standard levels, thus the B-spline interpolation is used to generate the values of water properties and their vertical derivatives on the isopycnals. The interpolated pressure, potential temperature and oxygen on the eight isopycnals are contoured in Figs3.6-3.8 (on the isopycnals, salinity contours are exactly in the form as those of potential temperature, thus are not shown here). These distributions will be analyzed later with the inverse results. For example,

the temperature (salinity) contours on levels 3 and 4 are very similar (both are nearly zonal), but we will show that they result from quite different balances.

Table 3.1 The Eight Isopycnals and The Water Masses

Level Numbers	Isopycnal Values	Water Masses	Depth Ranges (m)
1	σ_0 =26.88	Near Surface Water	250--550
2	σ_1 =31.88	AAIW	700--900
3	σ_1 =32.08	upper CPW	1050--1150
4	σ_1 =32.28	lower CPW	1350--1500
5	σ_2 =36.94	interface	1800--1900
6	σ_2 =37.00	upper NADW	2250--2400
7	σ_3 =41.46	mid NADW	2700--2950
8	σ_3 =41.50	lower NADW	3350--3500

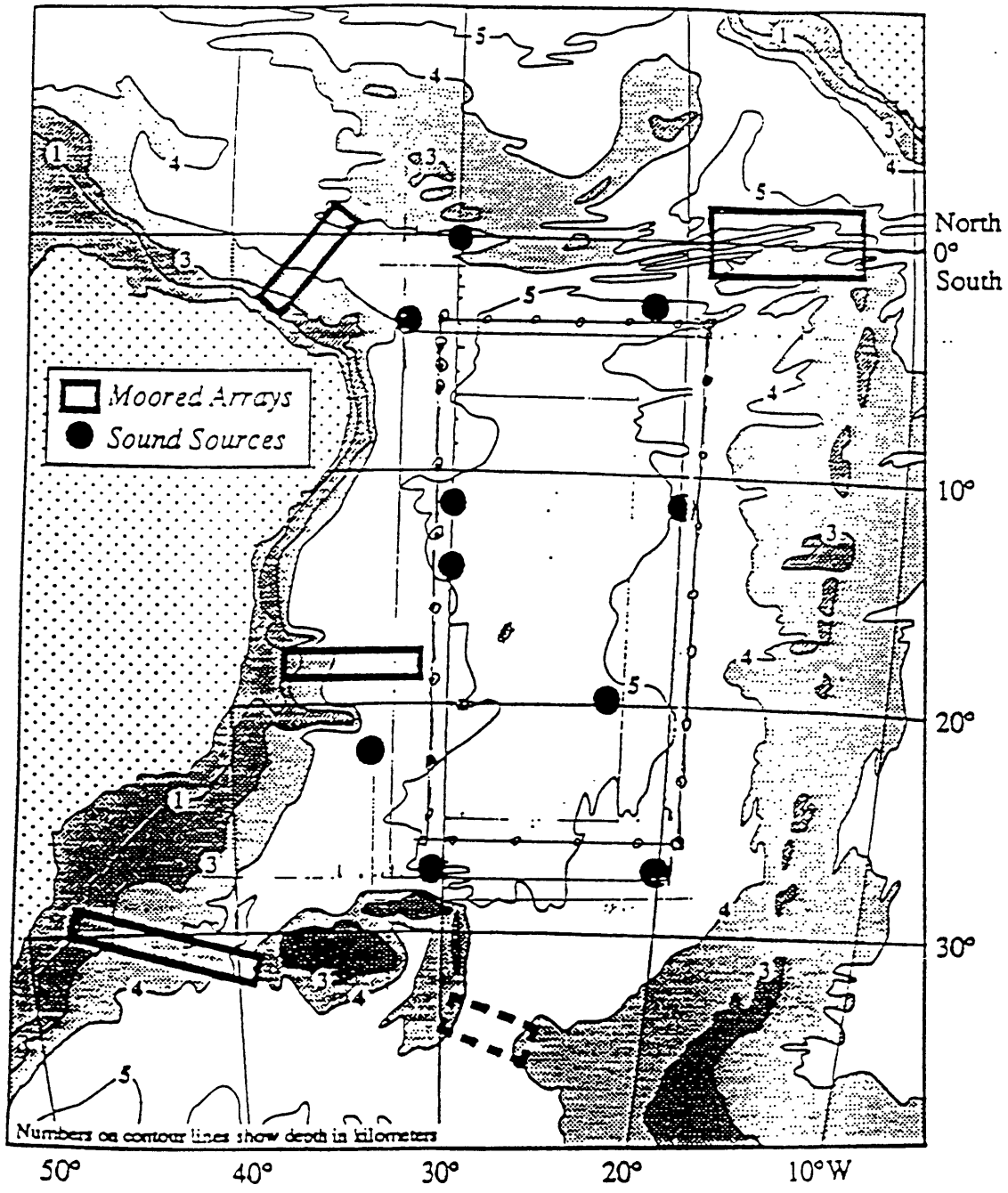

Fig.3.4 Modeled Area (circle-dotted lines) in this work

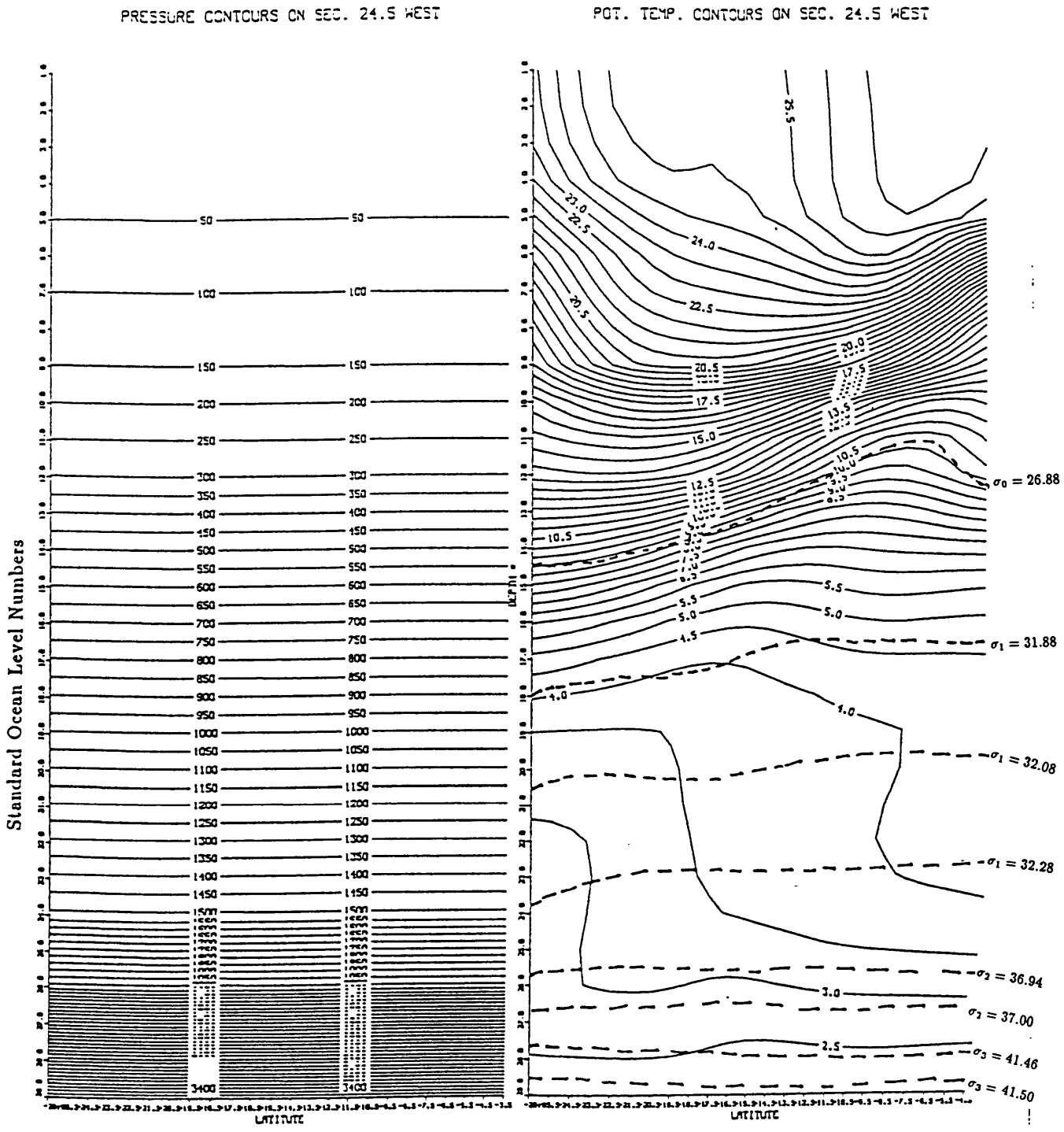

Fig.3.5 Vertical Section Contours along 24.5°W. (a) Pressure; (b) Potential Temperature

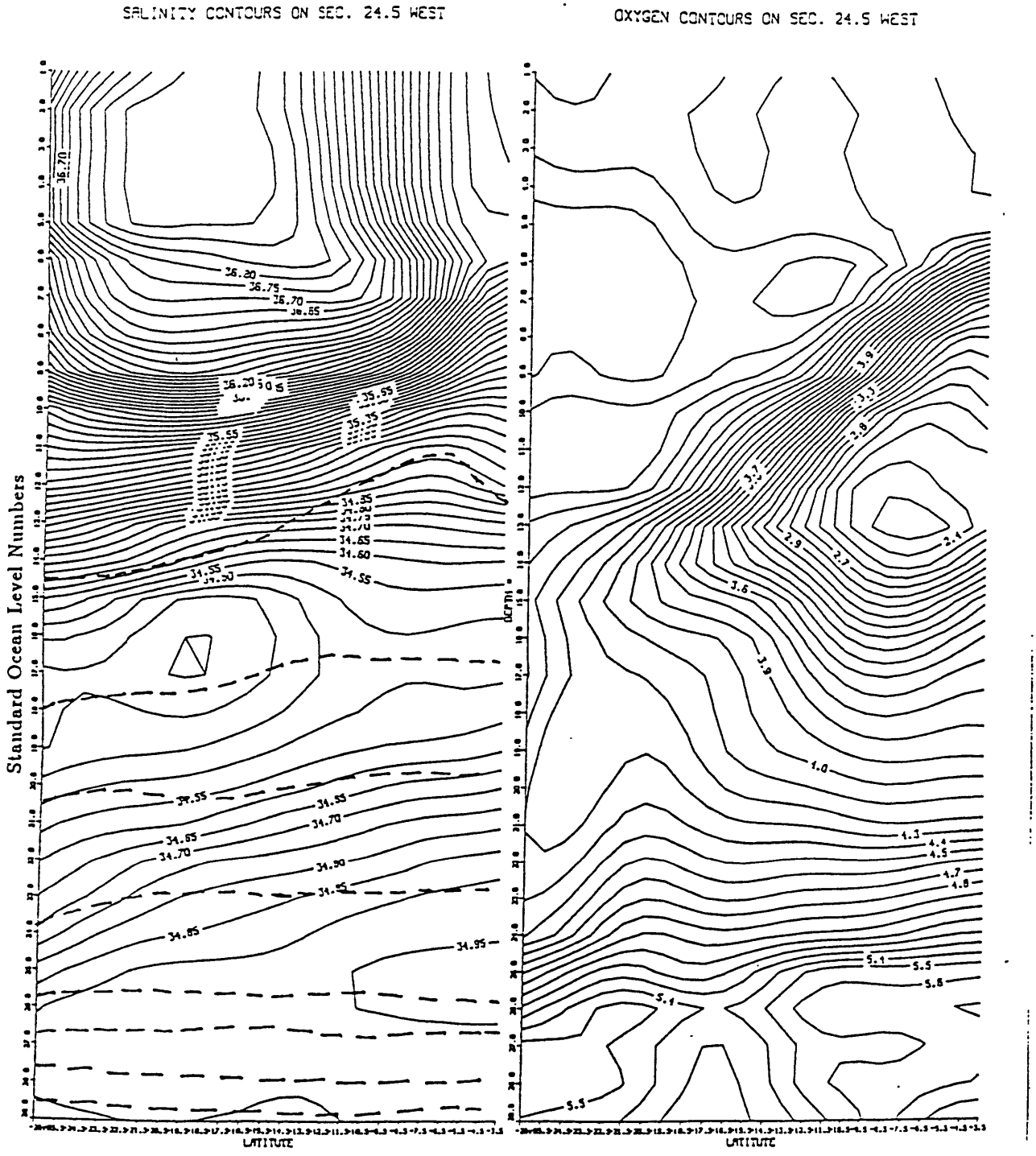

Fig.3.5 (continued) (c) Salinity; (d) Oxygen

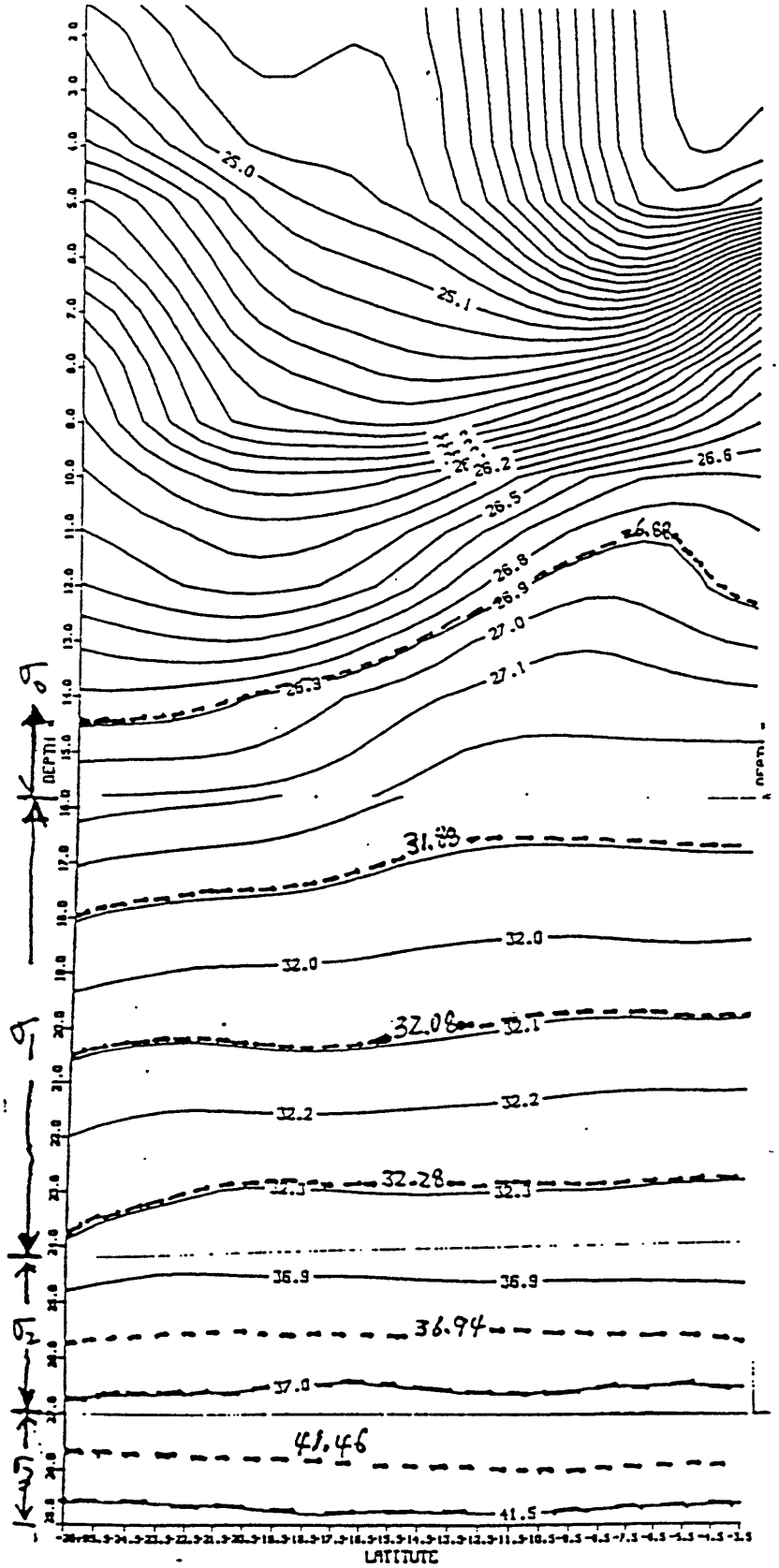

Fig.3.5 (continued) (e) Potential Density Anomalies.

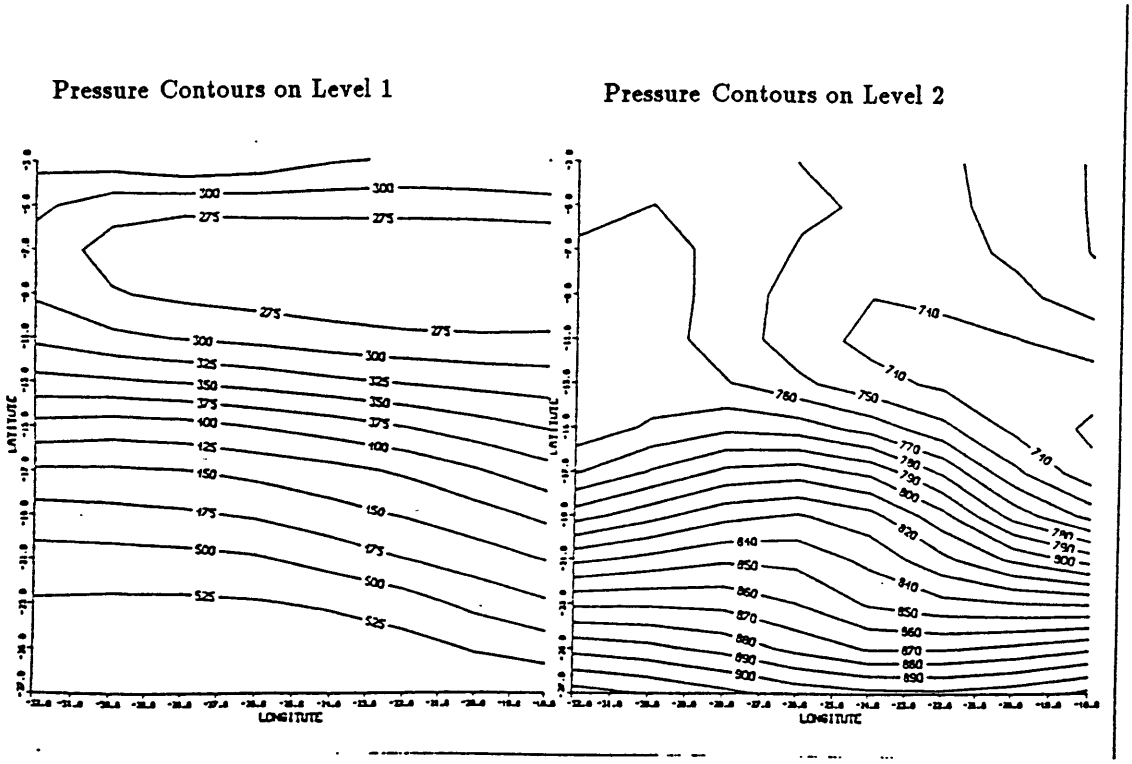

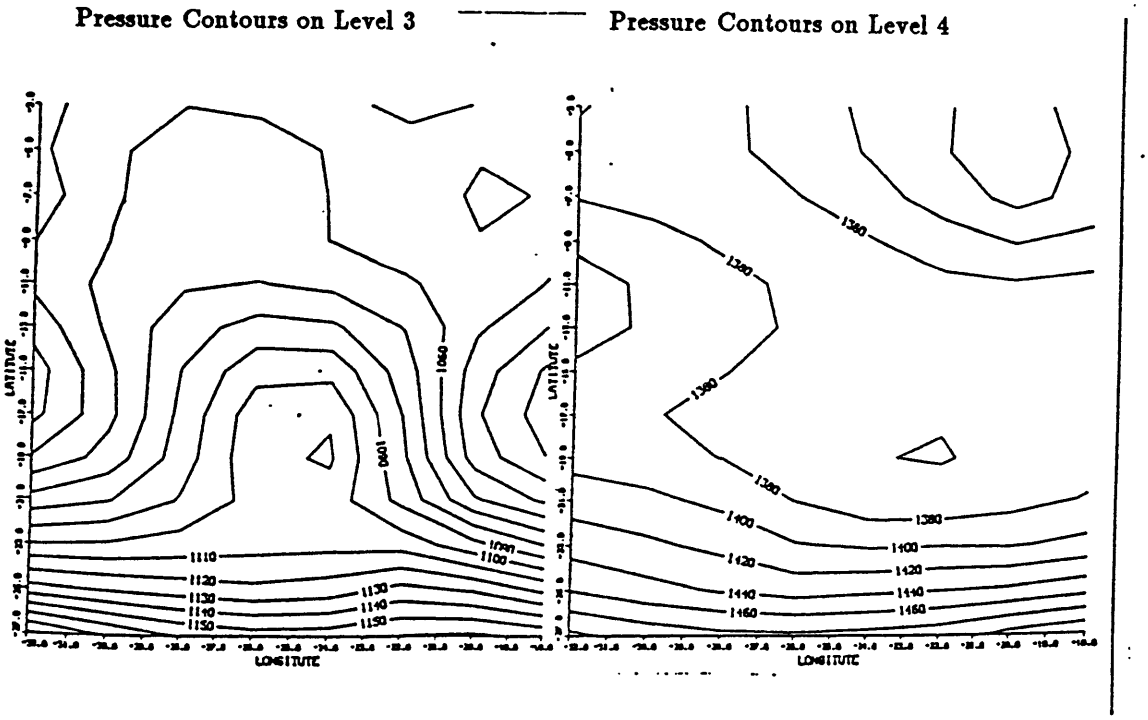

Fig.3.6 Pressure Contours on the eight isopycnals

Pressure Contours on Level 5

Pressure Contours on Level 6

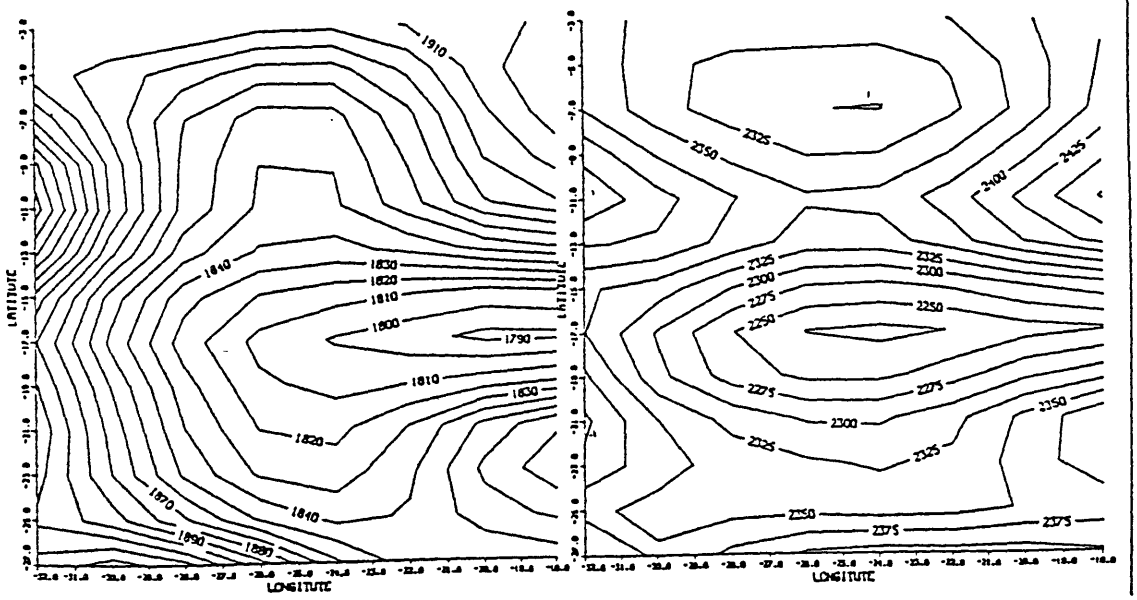

Pressure Contours on Level 7

Pressure Contours on Level 8

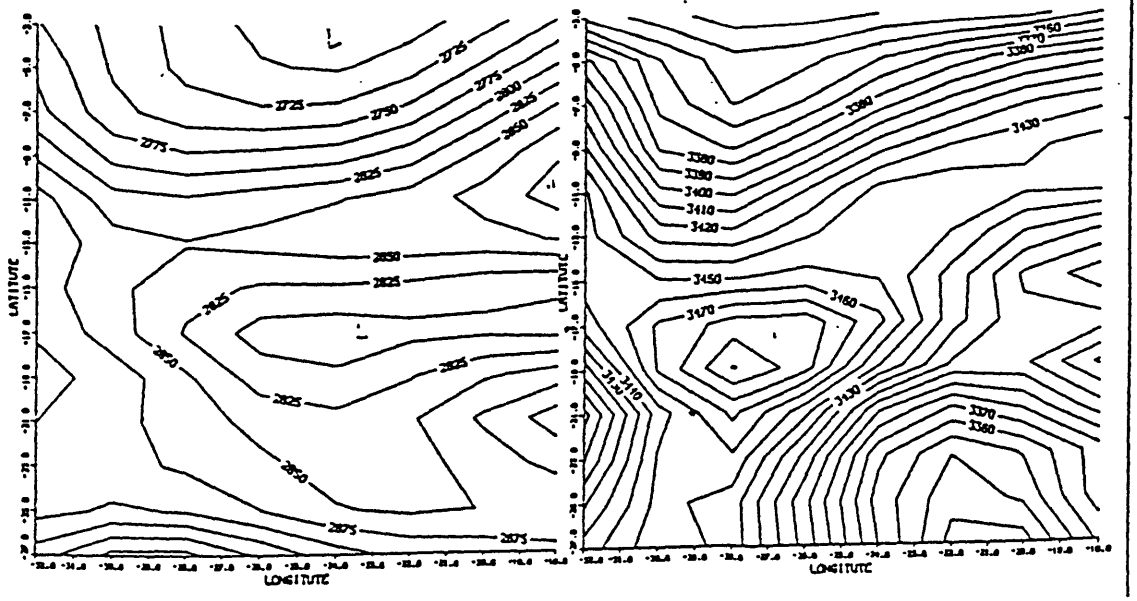

Fig.3.6 (continued)

Temperature Contours on Level 1

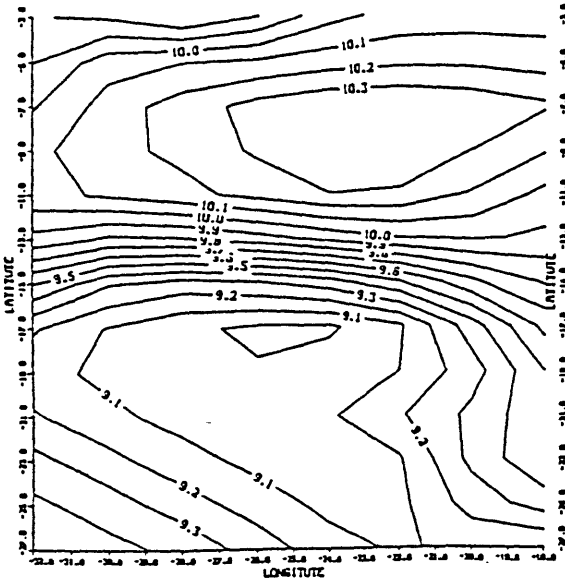

Temperature Contours on Level 2

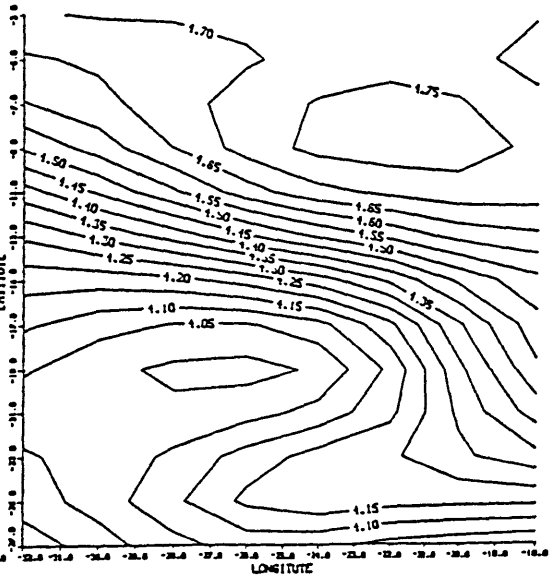

Temperature Contours on Level 3

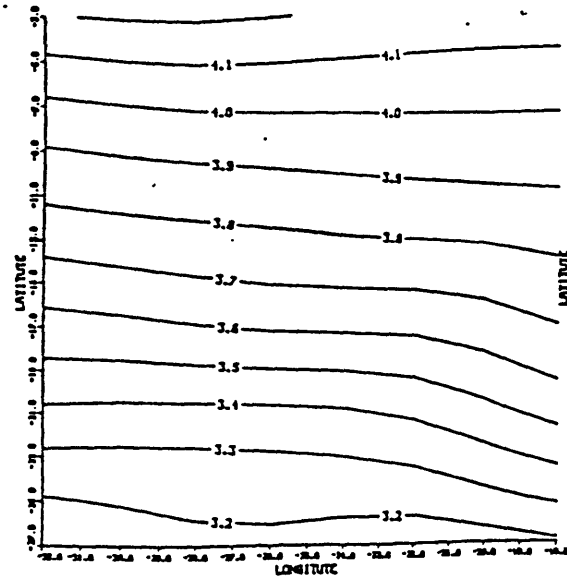

Temperature Contours on Level 4

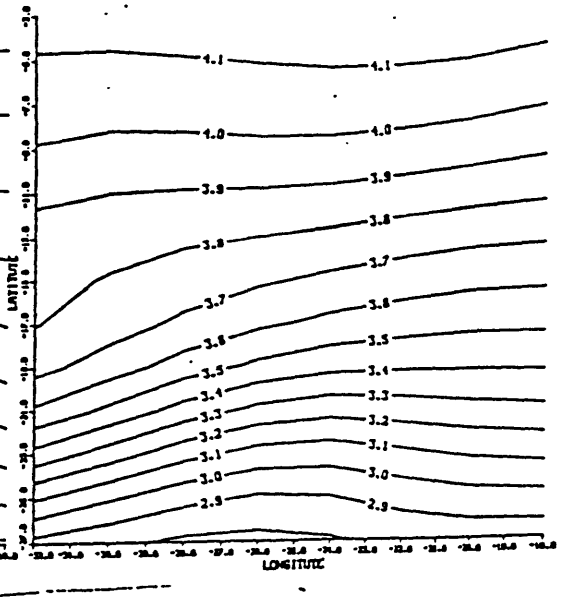

Fig.3.7 Potential Temperature Contours on the eight isopycnals

Temperature Contours on Level 5

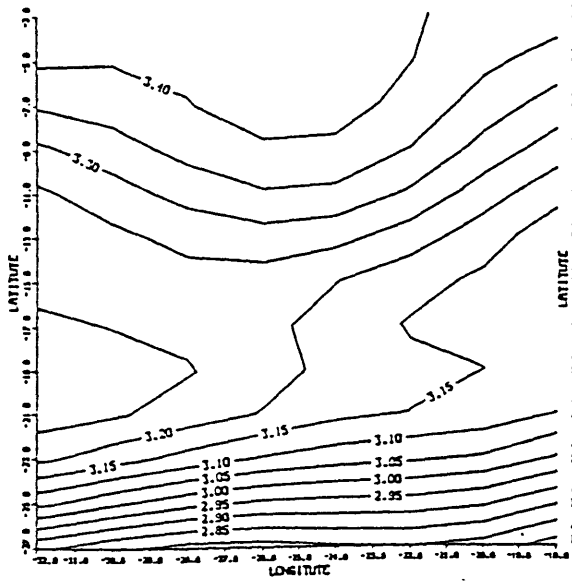

Temperature Contours on Level 6

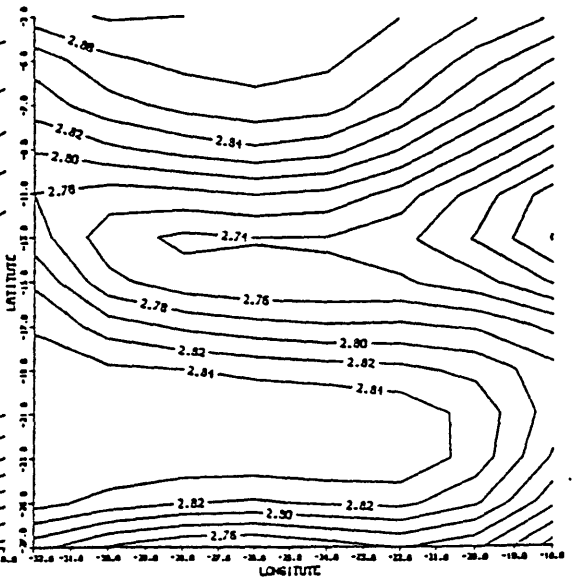

Temperature Contours on Level 7

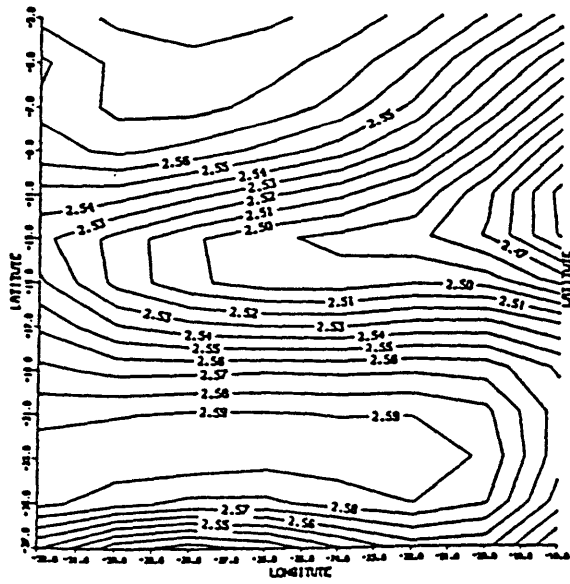

Temperature Contours on Level 8

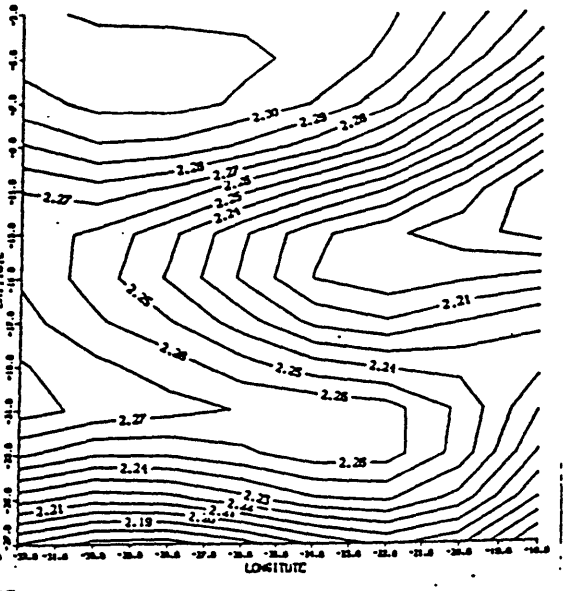

Fig.3.7 (continued)

Oxygen Contours on Level 1

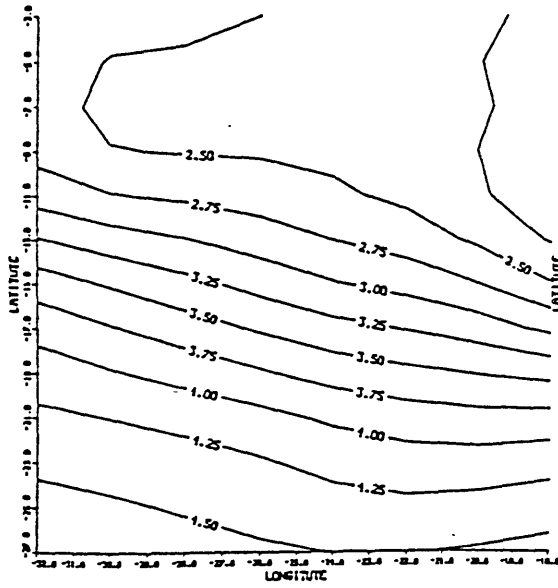

Oxygen Contours on Level 2

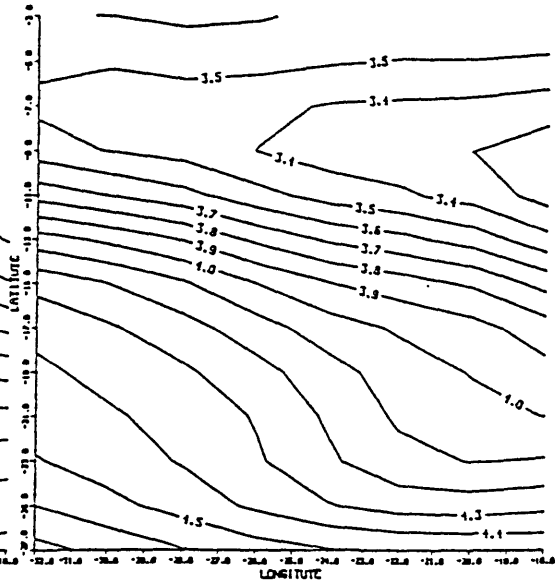

Oxygen Contours on Level 3

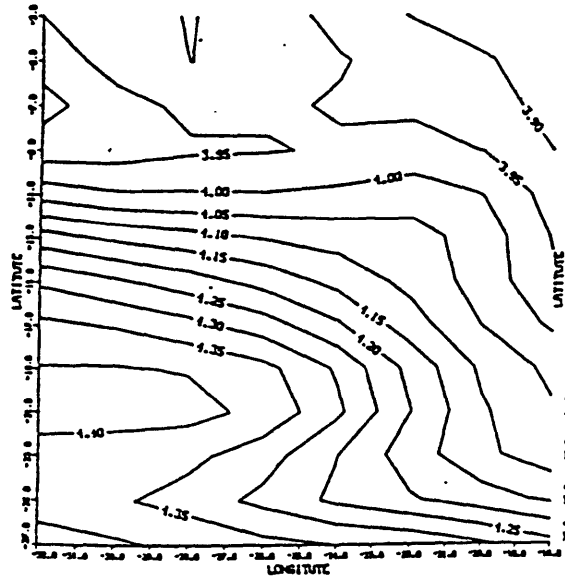

Oxygen Contours on Level 4

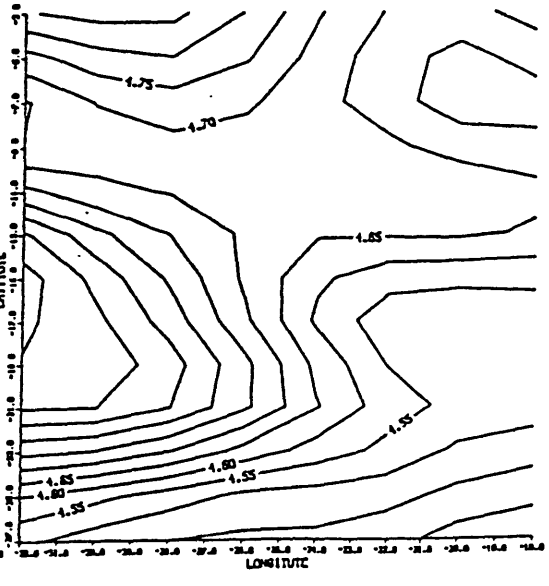

Fig.3.8 Oxygen Contours on the eight isopycnals

Oxygen Contours on Level 5

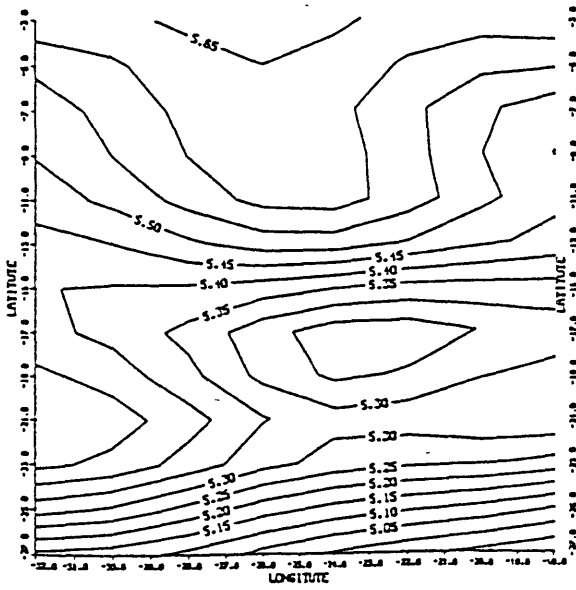

Oxygen Contours on Level 6

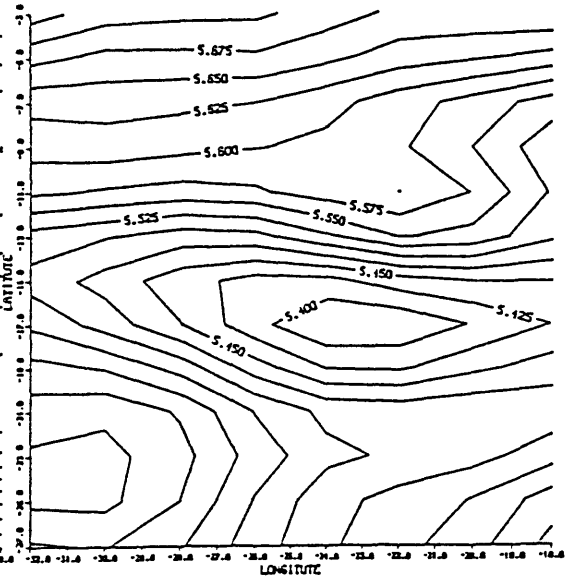

Oxygen Contours on Level 7

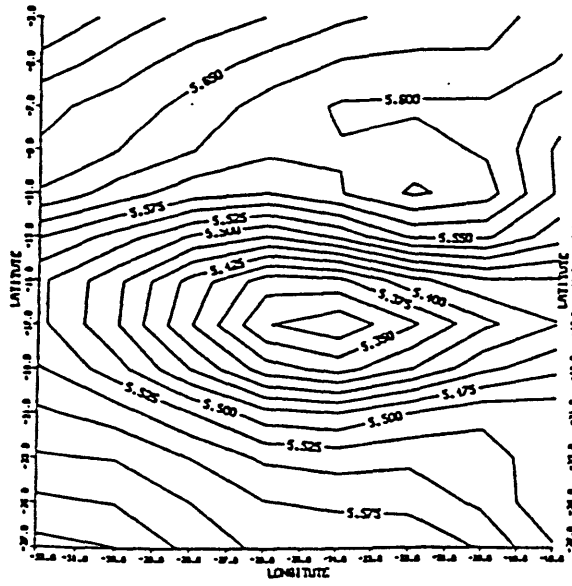

Oxygen Contours on Level 8

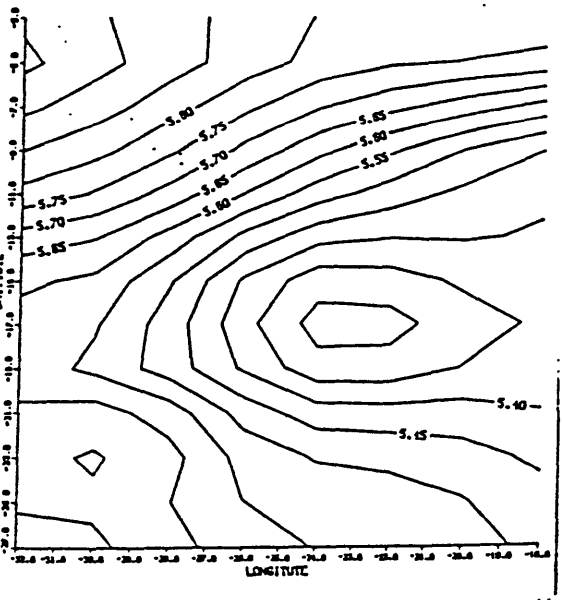

Fig.3.8 (continued)

3.4 Difference Equations and Additional Constraints

The equations in this model are the Dynamic Equation (3.1), Continuity Equation (3.14), Integrated Vorticity Equation (3.39) and Conservation Equations (3.56) for heat, salt and oxygen. In the purely advective model (no diffusion), the information from temperature and salinity are not independent, therefore only the potential temperature equation is used. These equations are written in the centered finite difference form on the grid shown in Fig.3.9, which is the same as that used by Hogg (1987) except that it is three dimensional now. The grid steps are 2-degrees latitude and longitude, and varying in the vertical between the isopycnal surfaces. An example is given in Appendix A. The problem is then written in the matrix form:

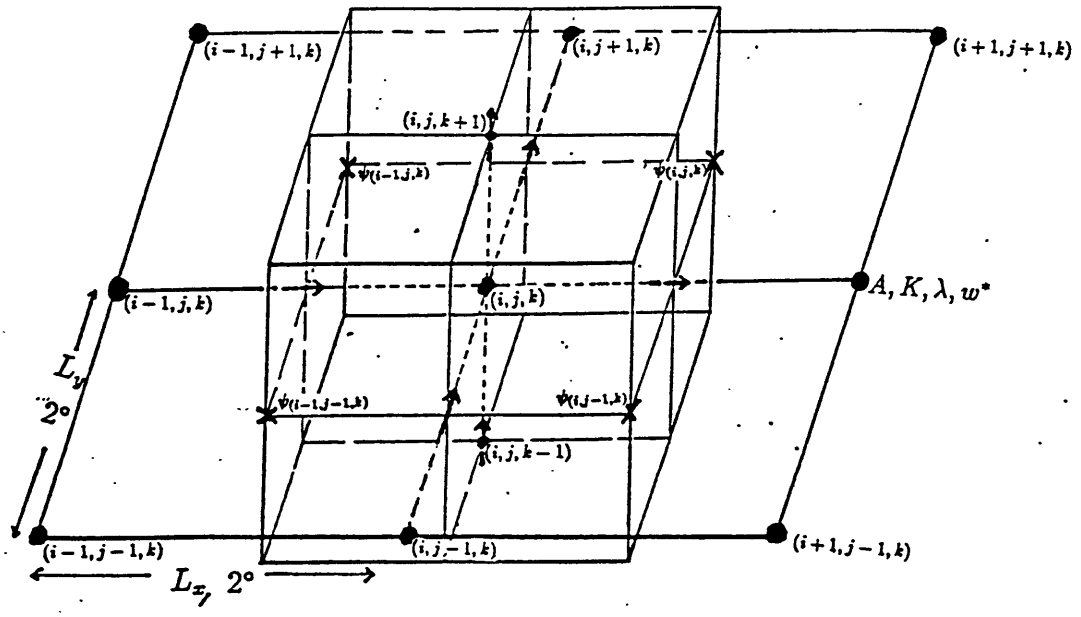

Fig.3.9 Staggered grid for the centered finite difference forms of the governing equations. Water properties and unknown diffusive parameters are at · points, and the unknown streamfunctions are at X points.

$$A \times X = Y \tag{3.73}$$

where A is the coefficient matrix, X is the vector containing the unknowns, and Y is the RHS including the known inhomogeneous terms from the Dynamic and Integrated Vorticity equations, which gives the system unique non-zero solutions. This equation system is solved by the inverse method, which will be discussed below.

The eddy diffusivities (A, K) are generally varying from place to place, and these variations have dynamic effects on the distributions of water properties, as discussed by Armi (1979) , Armi and Haidvogel (1982) as examples. In a steady-state diffusive model, Armi and Haidvogel (1982) show that the tongue-like property distributions can be generated by a purely diffusive field with variable and anisotropic diffusions. In this work, we parameterize the diffusive parameters in the same way as in Hogg's (1987) work, i.e. as third order Tchebychev polynomial (in discrete form) functions of x and y whose coefficients may differ from level to level. In this way, we will show that the equation system (3.73) is overdetermined not only formally, but also practically. Based on the assumption that all the eddy diffusive processes are dissipative, it is required that all the diffusivities (A and K) and the oxygen consumption rate (λ) are positive, i.e.

$$A, K, \lambda > 0 \tag{3.74}$$

By the definition of the streamfunction, there is an arbitrary additive constant, and we can set this constant equal to zero at a fixed location (x_0, y_0) on the top isopycnal

surface, i.e. let

$$\psi_{1(x_0,y_0)} = 0 \tag{3.75}$$

and hence from the dynamic relation we have

$$-\psi_{2(x_0,y_0)} = DYN1_{(x_0,y_0)} \tag{3.76}$$

is also a constant. Relative to location (x_0, y_0), we have

$$\psi_{1(x,y)} - \psi_{1(x_0,y_0)} - [\psi_{2(x,y)} - \psi_{2(x_0,y_0)}] = DYN1_{(x,y)} - DYN1_{(x_0,y_0)} \tag{3.77}$$

Define

$$\begin{aligned} \psi'_{1(x,y)} &= \psi_{1(x,y)} - \psi_{1(x_0,y_0)} = \psi_{1(x,y)} \\ \psi'_{2(x,y)} &= \psi_{2(x,y)} - \psi_{2(x_0,y_0)} \end{aligned} \tag{3.78}$$

then by definition, not only

$$\psi'_{1(x_0,y_0)} = 0, \tag{3.79}$$

but also

$$\psi'_{2(x_0,y_0)} = 0, \tag{3.80}$$

Note that only the derivatives of ψ are involved in all the other equations (conservation equation, continuity equation, integrated vorticity equation, etc.), thus the above equations are also true for the ψ'. Therefore if we solve for ψ' instead of ψ, the values of ψ'

at (x_0, y_0) on both isopycnal surfaces are known to be zero, and they can be taken out of the unknowns. Similarly, if we have N-level isopycnals in the model, we generally have

$$\psi_{k\ (x,y)} - \psi_{k\ (x_0,y_0)} - [\psi_{k+1\ (x,y)} - \psi_{k+1\ (x_0,y_0)}] = DYN1_{k\to k+1\ (x,y)} - DYN1_{k\to k+1\ (x_0,y_0)}, \tag{3.81}$$

or

$$\psi'_{k\ (x,y)} - \psi'_{k+1\ (x,y)} = DYN1'_{k\to k+1\ (x,y)}, \quad k = 1 \to N-1 \tag{3.82}$$

and in terms of ψ', the $\psi'_{(x_0,y_0)}$ on all the isopycnal levels are by definition equal to zero and thus can be taken out of the unknowns. In summary, we will solve for ψ', and let

$$\psi'_{(x_0,y_0)} = 0 \tag{3.83}$$

If the lateral grids are *ngx by ngy* and the vertical level number is $Nlev$, then the unknown number for streamfunction is

$$Nlev \times [(ngx-1)(ngy-1)-1].$$

If the polynomial degree for the diffusive parameters is *npl*, then the number of the unknown coefficients for each diffusivity on each isopycnal is $\frac{(npl+1)(npl+2)}{2}$. Thus the number for the total unknowns is

$$\begin{aligned}
N &= Nlev \times [(ngx-1)(ngy-1)-1] && \textit{for Purely Advective Model, or} \\
N &= Nlev \times [(ngx-1)(ngy-1)-1] + 4 \times \frac{(npl+1)(npl+2)}{2} && \textit{for } K_\theta = K_S, \textit{ or} \\
N &= Nlev \times [(ngx-1)(ngy-1)-1] + 5 \times \frac{(npl+1)(npl+2)}{2} && \textit{for } K_\theta \neq K_S
\end{aligned}$$

The number of the total equations is (no salinity equations are used in the Purely Advective model)

$$M = (4 \times Nlev - 1)(ngx - 2)(ngy - 2) + (Nlev - 1)[(ngx - 1)(ngy - 1) - 1]$$
$$for\ Purely\ Advective\ Model$$
$$M = (5 \times Nlev - 1)(ngx - 2)(ngy - 2) + (Nlev - 1)[(ngx - 1)(ngy - 1) - 1]$$
$$for\ Advective - diffusive\ Model$$

For the current problem, $ngx = 8, ngy = 13, Nlev = 8, npl = 3$. The number for the total unknowns is

$$N = 644 \qquad for\ Purely\ Advective\ Model$$
$$N = 984 \qquad for\ K_\theta = K_S$$
$$N = 1064 \qquad for\ K_\theta \neq K_S$$

The number for the total equations is

$$M = 2627 \qquad for\ Purely\ Advective\ Model$$
$$M = 3155 \qquad for\ Advective\ Diffusive\ Model$$

3.5 Basic Techniques in the Inverse Method

The inverse method is a powerful machinery for dealing with the not just-determined (under- or over- determined), inexact (due to measurement errors and appoximations in getting the simplified equations), or redundant systems of equations(not all equations are independent). Despite the nonuniqueness of the solutions for an underdetermined system, the inverse method itself can tell us how well the solutions adapt the equations, to what extent the solutions have been resolved, and what equations or processes control the solutions most efficiently. That is to say the method is self-consistent. It also has the

flexibility to add some physically meaningful contraints(in equality or in inequality) to the system to control the solutions. In this section, the basic techniques of the inverse mothod used in this work will be reviewed briefly. Details can be found from Wiggins(1972) or Wunsch(1978).

Equation Scaling

As different equations may have different noise levels, equation scaling is an important issuse in getting better solutions. The general principles for row and column scaling and their effectiveness for different regimes are presented in Appendix B. The basic idea is that equations with larger errors should be down weighted so that solutions will not be contaminated by the large noise. For formally and actually overdetermined system ($M > N$ *and* $Rank(A) = N$ where M is the equation number and N is the unknown number), only row scaling is effective;for formally underdetermined system with *full* rank($M < N$ *and* $Rank(A) = M$), only column scaling is effective; and for formally overdetermined and actually underdetermined system ($M > N$ *but* $Rank(A) < N$), both row and column scaling are effective. In the present work, the system is really overdetermined and full rank (see below), thus only row scaling is necessary (Actually in setting up the equation system, the coefficients for all unknowns to be calculated have been arranged to be of order one, and this is effectively doing the column scaling). In theory, if the equation errors are correlated, then row weighting factor should be based on the error variance. In practice, without any *prior* knowloge about the correlations, one usually assume they are not correlated, and the scaling factors are chosen such that the residuals for all equations are in the same noise level. In our model, there are overall eight vertical isopycnal levels with the first level in the thermocline. The equations at different levels have different errors. For example, write the conservation equation in the following simple form:

$$\vec{\mathbf{u}} \cdot \nabla C = other\ terms \tag{3.84}$$

There are practically two components in C: the real or mean $\bar{C}$ and error or standard deviation C'. Similarly, $\vec{\mathbf{u}} = \vec{\mathbf{U}} + \vec{\mathbf{u}}'$. Then the above equation becomes

$$\vec{\mathbf{U}} \cdot \nabla \bar{C} = other\ terms - \vec{\mathbf{U}} \cdot \nabla C' - \nabla \bar{C} \cdot \vec{u}' - \vec{u}' \cdot \nabla C' \tag{3.85}$$

The data show that the gradients for θ and S on the thermocline level are much greater than those on the deeper isopycnals, and we also expect that the flow in the thermocline is stronger than that in deeper levels. Thus unless the noise C' and $\vec{u}'$ in the themocline are much smaller than that in deep levels (contrarily, the Levitus atlas values shows that the standard deviations for θ and S and O_2 in the upper levels are larger than deep levels, see Fig.3.3), the equations on the isopycnals in the thermocline should be down weighted by factors of $\frac{1}{\nabla \bar{C}}$ and $\frac{1}{\vec{U}}$. More generally, the equations on each isopynal are scaled by factors $\frac{1}{C_{max}-C_{min}}$ where C_{max} and C_{min} are the maximun and minimum values of the concentration C on that isopynal. Expecting that the velocities below the thermocline all have the same magnitude, only the equations on the thermocline isopycnals are scaled by a factor of $\frac{\vec{U}_k}{\vec{U}_1}, k > 1$, which was chosen as 0.2 on the experimental basis so that the scaled residuals have the same magnitude on all levels.

The model experiments showed the necessity to use the above scalings. The model in the first run was for seven levels with no thermocline level. All the unknowns, including the diffusive parameters are well resolved (significantly different from zero), and the residuals for all equations and on all levels are of the same magnitude. When the thermocline level was included but without the above scalings, all the diffusive parameters are not resolved (from the noise level) and the residuals in the equations on the thermocline isopycnals are much larger than the ones below the thermocline. When the above scaling factors are added, all the parameters are well determined again, and all the equations have the same magnitude of residuals. In addition, the solutions are almost identical with

that of the former seven level run. In his two level model, Hogg(1987) didn't use the above scalings. But interestingly, in his Mediterranian salt tongue region, the gradients of temperature and salinity on the thermocline isopycnal are smaller than that on the isopycnal beneath the thermocline($\frac{\nabla_\sigma C_1}{\nabla_\sigma C_2} \sim \frac{1}{2}$) due to the Mediterranean outflow, and if one expects the flows in the thermocline to be stronger (his results show that $\frac{U_1}{U_2} \sim 2$), then the two scaling factors have opposite effects and the total scaling effects may be ineffective. But usually, the gradients and flows are stronger in the thermocline, and the scalings are important to get well determined solutions.

Oxygen is not conserved in the ocean and a consumption term is included as unknown in the oxygen equation. At first, we assume that the oxygen distribution constrains the flows and diffusion coefficients as equally important as temperature and salinity do, and thus the same weight is used. But the results show that the solutions for the oxygen consumption rate are unreasonably large from the biologists' point of view. To lessen the possible contamination of this badly determined parameter on other parameters, a small weight(.01) is given to the oxygen equations. In doing so, it really means that the flows and diffusion parameters are determined by temperature and salinity distibutions, and oxygen is *passively* advected and diffused by them, and the residuals are used to determine the oxygen consumption rates. In this way, the results show that the consumption rates compared with their errors do not significantly differ from zero.

Chose the Rank

As not all the equations are necessarily independent, a formally overdetermined system may be actually underdetermined. Since the solutions are proportional to $1/\lambda_i$, whereas the solution error variances are proportional to $1/\lambda_i^2$, the solution errors blow up much more quickly as the singular values decrease. To get significant solutions, it may be necessary to cut off some small eigenvalues and associated eigenvectors. Wiggins(1972) and Lawson and Hanson (1974) discuss several approaches to determine the effective rank

or where the singular values should be cut off. One way is displaying the distribution of the singular values (as function of numbers) to see if there is any abrupt decrease of the singular values. Another method is the so called Levenberg-Marquardt stablization technique (Lawson and Hanson, 1974) which is used to judge whether small eigenvalues contribute significantly to a reduction in residual variance without inordinate increases in parameter variance. A more direct (but after solution solving) method is to examine whether the solutions including the small eigenvalues are significant compared with the solution errors. For the problem in this work, it is shown that by all three judgements (see Figs.3.10, 3.11 and solutions in Chapter 4) it is full rank or really overdetermined.

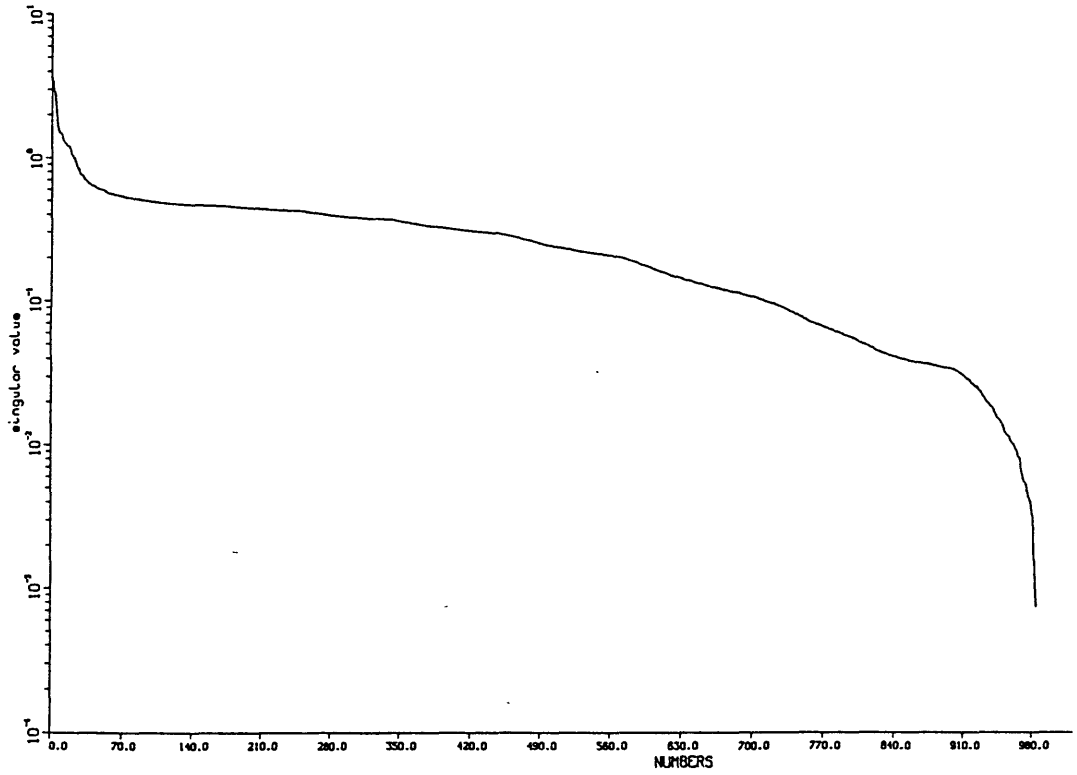

Fig.3.10 Singular Value Dirtributions for the Advective-Diffusive Model

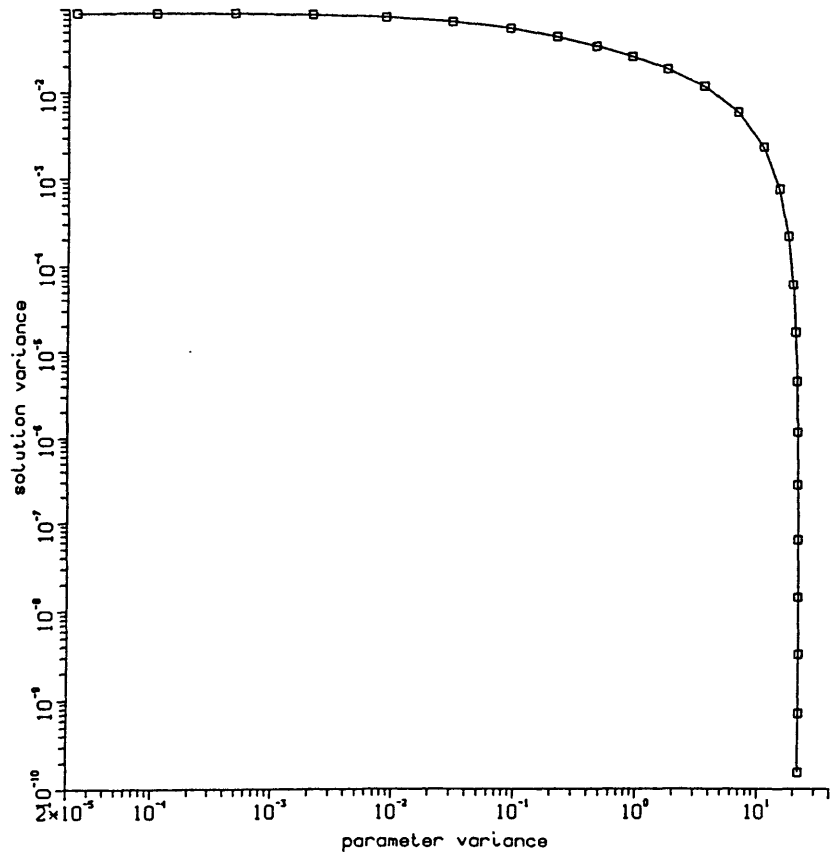

Fig.3.11 Solution Variance v.s. Parameter Variance

Data Resolution and Solution Resolution

After having the rank decided, the SVD solution for the weighted set of Eq.(3.73) is obtained as

$$\hat{X}_{N\times 1} = V_{N\times K}\Lambda^{-1}_{K\times K}U^T_{K\times M}Y_{M\times 1} \tag{3.86}$$

where only the first K eigenvalues and eigenvectors are used. Using the estimated solution $\hat{X}$, the estimated value for the Y is

$$\hat{Y} = A\hat{X} = U_{M\times K}\Lambda V^T_{K\times N}\cdot V_{N\times K}\Lambda^{-1}_{K\times K}U^T_{K\times M}Y_{M\times 1} = U_{M\times K}U^T_{K\times M}Y \tag{3.87}$$

This relation shows that if some diagonal values of the matrix UU^T equal one, then the corresponding estimated values of $\hat{Y}$ are exactly those of Y, or the cooresponding residuals are zeros. This means that these equations are exactly satisfied. On the contrary, however the equations corresponding to small diagonal values of UU^T have large residuals and are less satsfied. Thus matrix UU^T is called Data Resolution, and its diagonal values signify the contributions of the equations to the solutions. The data resolutions for the Advective- Diffusive model are ploted in Fig.3.12, which shows that the Dynamic Equations contribute most to the solutions.

A relation between the estimated solution $\hat{X}$ and its *real* value X can also be established as follows:

$$\hat{X} = V\Lambda^{-1}U^TY = V\Lambda^{-1}U^TAX = V\Lambda^{-1}U^TU\Lambda V^TX = VV^TX \tag{3.88}$$

The physical explanation for the matrix VV^T is that its diagonal values signify the extent to which the unknowns are resolved: large values indicate that the corresponding

unknowns are more like their true values and thus are well resolved, and vice versa. Therefore the matrix VV^T is called Solution Resolution matrix. For a real overdetermined system, $K = N$ and $VV^T = I$ and thus all the unknowns are fully determined (of course with their individual error bounds).

Error Bounds on the Solutions

Without any a *priori* knowledge about the correlations between the data noise (or residuals) of the equations, we assume that they are not correlated. With this assumption, the error variance for the solutions are determined by (e.g. Wunsch, 1978)

$$E = \epsilon^2 V \Lambda^{-2} V^T \tag{3.89}$$

where ϵ^2 is the expected error determined from the residual imbalances in the equations (Lawson and Hansen, 1974).

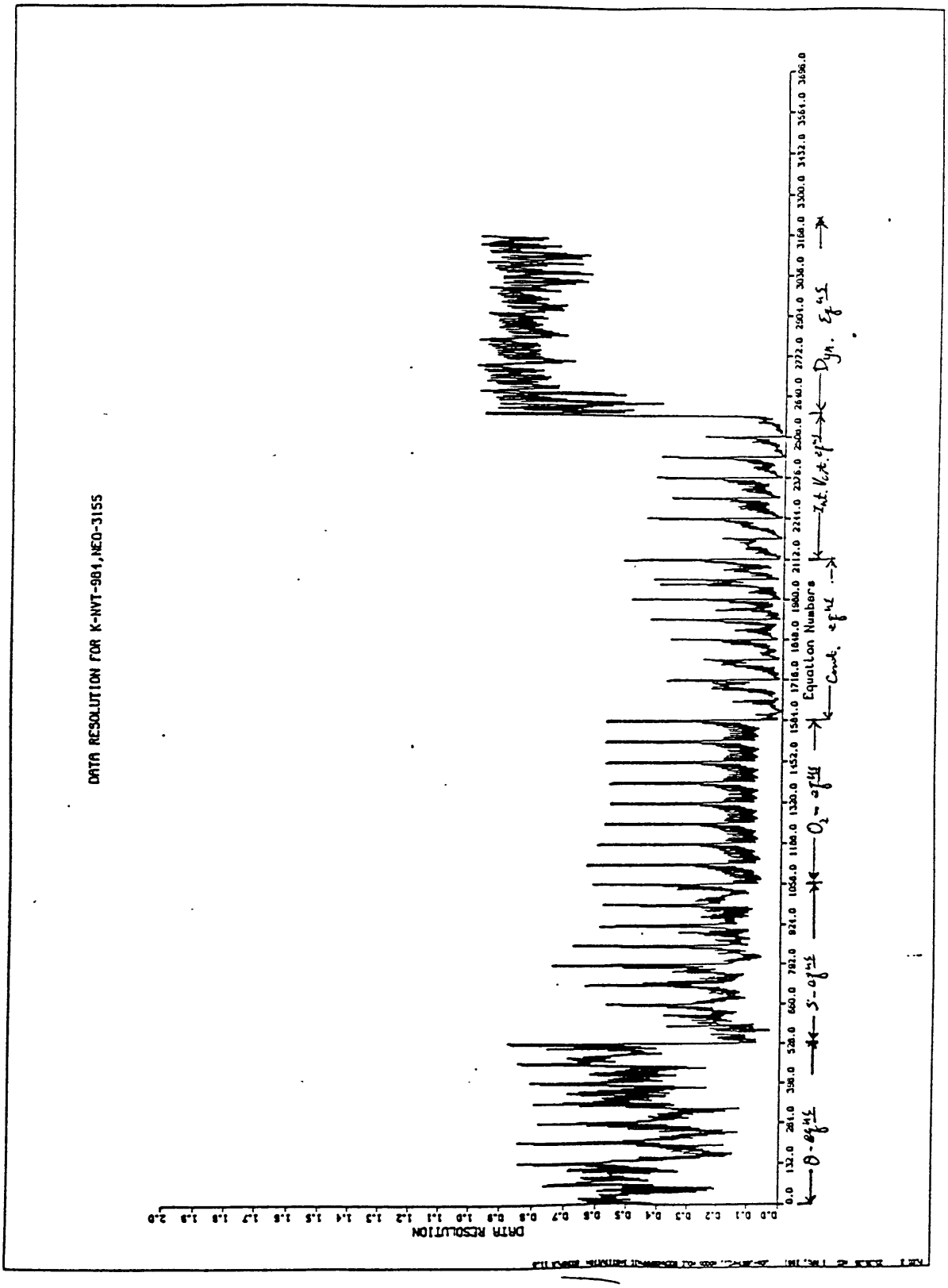

Fig.3.12 Data Resolutions for the Advective-Diffusive case

Chapter 4

RESULTS AND DISCUSSIONS

4.1 Introduction

The problem posed in the last chapter, i.e. the weighted set of eq.(3.73) augmented by the positive constraints of eq.(3.74), is now solved by the methods and programs given in Lawson and Hansen (1974). We have proposed three models for the water mass balances in the Brazil Basin, namely the Purely Advective (PADV hereafter) model (actually it is *lateral* advective model, because the diapycnal advection vanishes without diffusion as shown before), Advective-Diffusive (AVDF hereafter) model with the same diffusivities for heat and salt, and the Double Diffusion (DDF hereafter) model (i.e. advective-diffusive model with different diapycnal diffusivities for heat and salt by considering the possible double diffusion effects). Comparisons between the results of the PADV (Fig.4.1) and the AVDF (Fig.4.3) models show that both give similar circulation patterns on all the isopycnal surfaces, with only minor differences in magnitudes.

One direct method to judge the effectiveness of the model is to look at the solution errors. With less unknowns, if the PADV model is at least as physically realistic as the AVDF model, in which more unknowns (the diffusive parameters) are to be solved, one would expect that the solution errors for the streamfunctions should be smaller in the PADV model than in the AVDF model. However, the opposite is true. The

results show that the streamfunctions in the PADV model have larger errors. This means that larger residuals are left in the PADV model. But the slight error differences in Fig.4.1 and Fig.4.3 may not convince one that the AVDF model is better than the PADV model. Another more efficient way to judge the superiority of the model is to analyze the residuals. Usually some physics can be attached to the interpretations of the residuals: significant structures often represent the missing physical terms in the equations. There are large-scale significant amplitude structures in the residuals of the PADV results (see Fig.4.2), this suggests that some significant physical processes, namely the diffusion processes, have been left out of the model. On the contrary, the residuals in the AVDF results are rather small compared with the proposed physical terms, and are more or less *randomly* distributed (Fig.4.4). These small residuals represent the data noise and unimportant terms left out of the equations. With the above arguments the analysis evidently indicates that the purely advective model cannot sufficiently describe the water property balances.

The circulations resulting from the DDF model and from the AVDF model have not only similar flow patterns, but also similar magnitudes. Comparison of Fig.4.3 with Fig.4.6 shows that they are almost identical as far as the circulation is concerned. However, there are some differences in the diffusion parameters in the two models. We will depict our results based on the AVDF model in this section, and the effectiveness of the possible double diffusion and its roles will be explored later on.

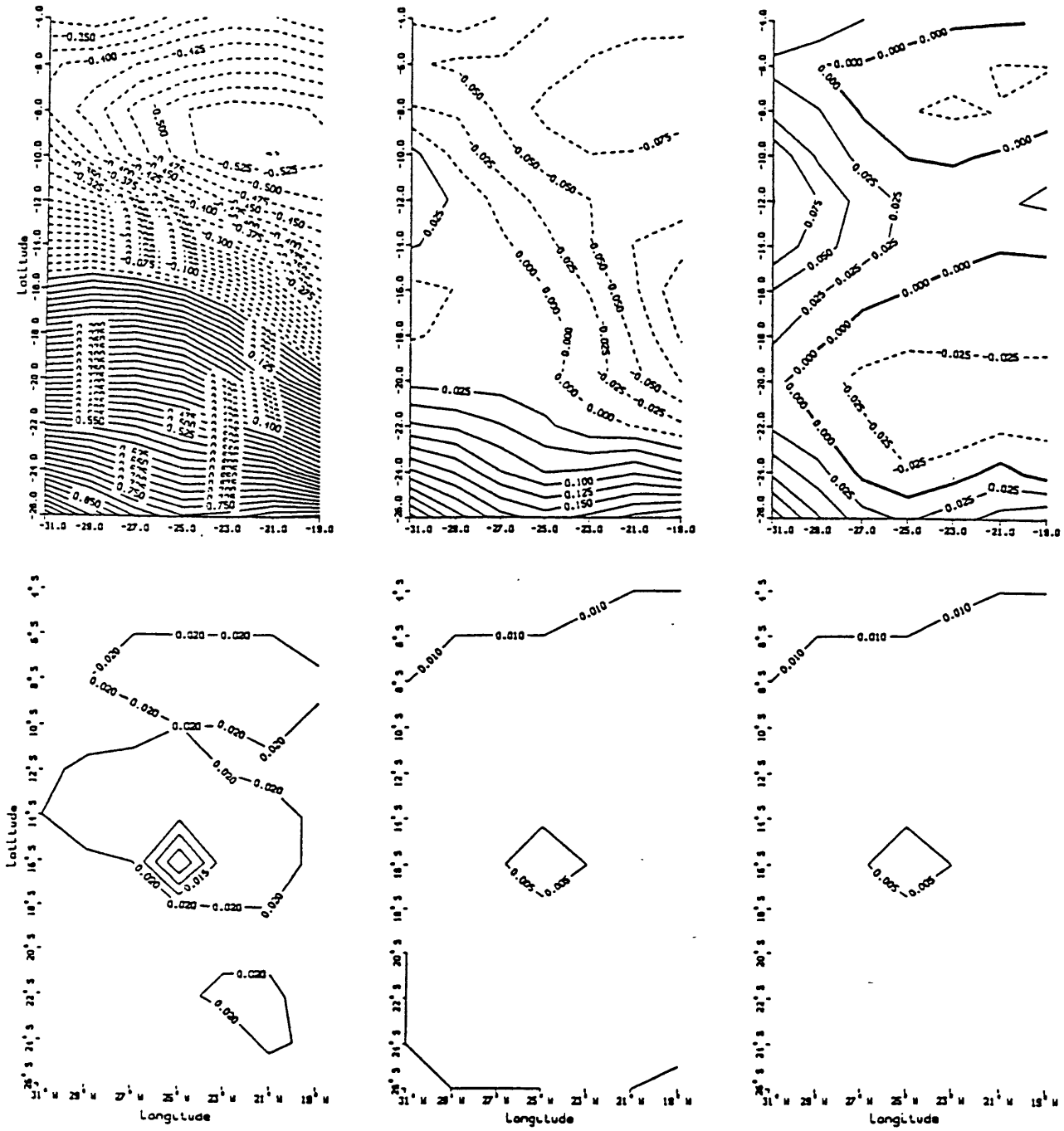

(a)Level 1 (b)Level 2 (c)Level 3

Fig.4.1. Purely Advective Model Results: Streamfunction (upper) and its expected error (lower) Contours On the 8 Isopycnals. Unit: m^2/s^2

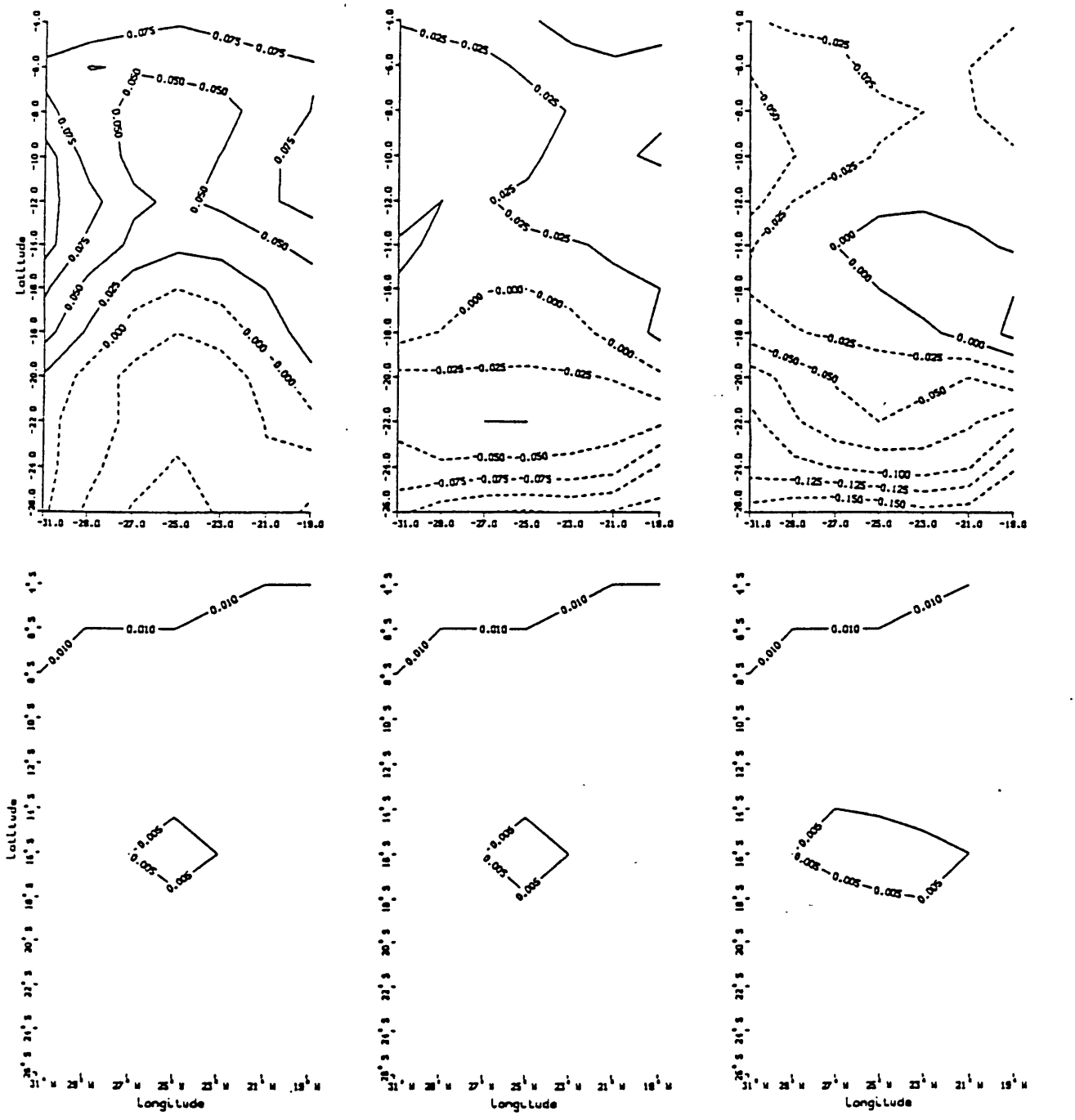

(d)Level 4 (e)Level 5 (f)Level 6

Fig.4.1 (continued)

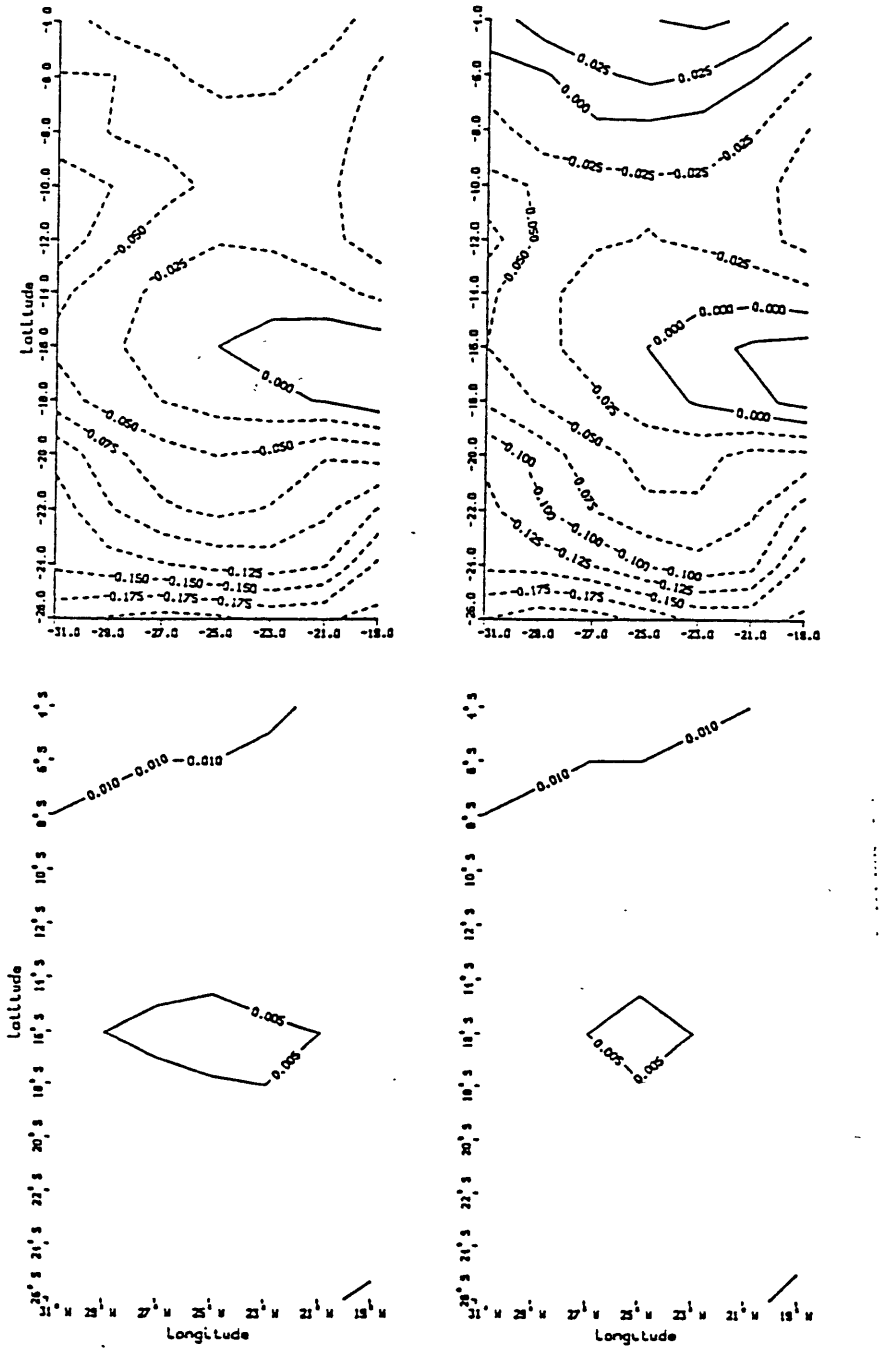

(g)Level 7 (h)Level 8

Fig.4.1 (continued)

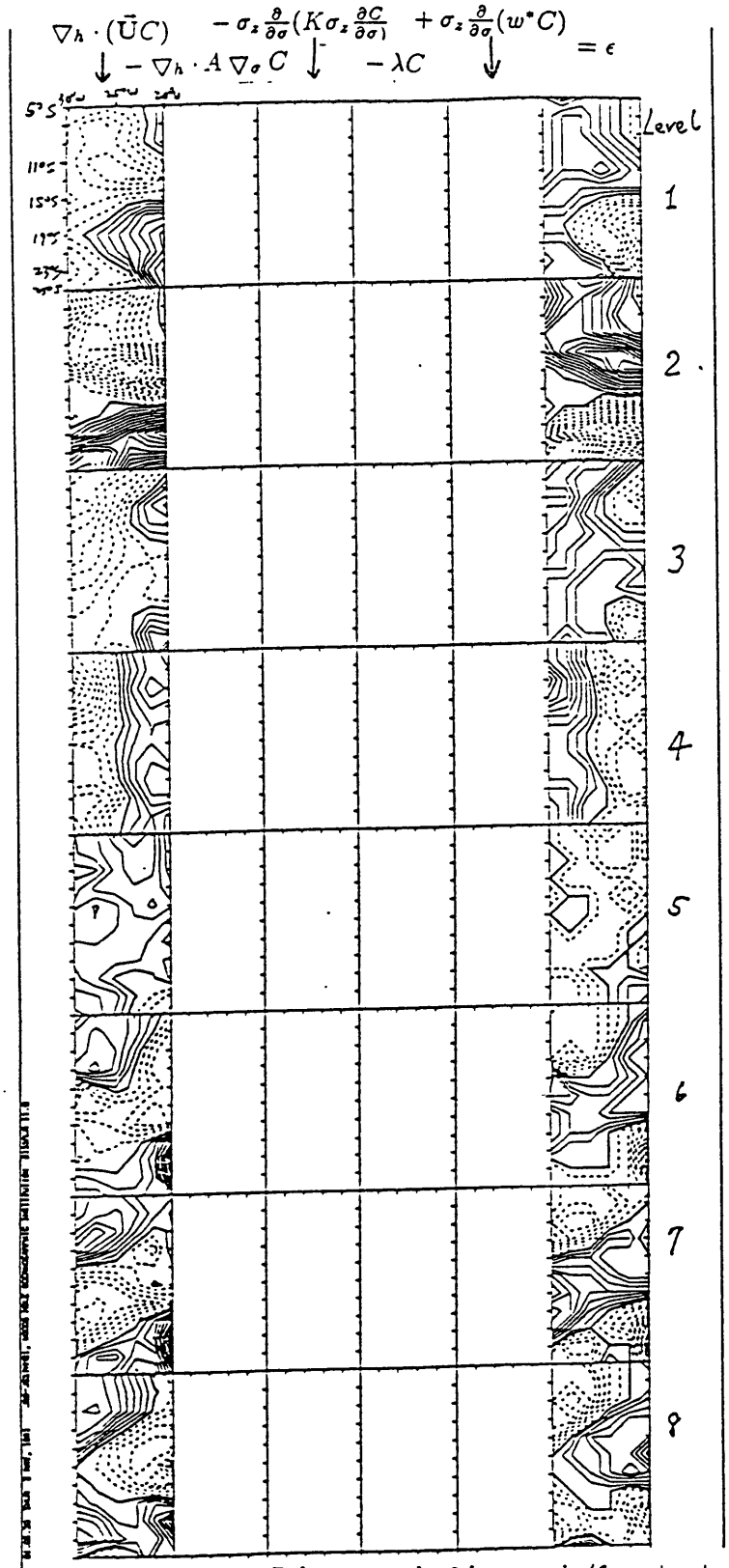

Fig.4.2a Potential Temperature Balances on the 8 isopycnals (from top to bottom panels) from the PADV model. Contour interval=.005 units

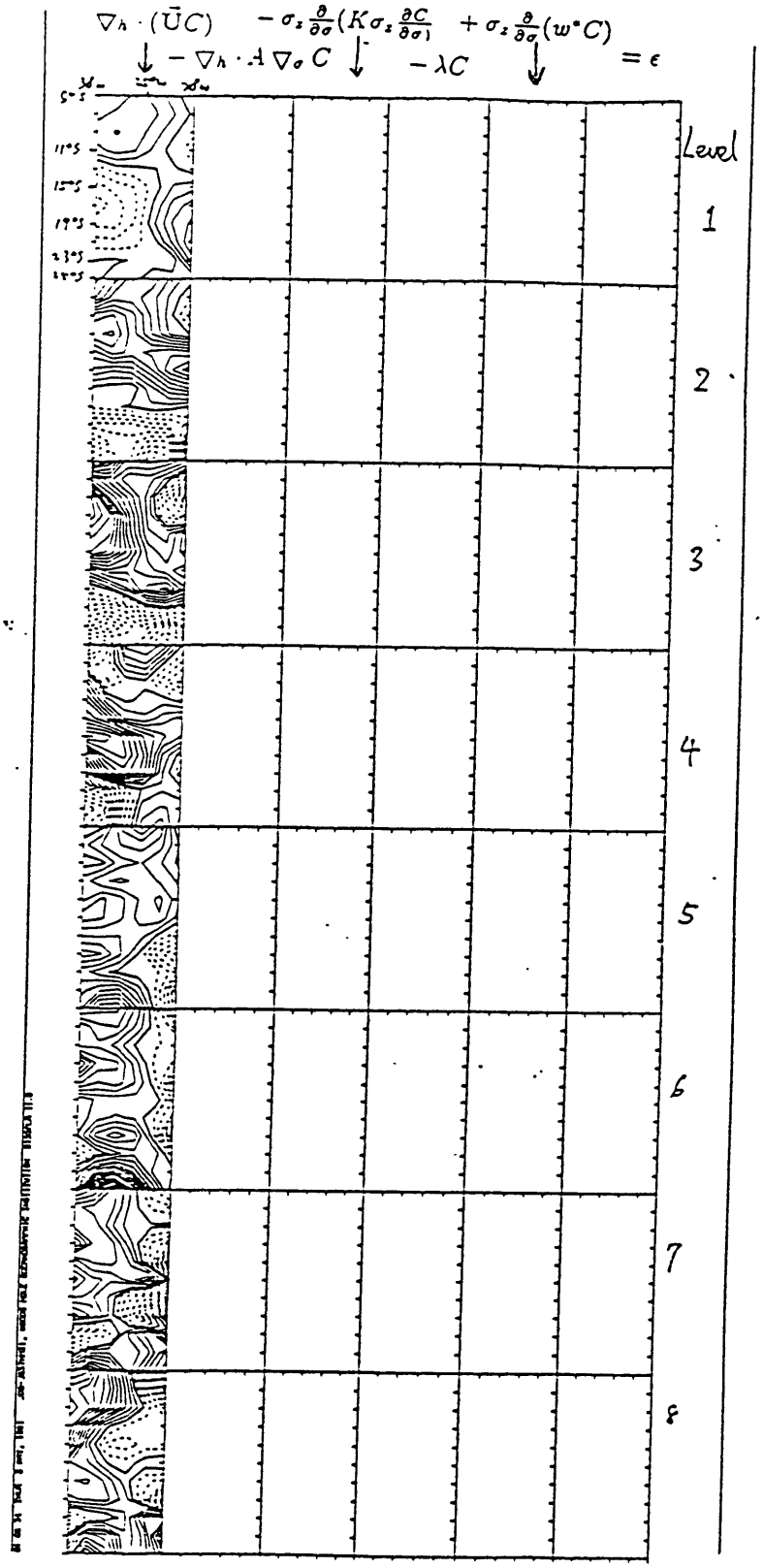

Fig.4.2b Oxygen Balances on the 8 isopycnals (from top to bottom panels) from the PADV model. Contour interval= .0005 units

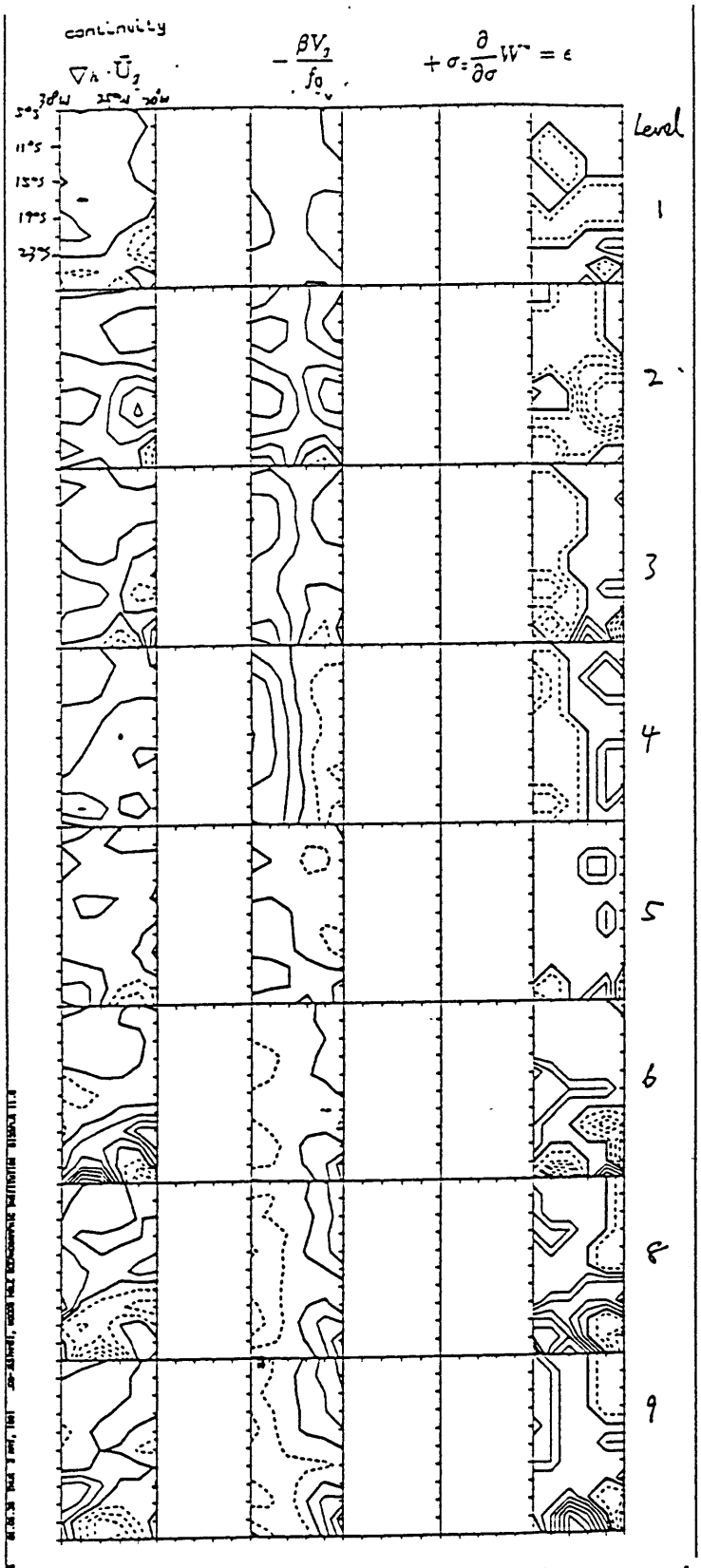

Fig.4.2c Continuity Equation Balances on the 8 isopycnals (from top to bottom panels) from the PADV model. Contour interval=.005 units

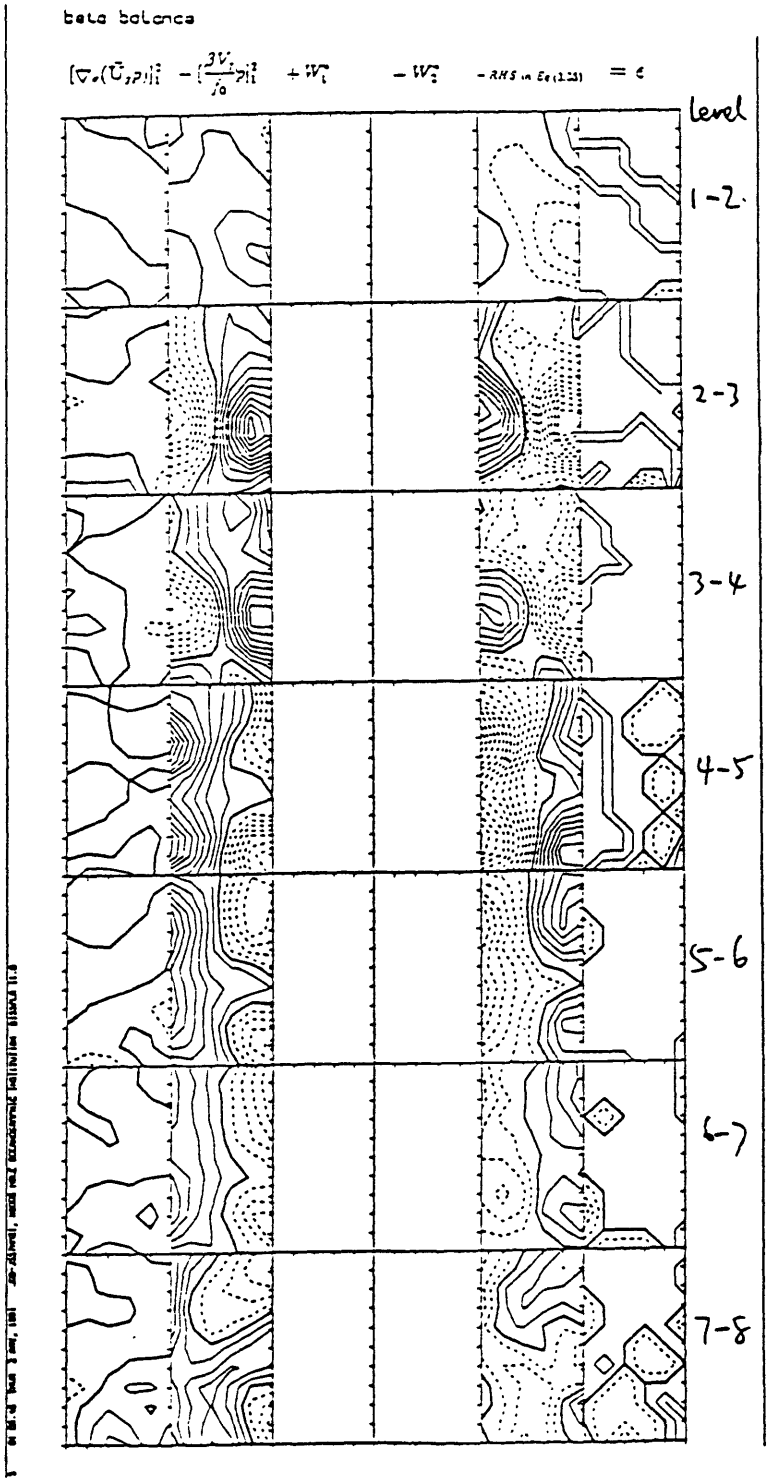

Fig.4.2d Integrated Vorticity Equation Balances on the 8 isopycnals (from top to bottom panels) from the PADV model. Contour interval=.005 units

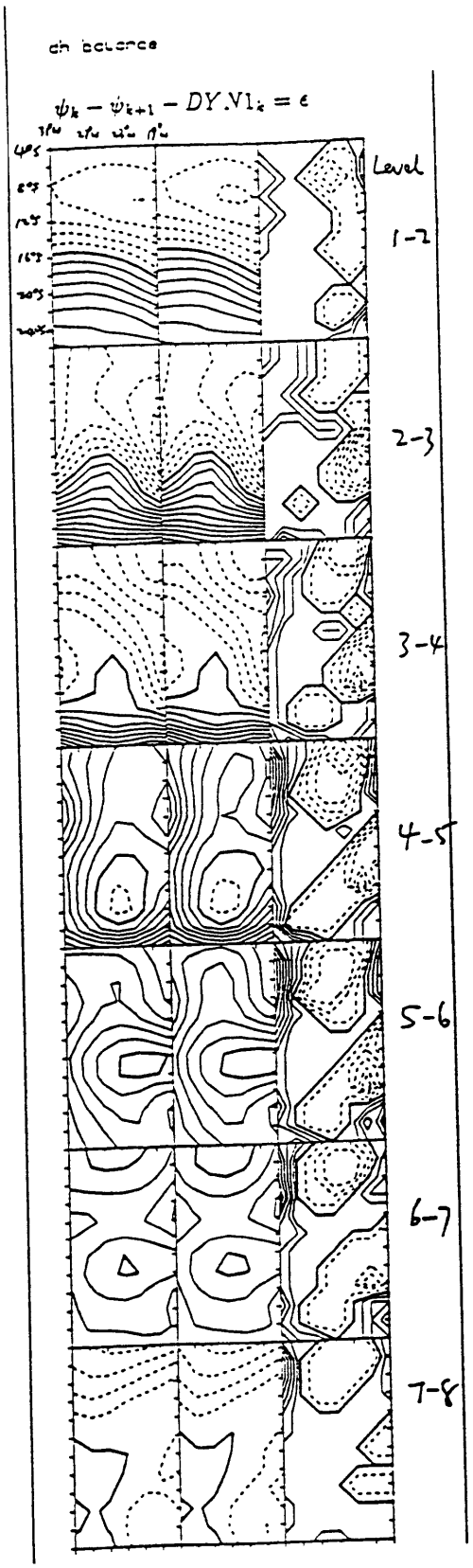

Fig.4.2e Dynamic Equation Balances on the 8 isopycnals (from top to bottom panels) from the PADV model. Contour interval=.005 units

4.2 Circulations Of The Water Masses In The Brazil Basin

Description of the Circulations The contours of streamfunction (for $f\vec{\mathbf{U}}$) on the eight isopycnals in the rectangular region in the Brazil Basin are shown in Figs.4.3, which will be discussed from the top to the deepest level. In this small area, one isopycnal usually represents one water mass, but different water masses may appear on the same isopycnal in different regions on certain special isopycnals, as we will see later on.

The isopycnal level in the thermocline of $\sigma_0 = 26.88$, which represents the South Atlantic Central Water, has gyre-like pressure contours (Fig.3.6a): it is shallowest near 7°S (about 250 *dbar*), and deepens to about 325 *dbar* at 3°S and to 550 *dbar* at 27°S. The circulation also has a gyre-like pattern (Fig.4.3a), but the gyre is centered a little south (at about (10°S, 21°W)). South of 12°S, the flows are nearly zonal and towards the west, with a zonal velocity of about 1.5 cm/s (Table.4.1). Nearer the equator (around 5°S), flows are zonally towards the east with the velocity of about 3 cm/s (Note that the gradients (spacing) of the streamfunction contour lines marks the strength of the quantity $f\vec{\mathbf{U}}$, thus the actual velocity near equator (where f is smaller) is stronger than it appears). It seems that the gyre system extends to the three immediate lower isopycnals (levels 2, 3, and 4), but the gyre center shifts southward as it deepens: near 16°S on level 2, 22°S on level 3, and 25°S on level 4. It disappears on the next level ($\sigma_2 = 36.94, \sim 1900 dbar$), but water mass analysis (to follow) shows that the southern eastward flow may be the extension of this gyre centered south of this area. At greater depths, another kind of (anticyclonic) gyre appears: it lies near 16°S on $\sigma_2 = 37.00$, and maintains and becomes stronger with depth ($\sigma_3 = 41.46, \sigma_3 = 41.50$).

Table 4.1 u and v-components of the lateral velocity (cm/s)

u						v					
level=			1								
3.132	3.322	3.609	3.095	3.061	2.955	-0.273	0.814	1.190	0.525	0.000	-0.496
0.278	1.025	1.582	2.050	2.278	2.531	0.685	0.964	0.752	0.417	0.123	-0.341
-1.045	-0.513	-0.128	0.217	0.483	0.572	1.258	1.188	1.002	0.647	0.223	-0.081
-1.729	-1.932	-1.713	-1.406	-1.164	-0.897	1.101	1.216	1.146	0.819	0.372	0.078
-1.919	-2.317	-2.523	-2.386	-1.892	-1.350	0.484	0.918	1.107	0.992	0.727	0.429
-1.668	-2.056	-2.479	-2.687	-2.389	-1.668	0.047	0.417	0.743	1.023	1.250	0.990
-1.582	-1.804	-1.930	-1.909	-1.883	-1.741	-0.137	0.049	0.444	0.949	1.401	1.452
-1.464	-1.393	-1.374	-1.416	-1.525	-1.809	-0.098	-0.031	0.372	0.871	1.178	1.266
-1.282	-1.192	-1.166	-1.390	-1.812	-2.108	-0.001	0.048	0.311	0.558	0.781	0.871
-1.255	-1.085	-1.006	-1.156	-1.429	-1.721	0.142	0.174	0.270	0.148	0.373	0.548
-1.751	-1.547	-1.328	-1.204	-1.401	-1.872	0.305	0.390	0.344	0.023	-0.032	0.084
level=			2								
1.292	1.610	1.203	0.338	1.044	1.009	-0.036	0.303	0.577	0.533	0.370	0.451
-0.620	-0.253	0.329	0.544	0.405	0.215	0.398	0.395	0.380	0.357	0.249	0.130
-0.818	-0.414	-0.345	-0.306	-0.246	-0.217	0.659	0.660	0.534	0.270	0.128	0.020
-0.323	-0.509	-0.396	-0.299	-0.194	-0.032	0.636	0.651	0.501	0.287	0.193	0.108
0.213	-0.069	-0.281	-0.178	0.069	0.288	0.226	0.425	0.461	0.401	0.345	0.276
0.453	0.292	0.042	-0.149	-0.083	0.131	0.053	0.087	0.239	0.430	0.526	0.439
0.053	0.021	-0.005	-0.037	-0.095	-0.105	-0.022	-0.043	0.061	0.317	0.544	0.519
-0.033	0.057	0.104	0.076	-0.047	-0.237	0.023	-0.022	0.060	0.223	0.376	0.387
-0.211	-0.151	-0.077	-0.086	-0.219	-0.435	0.078	0.076	0.082	0.140	0.148	0.138
-0.525	-0.418	-0.343	-0.383	-0.541	-0.639	0.148	0.170	0.132	-0.024	-0.061	0.001
-1.025	-0.909	-0.828	-0.839	-0.850	-0.883	0.253	0.284	0.165	-0.072	-0.141	-0.055
level=			3								
1.415	1.681	1.239	1.026	1.115	0.991	0.386	0.429	0.384	0.326	0.303	0.259
-0.569	-0.315	0.190	0.367	0.202	0.063	0.643	0.387	0.242	0.227	0.148	0.015
-0.828	-0.424	-0.375	-0.365	-0.335	-0.375	0.789	0.611	0.384	0.150	0.018	-0.054
-0.348	-0.420	-0.275	-0.186	-0.170	-0.129	0.835	0.624	0.376	0.156	0.026	-0.054
0.267	0.130	0.021	0.069	0.171	0.260	0.533	0.510	0.376	0.208	0.060	0.039
0.596	0.518	0.381	0.214	0.173	0.226	0.399	0.306	0.229	0.166	0.128	0.098
0.327	0.295	0.269	0.243	0.174	0.105	0.310	0.211	0.105	0.056	0.097	0.090
0.308	0.322	0.303	0.261	0.185	0.066	0.286	0.171	0.071	0.006	-0.013	-0.007
0.159	0.116	0.116	0.103	0.060	-0.013	0.228	0.161	0.042	-0.027	-0.100	-0.114
-0.142	-0.114	-0.079	-0.087	-0.146	-0.134	0.180	0.167	0.059	-0.068	-0.158	-0.105
-0.620	-0.558	-0.489	-0.463	-0.423	-0.398	0.201	0.220	0.104	-0.093	-0.138	-0.068
level=			4								
1.522	1.822	1.345	1.079	1.185	1.062	0.193	0.133	-0.015	-0.133	-0.148	-0.067
-0.278	-0.051	0.405	0.544	0.367	0.266	0.528	0.168	-0.104	-0.112	-0.149	-0.201
-0.483	-0.079	-0.039	-0.030	0.030	0.020	0.697	0.420	0.081	-0.112	-0.197	-0.175
-0.186	-0.202	-0.032	0.081	0.097	0.097	0.814	0.465	0.142	-0.053	-0.131	-0.184
0.199	0.185	0.178	0.240	0.274	0.288	0.614	0.448	0.224	0.019	-0.127	-0.128
0.471	0.471	0.465	0.381	0.298	0.244	0.540	0.377	0.200	-0.009	-0.135	-0.128
0.306	0.301	0.316	0.322	0.258	0.158	0.454	0.359	0.165	-0.072	-0.202	-0.186
0.422	0.374	0.303	0.251	0.223	0.142	0.387	0.298	0.122	-0.085	-0.255	-0.278
0.379	0.245	0.164	0.138	0.168	0.181	0.253	0.191	0.038	-0.083	-0.227	-0.332
0.185	0.130	0.118	0.134	0.138	0.229	0.117	0.100	0.017	-0.069	-0.185	-0.227
-0.124	-0.135	-0.102	-0.066	0.015	0.088	0.049	0.084	0.048	-0.041	-0.107	-0.105
level=			5								
1.522	1.681	1.132	0.867	0.955	0.814	-0.495	-0.407	-0.422	-0.392	-0.089	0.377
-0.076	-0.025	0.329	0.443	0.278	0.228	-0.108	-0.341	-0.412	-0.294	-0.112	0.145
-0.286	-0.020	-0.030	-0.010	0.118	0.168	0.021	-0.081	-0.191	-0.236	-0.112	0.137
-0.162	-0.218	-0.073	0.081	0.170	0.162	0.144	0.002	-0.098	-0.090	0.008	0.051
0.000	0.048	0.082	0.151	0.151	0.130	0.053	0.064	0.025	0.026	-0.012	0.035
0.209	0.286	0.328	0.262	0.161	0.071	0.128	0.096	0.056	-0.009	-0.078	-0.009
0.211	0.200	0.216	0.216	0.185	0.127	0.123	0.143	0.050	-0.072	-0.137	-0.087
0.436	0.336	0.232	0.199	0.227	0.218	0.052	0.078	0.007	-0.061	-0.131	-0.139
0.383	0.228	0.151	0.142	0.207	0.293	-0.093	-0.048	-0.059	-0.033	-0.048	-0.122
0.280	0.292	0.308	0.328	0.339	0.450	-0.177	-0.103	-0.061	-0.013	0.017	0.031
0.212	0.281	0.358	0.398	0.445	0.456	-0.130	-0.046	-0.009	0.004	0.063	0.110
level=			6								
1.362	1.274	0.566	0.354	0.655	0.690	-0.784	-0.511	-0.378	-0.207	0.274	0.754
0.013	-0.076	0.202	0.316	0.202	0.202	-0.499	-0.568	-0.435	-0.063	0.275	0.480
-0.197	0.039	0.010	0.000	0.079	0.089	-0.372	-0.321	-0.231	-0.061	0.193	0.402
-0.267	-0.339	-0.210	-0.057	0.024	-0.040	-0.195	-0.222	-0.139	0.034	0.225	0.213
-0.178	-0.123	-0.103	-0.123	-0.240	-0.295	-0.245	-0.127	-0.037	0.074	0.112	0.147
0.083	0.119	0.131	0.036	-0.113	-0.262	-0.161	-0.077	-0.036	-0.045	-0.051	0.079
0.211	0.185	0.185	0.195	0.190	0.148	-0.165	-0.038	-0.050	-0.105	-0.132	-0.031
0.526	0.459	0.374	0.360	0.426	0.464	-0.185	-0.093	-0.074	-0.071	-0.083	-0.070
0.443	0.323	0.254	0.250	0.323	0.422	-0.260	-0.187	-0.124	-0.028	0.030	-0.030
0.312	0.367	0.383	0.383	0.367	0.438	-0.272	-0.211	-0.133	-0.013	0.073	0.104
0.252	0.332	0.420	0.445	0.456	0.438	-0.182	-0.127	-0.086	-0.024	0.076	0.146
level=			7								
1.398	1.256	0.548	0.442	0.849	0.938	-1.183	-0.674	-0.400	-0.170	0.511	1.191
0.190	0.127	0.468	0.607	0.468	0.468	-0.811	-0.676	-0.401	0.030	0.446	0.829
0.039	0.345	0.296	0.246	0.306	0.306	-0.560	-0.373	-0.198	-0.009	0.306	0.685
-0.154	-0.234	-0.137	0.016	0.113	0.016	-0.280	-0.277	-0.146	0.074	0.315	0.407
-0.267	-0.233	-0.226	-0.274	-0.418	-0.494	-0.321	-0.198	-0.064	0.103	0.183	0.268
-0.018	-0.024	-0.042	-0.131	-0.280	-0.459	-0.265	-0.162	-0.079	-0.021	-0.013	0.160
0.195	0.148	0.153	0.153	0.164	0.169	-0.302	-0.133	-0.094	-0.083	-0.084	0.045
0.587	0.535	0.474	0.483	0.564	0.611	-0.331	-0.164	-0.100	-0.052	-0.007	0.025
0.486	0.396	0.344	0.331	0.374	0.456	-0.372	-0.230	-0.129	-0.014	0.086	0.063
0.324	0.418	0.434	0.418	0.383	0.430	-0.321	-0.233	-0.137	-0.025	0.100	0.174
0.292	0.401	0.496	0.522	0.536	0.500	-0.171	-0.131	-0.098	-0.044	0.092	0.175
level=			8								
1.734	1.575	0.955	0.991	1.592	1.787	-1.524	-0.866	-0.393	-0.059	0.637	1.450
0.380	0.354	0.810	1.050	0.949	0.949	-1.109	-0.735	-0.293	0.219	0.628	1.011
0.266	0.621	0.621	0.562	0.582	0.503	-0.794	-0.337	-0.047	0.155	0.429	0.772
0.040	-0.024	0.048	0.178	0.210	0.016	-0.432	-0.226	-0.021	0.175	0.353	0.378
-0.158	-0.103	-0.123	-0.240	-0.466	-0.617	-0.394	-0.176	0.015	0.128	0.136	0.158
0.060	0.054	-0.018	-0.173	-0.352	-0.518	-0.285	-0.167	-0.064	-0.075	-0.087	0.036
0.243	0.200	0.158	0.121	0.132	0.195	-0.286	-0.165	-0.153	-0.160	-0.150	0.003
0.549	0.502	0.422	0.426	0.554	0.658	-0.291	-0.209	-0.204	-0.112	-0.029	0.065
0.435	0.349	0.306	0.280	0.293	0.374	-0.326	-0.271	-0.235	-0.078	0.091	0.132
0.351	0.442	0.422	0.387	0.351	0.383	-0.265	-0.283	-0.253	-0.102	0.091	0.234
0.365	0.456	0.544	0.558	0.551	0.493	-0.122	-0.200	-0.231	-0.125	0.068	0.208

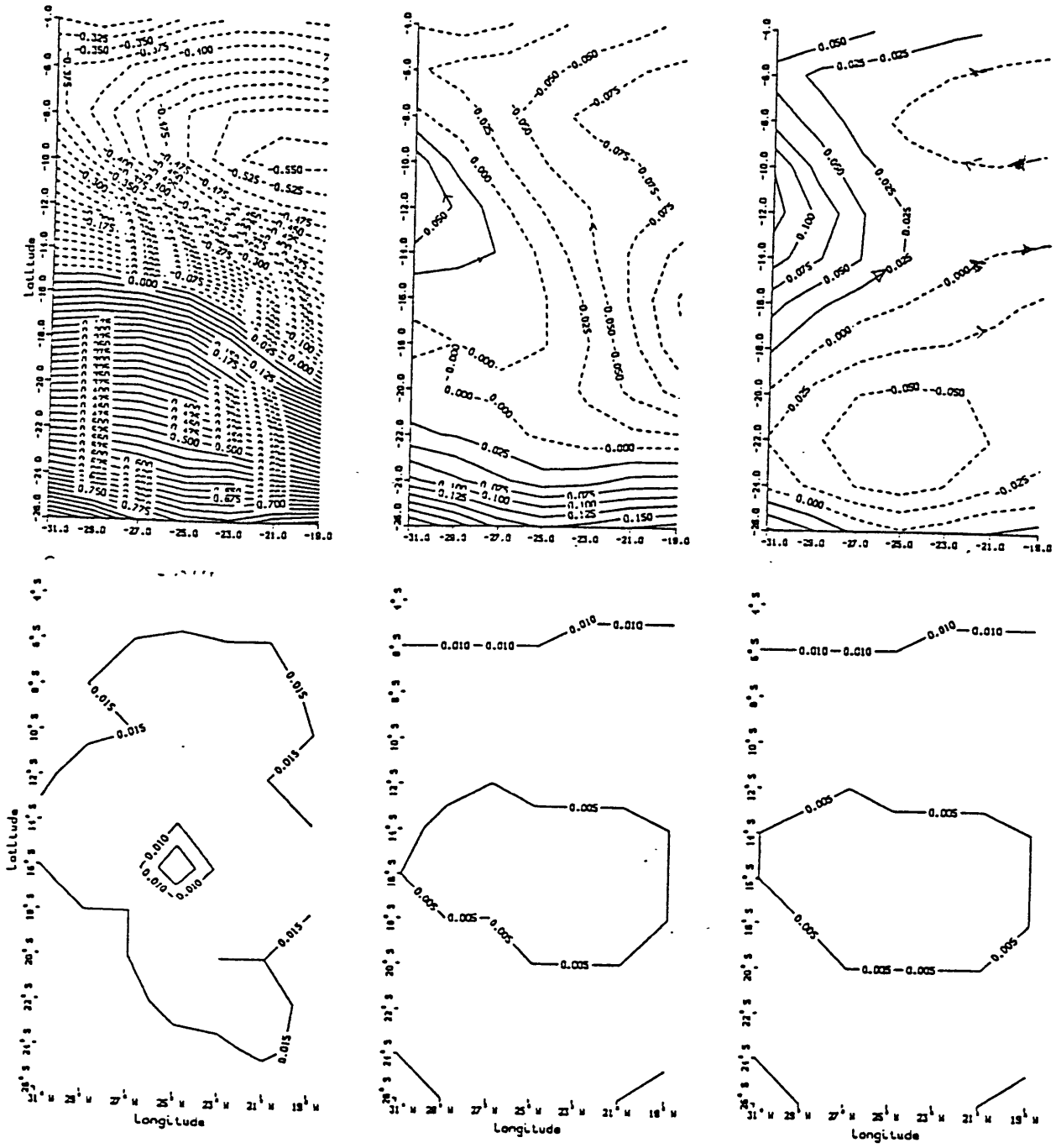

(a)Level 1 (b)Level 2 (c)Level 3

Fig.4.3. Advective-Diffusive Model Results: Streamfunction (upper) and its expected error (lower) Contours On the 8 Isopycnals. Unit: m^2/s^2

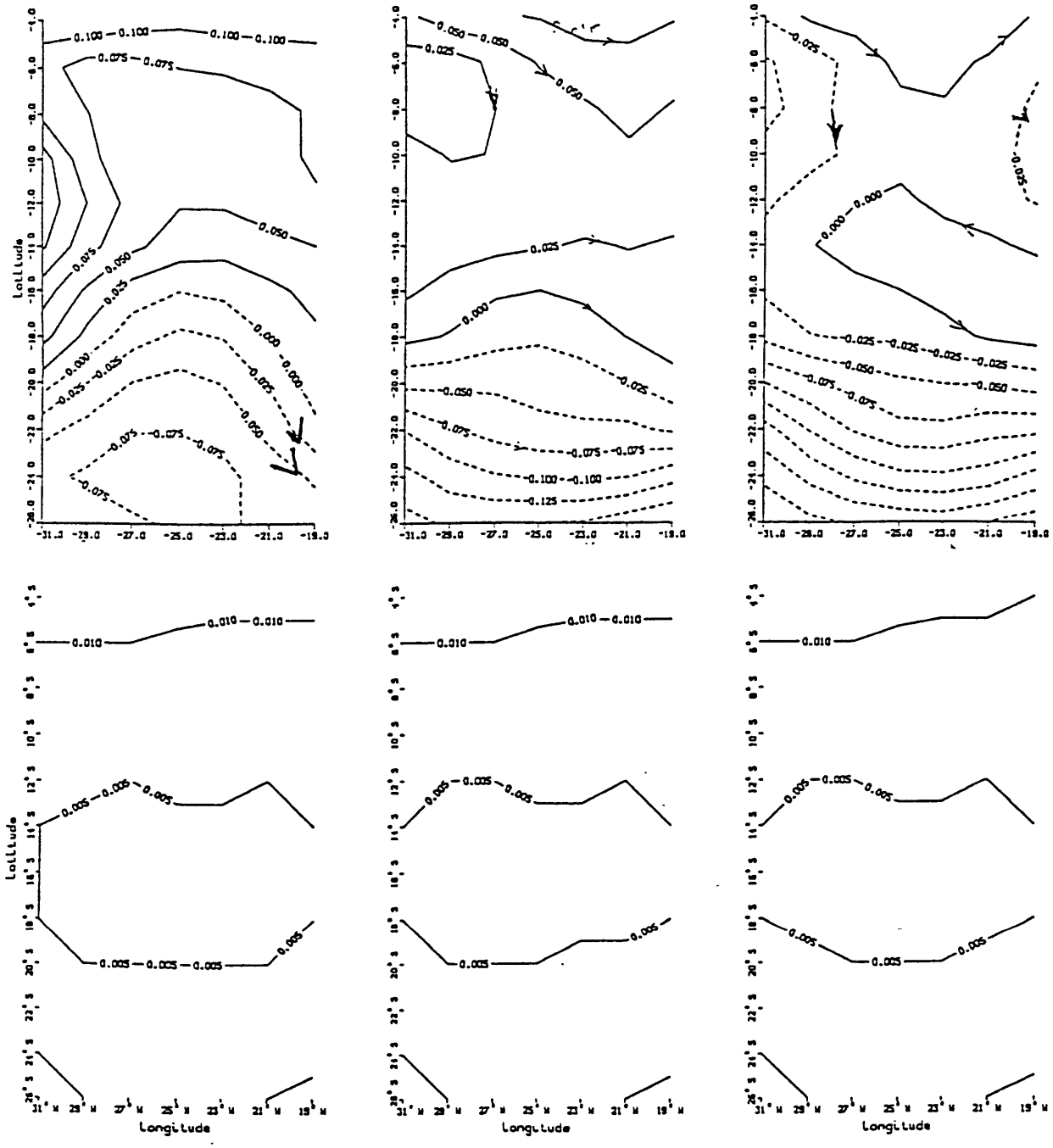

(d)Level 4 (e)Level 5 (f)Level 6

Fig.4.3 (continued)

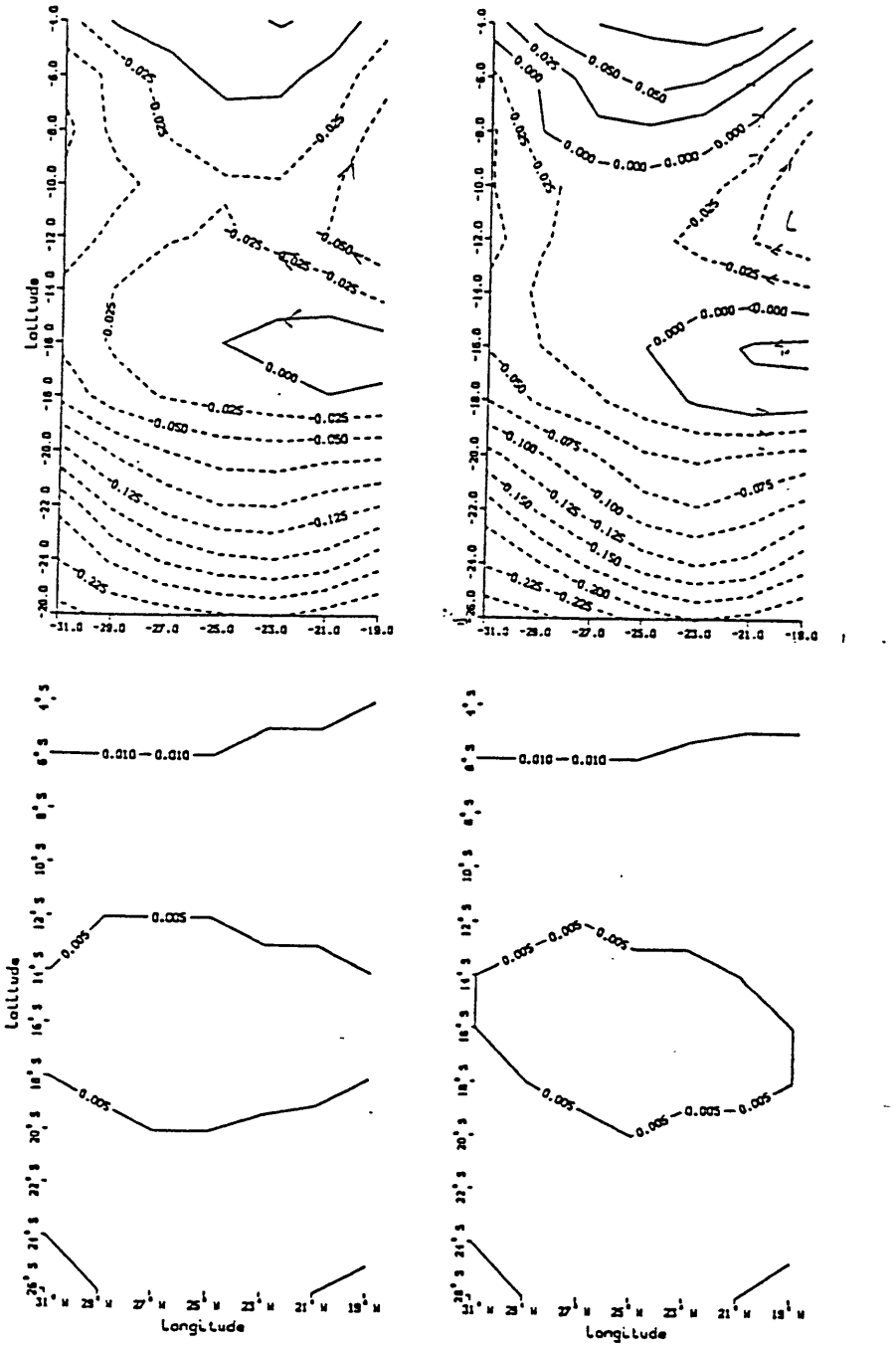

(g)Level 7 (h)Level 8

Fig.4.3 (continued)

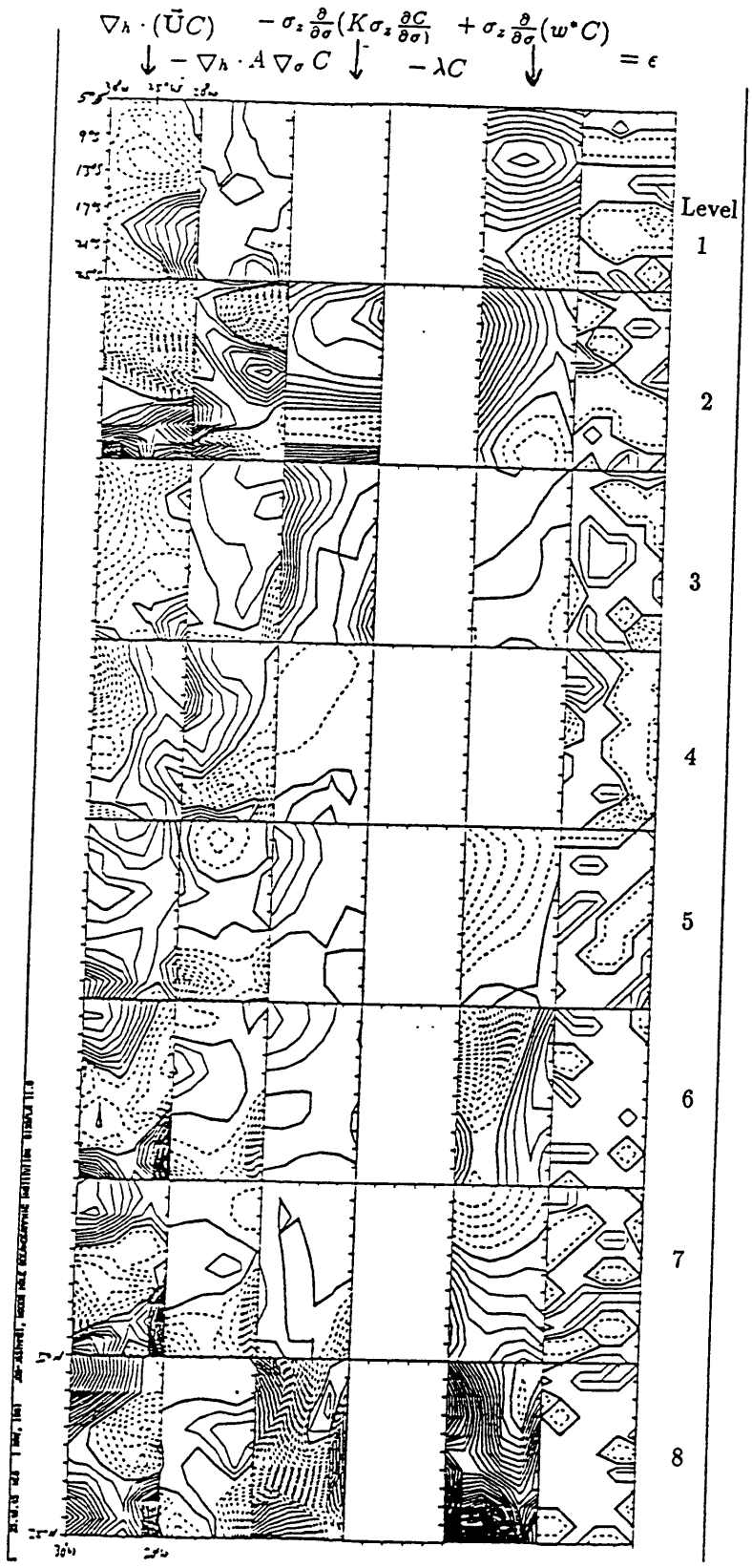

Fig.4.4a Potential Temperature Balances on the 8 isopycnals (from top to bottom panels) from the AVDF model. Contour interval=.005 units

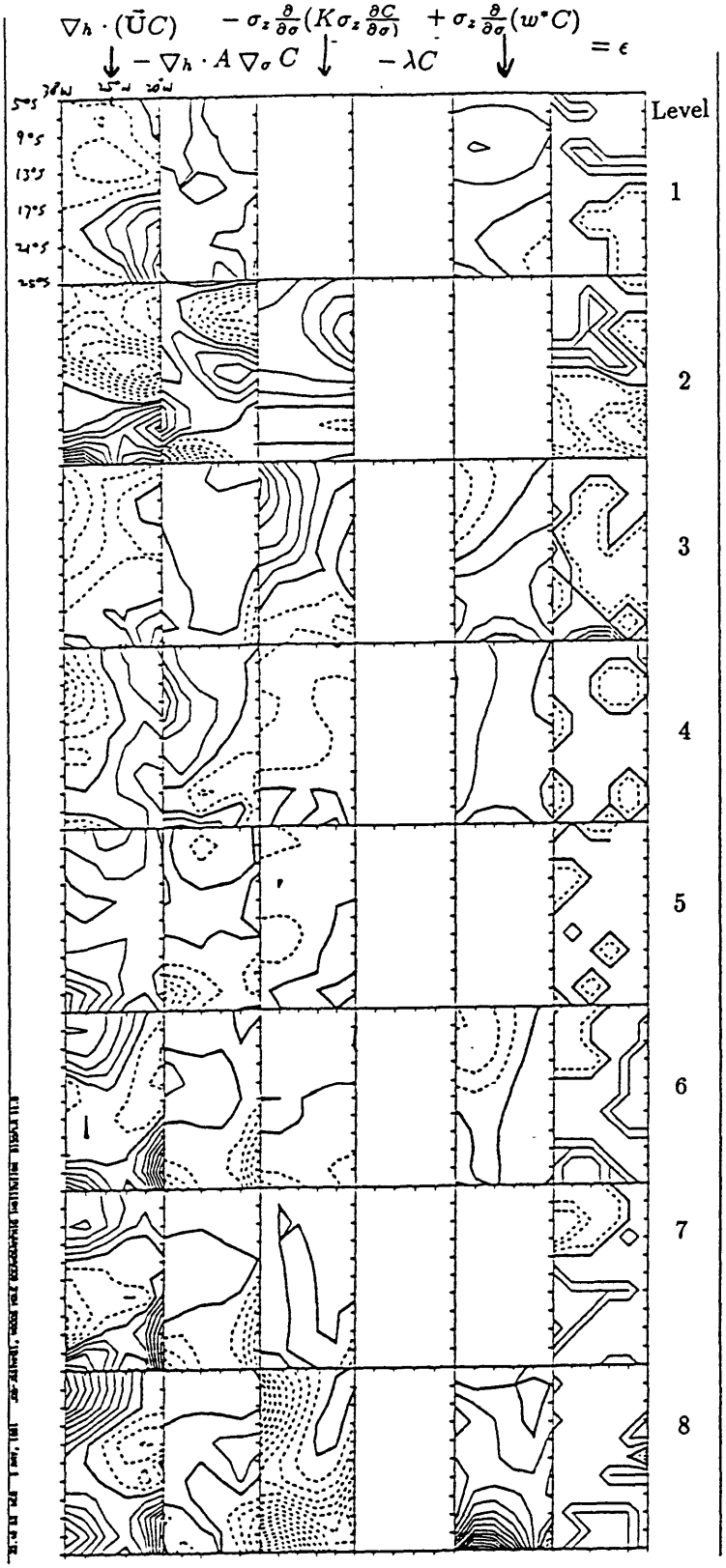

Fig.4.4b Salinity Balances on the 8 isopycnals (from top to bottom panels) from the AVDF model. Contour interval=.005 units

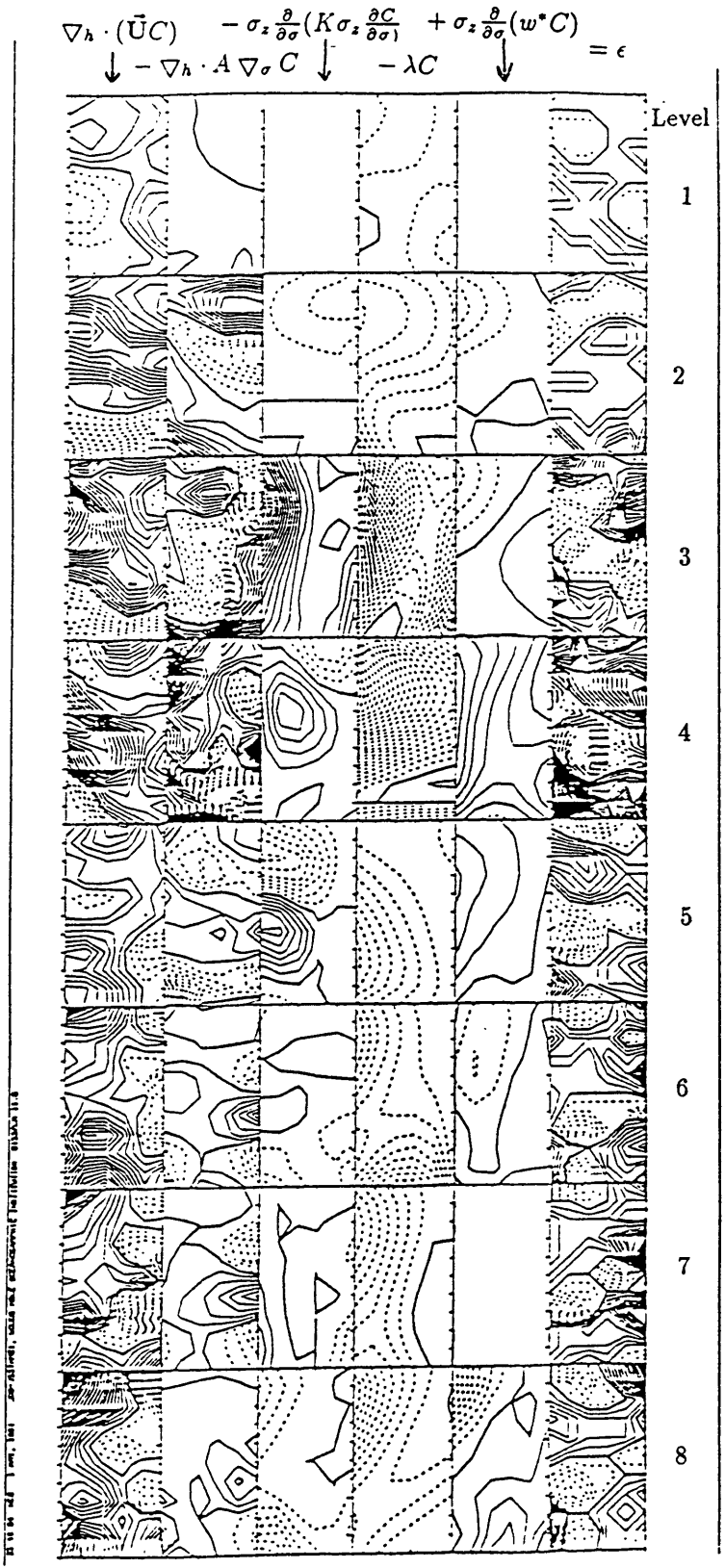

Fig.4.4c Oxygen Balances on the 8 isopycnals (from top to bottom panels) from the AVDF model. Contour interval= .0005 units

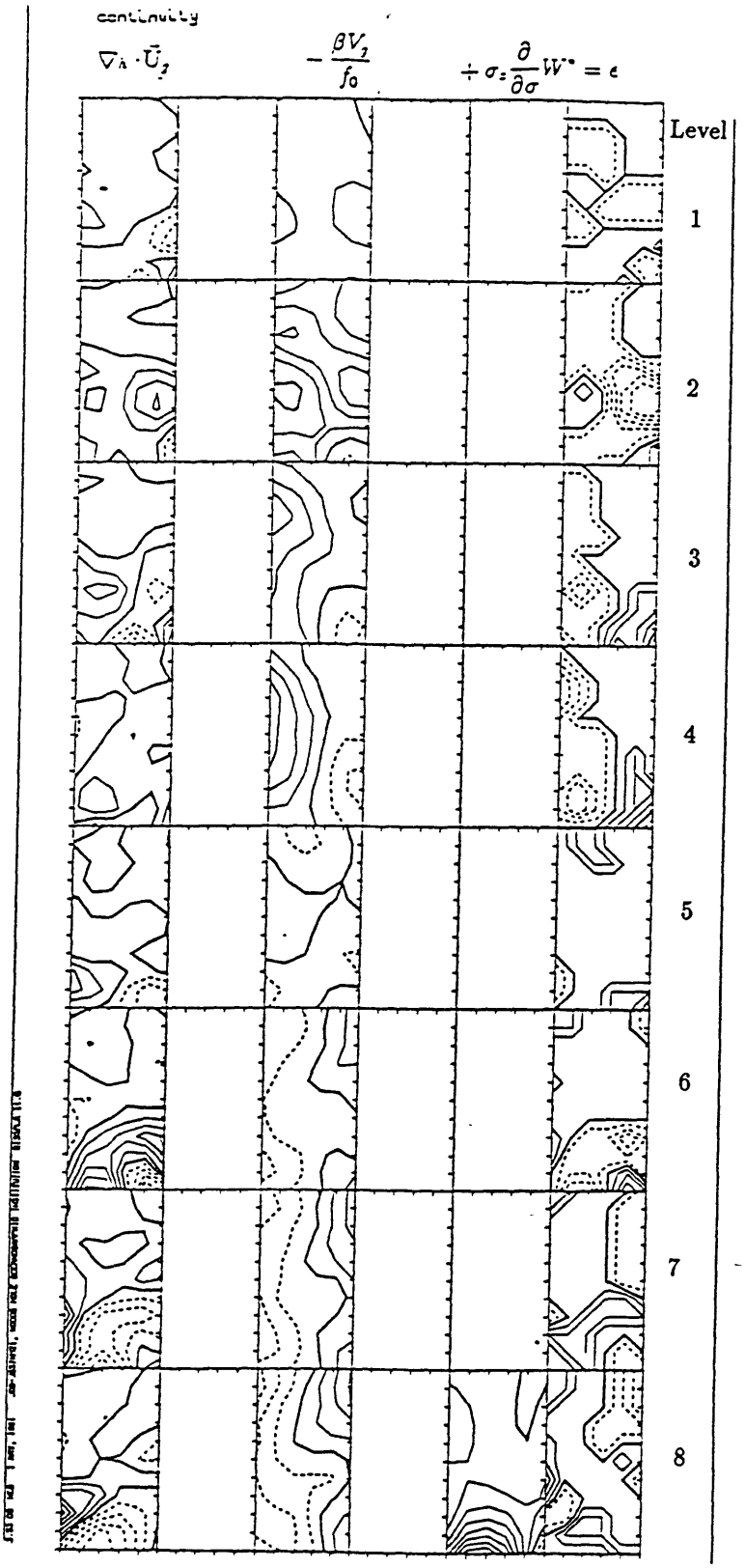

Fig.4.4d Continuity Equation Balances on the 8 isopycnals (from top to bottom panels) from the AVDF model. Contour interval=.005 units

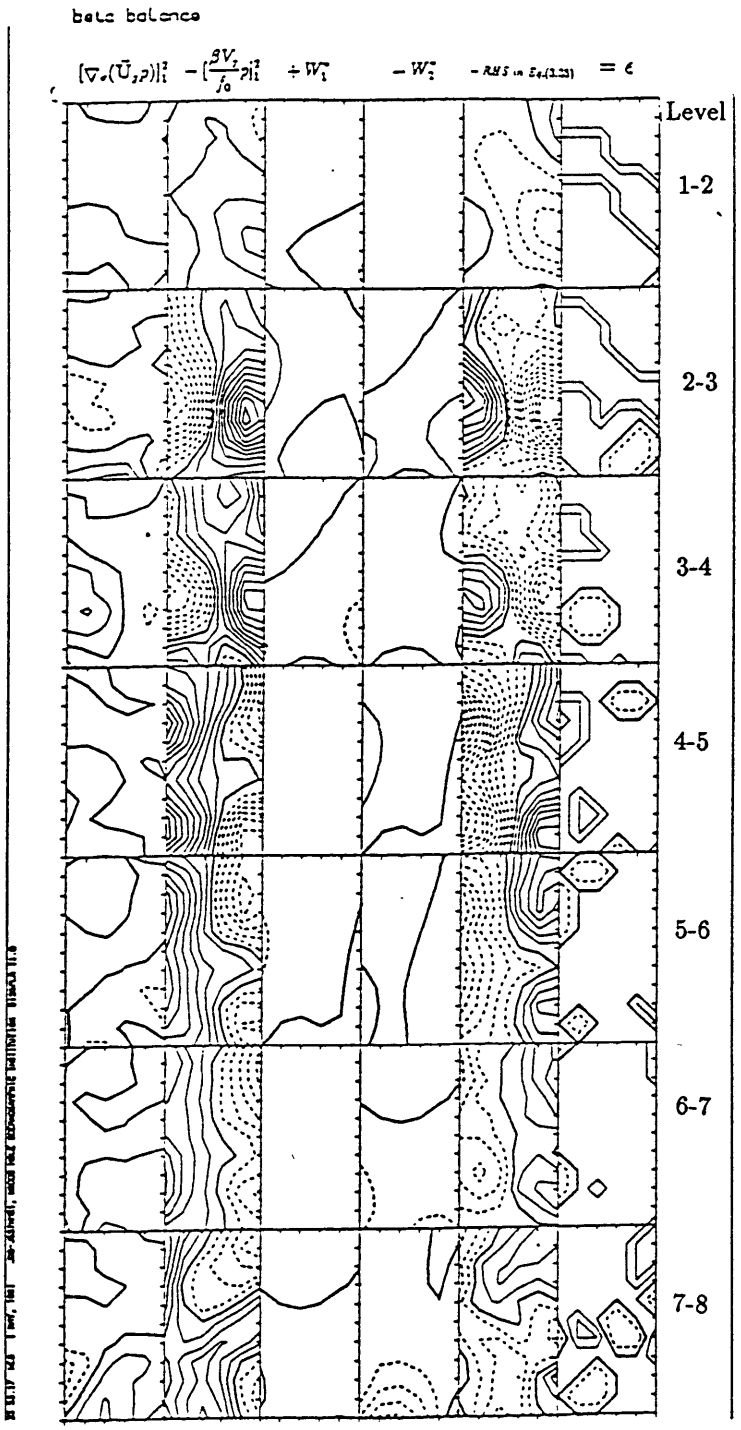

Fig.4.4e Integrated Vorticity Equation Balances on the 8 isopycnals (from top to bottom panels) from the AVDF model. Contour interval=.005 units

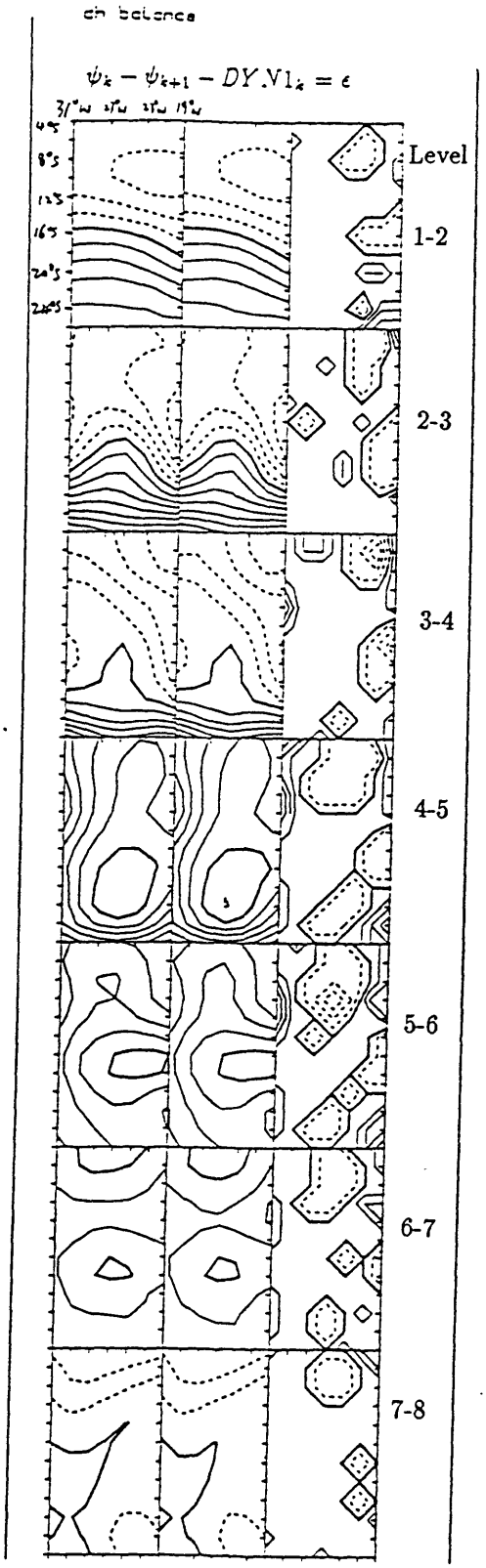

Fig.4.4f Dynamic Equation Balances on the 8 isopycnals (from top to bottom panels) from the AVDF model. Contour interval=.005 units

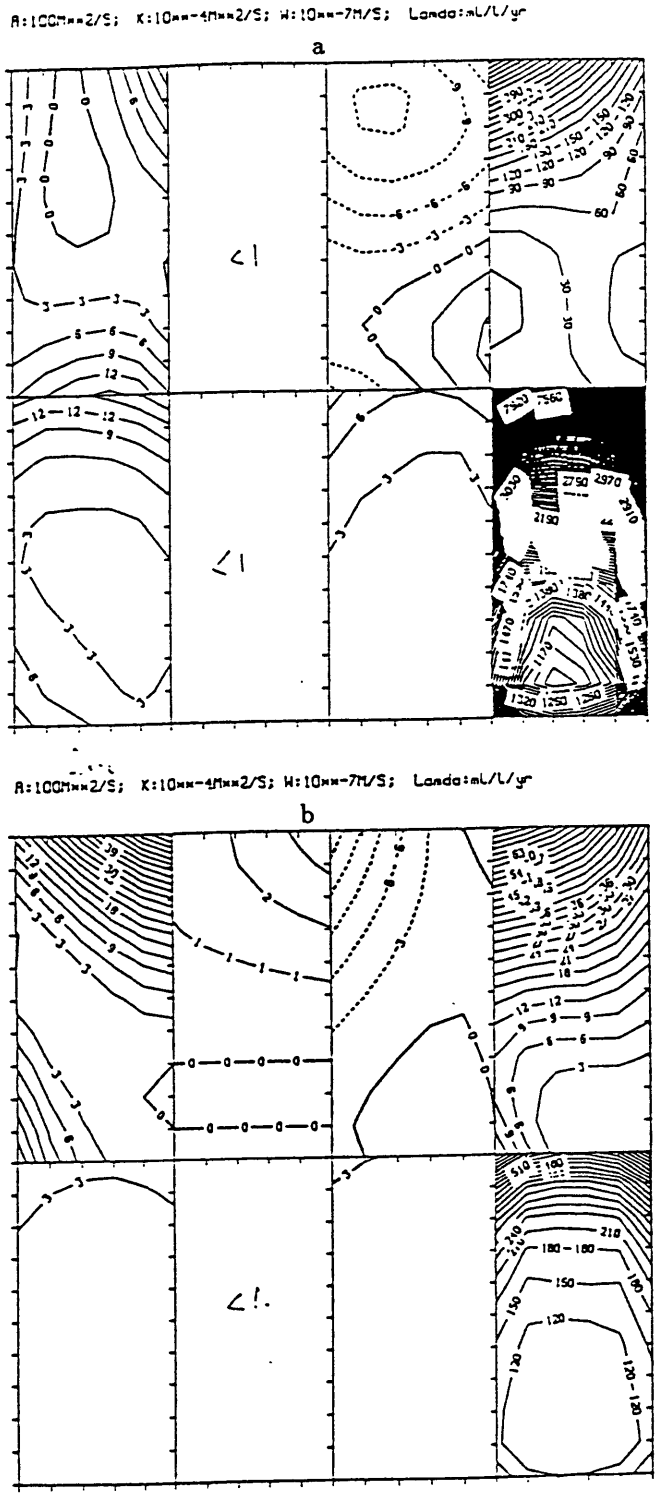

Fig.4.5 Solutions for Isopycnal and Diapycnal Diffusivities (A, K), Diapycnal Velocities ($\tilde{w}^*$), and Oxygen Consumption Rates (λ) as well as their Expected errors from the AVDF model. (a) Level 1; (b) Level 2

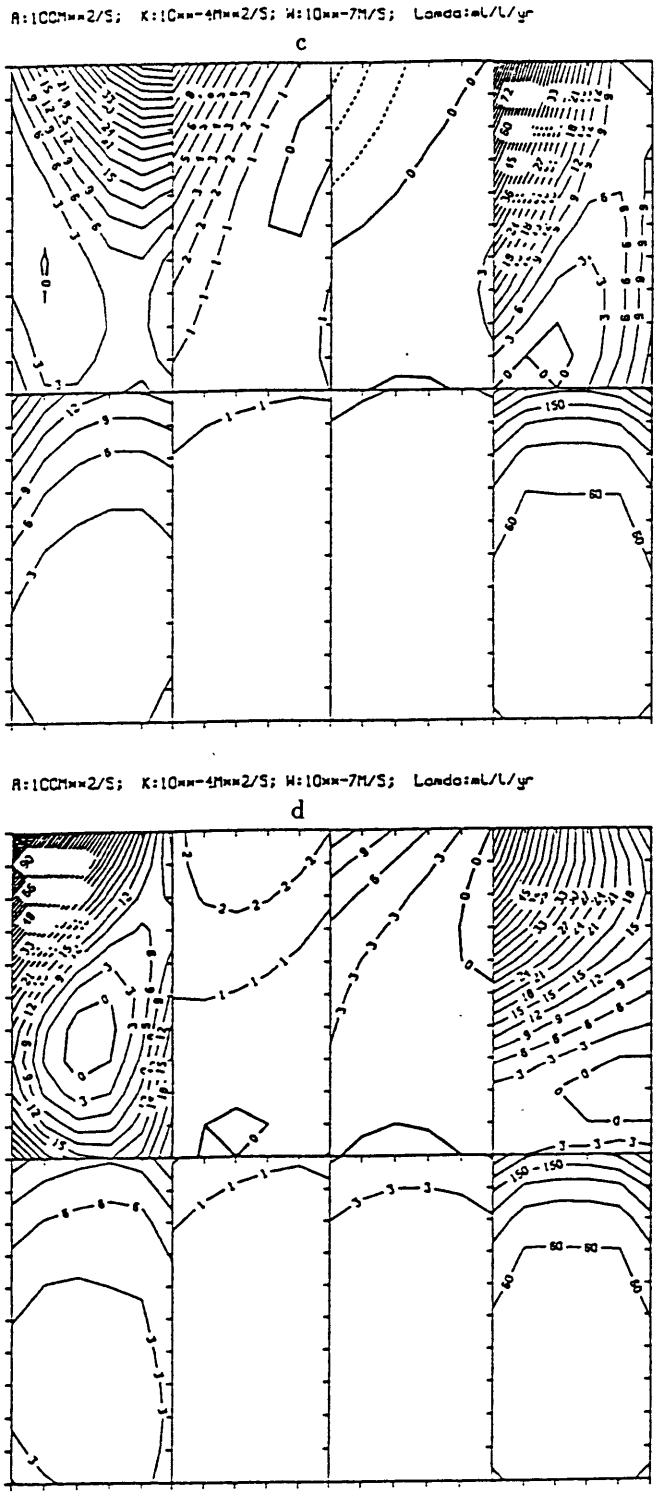

Fig.4.5 (continued) (c) Level 3; (d) Level 4

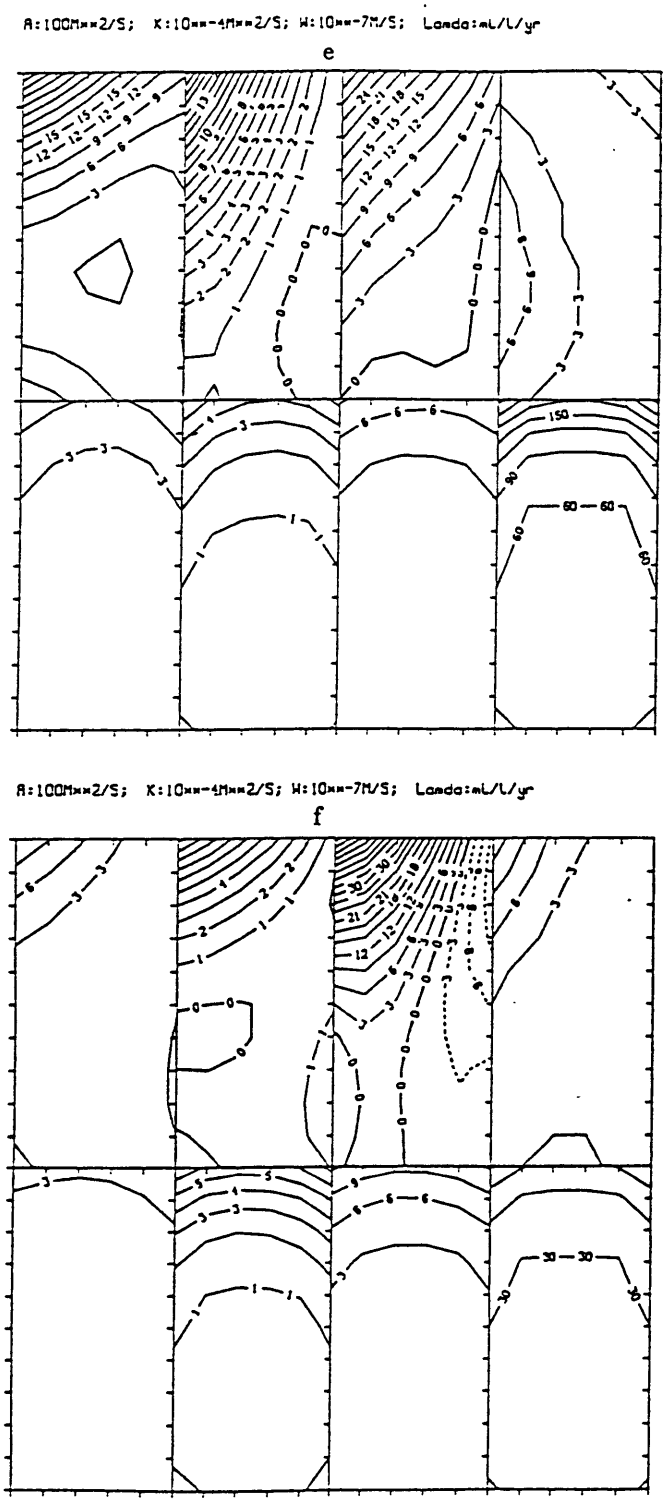

Fig.4.5 (continued) (e) Level 5; (f) Level 6

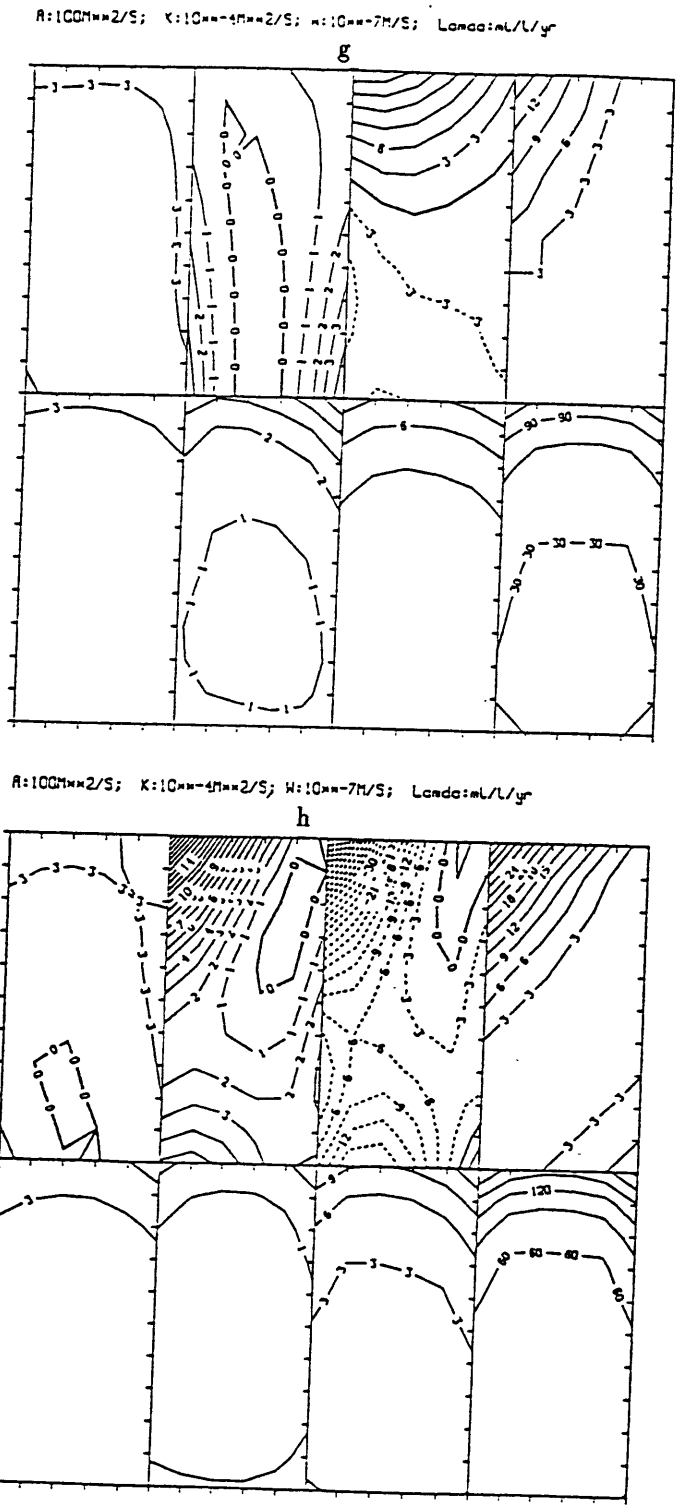

Fig.4.5 (continued) (g) Level 7; (h) Level 8

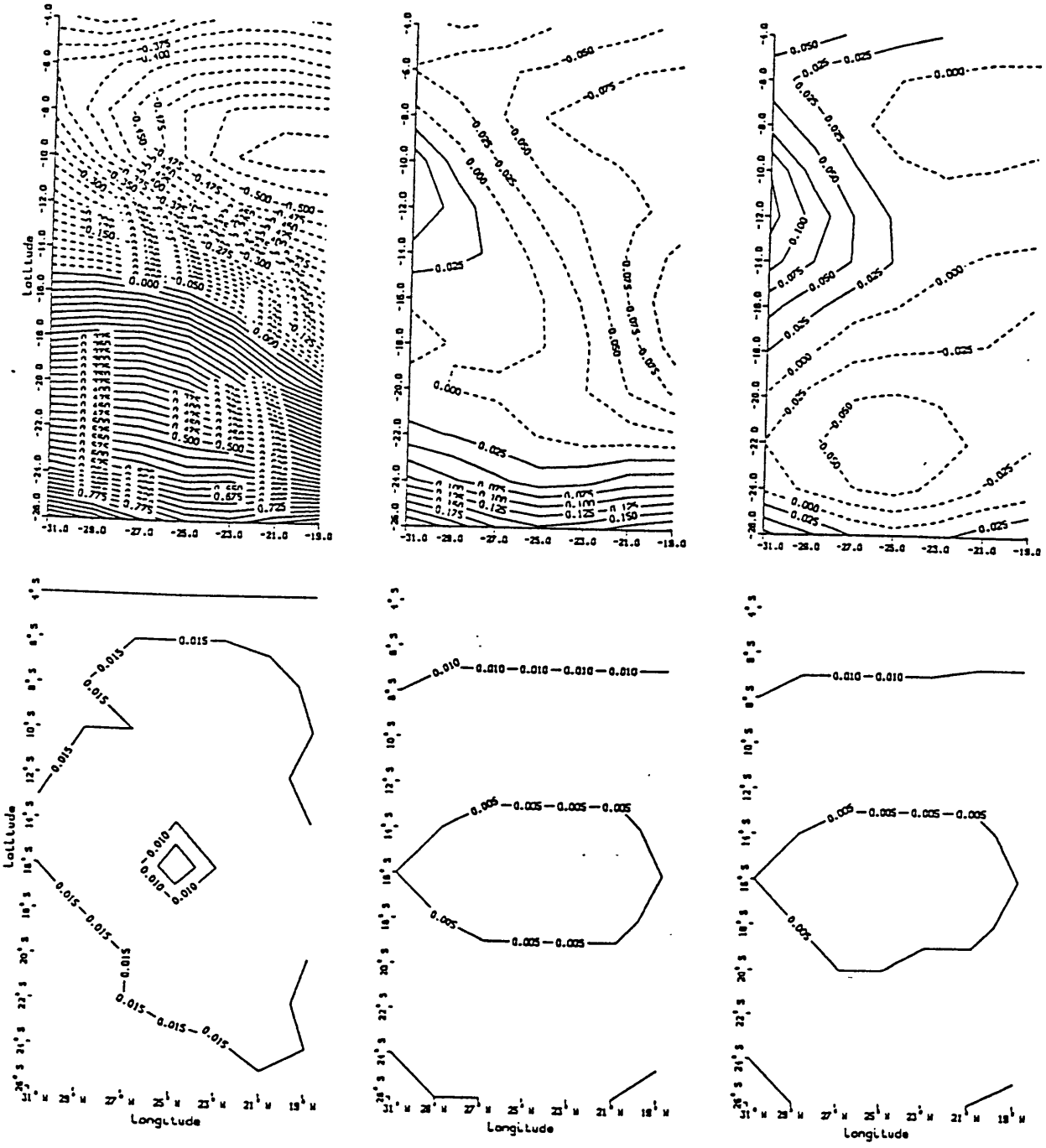

(a)Level 1 (b)Level 2 (c)Level 3

Fig.4.6 Double-Diffusive Model Results: Streamfunction (upper) and its expected error (lower) Contours On the 8 Isopycnals. Unit: m^2/s^2

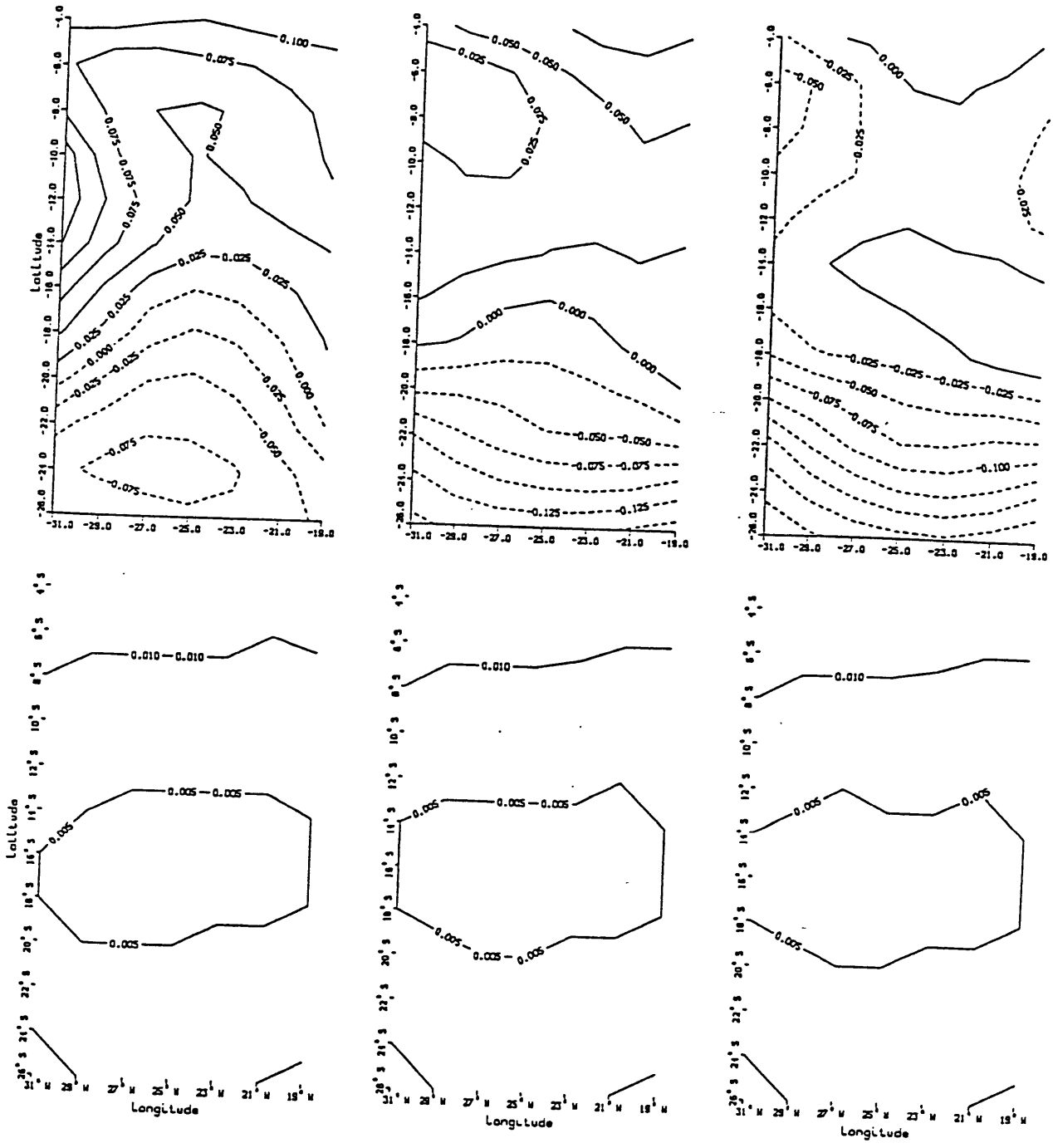

(d)Level 4 (e)Level 5 (f)Level 6

Fig.4.6 (continued)

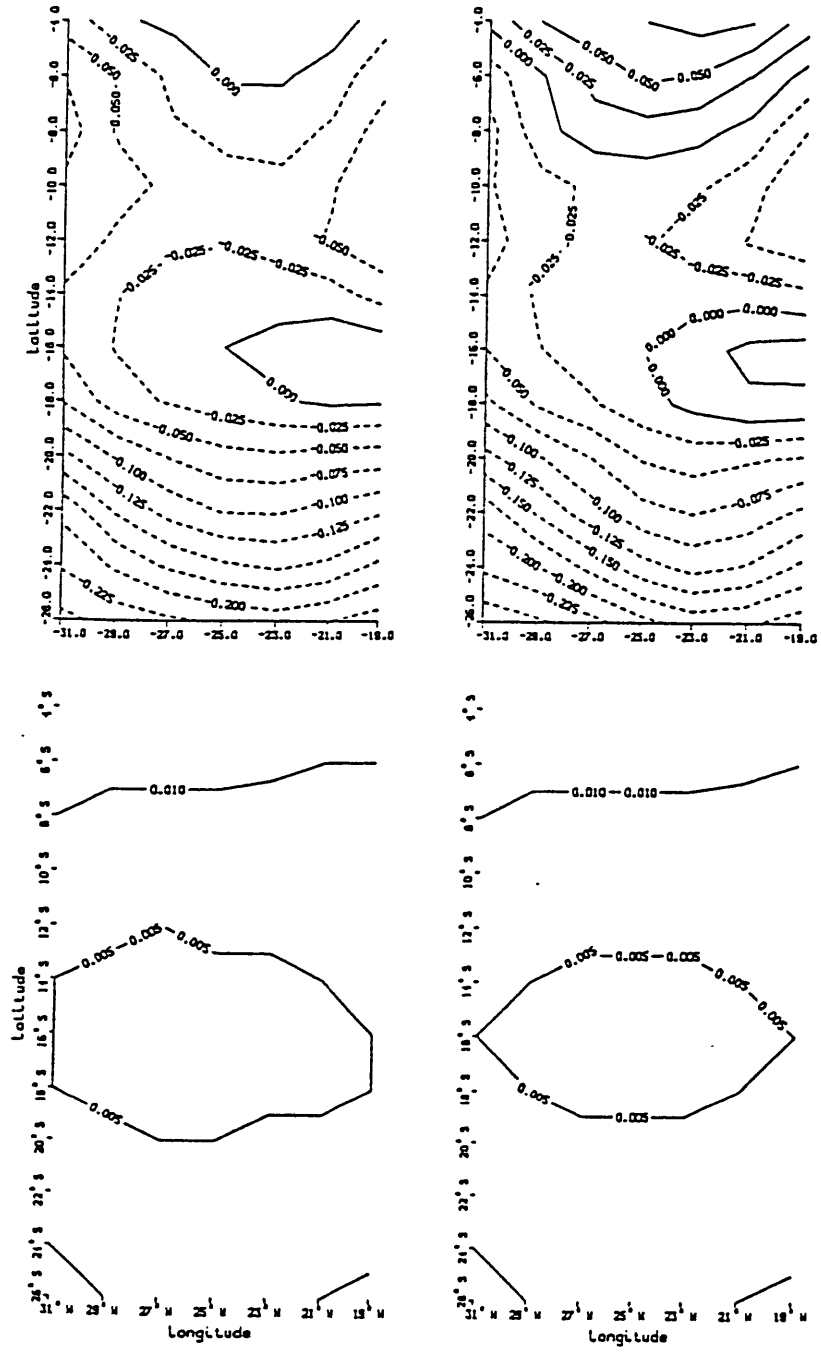

(g)Level 7 (h)Level 8

Fig.4.6 (continued)

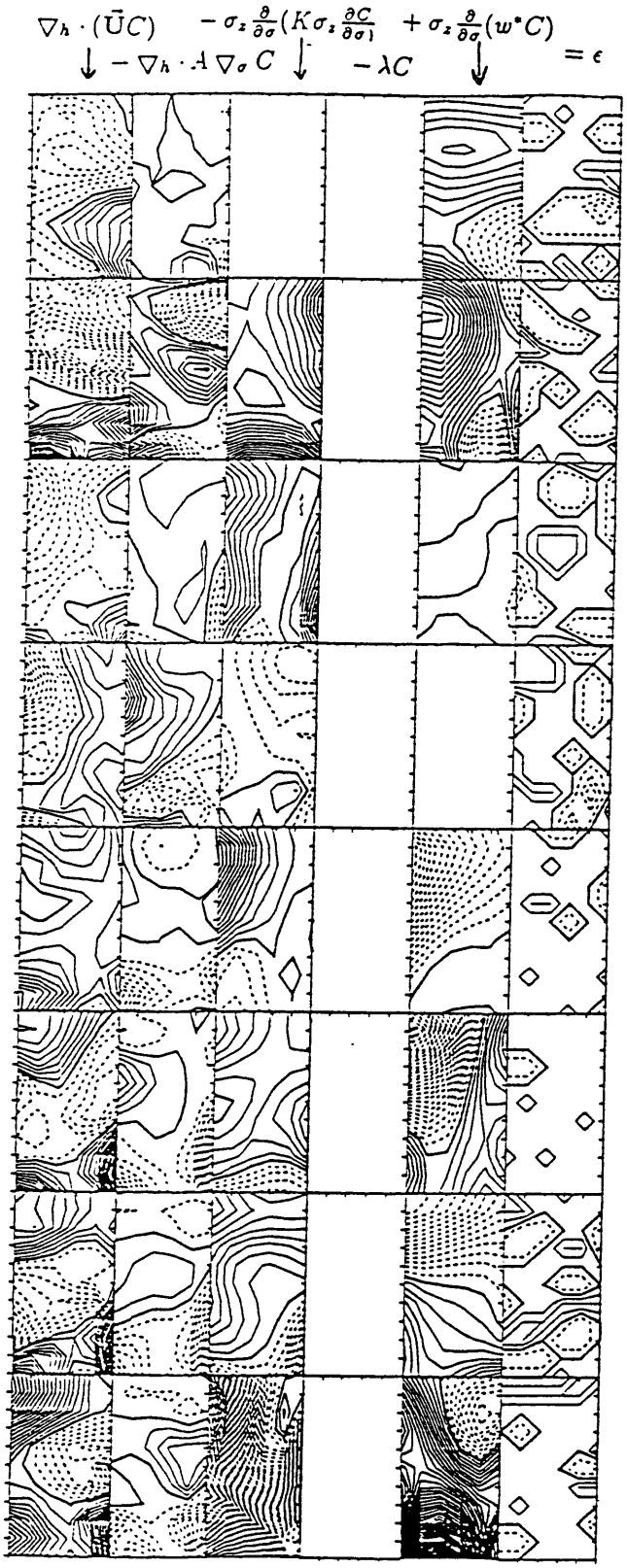

Fig.4.7a Potential Temperature Balances on the 8 isopycnals (from top to bottom panels) from the DDF model. Contour interval=.005 units

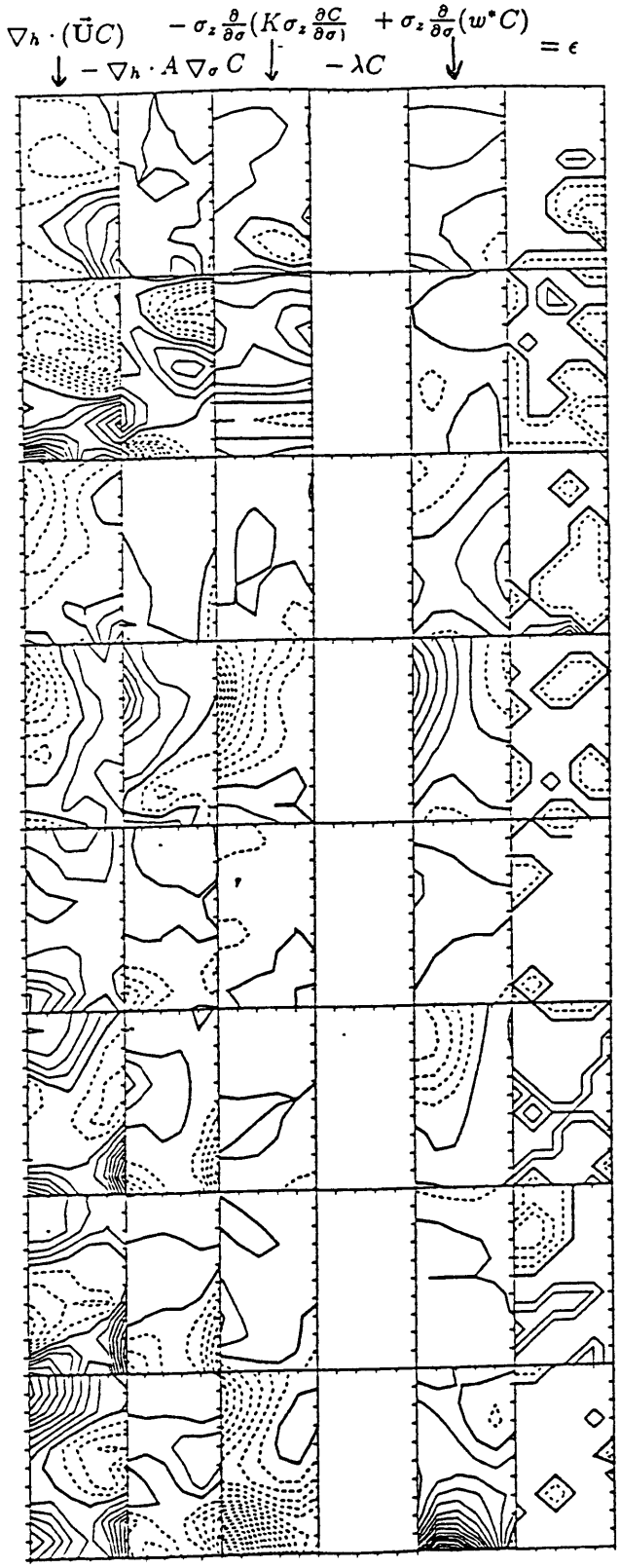

Fig.4.7b Salinity Balances on the 8 isopycnals (from top to bottom panels) from the DDF model.

Contour interval=.005 units

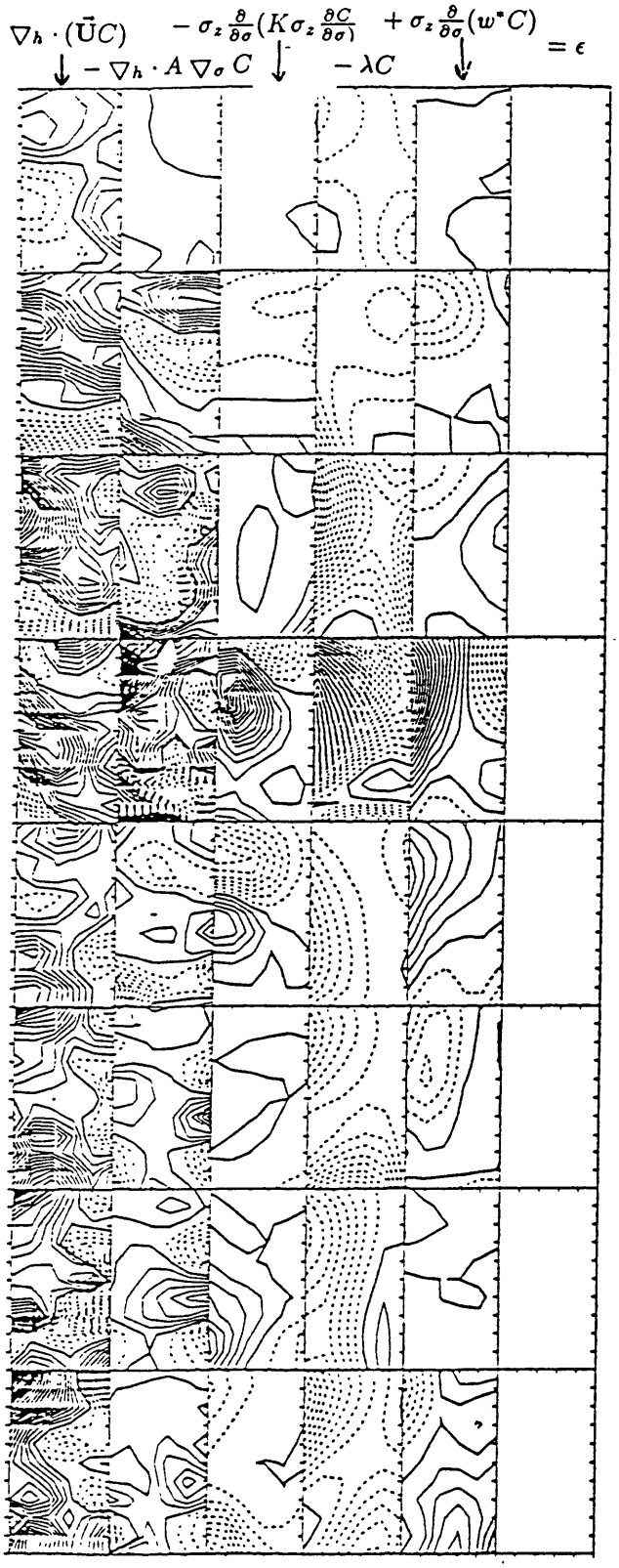

Fig.4.7c Oxygen Balances on the 8 isopycnals (from top to bottom panels) from the DDF model.

Contour interval=.0005 units

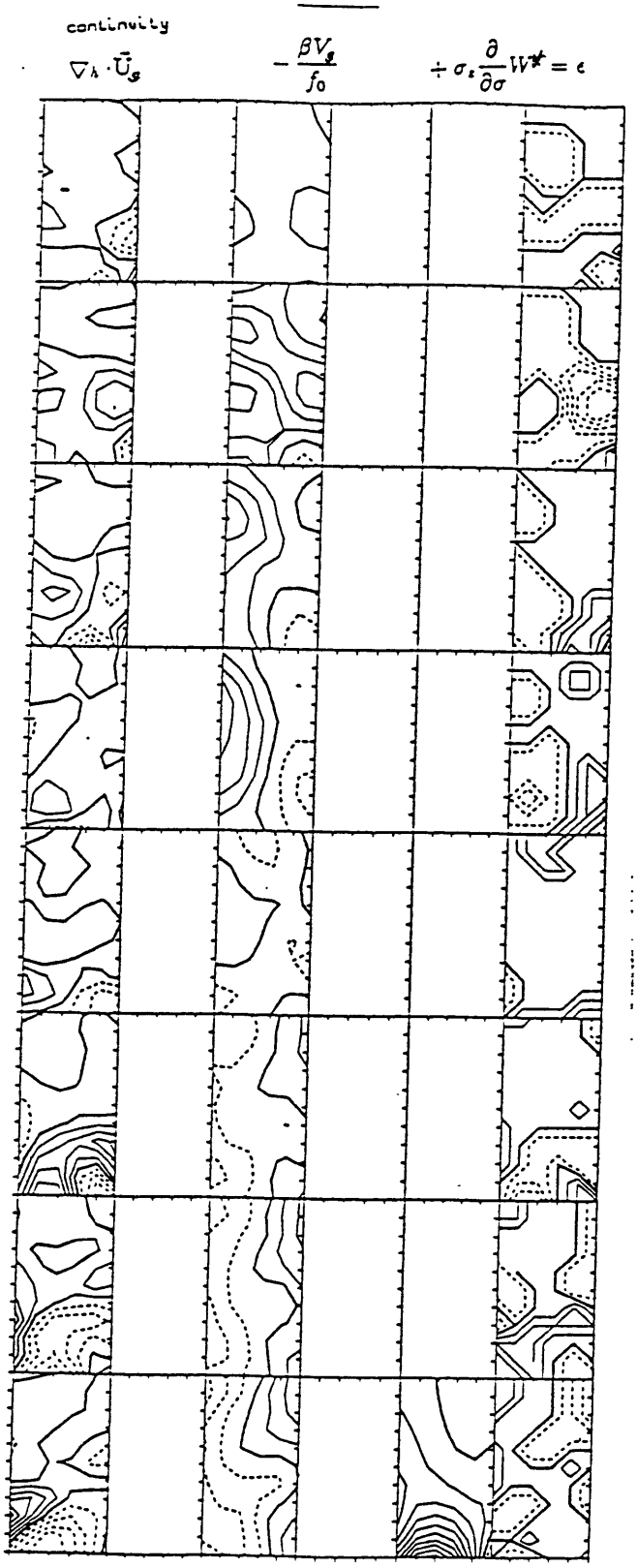

Fig.4.7d Continuity Equation Balances on the 8 isopycnals (from top to bottom panels) from the DDF model. Contour interval=.005 units

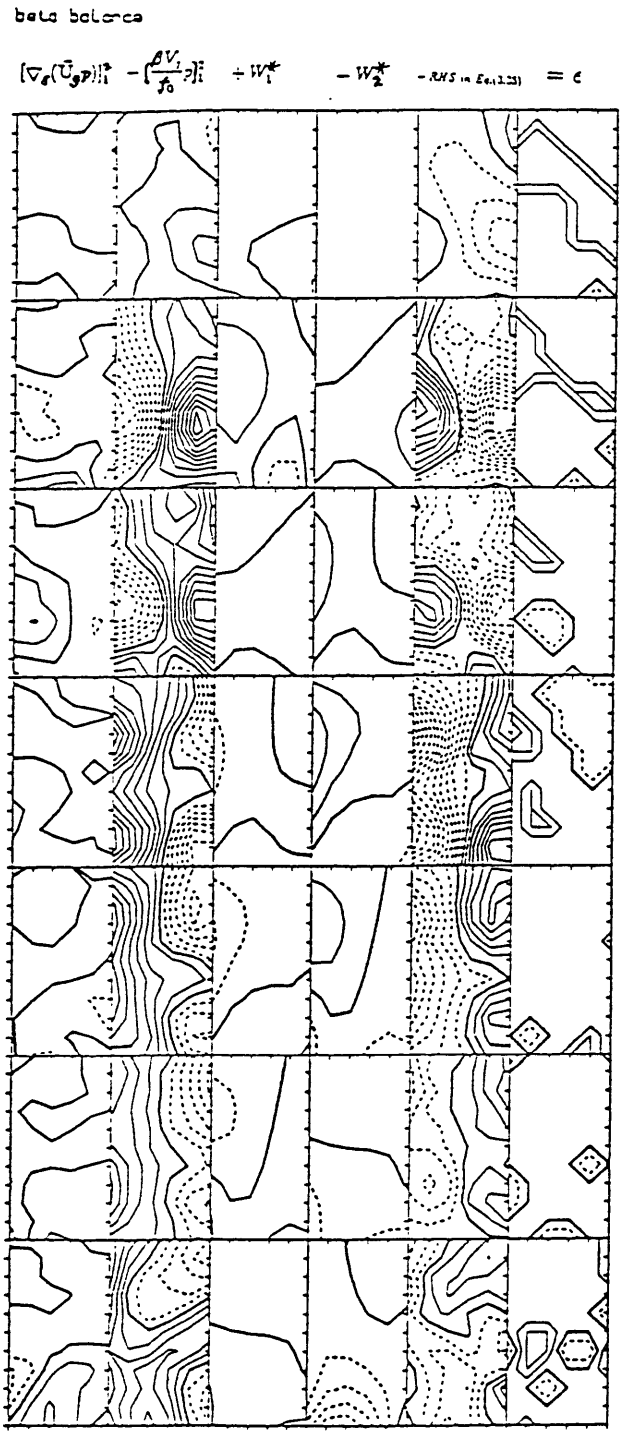

Fig.4.7e Integrated Vorticity Equation Balances on the 8 isopycnals (from top to bottom panels) from the DDF model. Contour interval=.005 units

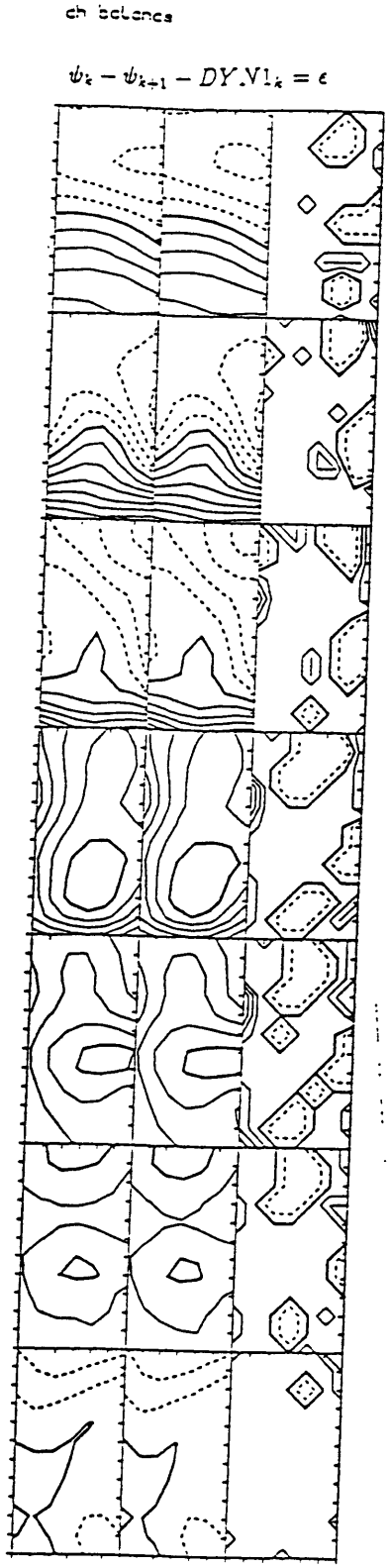

Fig.4.7f Dynamic Equation Balances on the 8 isopycnals (from top to bottom panels) from the DDF model. Contour interval=.005 units

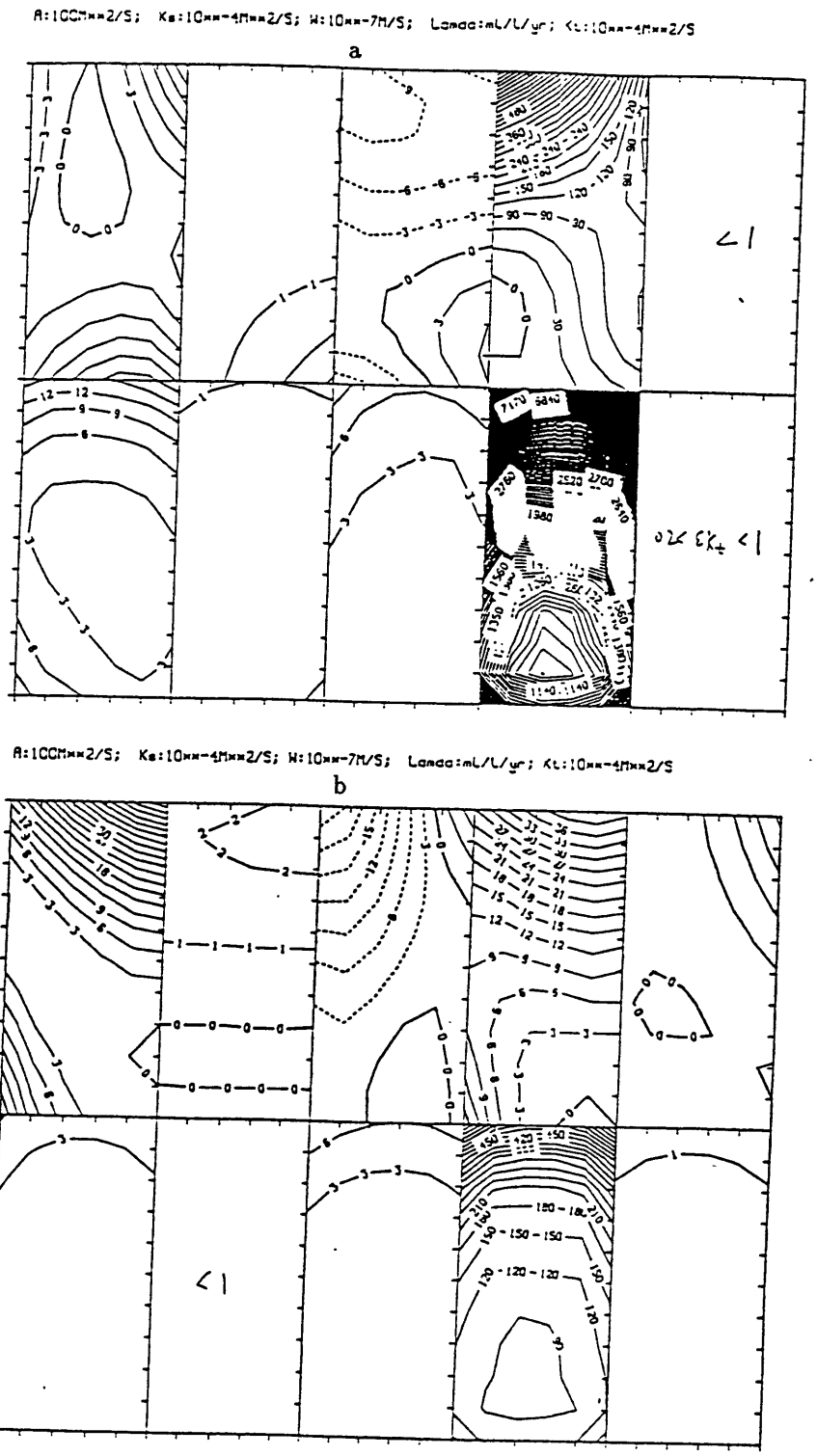

Fig.4.8 Solutions for Isopycnal and Diapycnal Diffusivities (A, K), Diapycnal Velocities (W), and Oxygen Consumption Rates (λ) as well as their Expected errors from DDF model. (a) Level 1; (b) Level 2

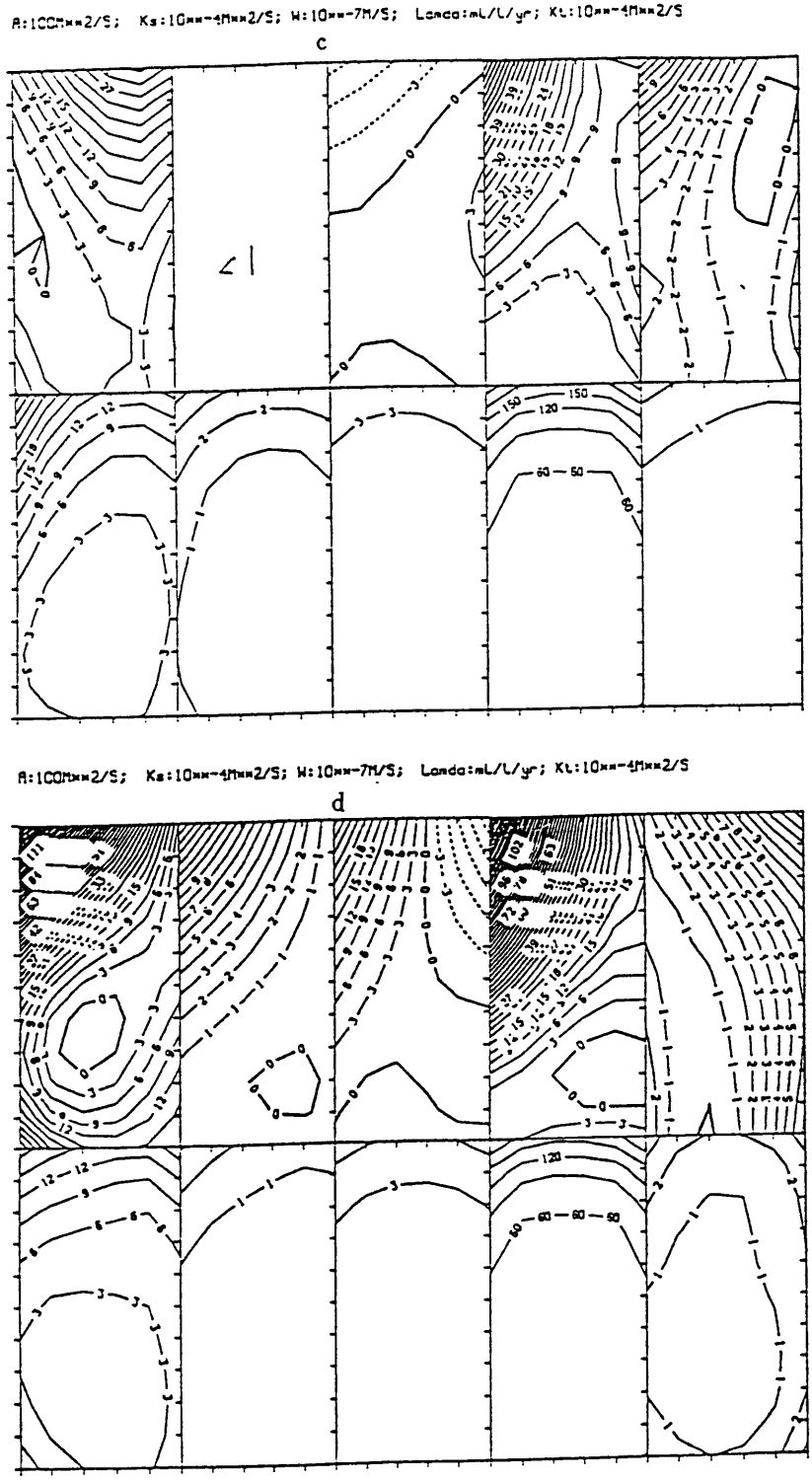

Fig.4.8 (continued) (c) Level 3; (d) Level 4

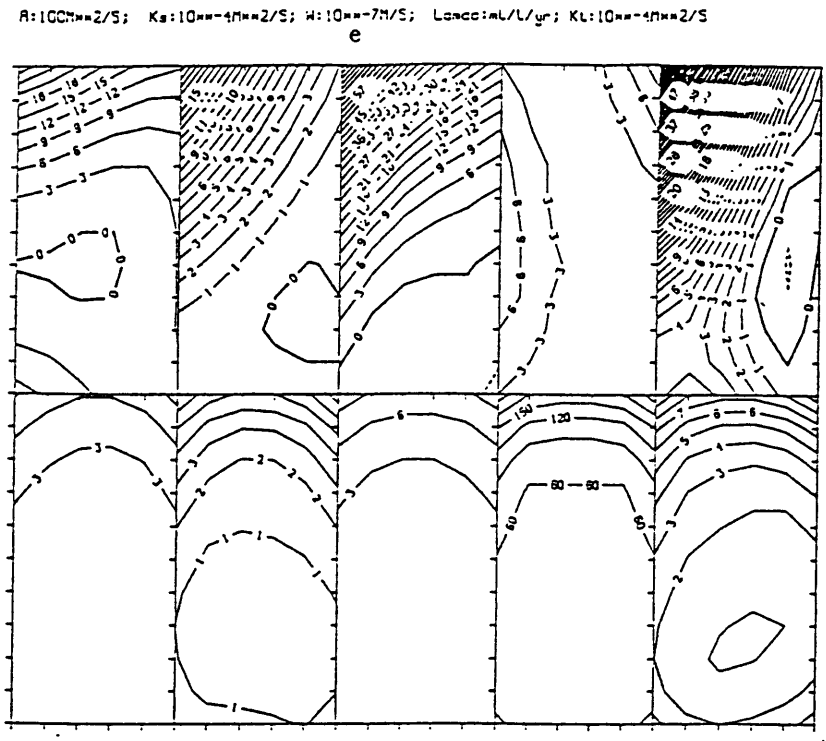

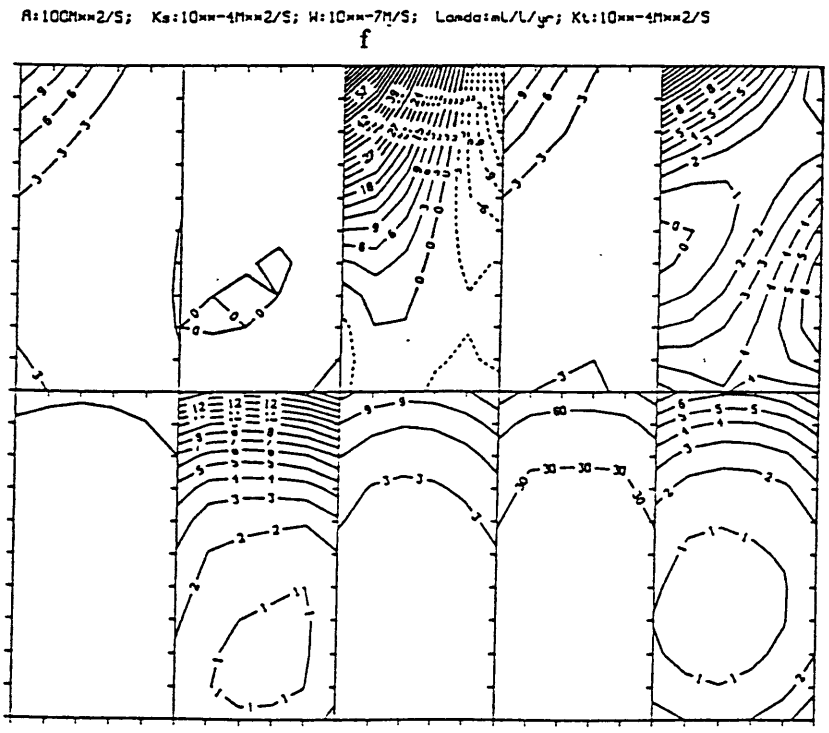

Fig.4.8 (continued) (e) Level 5; (f) Level 6

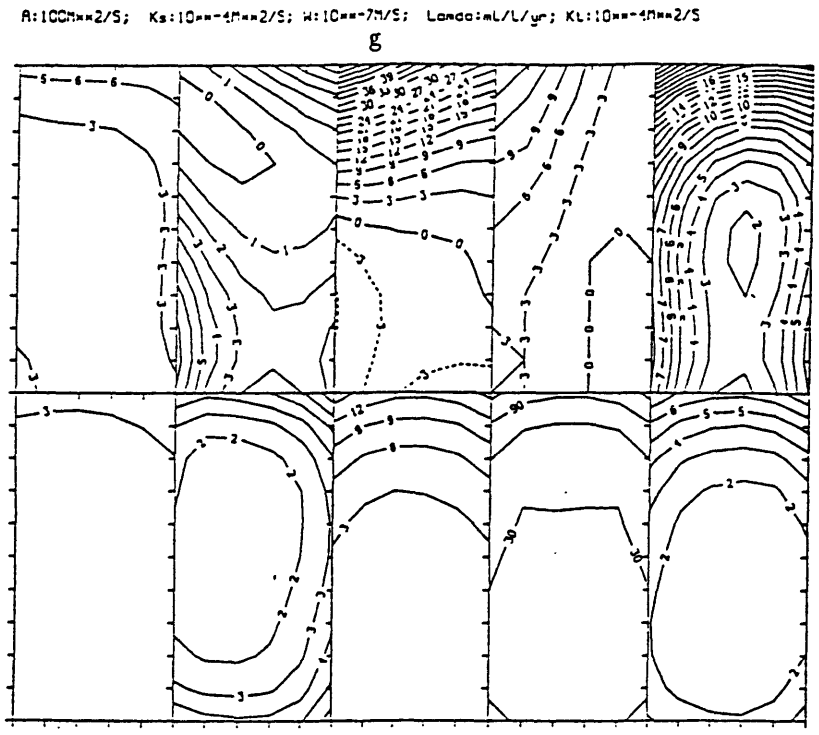

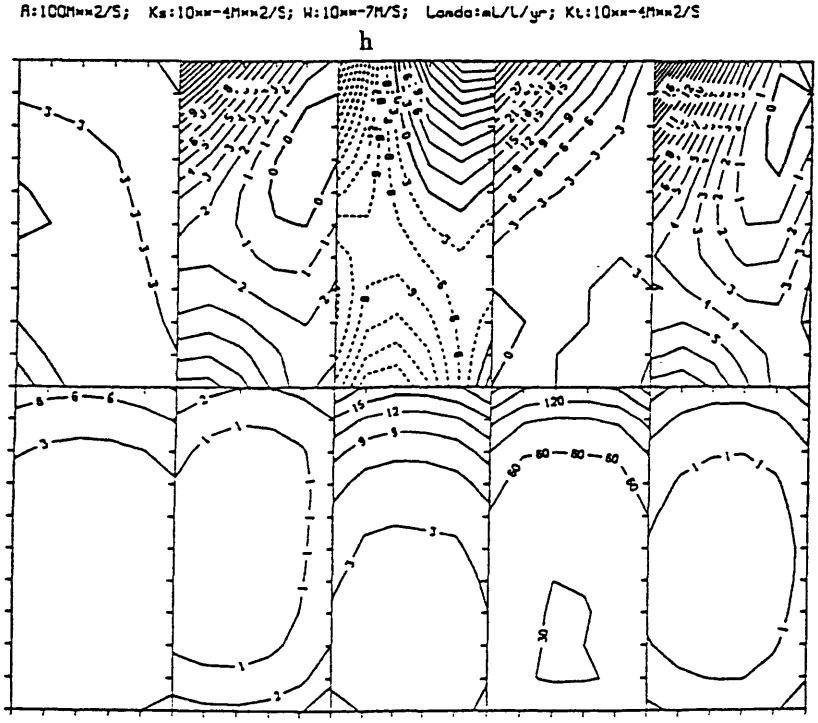

Fig.4.8 (continued) (g) Level 7; (h) Level 8

On the second level ($\sigma_1 = 31.88$), there are also some similarities between the circulation patterns and the pressure contours:a low pressure center appears at about 15°S and south of it lies the cyclonic gyre center (at $\sim$ 17°S). Flowing on this isopycnal are mainly the cold, fresher, oxygen rich Antarctic Intermediate Water(AAIW): it enters from the Southeast region in this area, and flows almost zonally with velocity at about 1 cm/s in the very south, on its north side it flows Northwestward as far as equator region, where it deflects to the northeast, flowing with a velocity of about 1.2 cm/s. Going deeper, since the slopes of the isopycnals become much smaller, the correspondence of the circulations and the pressure patterns are no longer apparent. Below the AAIW, the water on the next level ($\sigma_1 = 32.08$) is the Upper Circumpolar Water (UCPW) (except the northern edge), which is from south. It is cold, fresher, but oxygen poor. This water also enters from the southeastern region (Fig.4.3c), but with a smaller velocity (about 0.5 cm/s, about half of the velocity for the AAIW). Some of this water mass recirculating around a closed cyclonic gyre centered at (22°S, 25°W), and some of it escapes from the gyre and goes northwestward towards the equatorial region where it meets the oncoming NADW and flows eastward with velocity about 1.2 cm/s. The circulation pattern on the next isopycnal ($\sigma_1 = 32.28$) (Fig.4.3d) is basically the same as that of the UCPW, except with the center shifted about 3 degrees south. The next isopycnal ($\sigma_2 = 36.94$) was initially chosen to represent the upper NADW, but the circulation patterns and the more detailed water mass analysis reveal that on this isopycnal, the southern UCPW meets with the northern NADW around the center in this region. The flows shown in Fig.4.3e do indicate that the water enters from the northwest region of the area, and flows southeastward with velocity about 1 cm/s, to 10°S and 21°W where it turns northeastward. South of 16°S the flows are almost zonal, but we cannot judge wheather they are the extension of the NADW west of the area (31°W), as the flow on the next isopycnals indicate, or they are the recirculating part of the UCPW flow south of the area (26°S), as the flows on the upper isopycnal indicates. They can, however, be identified

by the distributions of the water properties. Figs.3.5 show the contours of the potential temperature, salinity and oxygen on a section along 24.5°W from 3.5°S to 26.5°S . The isopynal $\sigma_2 = 36.94$ lies at about 1900 *dbar*, and it is noted that there are two different water masses on this isopycnal: the warm, saline and oxygen rich NADW in the north and the cold, fresher and oxygen poor UCPW in the south. About 500 *dbar* deeper, on isopycnal $\sigma_2 = 37.00$ which is at about 2400 *dbar*, lies the center of the salinity maximum, and the potential temperature contours show that the warm NADW just extends to the south edge of this modeled area. This NADW layer is thick in this area and extends downwards through the next two levels, namely the $\sigma_3 = 41.46$ and the $\sigma_3 = 41.50$ isopycnals. The circulation patterns of the NADW on these three isopycnals are shown in Figs.4.3f,g,h. On $\sigma_2 = 37.00$, the NADW enters this area from the northwest corner, one part of it goes southeastward and then turns northeastward, another part in the west first flows southward and then it deflects eastward, then northeastward. The remaining part of the water recirculates anticyclonically with axis at about 16°S, through the region east of this modeled area. As the water recirculates , some of it leaves the gyre and bears northward and then joins the northern northeastward flowing NADW. Moving deeper, these features become more evident and flows are slightly stronger. The outflow at the northeast corner is about 1 cm/s on $\sigma_2 = 37.00$, about 1.5 cm/s on $\sigma_3 = 41.46$, and about 2.3 cm/s on $\sigma_3 = 41.5$. The eastward flow in the south edge is about 0.4 cm/s on $\sigma_2 = 37.00$ and about 0.5 cm/s on the two lower isopycnals.

Comparisons With Other Works Reid(1989) has proposed another method to study the *total* geostrophic flows in the whole South Atlantic Ocean. The basic idea of the method is that, on the lines of the selected hydrographic stations, the density fields are first used to calculate the geostrophic flows *relative* to the ocean bottom by the dynamic method (the relative flows are also called *baroclinic* flows), then a so-called *barotropic* component for each pair of stations is added to make the flows consonant with the tracer patterns (in this sense the idea of the $core - layer$ method has been used).

Then the adjusted flows are used to construct the steric height, and the barotropic components are adjusted to make the steric height continuously distributed. Finally the mass conservation for the whole Atlantic Ocean was used to further adjust the barotropic components, and the adjusted steric height for the total (adjusted) geostrophic flows are calculated and contoured. Note that the data sets he used are either from stations in a single cruise and/or some combinations of them where necessary (e.g., for the high latitude region). Thus the data sets he used are neither synoptic nor the averages of measurements taken over a long time period. In this section, we present some of his results in the Brazil Basin and compare his circulations for different water masses with ours. In what follows, the notation *steric height* refers to Reid's results, and *streamfunction* refers to ours (physically they are the same thing).

For the near surface water, Reid's adjusted steric height at 500 *dbar* are shown in Fig.4.9a. Comparing with our streamfunction patterns on $\sigma_0 = 26.88$ which extends from about 300 *dbar* in the north to about 530 *dbar* in the south (Fig.4.3a), it can be seen that both show a cyclonic gyre system in the selected Brazil Basin area. Water enters from the southeast and some of it flows almost zonally toward the west and leaves there. Some of it circulates around 10°S and flows out of this area from the northeast near the equator. Although the detailed structures and velocity values are not exactly the same (for example, the center of the gyre in the adjusted steric height contours is about five degree south of the center of the gyre in the streamfunction contours; Reid's flow patern shows a relatively narrow jet-like flow while our flows are much more uniform in the south region of the area), but the overall velocities in this area are in the same magnitudes (e.g., the adjusted steric height difference from 15°S to 25°S is about $(2.4 - 2.3) \times 10 m^2/s^2 = 1.0 m^2/s^2$ in this area, while our streamfunction difference in this same latitude band is also about $1.0 m^2/s^2$). Thus for the near surface water, the flows resulted from the two different models are quite consistant in the Brazil Basin.

The adjusted steric height contours at 800 *dbar* for the AAIW in Reid's results (Fig.4.9b) are also similar to our corresponding streamfunction contours (Fig.4.3b), i.e. on $\sigma_1 = 31.88$ for the AAIW which extends from about 750 *dbar* in the north to about 900 *dbar* in the south in this area. The cyclonic gyre center are located at the similar places (about 15°S). In the northwest region, the high streamfunction center at about 12°S in Fig.4.3b also has a corresponding high adjusted steric height center in Fig.4.9b, but it lies just west of this area. Reid's velocity seems a little stronger than ours (the adjusted steric height difference from 15°S to 25°S at the east edge of this area (about 19°W) is about $0.6m^2/s^2$, whereas the corresponding streamfunction difference is about $0.3m^2/s^2$).

On going deeper, although the circulation patterns of the two different approaches are different in detail, there are still broad similarities. The adjusted steric height at 1000 *dbar* and at 1500 *dbar* for the Upper Circumpolar Water in Reid's paper are represented in Fig.4.9c-d, and it can be seen that in this modeled area the flow patterns at these two depths are very similar to each other as well as to that of the AAIW above ($\sim 800dbar$): water enters this basin from the south, flows northwestward and deflects to east near equator. Looking at the larger (than our modeled) area, it can be seen that they are part of the closed cyclonic circulation gyres whose center is east of the Brazil Basin. Thus the flows are more meridional than zonal in the basin. However, our streamfunction contours for the UCPW (on $\sigma_1 = 32.08$ which extends from about 1050 *dbar* in the north to about 1150 *dbar* in the south, and on $\sigma_1 = 32.28$ extends from about 1350 *dbar* in the north to about 1500 *dbar* in the south, see Fig.4.3c,d) show different flow patterns in detail in this basin: there is a closed cyclonic gyre *within* the basin, and consequently on north and south sides of the gyre center the flows are more zonal than meridional. In a broad sense, however, both approaches result in the similar, cyclonic gyre flow patterns on these levels in the basin.

At depths greater than about 2000 *dbar*, the circulation patterns for the North Atlantic Deep Water determined from the two different methods are again different in detail, but broadly similar in the basin. Reid's adjusted steric height contours at 2000, 2500, 3000, and 3500 dbar are shown in Figs.4.9e,f,g,h. From these figures it can be seen that the flows on all the four depths in this area are very similar. Flowing on these levels in this basin are also the NADW, but it seems that they have recirculated back from the south, as south as 50°S. In addition, it can also be seen that the flows in this basin are more meridional than zonal, except in the region near the equator. Contrarily, the current model results suggest that the southward flowing NADW along the west boundary (i.e. Brazil coast) is *gradually* deflected to east and flows into the basin. The most easterly (i.e. furthest from the western boundary) part of the southward flowing NADW (in which weaker velocities are expected) is deflected first at relatively northern latitude, and the most westerly part (in which stronger velocities are expected) is deflected at a relatively southern latitude. Thus the flows in this basin are more zonal than meridional. Nonetheless, despite of the detailed differences of the flows between the different models, there is a common feature among both model results, i.e. the NADW goes firstly southward, deflects to east in the south, then returns to the north, and finally leaves the basin from the northeast corner flowing northeastward after having made the deep southern excursion. It is supposed that this water traverses the mid Atlantic ridge through the equatoral fracture zone passages and enters into the Angola Basin as the source water for that basin. The current model results (Fig.4.3) also suggest that the entering NADW from the northwest corner of this basin most likely has come through the Ceara Abysal Plain passage. These flow patterns are consistant with Wüst's core layer analysis (Fig.4.9i) and surprisingly similar to Defant's absolute flow fields (Fig.4.9j).

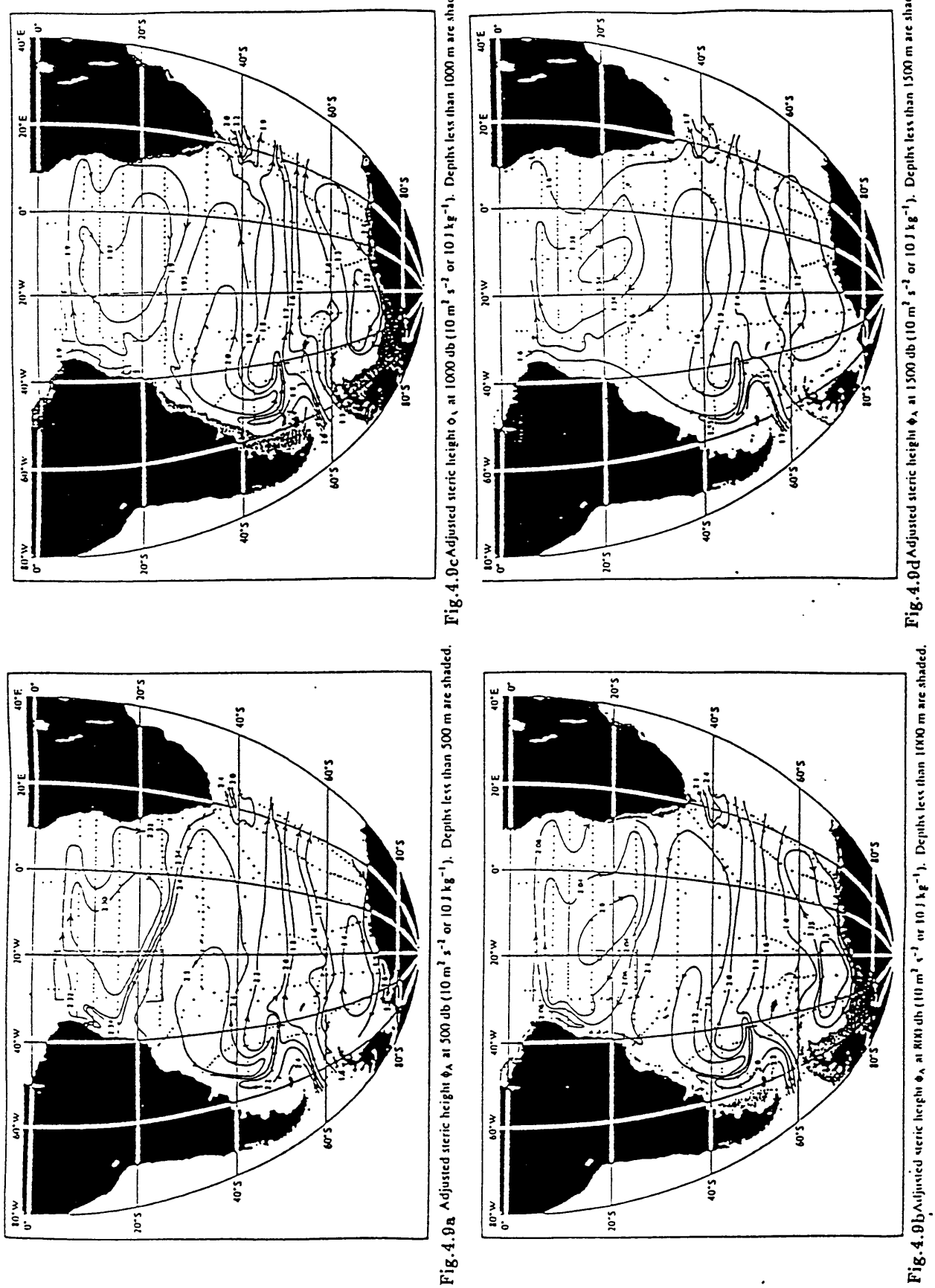

Fig.4.9a Adjusted steric height ϕ_A at 500 db (10 m^2 s^{-2} or 10 J kg^{-1}). Depths less than 500 m are shaded.

Fig.4.9b Adjusted steric height ϕ_A at 1000 db (10 m^2 s^{-2} or 10 J kg^{-1}). Depths less than 1000 m are shaded.

Fig.4.9c Adjusted steric height ϕ_A at 1000 db (10 m^2 s^{-2} or 10 J kg^{-1}). Depths less than 1000 m are shaded.

Fig.4.9d Adjusted steric height ϕ_A at 1500 db (10 m^2 s^{-2} or 10 J kg^{-1}). Depths less than 1500 m are shaded

Fig.4.9 Adjusted steric height at different depths in the South Atlantic (from Reid, 1989)

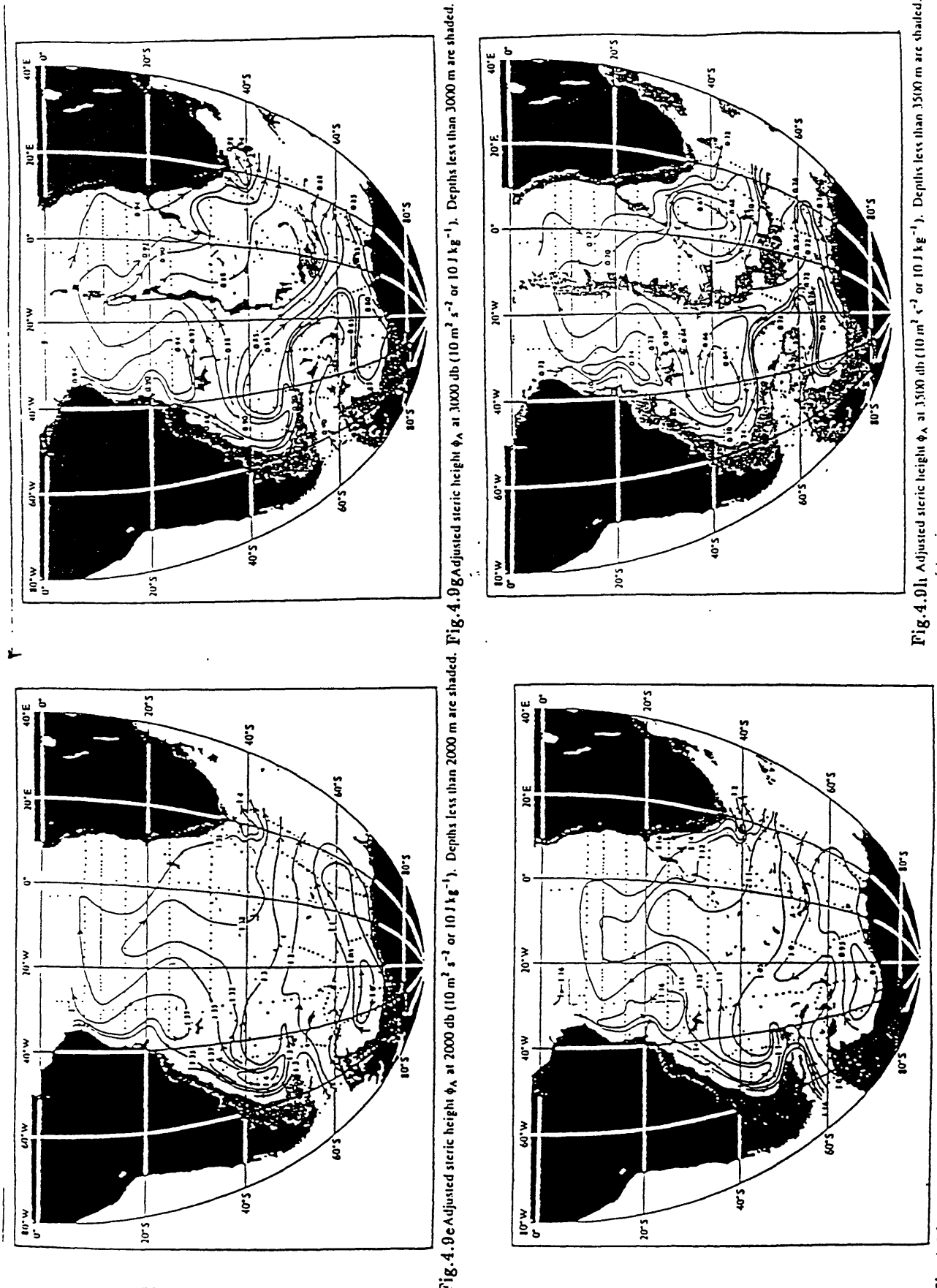

Fig.4.9e Adjusted steric height ϕ_A at 2000 db ($10\ m^2\ s^{-2}$ or $10\ J\ kg^{-1}$). Depths less than 2000 m are shaded.

Fig.4.9f Adjusted steric height ϕ_A at 2500 db ($10\ m^2\ s^{-2}$ or $10\ J\ kg^{-1}$). Depths less than 2500 m are shaded.

Fig.4.9g Adjusted steric height ϕ_A at 3000 db ($10\ m^2\ s^{-2}$ or $10\ J\ kg^{-1}$). Depths less than 3000 m are shaded.

Fig.4.9h Adjusted steric height ϕ_A at 3500 db ($10\ m^2\ s^{-2}$ or $10\ J\ kg^{-1}$). Depths less than 3500 m are shaded.

Fig.4.9 Adjusted steric height at different depths in the South Atlantic (from Reid, 1989)

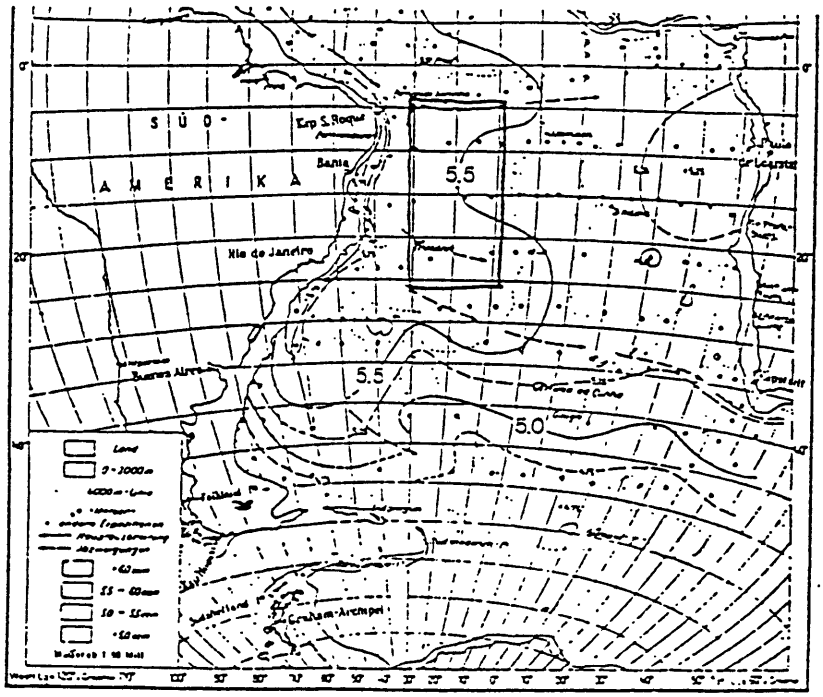

Fig.4.9i Oxygen (ml l⁻¹) of the core layer (intermediate oxygen maximum) of the Middle North Atlantic Deep Water. (Wüst 1935.) From Reid,1980.

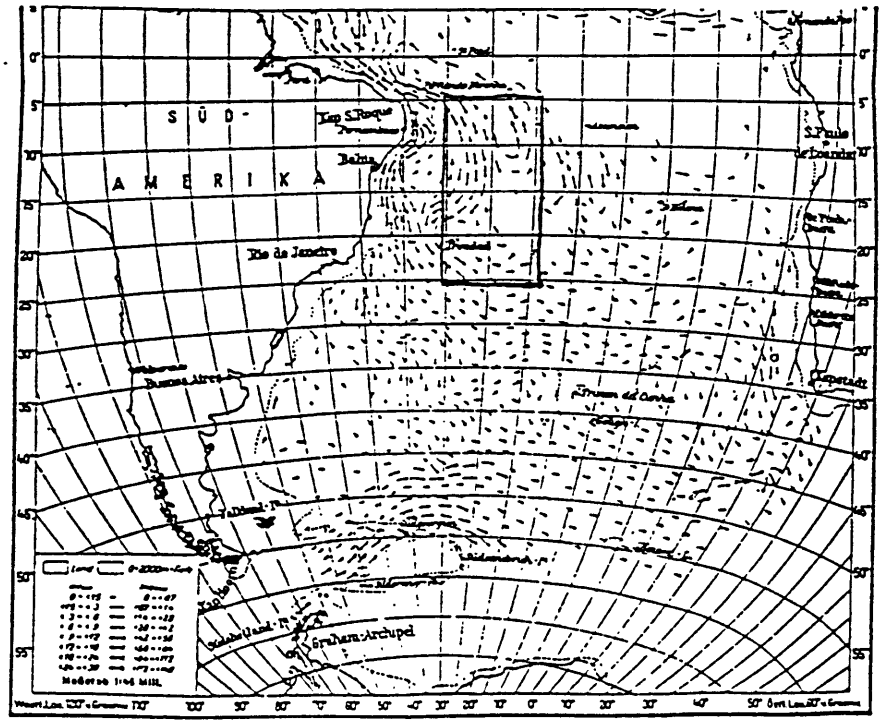

Fig.4.9j Defant's Absolute Flow Field at 2000m. From Reid,1980.

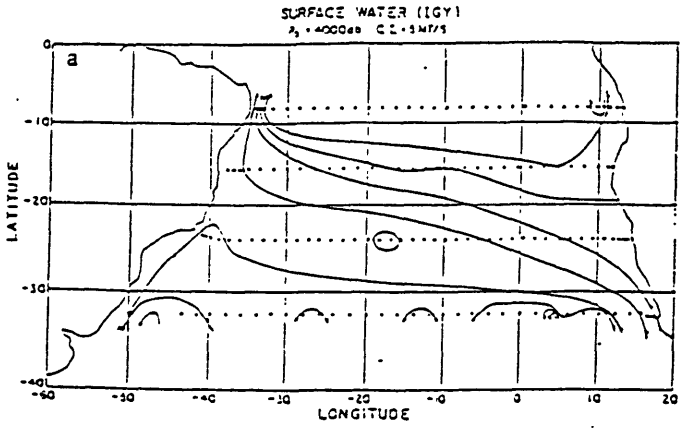

Fig.4.10a Transport streamlines for the Surface Water of the IGY sections with p_s = 4000 db. Contour interval (C.I.) is as indicated in the figure heading.

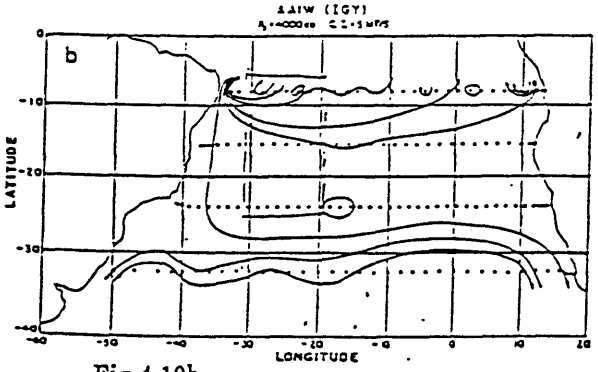

Fig.4.10b As in Fig.4.10a except for the AAIW.

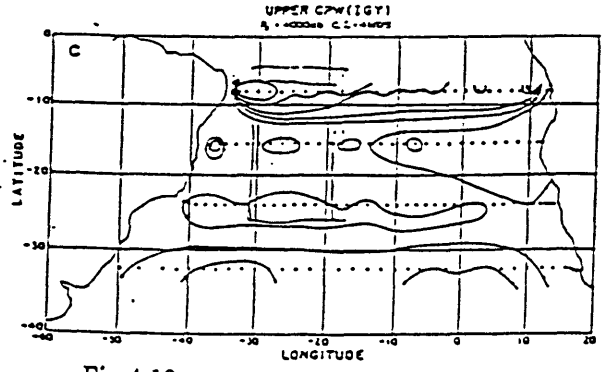

Fig.4.10c As in Fig.4.10a except for the Upper CPW.

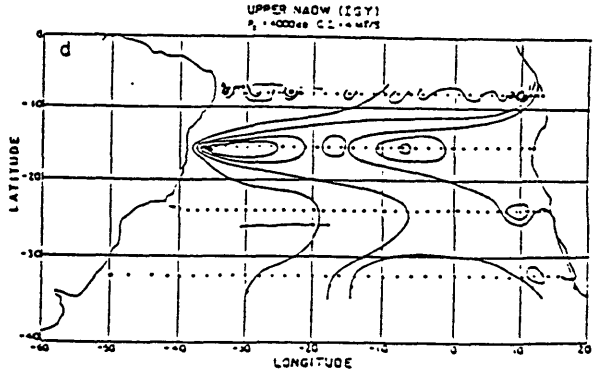

Fig.4.10d As in Fig.4.10a except for the Upper NADW.

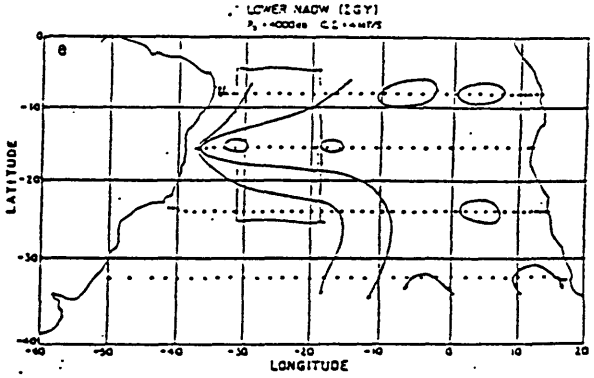

Fig.4.10e As in Fig.4.10a except for the Lower NADW.

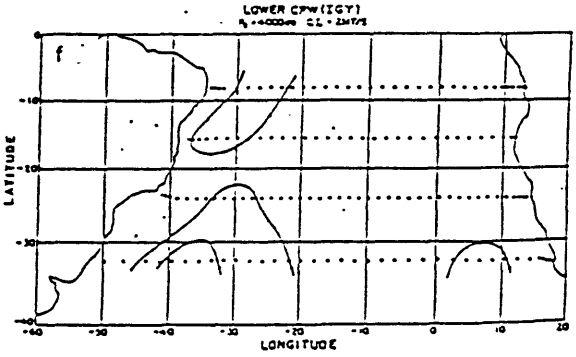

Fig.4.10f As in Fig.4.10a except for the Lower CPW.

Fig.4.10 Transport Streamfunctions for different water masses in the subtropical South Atlantic.

From Fu (1981)

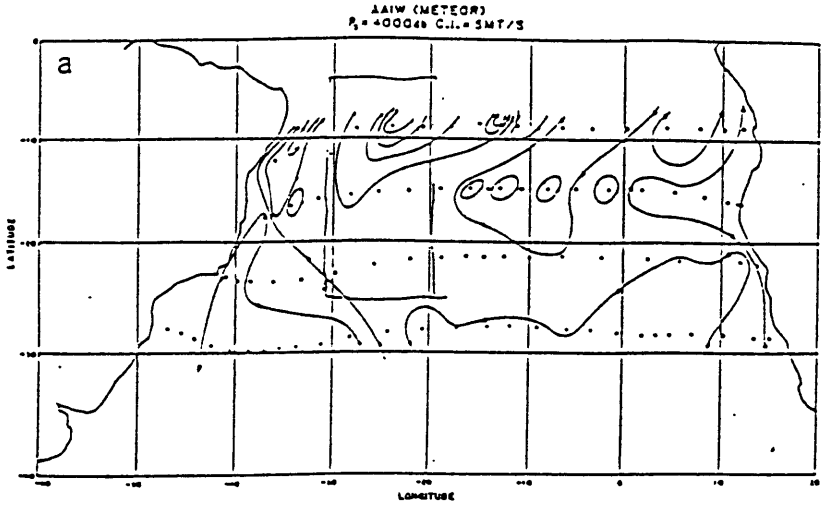

Fig.4.10g Transport streamlines for the AAIW of the METEOR sections with p_o = 4000 db (cf. Fig. 9b).

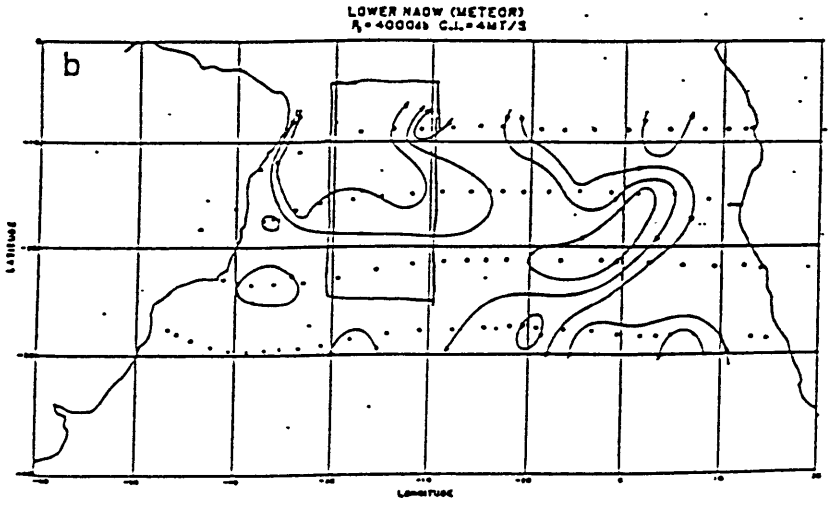

Fig.4.10h As in Fig. 10a except for the Lower NADW (cf. Fig. 9c).

Fig.4.10 (continued)

Fu (1981) uses the geostrophic box inverse model to study the general circulation and meridional heat transport of the subtropical South Atlantic Ocean. He uses two different data sets: four IGY (zonal) sections and four *Meter* (zonal) sections, and the two data sets are inverted individually. This method is good for determining the velocities and property transports (like the heat transport) *across* the vertical sections, but not good for studying the detailed horizontal circulation structures, as the distances between the sections may be too large. Fu's results do show that the meridional (across the sections) circulations and heat transports of the two data sets are pretty much the same, whereas the details of horizontal circulation of various water masses can be quite different between the two data sets. We cannot expect similarity between the different model results in detail, but it is of interest to examine any similarities or differences in the major features. Some of Fu's results are reprinted in Fig.4.10. For the IGY data set, the circulations for the Surface Water, the AAIW, and the UCPW do have some similarities to our and Reid's model results, whereas the circulations for the deep water, namely the NADW, are different from both of ours and Reid's. In the southern region (south of 15°S), his zonal flow is similar to ours (diffrent from Reid's quasi-meridional flow), but near the equatoral region, his flow pattern shows much small scale structure, quite different from the nearly zonal eastward flow in ours or Reid's results. For the *Meter* results, his circulation pattern for the lower NADW has some similarity to ours (and both different from Reid's almost meridional flow).

4.3 Isopycnal and Diapycnal Diffusivities, Diapycnal velocities and Oxygen Consumptions

The along isopycnal eddy diffusion coefficients (A), diapycnal diffusion coefficients (K), diapycnal velocities (W^*) and oxygen consumtion rates (λ) as functions of depth and the third order polynomial in lateral positions are calculated and shown in Fig.4.5. The isopycnal diffusivities for the water column in the basin have maximum values of $10^4 m^2/s$. The largest value (about $10^4 m^2/s$) appears on the isopycnal $\sigma_1 = 32.28$ on which lies the Upper Circumpolar Water in the south and the North Atlantic Deep Water in the north. Below this level lies the NADW, and it seems that the lateral diffusion coefficients decrease with depth and the solutions on the bottom two levels (the mid-NADW on $\sigma_3 = 41.46$ and the lower NADW on $\sigma_3 = 41.50$) are not significantly different from zero. The eddy diffusities are obviously not uniform in the whole area, and a general trend on all levels are that they are much larger in the north (near equator) than in the south. This implies that the eddy activities in the near equator region are much stronger, and this is consistant with Wyrtki et al (1976)'s eddy energy distribution map (here reprinted as Fig.4.11), although this map is for the statistics for the surface flow. On levels 2 and 3 on which it seems that the AAIW and UCPW reach the northeast region of the basin, the maximum values of the isopycnal diffusivity are at the northeast corner. On levels 4, 5, and 6 on which the NADW enters this basin from the northwest corner, the maximum values of the isopycnal diffusivity are at the northwest corner. Comparing with the streamfunction contours (Fig.4.3) reveals some correspondence between the distribution of the eddy diffusivity and the flow patterns: in the south, where the circulations are more uniform and larger scale, the diffusivities are smaller; in the north, the flows are more complicated and have smaller scales and the diffusities there are larger. On levels 7 and 8 , the smaller scale streamfunction structures appear along the northern half of the east edge of this area (Figs.4.3g,h), and it seems that the larger values of lateral diffusity

extend in the same way (Fig.4.5g,h). For the diapycnal diffusivities, the maximum value is about $20\times10^{-4}m^2/s$ (or $20cm^2/s$) which appears at the northwest corner on the bottom level ($\sigma_3 = 41.5$ for the lower NADW). The areal averaged values for K are no larger than $10 \times 10^{-4}m^2/s$. The general distrubutions on the isopycnals are very similar to that of the isopycnal diffusivities: they are larger in the north (near equator) than in the south region. The diapycnal diffusities for the near surface water (on $\sigma_0 = 26.88$) are very small and are not significantly different from zero. The solutions of K for the upper and mid NADWs are also not significantly different from zero, but those for the lower NADW are significant and are the largest in the water column in this basin. The general solutions for the diapycnal velocity have the magnitude of $10 \times 10^{-7}m/s$, and the extreme value can be as large as $70 \times 10^{-7}m/s$, which appears on the deepest level (the lower NADW). The lateral structures for the diapycnal velocities are similar to those of the diapycnal and isopycnal diffusivities in the main features: stronger in the north (near equator) and weaker in the south. It seems that on the top three levels (the Near Surface Water, AAIW and UCPW), waters are "downwelling". On the next four levels (lower CPW, interface of UCPW and NADW, upper NADW and mid NADW) waters are "upwelling". And on the lower NADW isopycnals, water is downwelling again. The solutions for oxygen consumption rates are unacceptalbly large, but they are not significantly different from zero.

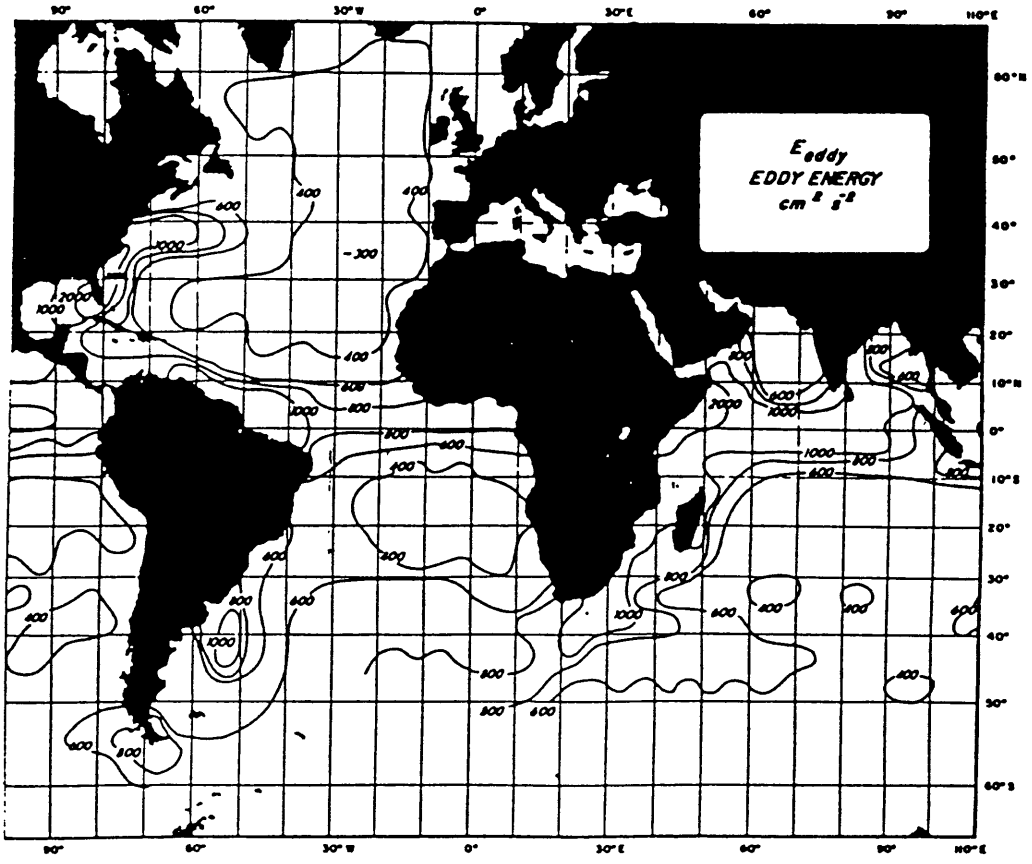

Fig.4.11 Eddy Energy Distributions in The World Oceans. From Wyrtki et al (1976)

There is a vast body of literature on different estimation methods for the eddy diffusivities in the ocean, with a wide range of values. By fitting the mean temperature and salinity profiles for the *interior* Pacific through a simple *vertical* advective-diffusive model, Munk's abyssal recipes (1966) gives a vertical diffusivity of $K = 1.3 \times 10^{-4} m^2/s$ and a vertical velocity of $W \sim 10^{-7} cm/s$. Needler and Heath (1975) modeled the Mediterianean out flow by a tongue diffusion as it spread across the Atlantic with a geostrophic velocity $v = (.2 \sim .4) cm/s$, and they found that $A = (15 \sim 30) \times 10^2 m^2/s$, and $K = (30 \sim 70) \times 10^{-4} m^2/s$. For the deep Pacific ocean, Fiadeiro and Craig (1978) pro-

posed a three dimensional model for the tracers and found that, with the upwelling below the thermocline at 3 m/year, the horizontal diffusivity A should be $10^2 \sim 10^3 m^2/s$ and the vertical diffusivity $5 \times 10^{-5} \sim 10^{-4} m^2/s$. By direct measurements, Gregg (1973,1977) calculated the vertical diffusivity for the Pacific and found that K is smaller than or the order of $10^{-6} m^2/s$. Gargett (1976) also found $10^{-6} m^2/s$ to be typical for the west Pacific although her values may range from 2×10^{-8} to $3 \times 10^{-4} m^2/s$. The box models of chemical tracers (e.g. Broecker and Peng, 1982; Li et al, 1984; Spitzer and Jenkins, 1989) usually yield results in the order of $10^{-4} m^2/s$ for the vertical diffusivity. By formulating an inverse model using the β-spiral method for the North Atlantic Oeean, and using the same Levitus atlas values, Olbers et al (1984) found a strong relation between the distributions of the eddy diffusivities and the energetics of the general circulation. Large eddy diffusivities appear in the strong current regions (e.g., Gulf Stream, the Equatoral Currents), and the small diffusivities appear at the center of the subtropical gyre. The upper limit for his diapycnal diffusivity is about $3 \times 10^{-4} m^2/s$ and appears in the Gulf Stream region. The upper limit for his lateral (isopycnal) diffusivity is about $35 \times 10^2 m^2/s$ and appears near the equator. However his solutions for the diffusive parameters are generally not significantly different from zero compared with their errors. In his original model, Hogg (1987) found the isopycnal diffusivity can be as large as $5 \times 10^2 m^2/s$, the diapycnal diffusivity as large as $5 \times 10^{-4} m^2/s$, and the diapycnal velocity can be as large as $5 \times 10^{-7} m/s$ for the Medteranian tongue region. Using a similar inverse model but in the Cartesian coordinate, Tziperman (1988) found that the value for the vertical difusivity is generally in the order of several cm^2/s, although being a function of depth and depending on the order of inverse calculation and averaging. Most of the works are for the Pacific and North Atlantic Oceans, and less work has been done for the South Atlantic. On the study of the flows of the AABW through the Vema Channel, Hogg et al (1982) found that values of $3.5 cm^2/s$ for the across isotherm diffusivity and $4 \times 10^2 m^2/s$ for the lateral diffusivity are necessary to maintain the heat balance. As discussed before, the so

called eddy diffusivities are model and data set dependent, so that one cannot expect to find *universal* or *constant* values for them. Pond and Pickard (1983) suggest the upper bounds for the horizontal and vertical diffusivities, which are $10^5 m^2/s$ and $10^{-1} m^2/s$ respectively. Compared with the previous works, our values for the diffusivities are not unresonable. In the literature of chemical and biological oceanography, the oxygen consumption rates are generally in the order of $1.0 ml/l/year$ (e.g. Jenkins, 1984,1989), and obviously our values are too large to be acceptable. Compared with their errors, however, these solutions are not significantly different from zero.

4.4 Water Mass Balances in the Brazil Basin

As the currents are generally not flowing along the isopleths of temperature, salinity, oxygen, etc., or equivalently, the water masses are changing their characteristics while flowing on their way. In this section we will show how the water masses modify their properties (by what kind of processes) while flowing, or how the steady fields of water properties (like temperature, salinity, and so on) are maintained in the flow fields. Literally, these are two different approaches: the first is the Lagrangian method, and the second the Eulerian method. But for the steady flows, the traces of the particles coincide with steamfunctions and these two methods are identical. As shown before, the Purely Advective model is not sufficient for the property balances in the basin, thus processes other than isopycnal advection (like diffusions etc.) are also important in the modifications of water properties.

Near Surface Water: $\sigma_0 = 26.88$ On the isopycnal surface for the near surface water ($\sigma_0 = 26.88$), there is dipole structure in the temperature (or salinity) contours: a hot, saltier center near (22°W,8°S) in the north and a cooler, fresher center near (25°W,18°S) in the south. In the southern region the flows are generally towards the northwest, and there is a gyre-like flow in the north. Thus the flows are generally down

the temperature (salinity) gradient in the southeast, and against temperature (salinity) gradient in the other regions. Therefore in the southeast, currents bring hot water down the stream so as to have the tendency to heat up the down stream, cooler region. But in reality, the temperature field is maintained steady, thus cooling processes must also be present there. This is accomplished mainly by the upwelling there, which carries the deep cooler waters up, as shown in Fig.4.4a (top panel). In the regions other than the southeast, the water is generally warmed up on its ways, and the warming is mainly accomplished by downwelling in those regions, which bring the upper warmer water down. Fig.4.4a also shows that on this isopycnal, both the lateral and the diapycnal diffusions are very weak, and they are generally not significant (with regards to the residuals).

As the potential density is only a function of potential temperature and salinity, thus on the isopycnals the salinity contours are the same as the potential temperature contours, and consequently the interpretation of the *isopycnal* advection and *isopycnal* diffusion for salinity is the same as for temperature. Despite the similarities between the temperature and salinity contours on the isopycnals, the diapycnal gradients for temperature and salinity may be very different, thus the relative importances of the diapycnal processes to lateral processes may be different in the temperature balance and in the salinity balance. For example, the salt balance maps (Fig.4.4b) show that the diapycnal advections are ineffective on levels 2, 5, and 7, but are effective in the temperature balances (Fig.4.4a). On the other hand, on levels 3 and 4, the diapycnal advections are effective in the salt balances, but ineffective in the temperature balances. (If double diffusion is in effect, cases become more subtle). But for this near surface water, Fig.4.4b shows that the salinity balance is very similar to the temperature balance: both are mainly balanced by advection—both lateral and diapycnal advections.

The oxygen concentrations generally decrease from south to north on this isopycnal in this area (Fig.3.8). They are distributed nearly zonally in the south, and gyre-like in

the north. There are some similarities between the oxygen contours and the flow patterns, and this implies that oxygen is mainly advected by the lateral flow. The oxygen balance maps (Fig.4.4c) do demonstrate that oxygen is mainly balanced by lateral advection. Diffusion (lateral and diapycnal) and diapycnal advection terms are very small, and although the consumption terms are larger, they are also not significant compared with the residuals. The residuals for oxygen on all the eight levels are large compared with the physical terms, and they do show large scale structures. Whereas the residuals for temperature and salinity are small in comparison with their physical terms, and randomly distributed. We know that the physical processes for the oxygen balance are different from those for the temperature and salinity balances: the former is not conserved while the latter ones are conservative. We added a consumption term in the oxygen balance equations, but unfortunately it turned out that this term is not well determined. There are two possible reasons for the indeterminacy of the oxygen consumption rates and for the large residuals: the proposed models are not appropriate for the oxygen balance (e.g., oxygen may have different diffusivities from those for temperature and salinity; and the consumption rates may not necessarily be proportional to the oxygen concentration), and the data noise for oxygen may be too large to have the less important terms (Fig.4.4 shows that the primarily important term for oxygen balance is the isopycnal advection) to be well determined.

AAIW: $\sigma_1 = 31.88$ On this isopycnal, all the four physical processes, namely the lateral and diapycnal advection and diffusion, are in effect in the temperature balance (Fig.4.4a, 2^{nd} pannel). In the northern region, the downwelling and diapycnal mixing are warming the water mass up, while the lateral mixing (diffusing the heat to the nearby cooler regions) and lateral advection (bring cooler water to this region) are cooling it down. The balance among them maintains the steady field of temperature. In the southern region, the warming associated with lateral advection and diapycnal mixing is balanced by the cooling associated with upwelling and lateral mixing. The interpretation

for the salinity balance is similar to that for temperature. However, as pointed out in the last paragraph, the impact of the diapycnal advection is very small and actually insignificant (Fig.4.4b). For oxygen, Fig.4.4c shows that the balance is mainly among the lateral advection, lateral diffusion, and oxygen consumption, but the diapycnal processes (advection and diffusion) are also effective in the northern region.

UCPW: $\sigma_1 = 32.08$ and $\sigma_1 = 32.28$ On levels 3 and 4 for the UCPW, the temperature (salinity) contours are very similar with each other, and surprisingly different from those on the upper and deeper isopycnals in that they are nearly zonal everywhere in this area. However the temperature (salinity) balance charts shown in Fig.4.4a (Fig.4.4b) suggest that these similar contours arise from different physical processes : on level 3 it represents the balance mainly between the *advection* processes (lateral advection and diapycnal advection), while on level 4, the balance is mainly between *isopycnal* processes (lateral advection and diffusion). On level 3, the flows are against the gradients almost everywhere except in the southeast corner. Accordingly the flows are cooling down in the down stream direction. This cooling effect is balanced by the warming effect of the diapycnal mixing , and thus a steady temperature field is attained.

On level 4, on the other hand, currents flow northeastward (against temperature gradients) in the western half of the region and flow southeastward (down temperature gradients) in the eastern half of this area, thus the water in the west is cooling down and that in the east is warming up as it flows on their way. These changes are mainly balanced by the lateral mixing so as to maintain the steady temperature field. On this level, there seems to be no correspondence between the lateral diffusion flux pattern and the temperature gradients: the temperature contours are nearly zonal while the lateral diffusion fluxes are more or less meridional. We know that there are two terms in the diffusive heat flux (e.g., $\frac{\partial}{\partial x}(A\frac{\partial \theta}{\partial x}) = A\frac{\partial^2 \theta}{\partial x^2} + \frac{\partial A}{\partial x}\frac{\partial \theta}{\partial x}$; $\frac{\partial}{\partial y}(A\frac{\partial \theta}{\partial y}) = A\frac{\partial^2 \theta}{\partial y^2} + \frac{\partial A}{\partial y}\frac{\partial \theta}{\partial y}$). Since there is no coorelation between the heat flux patterns and the temperature contours,

we can infer that there must be some correspondence between the lateral diffusion flux patterns and the patterns of lateral diffusivity gradients, and this inference is confirmed by Fig.4.5d, which gives the distribution of A on this level. The above discussion clearly demonstrates the dynamic importance of the inhomogenity of the diffusivities on the water mass balances, as discussed earlier using the extreme examples of Armi (1979) and Armi and Haidvogel (1982).

For the salinity balances on these two levels, the diapycnal advection also shows some importance, although it is not significant in the temperature balances. There is also some difference between the diapycnal diffusion flux patterns for heat and salt in the very south, because of the possible differences between the diapycnal gredients of temperature and that of salinity. Despite the simple zonal structure of temperature and salinity on these isopycnals, the oxygen contours are more complicated (Fig.3.8). The oxygen balances involve all the proposed physical processes, namely lateral advection and diffusion as well as diapycnal advection and diffusion, and oxygen consumptiom. The residuals are large, however, so that the oxygen balances are not well determined.

Interface between the UCPW and NADW:$\sigma_2 = 36.94$ As discussed before, on isopycnal $\sigma_2 = 36.94$ (level 5) lie the cold, fresh UCPW in the south and warm, saltier NADW in the north region, and this can also be seen from the temperature and salinity contours on this isopycnal as shown in Fig.3.7e. These figures also show that the gradients in the south are stronger than in the north. Corresponding to the strong gradients, the temperature (salnity) balance charts in Fig.4.4a (Fig.4.4b) (the 5^{th} panel) show that in the south, the balance is maintained mainly by the *lateral* processes, i.e. lateral advection is balanced by lateral diffusion. In the north region, the lateral gradients are smaller, thus the lateral processes are weaker and the diapycnal processes are stronger. The cooling of the diapycnal upwelling is balanced by the warming of diapycnal mixing. For the salinity balances, the diapycnal processes (advection and diffusion) are very weak. The oxygen

balances involve all the processes (Fig.4.4c), and because the oxygen increases with depth (actually with potential density), the upwelling brings higher oxygen up to this level.

NADW: $\sigma_2 = 37.00; \sigma_3 = 41.46; \sigma_3 = 41.50$ The temperature balances for the upper NADW (level 6,$\sigma_2 = 37.00$), the mid NADW (level 7,$\sigma_3 = 41.46$), and the lower NADW (level 8, $\sigma_3 = 41.50$) are shown in Fig.4.4a (the $6^{th} \sim 8^{th}$ panel). The corresponding balance charts for salinity and oxygen are shown in Figs.4.4b. Basically, all the processes are important in the mass balance, some more important in one region, and others more important in other regions. In the temperature balances on level 8 (lower NADW), the diapycnal processes (advection and diffusion) are very strong, however they generally have opposite effects (downwelling-warming and diapycnal mixing-cooling), their residuals balance the lateral advection terms, and also balance lateral mixing in the south region. As pointed out before, the circulation patterns on all the three isopycnals for the NADW are very similar with each other. The temperature (salinity, oxygen) contours on these levels shown in Figs.3.7f-h (Figs.3.8f-h) indicate that they are also very similar with each other on all the levels: a cold, fresher center near 13°S and a warm, saltier one near 23°S. Comparing the circulation patterns with the temperature (salinity) contours, one can also find a close correlation between them. The *permanent* anticyclonic gyre (appearing on all the three isopycnals) corresponds to the *permanent* cold, fresher center, with the gyre center just south of the cold center. If we draw a line along the cold, fresh tongue, we find that this line is just in the position of the northwestward flowing current and just north of the gyre center. In the south, the direction of the warm, saltier tongue corresponds to the strong southeastward flowing current of the NADW. Thus without *a priori* prejudice toward forcing the flows to go along the tongues of the water properties (θ or S), we do find the flows are along the tongues. Therefore the idea of the core-layer method is confirmed.

However the core-layer method cannot tell us the details of the flows, especially when the tongue disappears. Under this circumstance, we don't know where the flows are going. But our flow fields can tell us all about this. For example, the cold, fresh water first goes along the tongue, and when the tongue becomes weaker, the water leaves the tongue. In the north it flows toward the northeast and finally joins the northern northeast flowing NADW (there the flows are almost along the isotherms). In the south, the leaving the tongue water flows southeastward and joins the southeast flowing current of NADW (In the very south, the flow direction is also nearly along the isotherms). Of course we cannot say that the disappearing of the cold tongue is the reason of the splitting of the cold current, we should explain the problem in the other way: the northwest flowing cold, fresher current meets the oncoming warm, saltier NADW near (25°W,13 °S) and deflects to the north and south and joins the northern and southern NADWs respectively and because of this, the cold fresh tongue disappears.

Mass Conservation–Balances in the Coutinuity Equation In the formulation of the continuity equation, we have expanded the three dimensional nondivergence into three physical terms, namely the isopycnal divergence term (the lateral velocity is divergent), the planetary divergence term (advection of β, the variation of the Coriolis parameter), and the diapycnal divergence term. The balance of these terms are shown in Fig.4.4d, and it can be seen that on most of the isopycnals (all the levels except level 8), the balances are mainly between the lateral processes: that is the lateral divergence balances the planetary divergence. The diapycnal divergence is important only on the isopycnals for the lower NADW (level 8), on which the diapycnal velocity is large and is opposite in sign to those on upper (level 6) and mid NADW (level 7).

Integrated Vorticity Balances In the integrated vorticity equation between two isopycnal surfaces, Eq.(3.35) there are the following terms: the diapycnal velocity difference (or diapycnal stretching), the difference of isopycnal advections of p (or z),

or the *vertical* velocity difference resulting from the flows along sloping isopycnals (or vertical stretching), the difference of the advections of the planetary vorticity, and finally, the right hand side (RHS) inhomogeneous term associated with the sloping effects of the specific volume anomaly and pressure (or z) along the isopycnals. These terms for all the 8 levels are shown in Fig.4.4e and it can be seen that in the integrated vorticity equation the balance is mainly between the advection of the planetary vorticity and the RHS inhomogeneous term, all the other terms are much smaller except on the last level (level 8 for the lower NADW), on which diapycnal velocity manifests importance on the south boundary.

Balances in the Dynamic Equation In Fig.4.4f the balance terms in the Dynamic Equation, Eq.(3.1), are plotted. The first column is the streamfunction difference between two isopycnals, and the second column is the terms on the RHS—the theoretical difference for the streamfunctions by the geostrophy and hydrostatics. The very similarities of these two terms and the relatively very small residuals on all the levels assure us that the thermal wind relation is well satisfied by the computed flows.

4.5 Effects of Double Diffusion

In accordance with the fact that the seawater density is determined by two different properties of seawater, namely temperature and salinity, there is a special mixing mechnamism in the ocean, known as the double-diffusive mixing. The real stability of the ocean is determined not only by the distribution of the density field itself, but also by the respective distribution of the densities associated with the two properties. Even if the total density is stably distributed, if the density associated with one property is unstably distributed, the potential energy stored in this unstable component can be released through the instability due to the large difference between the molecular diffusivities of temperature and salinity ($\kappa_T/\kappa_S \sim 100$). Depending upon whether the instability is

induced by upper cold temperature (with larger diffusivity) or by higher salinity (with smaller diffusivity), the mixing is called diffusive mixing or salt-finger mixing. In the diffusive mixing, heat transport is more efficient than salt transport, and vice versa in the salt-finger mixing. In terms of $R_F = \alpha F_T/\beta F_S$, the ratio of heat density flux to salt density flux (where F_T and F_S are heat and salt flux respectively), $R_F > 1$ for the diffusive case, and $R_F < 1$ for the salt-finger case. R_F is generally a function of the stability parameter, $R_\rho = \alpha T_z/\beta S_z$. Expressing the heat and salt fluxes by the vertical eddy diffusivities (K_T, K_S) allows the R_F to be expressed in terms of K_T, K_S and R_ρ as follows:

$$R_F = \frac{\alpha F_T}{\beta F_S} = \frac{\alpha K_T T_z}{\beta K_S S_z} = \frac{K_T}{K_S}\frac{\alpha T_z}{\beta S_z} = \frac{K_T}{K_S} R_\rho \tag{4.1}$$

In the salt-finger case, we must have $R_\rho = \alpha T_z/\beta S_z > 1$ to maintain the total density stably distributed, and thus $R_F < 1$ implies that $\frac{K_T}{K_S} < R_\rho^{-1} < 1$, or $K_S > K_T$. Similarly, in the diffusive case, we must have $R_\rho = \alpha T_z/\beta S_z < 1$ to maintain the density stably distributed, and $R_F > 1$ for the diffusive case implies that $\frac{K_T}{K_S} > R_\rho^{-1} > 1$, or $K_T > K_S$. (For the diffusive case, one of Stern(1975)'s example shows that

$$\frac{K_T}{K_S} = R_\rho^{-1}(\kappa_T/\kappa_S)^{1/2} \sim 10 R_\rho^{-1}) \tag{4.2}$$

Simply stated, the eddy diffusivty for the driving component is larger than that for the driven component. In reality, not all the potential energy in the double diffusive instability can be released. For salt finger case, Schmitt (1979) finds that salt fingers have relatively low growth rates until $R_\rho < 2$. For both the diffusive and salt finger cases, laboratory results suggest that the instability growth rate increases as R_ρ approaches unity (e.g. Turner,1973). Besides the intrinsic relation of the growth rate, there is a more subtle question about the real importance of double diffusion in ocean mixing.

Double diffusion is only one of the mechanisms in ocean mixing, other processes (such as wave breaking, cabbeling, turbulance etc.) may also be important. If the other mixing processes are very strong, even effects of fully developed double difusion may not be evident at all. If one considers the importance of the double diffusion in the water mass (e.g., temperature, salinity) balances, the situation is even more subtle, because more processes are involved in the balances, such as advection, lateral difusion, and so on. Even when the distribution of temperature and salinity (or R_ρ) suggest that double diffusion is strong, its role in the water mass balances may be still relatively unimportant compared with other processes; examples can be found in Gargett (1989). These discussions indicate that the presence of distinctive double diffusive mixing may be used only as a *potential* indicator, and its real importance should be analyzed together with all other processes.

The profiles of the stability parameter R_ρ in the Brazil Basin (one example is shown in Fig.1.1) indicate that there are several *potential* regions for the double diffusion to occur. To reveal whether it is really important in the water mass balances, using our model and the Levitus atlas values, we ran the 8 level model with different unknowns for K_T and K_S (we assume that $K_{o2} = K_s$, because oxygen has a similar molecular diffusivity as salinity). The results are shown in Fig.4.6 to Fig.4.8. As far as the circulations are concerned, there are no differences in the solutions between the single and double diffusive model, as pointed out before. For the lateral diffusion coefficient A, the two model results are also not significantly different from each other. The solutions for the oxygen consumption rates are still not resolved, as in the former (single) model, thus no significant differences can be discussed. The lateral patterns of the diapycnal velocity solutions are respectively (level to level) the same for the two models on all the 8 levels , however there are some differences in numerical values on some levels. From the solutions for K_T and K_S themselves, it can be seen that the most significant differences between them are obtained on levels 3 and 6. But the solutions for level 6 are not significantly

different from zero as compared with their errors, thus the real diffrence between K_T and K_S is obtained on level 3, on which it can seen that $K_T > K_S$ (K_S is actually not significantly from zero). Corresponding to this level is a thin, weak inversion (increases with depth) in the temperature profiles (Fig.4.12a) and strongly stable salinity profiles (Fig.4.12b), so that the stability parameter R_ρ (Fig.1.1) falls into the temperature driven diffusive double diffusion regime, and $K_T > K_S$ is thus required as mentioned before.

There is another way to determine the effectiveness of the double diffusive mixing, i.e. by looking at the $\theta - S$ relations. If the double diffusion is not effective (compared with other mixings), i.e. the eddy diffusivities for temperature and salinity are the same, then the $\theta - S$ relation tends to be linear. On the other hand, in regions of effective double diffusive mixing, instead of the linear $\theta - S$ relationship, the $\theta - S$ relation tends to be along constant stability ratio ($R_\rho = const$), or $\alpha\theta - \beta S$ tends to be linear (Ingham,1966; Schmitt, 1981, 1990). The $\theta - S$ and $\alpha\theta - \beta S$ profiles in the several *potential* double diffusion ranges (shown on the R_ρ profiles, Fig.4.1.1) are shown in Fig.4.13, taken from a station at (28.5°W, 6.5°S) in the northwest corner (where diffusions are stronger) as an example. It can be seen that only in the region where the temperature inversion appears (corresponding to level 3), the $\alpha\theta - \beta S$ relation is more linear than $\theta - S$ relation, indicating the effectiveness of double diffusion in this region. In all the other regions, $\theta - S$ relations are more linear, and there are no indications of effective double difusive mixing.

a

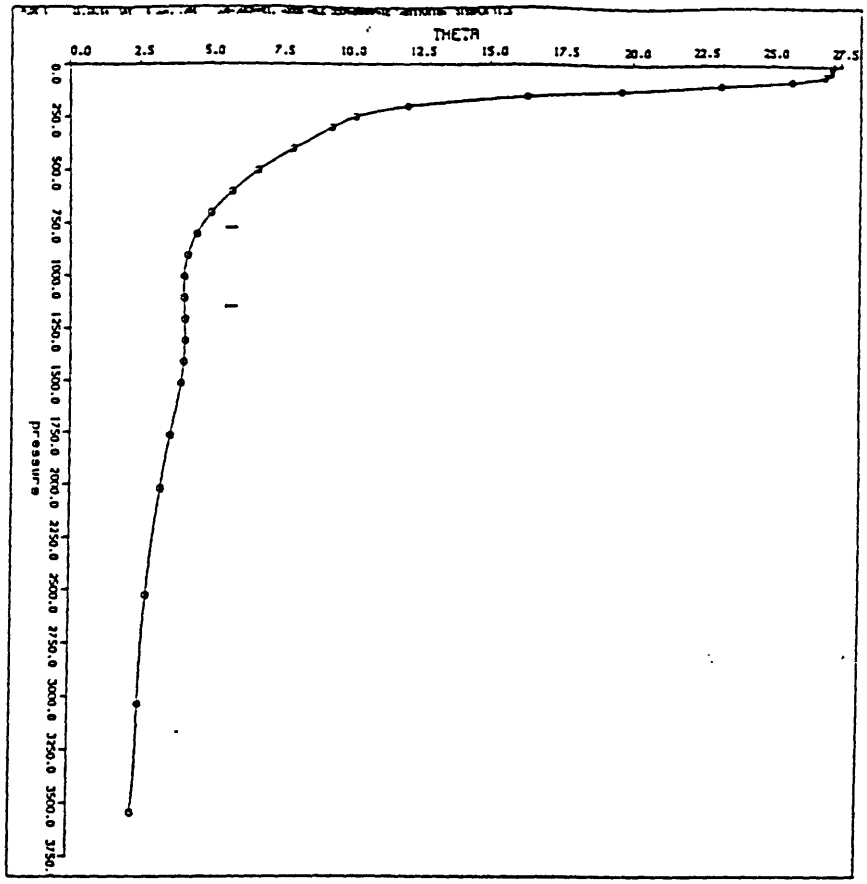

b

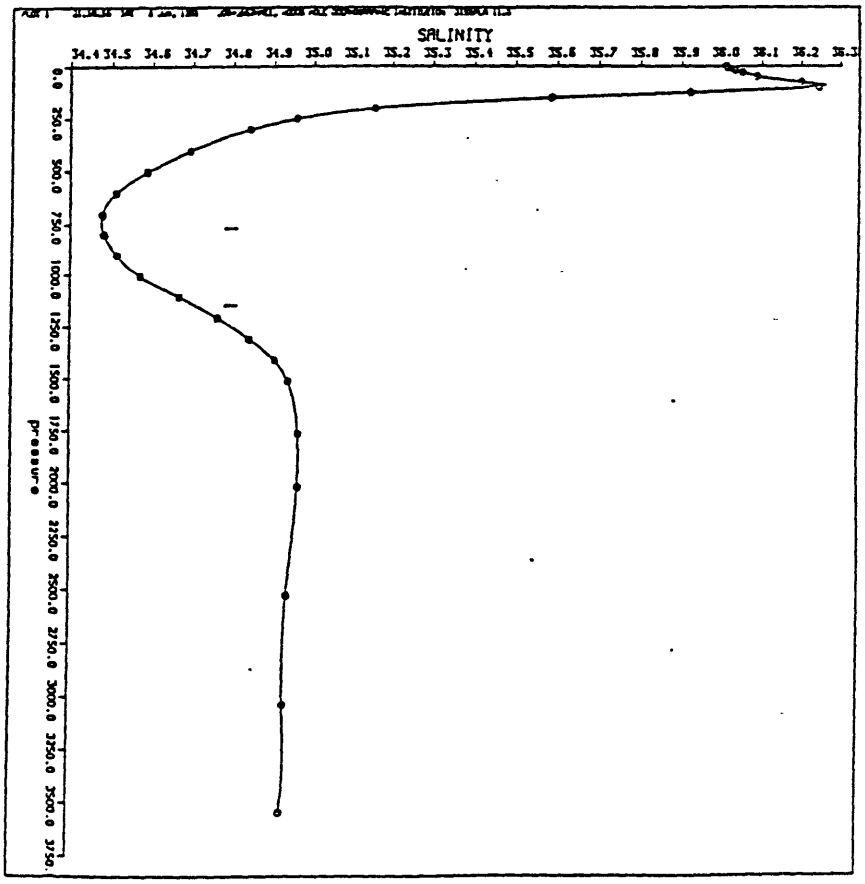

Fig.4.12 Profiles of (a) Potential temperature and (b) Salinity

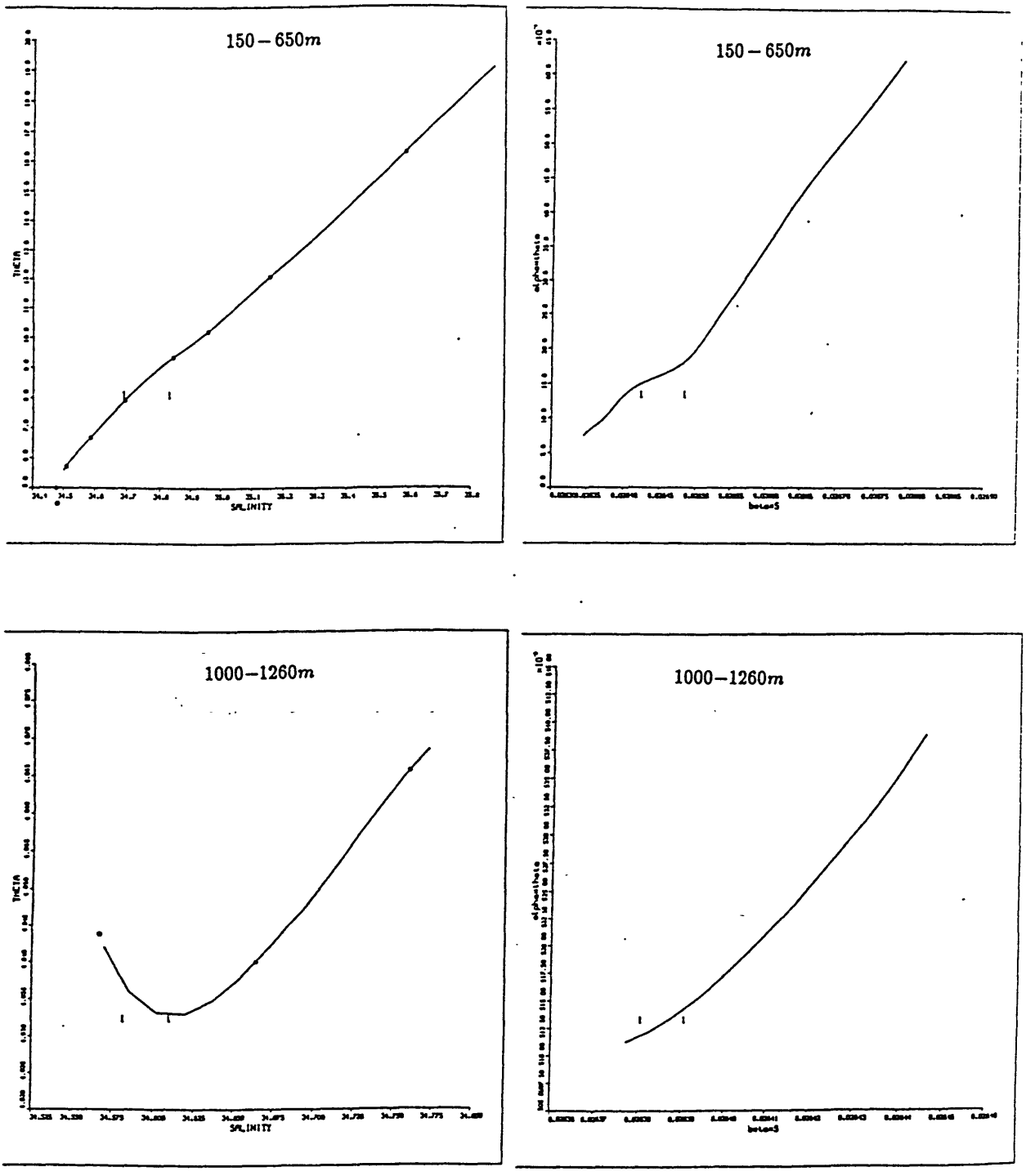

Fig.4.13 $\theta - S$ (left) and $\alpha\theta - \beta S$ (right) relations for several depth ranges

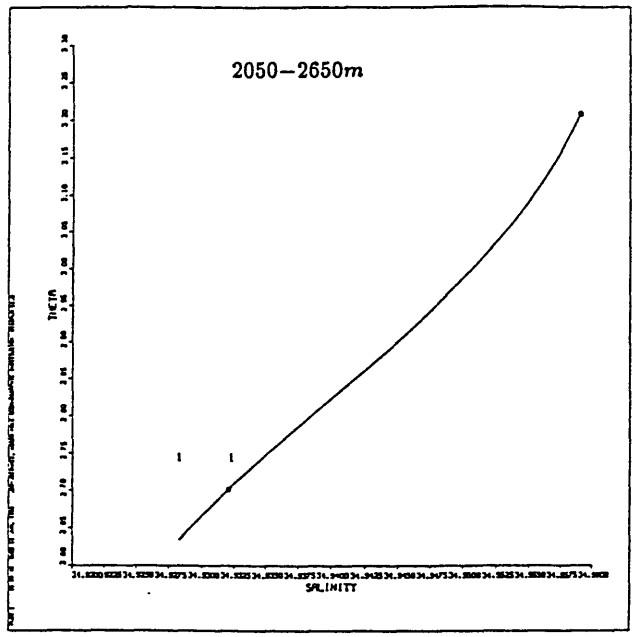

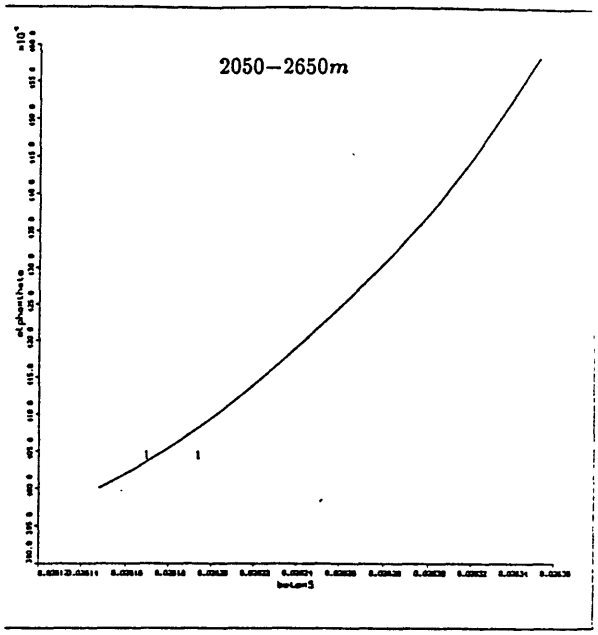

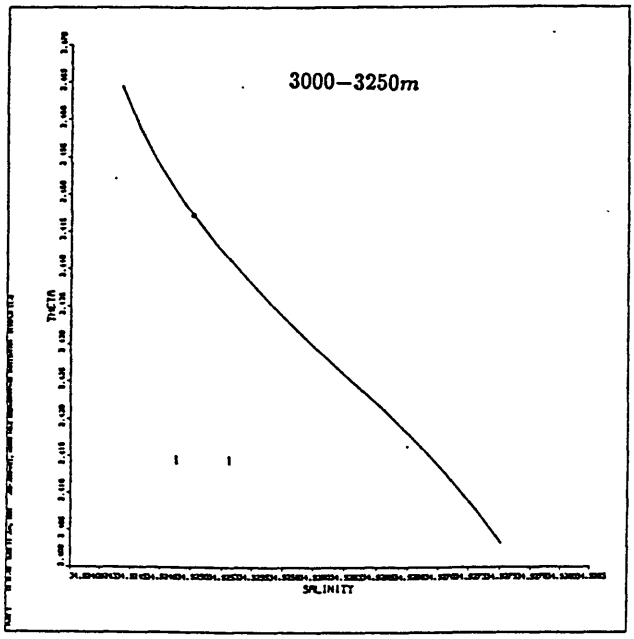

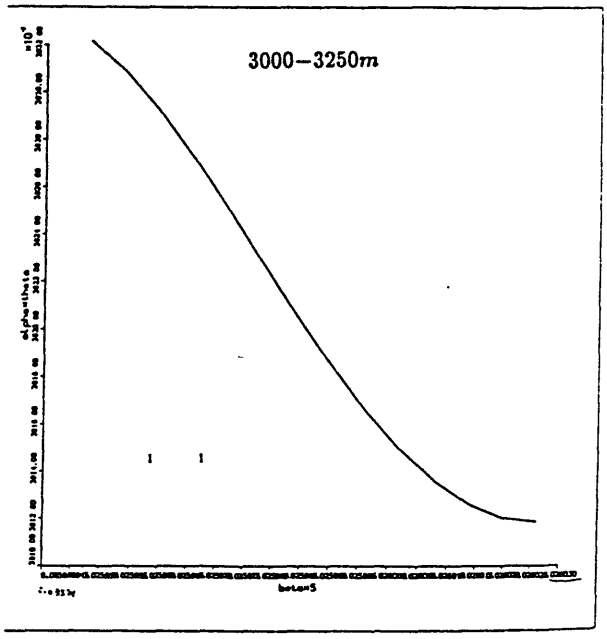

Fig.4.13 (continued)

CONCLUDING REMARKS

In the previous chapters, new streamfunctions (pressure anomaly and main pressure streamfunctions) have been proposed for use on potential density surfaces. By considering the variations of specific volume anomaly and pressure along isopycnal surfaces, the inverse model proposed by Hogg (1987) has been modified to make it more accurate in the potential density coordinates. Detailed estimates of the circulations, diffusions and water mass balances on the eight isopycnals have been studied by applying the modified model using the Levitus atlas values in the Brazil Basin.

Potential density analysis has long been used in descriptive oceanography, based on the assumption that water properties are advected mainly along isopycnal surfaces. Potential density coordinates have also been widely used recently in dynamic models. Some streamfunctions for certain vertical coordinates have been derived, but the exact form of streamfunctions for potential density coordinates is not known yet. Most previous works apply the Montgomery streamfunction to the potential density coordinates, in which the variation of specific volume anomaly along isopycnals has been ignored. In the first part of this work, I found that although the variation itself is small, its effects on the geostrophic velocity (product of pressure with the slops of δ) cannot be ignored because of the large value of the coefficient (p). By including the major part of this effect, the so called pressure anomaly and main pressure streamfumctions are suggested for use in potential density coordinates, in which the leftover part induces errors in velocity no larger than 10%. From this formulation, these streamfuntions can also be used in other gently sloping surfaces without producing large errors.

The inverse model used in this work comprises the dynamic method and water property conservations, as in most of the inverse models. But in this model, equations are written in the point-wise basis in potential density coordinates, in which are implied the water mass conservations over small volumes (boxes), thus detailed circulations and

mass balance processes can be studied. The current model results for the circulations for the upper levels in the Brazil basin show some consistency with previous works, but those at the deep levels are quite different. On the upper levels, there is a cyclonic gyre in the Brazil basin, and the gyre centre migrates southward as it goes deeper. Moreover, there is a close correlation between the circulation patterns and pressure contours , however this correlation is not apparent on the deep levels. The flows are generally stronger in the region near the equator than in the south. For the deep water, the present results show that the southward flowing NADW along the western boundary gradually turns to east into the Brazil basin from north to south, and in the north, the NADW leaves the basin northeastward and may traverse the mid-Atlantic ridge through the equatoral fracture zone passages and enter the Angola basin as the source water for that basin. Examples of the coincidence of the flow paths with the tongues of water properties are also found in this work.

The magnitudes of the diffusivities and diapycnal velocities differ from place to place, and they are not unreasonable compared with their values in the literature. They are larger in the region near equator than in the south, which is consistant with the previous study on eddy energy distributions. Diffusion plays an important role in the water mass balances. Since the flows are generally not along the isopleths of water properties, therefore the steady fields must be maintained by diffusive processes. Similar property fields at different depths and in different areas may result from quite different processes, as shown in this work and the work by Hogg (1987). In addition, variations of the diffusivities may also have dynamic importance in the water mass balances.

There are certain limitations in the current model. The exclusion of the topography and the irregular boundary limit further discussions on the flows of water masses. This work shows quite different pictures for the deep circulations from previous works, which should be verified by observations or theories. The balances in oxygen conserva-

tion are not well resolved, for reasons which are still unclear (one possibility is that the Levitus atlas values may not be accurate enough, more accurate data are needed).

Acknowledgments

I would like first to thank my thesis advisor, Nelson Hogg, for his patient guidance, encouragements and valuable discussions on this work, for the generously sharing of his time and ideas with me, for careful readings of the preliminary versions of this thesis, and for his teaching me the lively English. Talking with him is always fruitful and full of fun. In the period of this work, I have learned from him how to think critically and communicate more effectively .

My thanks also go to my thesis committee members, Carl Wunsch, Harry Bryden, Mike McCartney, and Breck Owens, for their encouragements and many helpful suggestions. Discussions with Susan Lozier, Ray Schmitt in the PO and Bill Jenkins in the Chemistry departmet are also helpful in understanding the problems and interpreting the results.

Support and friendship also come from the Joint Program students. Special thanks are for Changsheng Chen for his help in learning the Latex.

Finally, I thank my wife for her support in the past years.

REFERENCES

Armi, L., 1979. Effects of variations in eddy diffusity on property distributions in the ocean. *Journal of Marine Research*, **37**, 525–530.

Armi, L., and D.B. Haidvogel, 1982. Effects of variable and Anisotropic Diffusivities in a steady-state Diffusive Model. *Journal of Physical Oceanography*, **12**, 785–794.

Brecker, W.S. and T.H. Peng, 1982. *Tracers in the Sea.* New York, Eldigio Press. 690 pages.

Bryden, H.L., 1977. Geostrophic comparisons from moored measurements of current and temperature during the Mid-Ocean Dynamics Experiment. *Deep-Sea Research*, **24**, 667–681.

Ekman, V.W., 1934. Review of: Georg Wüst. "Das Bodenwasser und die Gliederung der Atlantsichen Tiefsee". *Journal du Conseil*,6, 102–104.

Fiadeiro, M.E., and H. Craig, 1978. Three-dimensinal modeling of tracers in the deep Pacific Ocean: I. Salinity and oxygen. *Journal of Marine Research*, **36**, 323–355.

Fiadeiro, M.E., and G. Veronis, 1984. Obtaining velocities from tracer distributions. *Journal of Physical Oceanography*, **14**, 1734–1746.

Fu, L.L., 1981. The General Circulation and Meridional Heat Transport of the Subtropical South Atlantic Determined by Inverse Methods. *Journal of Physical Oceanography*, **11**, 1171–1193.

Gargett, A.E., 1986. An investigation of the occurrence of oceanic turbulence with respect to finestructure. *Journal of Physical Oceanography*, **6**, 139–156.

Gargett, A.E., 1989. Ocean Turbulance. *Ann. Rev. Fluid Mech.*, **21**, 419–451.

Gill, A.E., 1982. *Atmospheric-Ocean Dynamics*. Academic Press. 662 pages.

Gregg, M.C., 1987. Diapycnal mixing in the thermocline: a review. *Journal of Geophysical Research*, **92(C5)**, 5249–5286.

Hogg,N., 1987. A least-squares fit of the advective-diffusive equations to Levitus Atlas data. *Journal of Marine Research*, **45**, 347–375.

Hogg,N., P.Biscaye, W.Gardner and W.J. Schmitz, Jr., 1982. On the transport and modification of Antarctic Bottom Water in the Vema Channel. *Journal of Marine Research*, **40**, 231-263.

Ingham, M.C., 1966. The Salinity Extrema of the World Ocean. Ph.D. Dissertation, Oregan State University, Corvallis, p.63.

Jenkins, W.J., 1984. The Use of Tracers and Water Mass to estimate Rates of Respiration. In *HETEROTROPHIC ACTIVITY IN THE SEA*, edited by J.E. Hobble and P.J. Williams, Plenum Publishing Corporation.

Jenkins, W.J., 1987. ^3H and ^3He in the Beta Triangle: Observations of Gyre Ventilation and Oxygen Utilization Rates. *Journal of Physical Oceanography*, **17**, 763–783.

Lawson, C.L., and R.J. Hanson, 1974.*Solving Least Squares Problems.* Prentice-Hall, Inc., Englewood Cliffs, NJ, 340 pages.

Levitus, S., 1982. *Climatological Atlas of the World Ocean.* NOAA Professional Paper 13, National Oceanic and Atmospheric Administration, Rockville, Maryland. 173 pages.

Li, Y.H., T.H. Peng, W.S. Broecker, and G. Östlund, 1984. The average vertical mixing coefficient for the oceanic thermocline. *Tellus*, **212–217.**

McDougall, T.J., 1987. Neutral Surfaces. *Journal of Physical Oceanography*, **17**, 1950–1964.

McDougall, T.J., 1989. Streamfunction for the lateral velocity vector in a compressible ocean. *Journal of Marine Research*, **47**, 267–284.

McDougall, T.J., 1991. Parameterizing Mixing in Inverse Models. (*to be published*)

Montgomery, R.B., 1938. Circulation in upper layers of southern North Atlantic deduced with use of isentropic analysis. *Papers in Physical Oceanography and Meterology*, **6**, 2,55 pp.

Munk, H.M.,1966. Abyssal Recipes. *Deep-Sea Research*, **63**, 707–730.

Needler, G.T., and R.A. Heath, 1975. Diffusion coefficients calculated from the Mediterranean salinity anomaly in the North Atlantic Ocean. *Journal of Physical Oceanography*, **5**, 173–182.

Olbers, D.J., M.Wenzel, and J. Willebrand, 1985. The inference of North Atlantic circulation patterns from climatological data. *Rev. Geophys.*, **23**, 313–356.

Pedlosky, J., 1987. *Geophysical Fluid Dynamics.* 2nd ed. Springer-Verlag, 710 pages.

Pond, S. and G. Pickart, 1983. *Introductory Dynamical Oceanography.* 2nd edition. Pergamon Press. 329 pages.

Reid, J., 1989. On the total geostrophic circulation of the South Atlantic Ocean: Flow patterns, tracers, and transports. *Prog. Oceanog.*, **23**, 149–244.

Reid, J., 1980. On the Mid-depth Circulation of the World Oceans. In *Evolution of Physical Oceanography*, edited by B.A. Warren and C. Wunsch. The MIT press. 623 pages.

Rintoul, S.R., 1988. Mass, Heat and Nutrient Fluxes in the Atlantic Ocean Determined by Inverse Methods. Ph.D Dissertation, MIT/WHOI Joint Program. 287 pages.

Schmitt, R.W.,Jr., 1979. The growth rate of super-critical salt fingers. *Deep-Sea Research*, **26A**, 23–40.

Schmitt, R.W.,Jr., 1981. Form of Temperature-Salinity Relationship in the Central Water: Evidence for Double-Diffusion Mixing. *Journal of Physical Oceanography*, **11**, 1015–1026.

Schmitt, R.W.,Jr., 1990. On the Density Ratio Balance in the Central Water. *Journal of Physical Oceanography*, **20**, 900-906.

Spitzer, W.S., and W.J. Jenkins, 1989. Rates of vertical mixing, gas exchange and new production: Estimates from seasonal gas cycles in the upper ocean near Bermuda. *Journal of Marine Research*, **47**, 169–196.

Stern, M.E., 1975. *Ocean Circulation Physics*, Chapter 11. Academia Press.

Stommel, H., and F. Schott, 1977. The beta spiral and the determination of the absolute velocity field from hydrographic station data. *Deep-Sea Research*, **24**, 325–329.

Turner, J.S., 1973. *Buoyancy Effects in Fluids.* Cambridge: Cambridge University Press. 367 pages.

Turner, J.S., 1980. Small Scale Mixing Processes. In *Evolution of Physical Oceanography*, edited by B.A. Warren and C. Wunsch. The MIT press. 623 pages.

Tziperman, E.,1987. Mixing and General Circulation Dynamics: Theory and Observations. Ph.D Dissertation, MIT/WHOI Joint Program. 162p.

Tziperman, E.,1988. Calculating the Time-Mean Oceanic General Circulation and Mixing coefficients from Hydrographic data. *Journal of Physical Oceanography*, **18**, 519–525.

Wiggins, R.A., 1972. The general linear inverse problem: Implication to Surface Waves and free osciltations on earth. *Rev. Geophys.* **10**, 251–285.

Wright, R., 1969. Deep Water Movement in the Western Atlantic as determined by use of a box model. *Deep-Sea Research*, **16**, 433-446.

Wunsch, C., 1977. Determing the General Circulation of the Ocean: A preliminary Discussion. *Science*, **196**, 871–875.

Wunsch, C., 1978. The general circulation of the North Atlantic west of 50°W determined from inverse methods. *Reviews of Geophysics and Space Physics*, **16**, 583–620.

Wüst, G., 1933. Schichtung und Zirkulation des Atlantischen Ozeans. Das Bodenwasser und die Gliederung der Atlantsichen Tiefsee. In *Wissenschaftliche Ergebnisse der Deuschen Atlantstchen Expedition auf dem Forschungs–und vermessungsschiff "Meter" 1925-1927, 6: 1st Part, 1, 106pp.*

Wüst, G., 1935. Schichtung und Zirkulation des Atlantischen Ozeans. Die Stratosphäre. In *Wissenschaftliche Ergebnisse der Deuschen Atlantstchen Expedition auf dem Forschungs–und vermessungsschiff "Meter" 1925-1927, 6: 1st Part, 2, 180pp.*

Wyrtki, K., L. Magaard, and J. Hager, 1976. Eddy energy in the oceans. *Journal of Geophysical Research*, **81**, 2641–2646.

Appendix A: Difference Equations

Use the centered difference scheme on the staggered grids shown in Fig.3.9, the controlling equations can be witten in the box balance form as follows, taken the conservation equations for water properties as an example.

In terms of the streamfunction, the conservation equation, Eq.(3.56), is rewritten as

$$\begin{aligned}\sigma_z \quad & \frac{1}{f_0}[-\frac{\partial}{\partial x}(\frac{C'}{\sigma_z}\frac{\partial \psi}{\partial y}) + \frac{\partial}{\partial y}(\frac{C'}{\sigma_z}\frac{\partial \psi}{\partial x})] - \frac{\beta C'}{f_0^2}\frac{\partial \psi}{\partial x} + \sigma_z C' {w^*}_\sigma + \frac{\partial C}{\partial z}w^* \\ = \quad & \sigma_z[\frac{\partial}{\partial x}(\frac{A}{\sigma_z}\frac{\partial C}{\partial x}) + \frac{\partial}{\partial y}(\frac{A}{\sigma_z}\frac{\partial C}{\partial y})] + \sigma_z \frac{\partial C}{\partial z}K_\sigma + \frac{\partial^2 C}{\partial z^2}\cdot K - C\cdot\lambda \qquad (4.3)\end{aligned}$$

Using the central difference, the difference form of the above equation at point (i,j,k) is witten as

$$\begin{aligned}\frac{\sigma_{zi,j,k}}{f_j}\{ \quad & - \frac{\frac{[(\frac{C'}{\sigma_z})_{i,j,k}+(\frac{C'}{\sigma_z})_{i+1,j,k}]}{2}[\frac{\psi_{i,j,k}-\psi_{i,j-1,k}}{L_y}] - \frac{[(\frac{C'}{\sigma_z})_{i-1,j,k}+(\frac{C'}{\sigma_z})_{i,j,k}]}{2}[\frac{\psi_{i-1,j,k}-\psi_{i-1,j-1,k}}{L_y}]}{L_x} \\ & + \frac{\frac{[(\frac{C'}{\sigma_z})_{i,j+1,k}+(\frac{C'}{\sigma_z})_{i,j,k}]}{2}[\frac{\psi_{i,j,k}-\psi_{i-1,j,k}}{L_x}] - \frac{[(\frac{C'}{\sigma_z})_{i,j-1,k}+(\frac{C'}{\sigma_z})_{i,j,k}]}{2}[\frac{\psi_{i,j-1,k}-\psi_{i-1,j-1,k}}{L_x}]}{L_y}\} \\ & - (\frac{\beta}{f_0^2})_j C'_{i,j,k}\frac{\frac{\psi_{i,j,k}-\psi_{i-1,j,k}}{L_x}+\frac{\psi_{i,j-1,k}-\psi_{i-1,j-1,k}}{L_x}}{2} \\ & + C'_{i,j,k}\frac{1}{2}(\frac{w^*_{i,j,k}-w^*_{i,j,k-1}}{z_{i,j,k}-z_{i,j,k-1}}+\frac{w^*_{i,j,k+1}-w^*_{i,j,k}}{z_{i,j,k+1}-z_{i,j,k}}) + C_{zi,j,k}{w^*}_{i,j,k} \\ = \quad & \sigma_{zi,j,k}[\frac{\frac{A_{i+1,j,k}+A_{i,j,k}}{\sigma_{zi+1,j,k}+\sigma_{zi,j,k}}\frac{C_{i+1,j,k}-C_{i,j,k}}{L_x} - \frac{A_{i,j,k}+A_{i-1,j,k}}{\sigma_{zi,j,k}+\sigma_{zi-1,j,k}}\frac{C_{i,j,k}-C_{i-1,j,k}}{L_x}}{L_x} \\ & + \frac{\frac{A_{i,j+1,k}+A_{i,j,k}}{\sigma_{zi,j+1,k}+\sigma_{zi,j,k}}\frac{C_{i,j+1,k}-C_{i,j,k}}{L_y} - \frac{A_{i,j,k}+A_{i,j-1,k}}{\sigma_{zi,j,k}+\sigma_{zi,j-1,k}}\frac{C_{i,j,k}-C_{i,j-1,k}}{L_y}}{L_y}] \\ & + C_{zi,j,k}\frac{1}{2}(\frac{K_{i,j,k}-K_{i,j,k-1}}{z_{i,j,k}-z_{i,j,k-1}}+\frac{K_{i,j,k+1}-K_{i,j,k}}{z_{i,j,k+1}-z_{i,j,k}}) + C_{zzi,j,k}K_{i,j,k} \\ & - C_{i,j,k}\lambda_{i,j,k} \qquad (4.4)\end{aligned}$$

or, collecting the coefficients for the same unknowns, we obtain

$$- \frac{\sigma_{zi,j,k}}{L_x L_y}\frac{1}{2f_j}\{[(\frac{C'}{\sigma_z})_{i+1,j,k}-(\frac{C'}{\sigma_z})_{i,j+1,k}]\psi_{i,j,k} + [(\frac{C'}{\sigma_z})_{i,j-1,k}-(\frac{C'}{\sigma_z})_{i+1,j,k}]\psi_{i,j-1,k}$$

$$+[(\frac{C'}{\sigma_z})_{i,j+1,k}-(\frac{C'}{\sigma_z})_{i-1,j,k}]\psi_{i-1,j,k}+[(\frac{C'}{\sigma_z})_{i-1,j,k}-(\frac{C'}{\sigma_z})_{i,j-1,k}]\psi_{i-1,j-1,k}\}$$

$$-\frac{\sigma_{zi,j,k}}{L_xL_y}(\frac{\beta L_y}{f})_j\frac{1}{2f_j}(\frac{C'}{\sigma_z})_{i,j,k}[\psi_{i,j,k}-\psi_{i-1,j,k}+\psi_{i,j-1,k}-\psi_{i-1,j-1,k}]$$

$$+\frac{1}{2}[\frac{C'_{i,j,k}}{p_{i,j,k}-p_{i,j,k-1}}w^*_{i,j,k-1}$$

$$+(\frac{C'_{i,j,k}}{p_{i,j,k+1}-p_{i,j,k}}-\frac{C'_{i,j,k}}{p_{i,j,k}-p_{i,j,k-1}}+2C_{zi,j,k})w^*_{i,j,k}-\frac{C'_{i,j,k}}{p_{i,j,k+1}-p_{i,j,k}}w^*_{i,j,k+1}]$$

$$=\frac{\sigma_{zi,j,k}}{L_x^2}[\frac{C_{i+1,j,k}-C_{i,j,k}}{\sigma_{zi+1,j,k}+\sigma_{zi,j,k}}(A_{i+1,j,k}+A_{i,j,k})-\frac{C_{i,j,k}-C_{i-1,j,k}}{\sigma_{zi,j,k}+\sigma_{zi-1,j,k}}(A_{i,j,k}+A_{i-1,j,k})]$$

$$+\frac{\sigma_{zi,j,k}}{L_y^2}[\frac{C_{i,j+1,k}-C_{i,j,k}}{\sigma_{zi,j+1,k}+\sigma_{zi,j,k}}(A_{i,j+1,k}+A_{i,j,k})-\frac{C_{i,j,k}-C_{i,j-1,k}}{\sigma_{zi,j,k}+\sigma_{zi,j-1,k}}(A_{i,j,k}+A_{i,j-1,k})]$$

$$+\frac{1}{2}[\frac{C_{zi,j,k}}{p_{i,j,k}-p_{i,j,k-1}}K_{i,j,k-1}$$

$$+(\frac{C_{zi,j,k}}{p_{i,j,k+1}-p_{i,j,k}}-\frac{C_{zi,j,k}}{p_{i,j,k}-p_{i,j,k-1}}+2C_{zzi,j,k})K_{i,j,k}-\frac{C_{zi,j,k}}{p_{i,j,k+1}-p_{i,j,k}}K_{i,j,k+1}]$$

$$-C_{i,j,k}\lambda_{i,j,k} \tag{4.5}$$

Note that $f_j \sim 10^{-4}$, in order to make the coefficients for the unknowns in $O(1)$, multipling the above equation by $L_xL_y10^{-4}$, and move the LHS to the RHS, we obtain

$$\sigma_{zi,j}\frac{10^{-4}}{2f_j}\{[(\frac{C'}{\sigma_z})_{i+1,j}-(\frac{C'}{\sigma_z})_{i,j+1}]\psi_{i,j}+[(\frac{C'}{\sigma_z})_{i,j-1}-(\frac{C'}{\sigma_z})_{i+1,j}]\psi_{i,j-1}$$

$$+[(\frac{C'}{\sigma_z})_{i,j+1}-(\frac{C'}{\sigma_z})_{i-1,j}]\psi_{i-1,j}+[(\frac{C'}{\sigma_z})_{i-1,j}-(\frac{C'}{\sigma_z})_{i,j-1}]\psi_{i-1,j-1}\}$$

$$+\sigma_{zi,j}(\frac{\beta L_y}{f})_j\frac{10^{-4}}{2f_j}(\frac{C'}{\sigma_z})_{i,j}[\psi_{i,j}-\psi_{i-1,j}+\psi_{i,j-1}-\psi_{i-1,j-1}]$$

$$-\frac{10^2}{2}[\frac{C'_{i,j,k}}{p_{i,j,k}-p_{i,j,k-1}}(L_xL_y10^{-6}w^*_{i,j,k-1})+(\frac{C'_{i,j,k}}{p_{i,j,k+1}-p_{i,j,k}}-\frac{C'_{i,j,k}}{p_{i,j,k}-p_{i,j,k-1}}$$

$$+2C_{zi,j,k})(L_xL_y10^{-6}w^*_{i,j,k})-\frac{C'_{i,j,k}}{p_{i,j,k+1}-p_{i,j,k}}(L_xL_y10^{-6}w^*_{i,j,k+1})]$$

$$+\sigma_{zi,j}\frac{L_y}{L_x}[\frac{C_{i+1,j}-C_{i,j}}{\sigma_{zi+1,j}+\sigma_{zi,j}}10^{-4}(A_{i+1,j}+A_{i,j})-\frac{C_{i,j}-C_{i-1,j}}{\sigma_{zi,j}+\sigma_{zi-1,j}}10^{-4}(A_{i,j}+A_{i-1,j})]$$

$$+\sigma_{zi,j}\frac{L_x}{L_y}[\frac{C_{i,j+1}-C_{i,j}}{\sigma_{zi,j+1}+\sigma_{zi,j}}10^{-4}(A_{i,j+1}+A_{i,j})-\frac{C_{i,j}-C_{i,j-1}}{\sigma_{zi,j}+\sigma_{zi,j-1}}10^{-4}(A_{i,j}+A_{i,j-1})]$$

$$+\frac{10^2}{2}[\frac{10^2C_{zi,j,k}}{p_{i,j,k}-p_{i,j,k-1}}(L_xL_y10^{-8}K_{i,j,k-1})+(\frac{10^2C_{zi,j,k}}{p_{i,j,k+1}-p_{i,j,k}}-\frac{10^2C_{zi,j,k}}{p_{i,j,k}-p_{i,j,k-1}}$$

$$+2\times 10^4 C_{zzi,j,k})(L_x L_y 10^{-8} K_{i,j,k}) - \frac{10^2 C_{zi,j,k}}{p_{i,j,k+1} - p_{i,j,k}}(L_x L_y 10^{-8} K_{i,j,k+1})]$$
$$-C_{i,j,k}(L_x L_y 10^{-4} \lambda_{i,j,k})$$
$$= 0 \tag{4.6}$$

Appendix B Scalings of the Equations

Before getting the solutions for the equation system

$$A_{M\times N} \times X \approx Y \qquad (I) \tag{4.7}$$

by the inverse method, it is usually necessary to do scalings on these equations first.

Row Scaling

Different equations may have different noises, and the noises may be even correlated with each other. Equations with large noises may contaminate the equations with small noises. In order to remove this contamination, row scaling is necessary. If the noise variance

$$N = (Y - \hat{Y})(Y - \hat{Y})^T \tag{4.8}$$

is known (where Y is the true solution and $\hat{Y}$ is the estimated solution), then the scaling factor is usually taken as $N^{-1/2}$ (where $N^{1/2}$ is defined as such that $N = N^{1/2}N^{T/2}$). The scaled system is now

$$N^{-1/2}A \times X = N^{-1/2}Y \quad or \quad A' \times X = Y' \qquad (II) \tag{4.9}$$

For the new system, a little of algebra shows that

$$N' = (Y' - \hat{Y}')(Y' - \hat{Y}')^T = I \ \ (unit\ matrix), \tag{4.10}$$

i.e. the noises in all the equations are in the same magnitude and uncorrelated.

For the overdetermined system ($M > N$), row scaling changes the solutions, as shown below. The SVD solution for the unscaled System (I) is

$$\hat{X} = (A^T A)^{-1} A^T Y \tag{4.11}$$

While the solution for the scaled System (II) is

$$\begin{aligned} \hat{X} &= (A'^T A')^{-1} A'^T Y' = (A^T N^{-T/2} N^{-1/2} A)^{-1} \cdot A^T N^{-T/2} N^{-1/2} Y \\ &\neq (A^T A)^{-1} A^T Y \end{aligned} \tag{4.12}$$

because the inverses for A^T and A do not exist.

However, for the undertermined system with full rank ($M < N$ and $Rank(A) = M$), as shown below that the row scaling does not change the solutions. The SVD solution for System (I) now is

$$\hat{X} = A^T (A A^T)^{-1} Y \tag{4.13}$$

and for System (II) is

$$\begin{aligned} \hat{X} &= A'^T (A' A'^T)^{-1} Y' = A^T N^{-T/2} (N^{-1/2} A A^T N^{-T/2})^{-1} N^{-1/2} Y \\ &= A^T N^{-T/2} N^{T/2} (A A^T)^{-1} N^{1/2} N^{-1/2} Y = A^T (A A^T)^{-1} Y \end{aligned} \tag{4.14}$$

i.e. exactly the same as for (I).

Column Scaling

The SVD solutions tend to give large values to the unknowns which have large coefficients. If one physically expected that the solutions for all the unknowns should be in the same order, then one should downweight the large coefficients. Chose a positive

definite matrix W (usually the squares of the lengths of the column coefficients), then System (I) is weighted as

$$AW^{-1/2} \cdot W^{1/2}X = Y \quad or \quad A' \cdot X' = Y \qquad (III). \tag{4.15}$$

For the overdetermined system with full rank ($M > N$ *and* $Rank(A) = N$), the following argument shows that column scaling does not change the solution: The SVD solution for (III) with $M > N$ is

$$\begin{aligned} \hat{X}' &= (A'^T A')^{-1} A'^T Y = (W^{-T/2} A^T A W^{-1/2})^{-1} W^{-T/2} A^T Y \\ &= W^{1/2} A^{-1} A^{-T} W^{T/2} W^{-T/2} A^T Y = W^{1/2} (A^T A)^{-1} A^T Y, \end{aligned} \tag{4.16}$$

thus

$$\hat{X} = W^{-1/2} \hat{X}' = (A^T A)^{-1} A^T Y \tag{4.17}$$

which is identical to the solution for (I).

However, for the underdetermined system ($M < N$), column scaling changes the solution, as shown below. The SVD solution for (III) with $M < N$ is

$$\hat{X}' = A'^T (A' A'^T)^{-1} Y = W^{-T/2} A^T (A W^{-1/2} W^{-T/2} A^T)^{-1} Y \tag{4.18}$$

thus

$$\begin{aligned} \hat{X} &= W^{-1/2} \hat{X}' = W^{-1/2} W^{-T/2} A^T (A W^{-1/2} W^{-T/2} A^T)^{-1} Y \\ &\neq A^T (A A^T)^{-1} Y \end{aligned} \tag{4.19}$$

becuse inverses for A and A^T do not exist.